

UC San Diego

Research Theses and Dissertations

Title

Modeling of Water Temperature, Dissolved Oxygen, and Fish Growth Rate in Stratified Fish Ponds using Stochastic Input Variables

Permalink

<https://escholarship.org/uc/item/59f3f23k>

Author

Lu, Zhimin

Publication Date

2003

Peer reviewed

Modeling of Water Temperature, Dissolved Oxygen, and Fish Growth Rate in Stratified
Fish Ponds using Stochastic Input Variables

By

Zhimin Lu

B.S. (Beijing Institute of Chemical Technology) 1976

M.S. (University of California, Davis) 1995

DISSERTATION

Submitted in partial satisfaction of the requirements for the degree of

DOCTOR OF PHILOSOPHY

in

Biological Systems Engineering

in the

OFFICE OF GRADUATE STUDIES

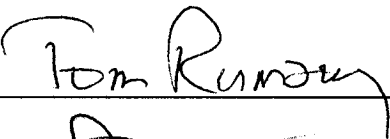
of the


UNIVERSITY OF CALIFORNIA

DAVIS

Approved:







Committee in Charge

2003

UMI Number: 3120970

INFORMATION TO USERS

The quality of this reproduction is dependent upon the quality of the copy submitted. Broken or indistinct print, colored or poor quality illustrations and photographs, print bleed-through, substandard margins, and improper alignment can adversely affect reproduction.

In the unlikely event that the author did not send a complete manuscript and there are missing pages, these will be noted. Also, if unauthorized copyright material had to be removed, a note will indicate the deletion.

UMI[®]

UMI Microform 3120970

Copyright 2004 by ProQuest Information and Learning Company.

All rights reserved. This microform edition is protected against unauthorized copying under Title 17, United States Code.

ProQuest Information and Learning Company
300 North Zeeb Road
P.O. Box 1346
Ann Arbor, MI 48106-1346

ACKNOWLEDGEMENTS

This study was supported by the Pond Dynamics/Aquaculture Collaborative Research Support Program.

Foremost, I would like to express my greatest gratitude to my major professor, Dr. Raul Piedrahita. Without his guidance and encouragement, I could not have accomplished this work. He was always open to assist me during the course of my research spending an immeasurable amount of time in guiding me through the challenges of coursework and model development. He reviewed my dissertation with amazing patience particularly due to my language difficulties.

I would like to express my appreciation to Dr. Tom Rumsey whose constant generosity, kindness, and confidence in me were the crucial for this endeavor. He advised me in graduate school and encouraged to continue into the Ph.D. program.

Furthermore, I am extremely thankful for the help of Dr. David Hills, who provided suggestions for my research concept as well as reviewed my dissertation.

Thanks to the staff of the Biological and Agricultural Engineering Department at UC Davis. Their willingness to help made me feel right at home.

Finally, I am grateful for the loving support from every member of my family. They reminded me every step of the way the value of my work which motivated me to finish.

ABSTRACT

A computer model has been developed to simulate water temperature, dissolved oxygen, and fish growth in a stratified fishpond using stochastic weather variables as input. The model consists of generated weather variables and calculated water quality and fish growth rate. The weather variables are generated using Monte Carlo methods, and include solar radiation, air temperature, and wind speed and direction. The water quality parameters are state variables that include water temperature, dissolved oxygen (DO), phytoplankton (in terms of chlorophyll a, Chla), and total ammonia nitrogen (TAN). Water temperature and DO are predicted at three depths in the water column and the other state variables are assumed to be uniformly distributed. Fish growth rates are predicted under the effects of weather variables and water quality for various pond fertilization treatments. The model has been calibrated and validated using data from the Pond Dynamics/Aquaculture Collaborative Research Program (PD/A CRSP) database. To evaluate the model's performance for different pond management strategies and different locations, model simulations were compared to data collected from 36 fishponds with 11 fertilization treatments in Thailand, Rwanda, and Honduras sites.

The comparisons of simulations and observed data indicate that the model is capable of predicting water temperature and DO stratification and fish growth for simulations up to six months long. The simulated results indicate that water temperature and DO are affected by weather variables, especially solar radiation. Changes in Chla and DO are affected by environmental conditions and fish grazing. The stochastically generated weather variables have little influence on fish growth. Fish growth rate is affected by

changes in Chla and fertilization rate because the model assumes that phytoplankton is the preferred food for tilapia.

The current model is limited by the uncertainty of available weather data and the corresponding limitations in the weather models. The model did not capture the Chla dynamics for some ponds for the Thailand site. These ponds also had a high variability in observed Chla for pond replicates, highlighting the complexity of the pond ecosystem. The fish growth simulations represent the effects of weather variables, DO and TAN concentrations.

CONTENTS

	Pages
ACKNOWLEDGEMENTS	ii
ABSTRACT	iii
CONTENTS	v
LIST OF TABLES	ix
LIST OF FIGURES	x
1. Introduction	1
1.1. Problem Statement	2
1.2. Objectives	5
1.3. Model Assumptions	6
2. Literature Review	8
2.1. Weather Models	9
2.1.1. Solar Radiation Models	10
2.1.2. Air Temperature Models	14
2.1.3. Wind Speed and Wind Direction Models	16
2.2. Water Quality Models	18
2.2.1. Characterization of Stratification	19
2.2.2. Water Temperature Models	20
2.2.3. Dissolved Oxygen Models	22
2.3. Fish Growth Models	26
3. Model Construction	28
3.1. Generation of Weather Values	28
3.1.1. Solar Radiation	30
3.1.2. Air Temperature	39
3.1.3. Wind Speed	41
3.1.4. Wind Direction	43
3.2. Water Quality Model	44
3.2.1. Water Temperature Model	44
3.2.1.1. Input Heat Sources	47
3.2.1.1.1. Solar Radiation Penetration	48
3.2.1.1.2. Atmospheric Radiation	50
3.2.1.1.3. Sensible Heat Transfer	51
3.2.1.1.4. Water Inflow	51
3.2.1.2. Heat Loss	52
3.2.1.2.1. Water Surface Radiation	52
3.2.1.2.2. Evaporative Heat	53

3.2.1.2.3. Heat Loss to the Sediment and Groundwater	54
3.2.1.2.4. Heat Loss from the Effluent	55
3.2.1.3. Heat Transport within the Water Column	56
3.2.1.3.1. Effective Diffusion	56
3.2.1.3.2. Convective Mixing	58
3.2.1.4. Temperature Calculation	58
3.2.2. Dissolved Oxygen Model	59
3.2.2.1. Input Sources	62
3.2.2.1.1. Photosynthesis	62
3.2.2.1.2. Reaeration	66
3.2.2.2. Oxygen Consumption	67
3.2.2.2.1. Phytoplankton Respiration	68
3.2.2.2.2. Fish Respiration	69
3.2.2.2.3. Organic Matter Oxidation	69
3.2.2.2.4. Nitrification	70
3.2.2.2.5. Sediment Respiration	70
3.2.2.3. Oxygen Diffusion between Adjacent Elements	70
3.2.2.4. Oxygen in the Water Influent and Effluent	71
3.2.2.5. Dissolved Oxygen Calculation	71
3.2.3. Phytoplankton Model	71
3.2.3.1. Chlorophyll a Production	72
3.2.3.2. Chlorophyll a Consumption	73
3.2.3.3. Chlorophyll a Calculation	74
3.2.4. Total Ammonia Nitrogen Model	74
3.2.5. Organic Matter Model	78
3.3. Fish Growth Model	80
3.3.1. Water Temperature Effects	82
3.3.2. Dissolved Oxygen Effects	84
3.3.3. Un-ionized Ammonia Effects	84
3.3.4. Food Supply Effects	85
3.3.5. Fish Population	87

4. Results: Model Calibration and Validation	89
4.1. Solar Radiation	91
4.2. Water Quality Simulation Results	101
4.2.1. Thailand Site	105
4.2.1.1. Calibration Run (Treatment 1: 100 kg/ha/wk chicken manure and 24.3 kg/ha/wk urea)	106
4.2.1.2. Validation Run (Treatment 2: 44 kg/ha/wk chicken manure and 10.8 kg/ha/wk urea)	111
4.2.1.3. Validation Run (Treatment 3: 200 kg/ha/wk chicken manure and 48.6 kg/ha/wk urea)	115
4.2.1.4. Frequency Distributions	120
4.2.2. Rwanda Site	124
4.2.2.1. Calibration Run (Treatment 1: 100 kg/ha/wk chicken manure and 400 kg/ha/wk grass)	124
4.2.2.2. Validation Run (Treatment 2: 150 kg/ha/wk chicken manure and 600 kg/ha/wk grass)	128
4.2.2.3. Validation Run (Treatment 3: 200 kg/ha/wk chicken manure and 800 kg/ha/wk grass)	133
4.2.2.4. Validation Run (Treatment 4: 100 kg/ha/wk chicken manure, 400 kg/ha/wk grass, and 28.6 kg/ha/wk urea)	138
4.2.2.5. Frequency Distributions	143
4.2.3. Honduras Site	147
4.2.3.1. Calibration Run (Treatment 1: 500 kg/ha/wk chicken manure)	147
4.2.3.2. Validation Run (Treatment 2: 250 kg/ha/wk chicken manure)	152
4.2.3.3. Validation Run (Treatment 3: 125 kg/ha/wk chicken manure)	156
4.2.3.4. Validation Run (Treatment 4: 1000 kg/ha/wk chicken manure)	160

4.2.3.5. Frequency Distributions	165
4.2.3.6. Long Term Simulations	171
4.3. Fish Growth Simulation Results	179
4.3.1. Thailand Site	180
4.3.2. Rwanda Site	182
4.3.3. Honduras Site	185
5. Discussion	188
5.1. Solar Radiation Generation	188
5.2. Water Temperature	191
5.3. Dissolved Oxygen and Phytoplankton	194
5.4. Fish Growth	200
6. Conclusions	204
6.1. Model Approach and Performance	204
6.2. The CRSP Database	207
6.3. Future Work	208
REFERENCES	210
APPENDICES	217
A. Stella Icon Diagram	217
B. Stella Equations	242

LIST OF TABLES

Table	Page
3-1. Characteristics of selected sites	31
3-2. Estimated parameters for the CFD curves	34
3-3. Estimated parameters for wind speed curves	42
4-1. Selected ponds and treatments used for model calibration and validation	90
4-2. Summary of monthly average clearness index values \bar{K}_t calculated from data in the PD/A CRSP database	92
4-3. Initial water quality input values	101
4-4. Site specific calibrated parameters for water quality models	103
4-5. Initial conditions for the fish growth model	179
4-6. Calibrated parameters for the fish growth model	179
4-7. Fish mass means for different treatments (Thailand site)	182
4-8. Fish mass means for different treatments (Rwanda site)	184
4-9. Fish mass means for different treatments (Honduras site)	187
5-1. Average and standard deviations of measured and simulated water temperature for each treatment	193

LIST OF FIGURES

Figure	Page
3.1. Conceptual diagram of an aquaculture pond model. It shows the relationship among fish, phytoplankton, DO, Temperature, and TAN. The three water layers are of the same depth and most of the processes shown for the surface layer also take place in the other layers.	29
3.1.1. Calculated monthly CFD curves from January to June for the Thailand site	32
3.1.2. Calculated monthly CFD curves from January to June for the Rwanda site	32
3.1.3. Calculated monthly CFD curves from January to June for the Honduras site	33
3.2.1. Water Temperature Model (Energy balance)	45
3.2.2. Schematic diagram of the dissolved oxygen model	61
4.1.1. Calculated CFD for three different months at the Thailand site	93
4.1.2. Comparison of CFD curves with same \bar{K}_l values for the Thailand and Honduras sites	93
4.1.3a. Generated and measured CFD curves for May for the Thailand site	94
4.1.3b. Generated and measured CFD curves for October for the Thailand site	94
4.1.4a. Generated and measured CFD curves for September for the Rwanda site	95
4.1.4b. Generated and measured CFD curves for January for the Rwanda site	95
4.1.5a. Generated and measured CFD curves for August for the Honduras site	96
4.1.5b. Generated and measured CFD curves for February for the Honduras site	96
4.1.6. Comparison of CFD curves generated using two different ρ values	99
4.1.7. Comparison of hourly solar radiation for the Thailand site	99
4.1.8. Comparison of hourly solar radiation for the Rwanda site	100
4.1.9. Comparison of hourly solar radiation for the Honduras site	100
4.2.1.1. Temperature of the surface layer for Treatment 1 for the Thailand site	106

4.2.1.2. Temperature of middle layer for Treatment 1 for the Thailand site	107
4.2.1.3. Temperature of bottom layer for Treatment 1 for the Thailand site	107
4.2.1.4. Surface layer DO for Treatment 1 for the Thailand site	109
4.2.1.5. Middle layer DO for Treatment 1 for the Thailand site	109
4.2.1.6. Bottom layer DO for Treatment 1 for the Thailand site	110
4.2.1.7. Chlorophyll a for Treatment 1 for the Thailand site	110
4.2.1.8. Temperature of surface layer for Treatment 2 for the Thailand site	112
4.2.1.9. Temperature of middle layer for Treatment 2 for the Thailand site	112
4.2.1.10. Temperature of bottom layer for Treatment 2 for the Thailand site	113
4.2.1.11. Surface layer DO for Treatment 2 for the Thailand site	113
4.2.1.12. Middle layer DO for Treatment 2 for the Thailand site	114
4.2.1.13. Bottom layer DO for Treatment 2 for the Thailand site	114
4.2.1.14. Chlorophyll a for Treatment 2 for the Thailand site	115
4.2.1.15. Temperature of surface layer for Treatment 3 for the Thailand site	116
4.2.1.16. Temperature of middle layer for Treatment 3 for the Thailand site	117
4.2.1.17. Temperature of bottom layer for Treatment 3 for the Thailand site	117
4.2.1.18. Surface layer DO for Treatment 3 for the Thailand site	118
4.2.1.19. Middle layer DO for Treatment 3 for the Thailand site	118
4.2.1.20. Bottom layer DO for Treatment 3 for the Thailand site	119
4.2.1.21. Chlorophyll a for Treatment 3 for the Thailand site	119
4.2.1.22. Frequency distributions for surface layer temperature (Treatment 1, Thailand site)	121
4.2.1.23. Frequency distributions for middle layer temperature (Treatment 1, Thailand site)	121

4.2.1.24. Frequency distributions for bottom layer temperature (Treatment 1, Thailand site)	122
4.2.1.25. Frequency distributions for surface layer DO (Treatment 1, Thailand site)	122
4.2.1.26. Frequency distributions for middle layer DO (Treatment 1, Thailand site)	123
4.2.1.27. Frequency distributions for bottom layer DO (Treatment 1, Thailand site)	123
4.2.2.1. Temperature of surface layer for Treatment 1 for the Rwanda site	125
4.2.2.2. Temperature of middle layer for Treatment 1 for the Rwanda site	125
4.2.2.3. Temperature of bottom layer for Treatment 1 for the Rwanda site	126
4.2.2.4. Surface layer DO for Treatment 1 for the Rwanda site	126
4.2.2.5. Middle layer DO for Treatment 1 for the Rwanda site	127
4.2.2.6. Bottom layer DO for Treatment 1 for the Rwanda site	127
4.2.2.7. Chlorophyll a for Treatment 1 for the Rwanda site	128
4.2.2.8. Temperature of surface layer for Treatment 2 for the Rwanda site	129
4.2.2.9. Temperature of middle layer for Treatment 2 for the Rwanda site	130
4.2.2.10. Temperature of bottom layer for Treatment 2 for the Rwanda site	130
4.2.2.11. Surface layer DO for Treatment 2 for the Rwanda site	131
4.2.2.12. Middle layer DO for Treatment 2 for the Rwanda site	131
4.2.2.13. Bottom layer DO for Treatment 2 for the Rwanda site	132
4.2.2.14. Chlorophyll a for Treatment 2 for the Rwanda site	132
4.2.2.15. Temperature of surface layer for Treatment 3 for the Rwanda site	134
4.2.2.16. Temperature of middle layer for Treatment 3 for the Rwanda site	134
4.2.2.17. Temperature of bottom layer for Treatment 3 for the Rwanda site	135

4.2.2.18. Surface layer DO for Treatment 3 for the Rwanda site	135
4.2.2.19. Middle layer DO for Treatment 3 for the Rwanda site	136
4.2.2.20a. Bottom layer DO for Treatment 3 for the Rwanda site	136
4.2.2.20b. Bottom layer DO for Treatment 3 for the Rwanda site (extended y-axis scale)	137
4.2.2.21. Chlorophyll a for Treatment 3 for the Rwanda site	137
4.2.2.22. Temperature of surface layer for Treatment 4 for the Rwanda site	139
4.2.2.23. Temperature of middle layer for Treatment 4 for the Rwanda site	139
4.2.2.24. Temperature of bottom layer for Treatment 4 for the Rwanda site	140
4.2.2.25. Surface layer DO for Treatment 4 for the Rwanda site	140
4.2.2.26. Middle layer DO for Treatment 4 for the Rwanda site	141
4.2.2.27a. Bottom layer DO for Treatment 4 for the Rwanda site	141
4.2.2.27b. Bottom layer DO for Treatment 4 for the Rwanda site (extended y-axis scale)	142
4.2.2.28. Chlorophyll a for Treatment 4 for the Rwanda site	142
4.2.2.29. Frequency distributions for surface layer temperature (Treatment 1, Rwanda site)	144
4.2.2.30. Frequency distributions for middle layer temperature (Treatment 1, Rwanda site)	144
4.2.2.31. Frequency distributions for bottom layer temperature (Treatment 1, Rwanda site)	145
4.2.2.32. Frequency distributions for surface layer DO (Treatment 1, Rwanda site)	145
4.2.2.33. Frequency distributions for middle layer DO (Treatment 1, Rwanda site)	146
4.2.2.34. Frequency distributions for bottom layer DO (Treatment 1, Rwanda site)	146

4.2.3.1. Surface layer temperature for Treatment 1 for the Honduras site	148
4.2.3.2. Middle layer temperature for Treatment 1 for the Honduras site	149
4.2.3.3. Bottom layer temperature for Treatment 1 for the Honduras site	149
4.2.3.4. Surface layer DO for Treatment 1 for the Honduras site	150
4.2.3.5. Middle layer DO for Treatment 1 for the Honduras site	150
4.2.3.6. Bottom layer DO for Treatment 1 for the Honduras site	151
4.2.3.7. Chlorophyll a for Treatment 1 for the Honduras site	151
4.2.3.8. Temperature of surface layer for Treatment 2 for the Honduras site	152
4.2.3.9. Temperature of middle layer for Treatment 2 for the Honduras site	153
4.2.3.10. Temperature of bottom layer for Treatment 2 for the Honduras site	153
4.2.3.11. Surface layer DO for Treatment 2 for the Honduras site	154
4.2.3.12. Middle layer DO for Treatment 2 for the Honduras site	154
4.2.3.13. Bottom layer DO for Treatment 2 for the Honduras site	155
4.2.3.14. Chlorophyll a for Treatment 2 for the Honduras site	155
4.2.3.15. Temperature of surface layer for Treatment 3 for the Honduras site	157
4.2.3.16. Temperature of middle layer for Treatment 3 for the Honduras site	157
4.2.3.17. Temperature of bottom layer for Treatment 3 for the Honduras site	158
4.2.3.18. Surface layer DO for Treatment 3 for the Honduras site	158
4.2.3.19. Middle layer DO for Treatment 3 for the Honduras site	159
4.2.3.20. Bottom layer DO for Treatment 3 for the Honduras site	159
4.2.3.21. Chlorophyll a for Treatment 3 for the Honduras site	160
4.2.3.22. Temperature of surface layer for Treatment 4 for the Honduras site	161
4.2.3.23. Temperature of middle layer for Treatment 4 for the Honduras site	162

4.2.3.24. Temperature of bottom layer for Treatment 4 for the Honduras site	162
4.2.3.25. Surface layer DO for Treatment 4 for the Honduras site	163
4.2.3.26. Middle layer for Treatment 4 for the Honduras site	163
4.2.3.27. Bottom layer DO for Treatment 4 for the Honduras site	164
4.2.3.28. Chlorophyll a for Treatment 4 for the Honduras site	164
4.2.3.29. Frequency distributions for surface layer temperature (Treatment 1, Honduras site)	165
4.2.3.30. Frequency distributions for middle layer temperature (Treatment 1, Honduras site)	166
4.2.3.31. Frequency distributions for bottom layer temperature (Treatment 1, Honduras site)	166
4.2.3.32. Frequency distributions for Surface layer DO (Treatment 1, Honduras site)	167
4.2.3.33. Frequency distributions for middle layer DO (Treatment 1, Honduras site)	168
4.2.3.34. Frequency distributions for bottom layer DO (Treatment 1, Honduras site)	168
4.2.3.35. The frequency distributions of the simulated and measured surface layer DO for Treatment 1 for the Honduras site	169
4.2.3.36. The frequency distributions of the simulated and measured middle layer DO for Treatment 1 for the Honduras site	170
4.2.3.37. The frequency distributions of the simulated and measured bottom layer DO for Treatment 1 for the Honduras site	170
4.2.3.38. Simulated water temperatures for the surface layer (Treatment 1, Honduras)	172
4.2.3.39. Simulated water temperatures for the surface layer for the first 600 hours (Treatment 1, Honduras)	172
4.2.3.40. Simulated water temperatures for the middle layer (Treatment 1, Honduras)	173

4.2.3.41. Simulated water temperatures for the middle layer for the first 600 hours (Treatment 1, Honduras)	173
4.2.3.42. Simulated water temperatures for the bottom layer (Treatment 1, Honduras)	174
4.2.3.43. Simulated water temperatures for the bottom layer for the first 600 hours (Treatment 1, Honduras)	174
4.2.3.44. Simulated DO for the surface layer (Treatment 1, Honduras)	176
4.2.3.45. Simulated DO for the surface layer for the first 600 hours (Treatment 1, Honduras)	176
4.2.3.46. Simulated DO for the middle layer (Treatment 1, Honduras)	177
4.2.3.47. Simulated DO for the middle layer for the first 600 hours (Treatment 1, Honduras)	177
4.2.3.48. Simulated DO for the bottom layer (Treatment 1, Honduras)	178
4.2.3.49. Simulated DO for the bottom layer for the first 600 hours (Treatment 1, Honduras)	178
4.3.1.1. Fish masses for Treatment 1 for the Thailand site	180
4.3.1.2. Fish masses for Treatment 2 for the Thailand site	181
4.3.1.3. Fish masses for Treatment 3 for the Thailand site	181
4.3.2.1. Fish masses for Treatment 1 for the Rwanda site	182
4.3.2.2. Fish masses for Treatment 2 for the Rwanda site	183
4.3.2.3. Fish masses for Treatment 3 for the Rwanda site	183
4.3.2.4. Fish masses for Treatment 4 for the Rwanda site	184
4.3.3.1. Fish masses for Treatment 1 for the Honduras site	185
4.3.3.2. Fish masses for Treatment 2 for the Honduras site	186
4.3.3.3. Fish masses for Treatment 3 for the Honduras site	186
4.3.3.4. Fish masses for Treatment 4 for the Honduras site	187

1. Introduction

To obtain high yields and high quality products from earthen fish ponds, water quality and food supply must meet the requirements for the cultured species over an entire growing season. However, it is difficult to maintain pond water quality at optimal conditions because most pond culture systems are open to the atmosphere. Water quality parameters are affected by climate and topography. Solar radiation, air temperature, wind speed, and wind direction significantly affect water quality, especially water temperature and dissolved oxygen (DO). Water temperature is a critical factor that regulates all biological, chemical, and physical processes in a pond. The survival and growth of cultured organisms depend on the concentration of DO. The depletion of DO may cause stress, slow growth, and even fish death.

Most fish ponds have high phytoplankton concentrations. Changes in the weather cause water temperature and DO to fluctuate seasonally and diurnally (Cuenco, et al., 1985c). Although the amount of solar radiation impinging on a horizontal surface under a clear sky can be predicted analytically for any given location, the effects of the atmosphere on radiation are subject to seasonal, geographic, and random variable changes including cloud cover, vapor pressure, dust, and ozone (Straskraba and Gnauck, 1985). Strong winds, clouds, cold rain, and unseasonably cool weather may suddenly happen at a pond site. Under such unpredictable weather conditions, low DO and low water temperature may occur and seriously affect fish growth and survival. Predicting the effects of water temperature and DO on fish growth under natural weather conditions will help improve

pond management, site selection, and the assessment of risk associated with specific management practices at a given site.

1.1. Problem Statement

Computer modeling is a useful tool for predicting water quality and fish growth in fish ponds. Various computer models have been developed to simulate water quality for fish ponds based on different applications (Piedrahita, 1984; Svirezhev et al., 1984; Losordo, 1988; Culberson, 1993; Nath, 1996; Jamu, 1998). The existing models include the simulation of the whole pond ecosystems over a growing season (Piedrahita, 1984; Svirezhev et al, 1984) and the simulation of water temperature and DO stratification for a 24 hour period (Losordo, 1988; Culberson, 1993). Nath (1996) developed a comprehensive model for assisting in pond site selection and pond management practices. The model includes the effects of water temperature, fertilization, and food supply on fish growth rate. Jamu (1998) developed a model to predict the effects of organic matter and nitrogen cycling pathways in integrated aquaculture/agriculture systems on fish growth. Most of the models mentioned were developed for well mixed ponds. None of the existing models include the effects of stratification over long periods. It is difficult to include the effects of local weather conditions over the long term using these models because the models are deterministic and the effects of random natural variations cannot be included in the simulated variables.

Water temperature and DO stratification in shallow earthen ponds often occur (Losordo, 1988). During windless days, the upper part of the water column can warm up and

become supersaturated in DO while the bottom water remains cooler and with lower DO. During the daytime, the upper water column may not be suitable for fish growth because of supersaturated DO and high temperature and the bottom water may lack oxygen. During the late night and early morning, ponds often destratify resulting in uniform DO and temperature throughout the water column. The daily stratification pattern may be destroyed using aerators or mixers. However, the continuous use of mechanical equipment is not economically practical for many fish farms. In addition, operation of the aerators based on normal daily patterns cannot guarantee the elimination of the risk of losing a crop because the water quality can be affected by unexpected changes of some environmental variables.

Realizing the importance of the stratification of temperature and DO in fish ponds, Losordo (1988) developed a model for predicting the stratification of water temperature and DO over a 24-hour period. The assumptions behind this model were that the water was mixed in the horizontal direction and stratified in the vertical direction. The temperature and DO values along the depth of a pond could then be predicted. In Losordo's model, detailed weather data were obtained for model validation and calibration. The model is limited in its application because it requires large, complete, and complex weather inputs. Culberson (1993) simplified Losordo's model by reducing the input data requirements. Simulation with Culberson's (1993) model was still for 24-hour periods.

Existing long term (complete growing period) and short term (24 hours) models can be used to improve the management of water quality in fish ponds. However, determining the conditions for optimum production is still a challenge because of the randomness of climatic and environmental conditions. For example, variations in solar radiation striking the water surface are likely to cause changes in water temperature and photosynthesis. As a result, water quality and fish growth cannot be determined exactly when pond conditions are projected into the future.

Further understanding of the effects of seasonal and diurnal cycles of water temperature and DO stratification on fish growth will improve fish pond management. Improvements may focus on management of oxygen concentration and the efficient operation of aeration systems, but they may also serve to determine the best season and time to stock the animals, and other management actions.

Most current fish pond models are deterministic, both the input and state variables are fixed. The outcomes of these models are always fixed by the given input variables. However, the behavior of a natural ecological system is often affected by random variables, such as weather parameters. To include the effects of random weather variables on water quality and fish growth in a fish pond model, long term historical data from the pond location are required. These data can be used to develop stochastic models to simulate weather parameters that can be used as inputs for water quality models. However, there are not enough observed weather data for most pond sites. The Pond Dynamics/Aquaculture Collaborative Research Support Program (PD/A CRSP) has been

conducted for over ten years to determine the effects of various factors on fish growth. Relatively long term observations of weather, water quality, and fish growth data are available from the PD/A CRSP database (PD/A CRSP, 2003). The program was designed to improve the efficiency of pond aquaculture systems in developing countries. In 1988 and 1989, the experiments were carried out to investigate the tilapia yield under different levels of organic fertilization in fresh water fish ponds in Thailand, Rwanda, and Honduras research sites. All fish ponds at these sites were fertilized with chicken manure, urea, and other organic wastes (such as fresh cut grass) to achieve a given nitrogen input rate. The fertilizers were applied on a weekly basis. Water temperature and DO were measured at four hours intervals at three water levels (surface, middle, and bottom water layers) one day every two weeks. Other parameters, such as chlorophyll a (Chla), total ammonia (TAN), and fish weight were measured monthly. Weather variables such as daily solar radiation, air temperature, and wind speed were measured daily. In addition, hourly solar radiation were measured occasionally. Some of the hourly water quality data were used for 24-hour simulations by Losordo (1988) and Culberson (1993), and the data also can be used for long term simulations.

1.2. Objectives

The objective of the project was to develop a model to simulate water temperature, DO, and fish growth in a stratified fish pond using stochastic weather input variables. The model consists of three components: weather parameter generation, the calculation of water quality, and the calculation of fish growth. Hourly values of solar radiation, air temperature, wind speed, and wind direction are generated using stochastic methods. The

water quality component includes the simulation of water temperature, DO, total ammonia nitrogen, and phytoplankton (in terms of chlorophyll a) using deterministic methods. The fish growth component includes the simulation of fish biomass under the effects of water quality and food supplies using a bioenergetics model. The variations of solar radiation, water temperature, DO, and fish growth in a stratified fish pond can be predicted over one growing season. The model is intended to predict the ranges and variability of water temperature, DO, and fish growth rate values under certain management strategies for a given site.

1.3. Model Assumptions

It is practically impossible to include all variables in a computer model for an aquaculture pond because it is a very complex ecological system. In this model, solar radiation, air temperature, wind speed, and wind direction are considered as random variables. Water quality state variables include temperature, DO, chlorophyll a, and total ammonia nitrogen. The model is based on the following assumptions:

1. Temperature and DO in a pond are uniform in the horizontal direction and stratify in the vertical direction. The water column is divided into three simulation layers in the vertical direction. In each layer, the temperature and DO are assumed to be uniform.
2. The water depth in the pond is constant. Water loss due to evaporation is assumed to not affect water depth significantly. The water inflow and outflow rates are always the same to keep a constant water depth. The influent and effluent enter and leave the pond at the surface layer.

3. Precipitation and its effects on temperature and stratification are not included in the model.
4. The phytoplankton concentration is calculated in terms of chlorophyll a.
Phytoplankton species differences are not considered in the model. The distribution of phytoplankton in the water column is uniform.
5. Nitrogen is considered as a limiting nutrient for phytoplankton growth. Phosphorus is not considered as a limiting nutrient because all ponds received chicken manure that has a high concentration of phosphorus. The distribution of nitrogen concentration is uniform.
6. pH and alkalinity are constant and do not affect pond conditions during the simulation periods.

2. Literature Review

A variety of computer models have been developed to simulate temperature, DO, and other water quality parameters in fish ponds (Meyer, 1980; Piedrahita, 1984; Svirezhev, et al., 1984; Losordo, 1988; Nath, 1996; Jamu, 1998, Ernst, 2000). Computer models for freshwater ecosystems can be classified as empirical or mechanistic. Empirical models are built based on the analysis of data and statistics. Those models have limited general application because the equations tend to be site-specific. In contrast, mechanistic models are based on an understanding of the theoretical relationship among the model variables. The equations in a mechanistic model describe the detailed processes among the system variables. Therefore, a mechanistic model can be easily adapted for different situations. A pond system involves complex environmental, chemical, physical, and biological relationships, and mechanistic models can only describe selected state variables. Most parameters in a mechanistic model are estimated based on data or adjusted by model tuning.

In general, the early efforts in pond model development were primarily empirical because of insufficient information about the interactions taking place within a pond system (Bolte et al., 1986). The relationships among biochemical and physical processes were estimated using regressions, correlation, probability distributions, factor analysis, etc. Recently developed models have been mostly mechanistic. Mass and energy balances have been used for the simulation of DO and temperature in pond ecosystems, respectively (Piedrahita, 1984; Svirezhev, et al., 1984; Losordo, 1988; Culberson, 1993). The existing models can simulate either long term (several months) or short term (24

hour) periods. The long term simulations have focused on water quality and have included many parameters but use the assumption that the pond water is well mixed (e.g. Piedrahita, 1984; Svirezhev, et al., 1984). Short term simulations have been used to model water quality stratification with a focus on DO and water temperature (Losordo, 1988; Culberson, 1993).

The simulation of diurnal water quality requires detailed meteorological data. The weather parameter values must be obtained either by observation or through simulations. Models have been developed using deterministic and stochastic methods to generate the weather parameter values for different applications. The techniques used in generating weather parameter values and in modeling water temperature, DO, and fish growth are reviewed in order to construct a water quality model for the long term simulation of stratified fish ponds.

2.1. Weather Models

Weather variables are the main environmental factors that affect water temperature and DO. The major variables include solar radiation, air temperature, wind speed and direction, relative humidity, atmospheric pressure, and precipitation. These variables are difficult to generate using deterministic methods because of their stochastic nature. An indication of the stochastic characteristics of the variables can be obtained from the statistical analysis of historical data. It is very difficult to construct a stochastic model with limited data sets, such as those available for CRSP sites. Several models have been developed to generate daily and hourly solar radiation, air temperature, wind speed, and

wind direction for different applications (e.g. Amato et al., 1986; Graham et al., 1988; Graham and Hollands, 1990; Gordon and Reddy, 1988a and b; Huang and Chalabi, 1995). Some of those models are described here.

2.1.1. Solar Radiation Models

Solar radiation values may be assumed to include two components: deterministic and stochastic (Graham et al., 1988). The deterministic component represents the long term characteristics at a given geographical location and account for factors such as seasonal variations. Therefore, the daily extraterrestrial irradiation variation can be predicted with mechanistic models. The stochastic component reflects the dynamic behavior of natural phenomena during short periods of time and accounts for factors such as the effects of clouds. The effects of clouds have been described using the clearness index (the clearness index is defined as the ratio of the solar irradiation on a horizontal plane to the extra-atmospheric irradiation) (Graham et al., 1988). The clearness index is a stochastic variable that can be described with probability distributions obtained from site data.

Once a mathematical model is developed based on detailed historical data for a site, solar radiation values can be generated for use in simulations. The essential step is to construct a model using equations incorporating the probability characteristics of long term historical data. Because of the lack of long historical data for many sites, much effort has been made to develop ways of using limited data sets.

Pioneering work in analyzing the characteristics of solar radiation was undertaken by Liu and Jordan (1960). A large number of solar radiation data from different locations and climate conditions were analyzed and checked for universal characteristics. Liu and Jordan (1960) treated atmospheric transmittance as the random variable instead of solar radiation itself. They found that for a given monthly average daily clearness index, \bar{K}_t , there is a unique frequency distribution of the daily clearness index, K_t (Cumulative Frequency Distribution or CFD). They found that the same values of \bar{K}_t have similar cumulative distribution curves. However, it is doubtful that the CFD curve is unique for a given value of \bar{K}_t especially considering site differences in latitude and elevation. More than 20 years of daily solar radiation data for 90 locations in the U. S. and Canada were analyzed by Bendt and co-workers (1981) confirming that the frequency distributions of the daily clearness index were dependent on the monthly average daily clearness, \bar{K}_t and were almost independent of the month and location. Therefore, although solar radiation is a random variable, the cumulative distribution curve is deterministic. A deterministic equation was derived to generate the cumulative distribution curves based on a maximum clearness index K_t of 0.8 for a clear day and a minimum K_t of 0.05 for a heavily clouded day (Bendt et al., 1981). Saunier and co-workers (1987) observed the monthly probability distributions of daily global irradiation values for both temperate and tropical climates and pointed out that the CFD curves proposed by Liu and Jordan (1960) did not suit tropical locations. They also found that the equations provided by Bendt and his co-workers (1981) for estimating the clearness index distribution needed to be adjusted for humid tropical climates.

Other researchers have attempted to develop models using a few parameters and no detailed historical data. After examining the sequences of the daily solar radiation data from 17 stations in Italy, Amato and co-workers (1986) proposed a model to generate daily solar radiation values using Markov processes and Fourier series. More than 20 years of daily solar radiation data from four stations in Italy were used to calibrate and validate their models. They found that the frequency distributions of the time series residuals, the means, and the variances were not Gaussian. However, data could be transformed into a Gaussian distribution by the use of an error function. A first order autoregressive model was applied to generate random numbers in a normal distribution, and the values of mean and variance were obtained through the use of Fourier series. Considering the sequential properties of solar radiation data, a one-day discrete time series was used in the model. The results of the data analysis showed that the first order autocorrelation coefficient was independent of location and the distributions of the residual values were independent of season. According to the authors (Amato, et al., 1986), the model could be used to generate daily solar radiation values for any location in Europe even when there were no directly measured data, but only monthly average values. However, their work did not allow for any changes in the distribution. In addition, the approach can only be applied to the locations studied because the solar radiation values for each site were used in model development.

Graham and his co-workers (1988) proposed a stochastic model to generate daily solar radiation values using only the monthly average daily clearness index. The model is

based on the fundamental observation of Liu and Jordan (1960) that the monthly average daily clearness index value, \bar{K}_t , has a unique cumulative frequency distribution (CFD) and is independent of location and month. After studying the ten-year daily solar radiation data sets from three different locations in Canada, the authors chose a first order autoregressive model for generating daily solar radiation values. The autocorrelation coefficients varied with the locations and months, from 0.253 to 0.348, and an average value of 0.29 was used for all three locations. Graham and his co-workers (1988) also found that the annual series of residuals had a normal distribution, which was different from the results obtained by Amato and coworkers (1986) who found that the distribution of K_t values is not Gaussian and varied monthly. The model of Graham and co-workers (1988) can be used to generate daily solar radiation values requiring only a monthly average value, \bar{K}_t , since cumulative frequency distribution curves or functions for daily solar radiation have been published for many locations. Therefore, the model can be applied for any location if one has the value of \bar{K}_t . The authors suggested that the model could be applied to all locations around the world but the model was validated only for three locations in Canada.

There are fewer published models for generating hourly values than daily values, due in part to the lack of suitable databases. Gordon and Reddy (1988a and b) compared the probability distributions of daily and hourly values, and concluded that the stationary statistics for individual hours were similar to those of daily solar radiation. Graham and co-workers (1990) developed a stochastic model to generate hourly values, in which the hourly values are dependent on the statistics of hourly data and the values of the daily

clearness index. The standard deviation was strongly dependent on the daily clearness index value but not dependent on the location. Three probability distribution functions were developed to generate hourly values based on the atmospheric transmittance that is a function of the daily clearness index. Knight and co-workers (1991) simplified the three probability functions into one function.

2.1.2. Air Temperature Models

A few models have been developed to generate hourly air temperature values (Card et al., 1976; Knight et al., 1991; Ephrath et al., 1996). The model developed by Card and co-workers (1976) used a Fourier series equation and the monthly average daily values to calculate the daily values. With the daily values, the hourly values could then be calculated using a normalized diurnal profile and the daily maximum and minimum values. The magnitude and the shape of the diurnal temperature depended on season, cloud cover, and other factors. A daily temperature profile was assumed such that the highest temperature was always at 3:00 p.m. and the lowest temperature was always at 6:00 am. Therefore, a sinusoid equation with a frequency of one cycle per day plus a second harmonic was used for the daily profile year round. The diurnal profile equation was applied by Culberson (1993) to estimate the hourly air temperature in a water quality model for 24 hour simulations. The model developed by Card and co-worker (1976) may not be suitable for long term water quality simulations because the effects of random variables cannot be ignored.

Although the effect of random components in hourly temperature simulations maybe small for solar heating systems, Knight and co-workers (1991) constructed an air temperature generation model using a random term. The hourly temperature was generated from the daily values with a series of normally distributed numbers that were transferred through a cumulative distribution function. The hourly temperature model consisted of deterministic and random components. The deterministic component was a cosine equation that generated the diurnal average hourly values. The random component was a second order autoregressive model (AR2). The analysis of the autocorrelation structure and residuals from various locations showed that the AR2 model was suitable for the generation of hourly air temperature. The authors found that the effects of the two autoregressive coefficients on the generation of hourly values were small, therefore the values of the two coefficients from one location can be used for all months and locations. The required input variables consist of monthly average daily air temperatures and the standard deviations of the monthly average daily values. The model may be more realistic than the model developed by Card et al (1976). The shape of the distribution is the same for the whole month, and the values for each hour are randomly changed in a normal distribution.

Ephrath and co-workers (1996) proposed using two equations to generate the hourly air temperature values: a sinusoidal equation to generate the daytime values and an exponential equation to generate nighttime values. Hourly air temperature values showed that the air temperature profile increased faster after sunrise, reached a plateau and maximum in the middle of day, and then decreased rapidly after sunset. The time of the

peak value on each day depended on the day length. The diurnal curve depended on the day length, maximum air temperature, minimum air temperature, the next day's minimum air temperature, and the time of sunrise and sunset. The equations were calibrated and validated using three locations in a temperate climate (latitude from 32 °N to 52.2 °N).

The application of Knight's model is limited by the need to obtain the probability distribution of the air temperature. Having the daily maximum and minimum daily values, the models developed by Ephrath and Card are easy to implement.

2.1.3. Wind Speed and Wind Direction Models

Wind speed is a key variable for predicting heat and oxygen transfer across the air-water interface. The wind speed is a non-stationary and non-Gaussian variable. There have been several studies on the simulation of daily and hourly wind speed (e.g. Balousktsis, et al., 1986; Ephrath et al., 1996; Huang and Chalabi, 1995).

A common method for the generation of wind speed values is based on the Weibull distribution using a conditional mean and variance (Huang and Chalabi, 1995). The seasonal and diurnal variations have to be removed using the means and standard deviations from the daily and hourly wind speed data, respectively (Balousktsis et al., 1986). After removing the periodicity, the frequency distribution of the measured data could be fitted into a Weibull distribution; therefore, the first order Markov transition matrix could be used to generate the wind speed data. The model was tested with data from three locations in Greece with latitudes from 35 to 40 °N. The model is simple

because the autocorrelation coefficients were found to be location independently. Moreover, the model requires only the monthly averages and standard deviations of measured daily values. The hourly average values can be generated using the generated daily values and the monthly variance of observed hourly data. However, the autoregressive-moving average (ARMA) model could not provide the accuracy of wind speed forecast needed for a greenhouse heating control system (Huang and Chalabi, 1995). Huang and Chalabi analyzed a set of 2024 hourly wind speed data. The means and variances of hourly wind speed indicated that an ARMA model was not suitable for real-time forecasting. Therefore, a linear, time-varying autoregressive (AR) process was used to simulate hourly wind speed. The difficulty of using an AR model is the complexity of the simultaneous estimation of moving average and autoregressive coefficients. The autoregressive coefficients were estimated from one set of observed hourly wind speed data.

It is always important to balance the accuracy of the simulation results and the simplicity of model implementation. Considering that only daily total, maximum, and minimum wind speed data may be available for many cases, a simple model was developed to derive the diurnal curves from daily data (Ephrath et al., 1996). The wind speed data from three different locations showed that the daily profile was similar. The hourly wind speed increased from the early morning until later afternoon, and then decreased to the minimum value in the evening. The diurnal cycle was described using two sine equations. The shape of the sine curves varied as the wind increased and decreased. The time of the maximum wind speed value was estimated from site data. The sunset and

sunrise time was also used to determine the shape of the sine curves. If the maximum and minimum values were not available, a total daily accumulated wind speed could be used to estimate the daily maximum value. The simulations and measurements showed good agreement (Ephrath et al., 1996).

It is difficult to determine the autoregressive coefficients with limited datasets. dos Santos Neto and Piedrahita (1994) used a very simple equation to generate wind speed in a preliminary water quality model. The wind speed was assumed to follow a normal distribution and hourly wind speed values were generated using means and standard deviations of observed historical data. There were no seasonal and diurnal patterns included in the equation.

Wind direction affects water quality through its impact on fetch. However, there are very few wind direction data available for fish ponds. Wind direction values were generated for a water quality model by dos Santos Neto and Piedrahita (1994) using a skewed normal distribution. The means and standard deviations were calculated from the few data available.

2.2. Water Quality Models

The consequences of thermal and DO stratification in semi-intensive fish ponds have been described by several researchers. This review focuses on fish pond water characterization and the modeling of water temperature and DO.

2.2.1. Characterization of Stratification

Thermal and DO stratification in lakes and reservoirs generally follows a seasonal or annual cycle. However, stratification in shallow fish ponds often occurs in diurnal cycles. Most fish ponds have a high density of phytoplankton and other suspended particles, which result in high turbidity. The high turbidity reduces the light penetration into the water column resulting in strong stratification. Because oxygen production is a function of light intensity and temperature, a low light intensity and a low temperature will result in a low oxygen production rate. DO concentration is determined by the net oxygen production and oxygen consumption rates. In a pond, the oxygen production rate drops with the increasing water column depth due to the reduced light intensity. However, the oxygen consumption rate does not decrease as depth increases resulting in low DO in the bottom layers of most ponds. Stratification in a one meter deep catfish pond was measured by Losordo (1988), who found differences in the temperature and DO exceeding 10 °C and 21 mg/L, respectively, between 5 and 80 cm below the pond surface. Similarly, the stratification data in the PD/A CRSP database showed that the maximum differences in temperature and DO were up to 6.0 °C and 10 mg/L per meter, respectively. In contrast, in deep lakes and reservoirs, the temperature difference varies from 0.2°C to 1 °C per meter (Goldman and Horne, 1983).

The maximum stratification in aquaculture ponds is often observed in the late afternoon before sunset, and destratification often occurs in late evening and after midnight.

Stratification in a highly turbid fish pond often consists of high temperature combined with supersaturated DO in the surface layer, and low temperature combined with low DO

in the bottom layer. Under these conditions, cultured fish may limit their movements in extreme areas and the culture volume may be effectively reduced. Recognizing the importance of predicting stratification in fish culture ponds, Losordo (1988) developed a model to simulate the stratification of water temperature and DO in fish ponds.

2.2.2. Water Temperature Models

Water temperature models for aquaculture ponds have been developed based on energy balances for the water. The net heat transfer in a pond is estimated by accounting for the heat inputs and heat outputs. The major heat source is solar radiation. The outputs include heat loss due to evaporation, convection, and heat transfer between water layers. Typically, one dimensional models have been used since the temperature gradient in the horizontal direction is much less than in the vertical direction (Cathcart and Wheaton, 1987; Losordo, 1988). A one dimensional model was developed by Cathcart and Wheaton (1987) for predicting temperature in several discrete layers in the vertical direction. Considering the difficulty in obtaining the input weather data, the authors used only hourly measurement of solar radiation. The model includes heat transfer between the water layers, which was estimated using a Fickian diffusion function based on the assumption of molecular diffusion. The light attenuation at each water layer was estimated using an exponential equation that was a function of pond depth. The effect of wind speed on the heat distribution was considered in the model based on the density gradient in the water column.

Losordo (1988) argued that it was important to include the detailed weather variables when simulating surface water temperature. He developed a model including detailed weather data: solar radiation, air temperature, humidity, wind speed, wind direction, and rain fall. The weather data were sampled every minute, and recorded every 20 minutes. The heat balance used by Losordo (1988) for the surface water was more complete than in the model developed by Cathcart and Wheaton (1987). The effect of wind speed on turbulent heat mixing of surface water was modeled by accounting for the wind shear force in addition to the density gradient. In Losordo's model, a one meter deep fish pond was divided into five layers in the vertical direction. The simulated temperatures for the five layers were started at a depth of 5 cm below the water surface and repeated at 20 cm intervals. An energy balance was applied for each water layer. The input variables included initial pond conditions and measured weather data. Since the detailed observed data were used for model calibration, the model proved reliable in its application to several pond locations in Northern California. However, model application is limited because the detailed input variables are difficult to obtain for other pond sites.

Culberson (1993) modified Losordo's model to be used for a wide range of geographical sites, from temperate to tropical climates. In Culberson's model, the simulation water elements were reduced from five to three. The detail of the input variables was reduced based on the available data from the test sites. The model was verified for several pond locations and yielded satisfactory simulation results.

2.2.3. Dissolved Oxygen Models

The most critical water quality parameter in fish ponds is DO. Many models have been developed to predict DO dynamics in fish ponds (Romaine and Boyd, 1979; Meyer and Brune, 1982; Piedrahita, 1984; Svirezhev et al, 1984; Losordo, 1988). The principle of mass balance has been applied in these models. DO concentration is calculated from the rates of oxygen production, consumption, and transformation. The oxygen source terms are photosynthesis in the water column and reaeration at the water surface; the consumption consists primarily of respiration by phytoplankton, fish, and other organisms. The rates of oxygen production and consumption can be estimated using either empirical or mechanistic approaches. The early published models were mostly empirical (Romaine and Boyd, 1979), in which the oxygen production and consumption rates were estimated using regression equations that were obtained from data. Later models have been mostly mechanistic (Meyer and Brune, 1982; Piedrahita, 1984; Svirezhev et al, 1984; Losordo, 1988). With a few exceptions, existing DO models are suitable for mixed ponds and cannot be used to describe conditions in a stratified pond.

Boyd and co-workers (1978) developed a model for predicting DO in catfish ponds. In their model, the oxygen production by photosynthesis was described as a function of solar radiation, chlorophyll-a, and oxygen concentrations at dawn. The oxygen consumption due to phytoplankton was estimated as a function of fish biomass, Secchi disk depth, and oxygen concentration at dusk. The diffusion of oxygen between the water surface and the environment was characterized as a function of wind speed and water temperature.

Chlorophyll-a concentration was obtained from the Secchi disk depth through a

correlation equation. In the model, all functions were regression equations using data from a catfish pond. Input values, such as solar radiation, wind speed, and water temperature came directly from the data.

Meyer and Brune (1982) developed a model using a mechanistic approach to predict DO in a hypothetical catfish pond. The authors intended to identify and describe some interactions between biochemical and physical processes. Because of the limited information available from fish culture ponds, many equations were adapted from systems such as shallow lakes, reservoirs, eutrophic ponds, and wastewater stabilization ponds. Oxygen production sources and sinks were described theoretically. The constants, coefficients, and parameters in the mathematical equations were calibrated and validated using different sets of data from previous studies. Photosynthesis was described as a function of light attenuation, nutrient conditions, water temperature, and the concentration of chlorophyll-a. Oxygen consumption due to respiration by phytoplankton was modeled as a function of temperature and the initial rate of respiration of decaying phytoplankton. The diffusion between the water surface and the air was estimated as a function of DO concentration, water temperature, and wind velocity. Hourly solar radiation values under a clear sky were estimated based on the geometry of the earth's rotation, variations in the inclination of the earth's axis, and the elliptical rotation of the earth around the sun. Water temperature values were given and pond water was assumed to be completely mixed. The model was used for short term (24 hour) simulations, and use of this model for long term simulations is limited because the dynamics of

phytoplankton concentration, Secchi disk values, and weather input variables were not included.

Two similar models that can be used to predict water quality and fish growth rate in fish ponds were developed separately by Piedrahita (1984) and Svirezhev et al. (1984). There were 22 state variables in Piedrahita's model and 11 in Svirezhev's model.

Phytoplankton production rate was modeled as a function of nutrient concentration, light intensity, and temperature. Phytoplankton consumption rate was estimated by the inclusion of the mortality of phytoplankton, grazing by fish and zooplankton, and sinking to the sediment. Oxygen production rate was assumed to be proportional to phytoplankton production rate and was described using a linear equation.

Another long-term model was developed by Lee and co-workers (1991a,b) for the prediction of DO in a marine fish culture zone. The authors took into account the effects on the accuracy of the prediction of DO of wide fluctuations in the saturation light intensity and the ratio of carbon to chlorophyll-a. In their model, the saturation light intensity was calculated from the previous three days' light intensity. The ratio of carbon to chlorophyll-a was estimated as a function of the maximum phytoplankton growth rate, the temperature limit factor, the saturation light intensity, and the initial slope of the phytoplankton-light intensity curve. The model was developed for a completely mixed shallow coastal bay with weak tidal flushing. The solar radiation, water temperature, nutrient loading, and the tidal flushing range were given values on a daily basis. The DO prediction was described as satisfactory, but the phytoplankton concentration was not.

A model developed by Losordo (1988) attempted to predict the stratification of temperature and DO in fish ponds. Similar to his temperature model, oxygen concentration was predicted in the five volume elements or water layers. The oxygen concentration in each element was assumed to be homogeneous. Light attenuation in the water column was described using the Lambert-Beer Law. The effects of the solar radiation incident angle and water turbidity were taken into account in the model. Oxygen diffusion between the elements was based on the concepts of molecular and turbulent diffusions. The major force for turbulent transport at the water surface was wind shear. Wind shear is calculated in Losordo's model using an empirical equation based on air density, coefficient of aerodynamic resistance, and wind speed. Because the model's approach was based on mechanistic principles, the predicted results were verified for different locations. The simulation results were satisfactory. However, the application of the model was limited because a large number of detailed input variables are required, such as detailed weather data (every 20 minutes).

Considering the lack of detailed data available for most fish ponds, Culberson (1993) modified Losordo's model by making it more "user friendly". The most significant changes in the model were the reduction of the input data from 440 to 60 data points, which substantially reduce the data requirement especially for some difficult to obtain data. Culberson also reduced the simulated thermal elements in a water column from five to three. The simplified model demonstrated that the mass balance approach is appropriate and that the simulation results remain accurate after verification of the model using three different geographical locations. However, the model cannot be used for long-

term simulations directly because the long-term changes in variables, such as Secchi disk, fish respiration, and weather input variables were not modeled. For a short-term simulation, the saturating light intensity and the ratio of carbon and chlorophyll-a were considered to be constants (Losordo, 1988).

2.3. Fish Growth Models

The relationships among fish growth, water quality, and feeding are of major concern in predicting fish weight. It is difficult to conduct experiments to examine the effects of one factor only because various biotic factors, such as fish size, species, and behavior influence fish growth. Most fish growth models have been developed based on the concept of bioenergetics (Cuenco et al., 1985c; Liu and Chang, 1992; Bolte et al., 1994; Nath, 1996). The basic principle of bioenergetics is that all energy intake through food consumption is lost as waste (feces or excretion), used in metabolic processes or stored as new body tissue (Jobling, 1994). Since food consumption is a function of fish size, the energy balance within a fish body is usually described based on fish biomass.

Variables affecting food intake include fish size, food availability, photoperiod, temperature, DO, and un-ionized ammonia concentrations (Cuenco et al., 1985a). Water temperature is the factor that affects the fish growth rate the most. A sensitivity analysis performed by Cuenco and co-workers (1985b) showed that parameters for food consumption are more sensitive than parameters related to the metabolic terms. Liu and Chang (1992) developed a bioenergetics model to examine the effects of pond fertilization, stocking density, and spawning on the growth of Nile tilapia. A non-linear

regression method was used to estimate the parameters in the growth model. The model provided fairly accurate results of the estimated parameters from PD/A CRSP Thailand data (Liu and Chang, 1992).

A more complete bioenergetics model was developed for Nile tilapia (Bolte et al., 1994; Nath 1996). The model accounted for the effects of water temperature, DO, un-ionized ammonia, photoperiod, fish size, and food availability. The model can be used to predict fish growth under different pond management strategies. Three different food sources (two types of phytoplankton and one of zooplankton) were included in the model. The different types of food sources were described based on their carbon content. The coefficients of food intake rate for each food source were determined by model calibration. The model was used to simulate fish growth at different stocking densities and different fertilization rates at several locations. The simulation results indicated that the model could not describe the effects of fertilization on fish growth because the nutrient content of food sources was not included. The authors suggested that future work should include the effect of factors such as climate.

3. Model Construction

The model described in this dissertation includes three parts: Weather, Water Quality, and Fish Growth. Each part consists of several sub-models, which describe different variables. The schematic diagram of the water quality model is shown in Figure 3.1. The Weather Part includes solar radiation, air temperature, wind speed, and wind direction sub-models, which are constructed using stochastic methods. The Water Quality Part includes water temperature, DO, phytoplankton (in terms of chlorophyll a), and total ammonia nitrogen (TAN) sub-models, which are constructed using deterministic methods. The Fish Growth Part accounts for the effects of water quality, environmental conditions, feed, and genetic parameters on fish growth. The model was constructed to make maximum use of the information available from the PD/A CRSP database.

3.1. Generation of Weather Values

The weather values generation includes hourly solar radiation, air temperature, and wind speed. Time series methods were used for generating these values. The solar radiation model has been modified from the model developed by Graham and co-workers (1988, 1990). The air temperature model is a combination and modification of several published methods (Card et al., 1976; Knight et al., 1991). The wind speed model was constructed using a first order Markov process. Data to construct and test the weather models were obtained from the PD/A CRSP database.

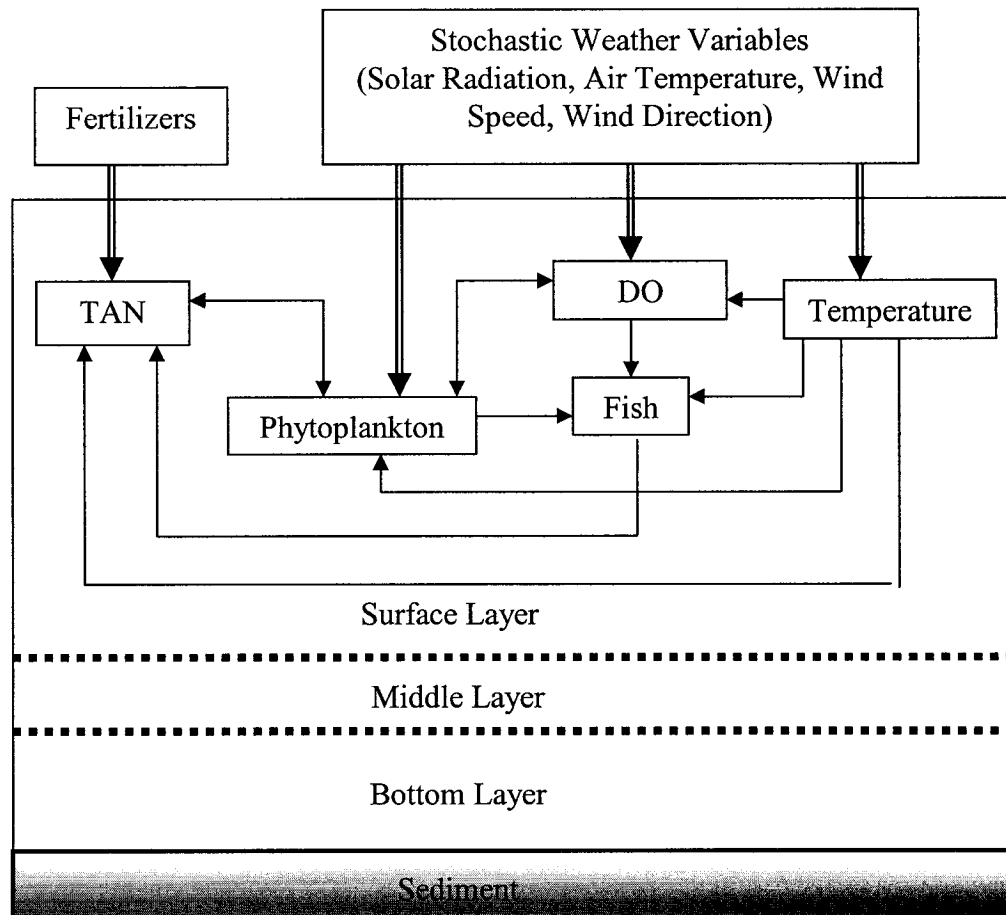


Figure 3.1. Conceptual diagram of an aquaculture pond model. It shows the relationship among fish, phytoplankton, DO, Temperature, and TAN. The three water layers are of the same depth and most of the processes shown for the surface layer also take place in the other layers.

3.1.1. Solar Radiation

Several researchers have found that a first order autoregression equation is suitable for generating a series of daily solar radiation values (Liu and Jordan, 1960; Amato, et al., 1986; Graham et al., 1988). Graham and co-workers (1988) developed a model which requires only monthly average daily solar radiation values. The model was based on the discovery by Liu and Jordan that the frequency distribution of clearness index was only a function of monthly average daily solar radiation values, and independent of location and season. Graham's model was intended to be used for locations for which the average monthly daily clearness index values were known. Considering the lack of long-term solar radiation data from fish pond sites around the world, the weather model was developed using the approach proposed by Graham and co-workers (1988 and 1990).

The model was constructed based on the statistics of daily clearness indices. The cumulative frequency distribution (CFD) of the daily clearness index for each month was obtained from the PD/A CRSP database, which constitutes a data set that is less complete than what is normally available from long-standing meteorological installations. Three sites were selected from the PD/A CRSP database to examine the correlation of the CFD and monthly average daily clearness index and to test the procedure presented below for the generation of hourly solar radiation values. The fish pond sites are in Thailand, Honduras, and Rwanda (Table 3-1).

Table 3-1. Characteristics of selected sites
(PD/A CRSP, 1987)

	Thailand (Bang Sai)	Rwanda (Rwasave)	Honduras (El Carao)
Latitude	14°45'N	2°40'S	14°26'N
Longitude	100°32'E	29°45'E	87°26'W
Elevation (m)	5	1700	583
Data Length (years)	6	8	6
Ave. Annual Air Temperature (°C)	28.0	21.0	25.3
Ave. Annual Rainfall (mm)	1372	1200	765
Pond dimension (m) (Length x Width x Depth)	22 x 10 x 1.0	30 x 20 x 1.3	50 x 30 x 0.9

The data sets used to calculate the daily clearness index probability distributions cover periods of six years (1990 to 1995), six years (1986 to 1991), and eight years (1984 to 1991) from Thailand, Rwanda, and Honduras, respectively. However, the data sets are not complete, with data missing from periods of up to three months. The extraterrestrial solar radiation was calculated using the equations of Duffie and Beckman (1991), for the calculation of K_t and \bar{K}_t .

For each month, the clearness index values ranged from 0.10 to 0.85 and were divided into 30 groups with intervals of 0.025 to generate the cumulative frequency distributions. As an example, six monthly CFD curves for each location are shown in Figures 3.2 to 3.4 for the Thailand, Rwanda, and Honduras sites, respectively.

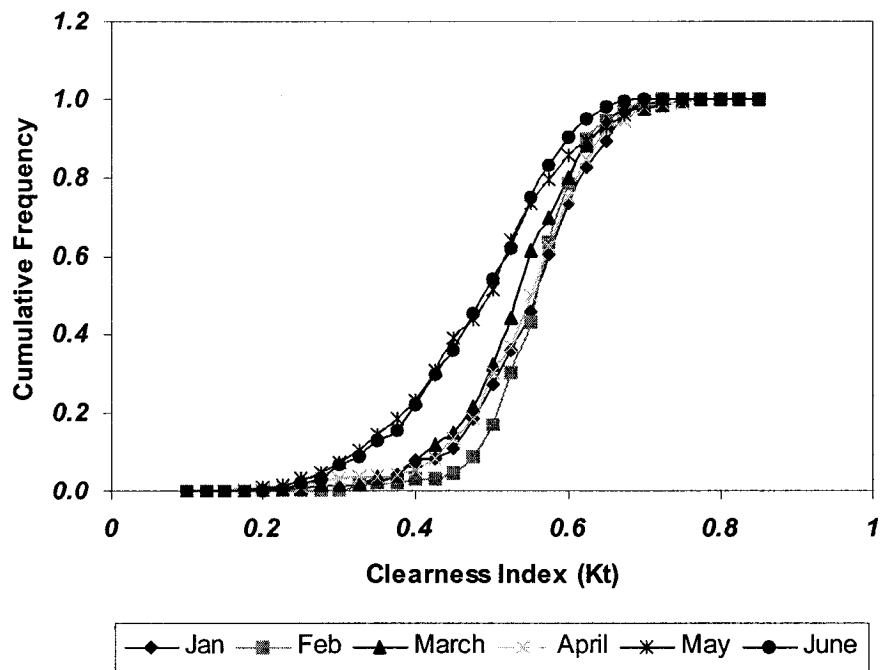


Figure 3.1.1. Calculated monthly CFD curves from January to June for the Thailand site

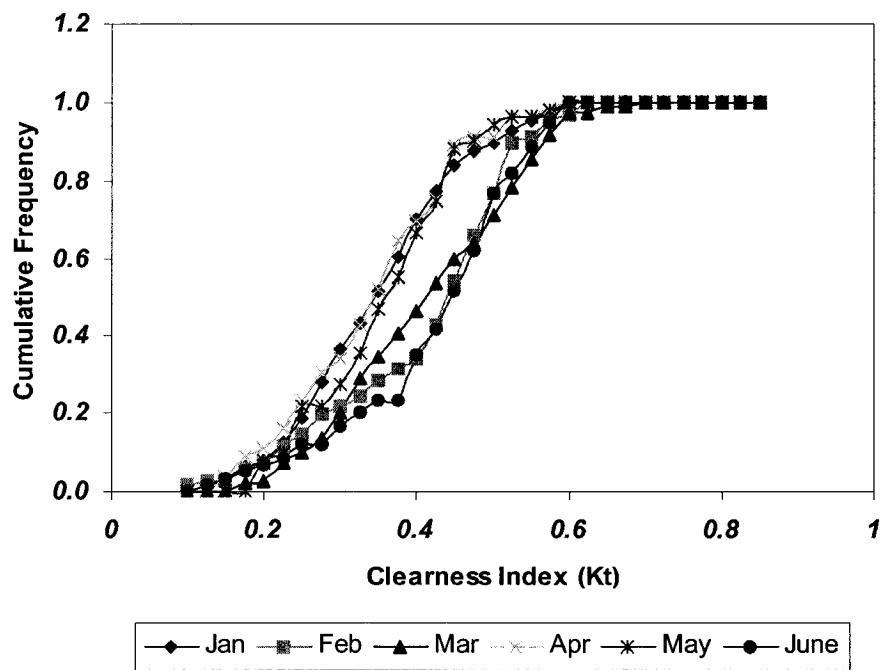


Figure 3.1.2. Calculated monthly CFD curves from January to June for the Rwanda site

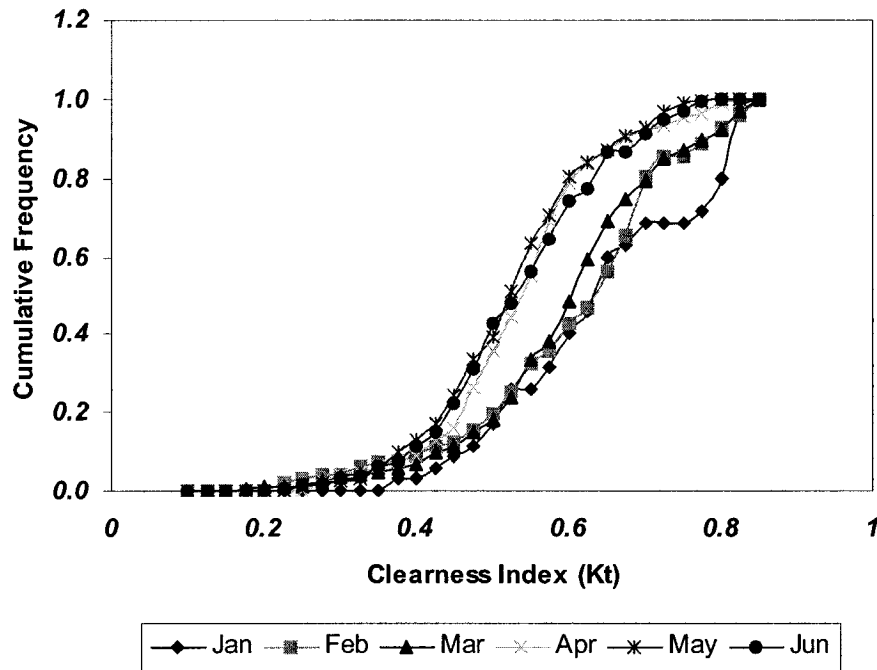


Figure 3.1.3. Calculated monthly CFD curves from January to June for the Honduras site

Since the monthly CFD curves were of similar shapes, a single equation form was selected for all the CFD curves after exploratory analysis of the data (TableCurve™). The equation was selected on the basis of the quality of fit as indicated by the correlation coefficient (R^2), and is of the form:

$$F(K_t) = -0.01 + \frac{a}{1 + \exp\left(\frac{b - K_t}{c}\right)} \quad (3-1-1)$$

Where a , b , and c can be estimated by curve fitting (e.g. TableCurve™) for a given K_t .

To reduce the number of equations used while also maintaining the accuracy of the model, it was decided to combine similar CFD curves into a single equation as long as the

R^2 for the combined equation could be maintained above 0.98. As a result, there were four groups for the Thailand site, two for the Rwanda site, and three for the Honduras site (Table 3-2).

Table 3-2. Estimated parameters for the CFD curves

Location	Months	a	b	c
Thailand	Jan. to Apr.	1.0238	0.5473	0.0476
	May to Sept.	1.0264	0.4742	0.0649
	Oct.	1.0322	0.5139	0.0783
	Nov. & Dec.	1.0722	0.6239	0.0634
Honduras	Jan. to Mar.	1.0557	0.6260	0.0888
	Apr. to Oct.	1.0177	0.5301	0.0725
	Nov. & Dec.	1.0260	0.4898	0.1141
Rwanda	Jan, Apr., May, & Aug. to Dec.	1.0127	0.3387	0.0598
	Feb., Mar., June, & July	1.0356	0.4172	0.0730

After the CFD curves of K_t were obtained from the historical data, the procedure for the generation of the hourly solar radiation values had two steps. The first step consisted of generating solar radiation values for each day based on the CFD of K_t for each month. In the second step, a series of hourly values was obtained by disaggregation of the daily value using a first order autoregressive model (AR1).

Step 1. Generation of Daily Clearness Index, K_{tg}

Daily solar radiation typically exhibits strong correlation between day t and day $t-1$ values (Amato et al., 1986; Graham et al, 1988) and an AR1 model may be used for the

stochastic generation of daily values. An AR1 model can be expressed as (Box and Jenkins, 1970):

$$\chi(t) = \rho\chi(t-1) + \omega \quad (3-1-2)$$

χ = first order autoregressive term for daily radiation

ρ = first order autocorrelation coefficient for K_t

ω = normally distributed random number with a mean of zero and a variance of $1-\rho^2$

t = Julian day, ranging from 1 to 365

Where the value of the autocorrelation coefficient can be calculated from the daily data using (Box and Jenkins, 1970)

$$\rho = \frac{\sum_{t=1}^{n-1} x_t x_{t+1} - \frac{1}{n-1} \sum_{t=1}^{n-1} x_t \sum_{t=2}^n x_t}{\left[\sum_{t=1}^{n-1} x_t^2 - \frac{1}{n-1} \left(\sum_{t=1}^{n-1} x_t \right)^2 \right]^{1/2} \left[\sum_{t=2}^n x_t^2 - \frac{1}{n-1} \left(\sum_{t=2}^n x_t \right)^2 \right]^{1/2}} \quad (3-1-3)$$

where

x_t = measured daily clearness index on day t

n = length of the data set in days

The autocorrelation coefficient is a dimensionless factor, which ranges from -1 to +1. An autocorrelation coefficient of zero indicates that there is no correlation between consecutive x values. The ω term represents the random day to day variation.

As shown in Figures 3-2 to 4, K_t is not a normally distributed variable. The AR1 model can be applied after transforming K_t into a normal variable using a Gaussian mapping

technique (Amato et al, 1986; Graham et al., 1988). The mapping technique consists of equating the CFD of K_t to the CFD of a Gaussian variable, $\chi(t)$ by transforming the CFD function from the K_t domain to the $\chi(t)$ domain. The Gaussian variable $\chi(t)$ can be generated using Equation 3-1-2, and its CFD function can be calculated from (Graham, et al., 1988):

$$G(\chi(t)) = \frac{1}{2} \left[1 + \operatorname{erf} \left(\frac{\chi(t)}{\sqrt{2}} \right) \right] \quad (3-1-4)$$

where

$G(\chi)$ = CFD for χ

$\operatorname{erf}()$ = error function

The CFD function of the measured K_t is obtained from Equation 3-1-1. Applying the mapping technique to generate the normalized CFD function, $G(\chi(t))$ is set equal to

$F(K_{tg})$

$$\frac{1}{2} \left[1 + \operatorname{erf} \left(\frac{\chi(t)}{\sqrt{2}} \right) \right] = -0.01 + \frac{a}{1 + \exp \left(\frac{b - K_{tg}}{c} \right)} \quad (3-1-5)$$

where

a, b, c = estimated parameters for the CFD function for daily clearness index

K_{tg} = generated daily clearness index which can be rearranged to solve for daily clearness

index, K_{tg} :

$$K_{tg} = b - c \ln \left[\frac{a}{\left(\frac{1}{2} \left[1 + \operatorname{erf} \left(\frac{\rho \chi(t-1) + \omega}{\sqrt{2}} \right) \right] + 0.01 \right)} - 1 \right] \quad (3-1-6)$$

A new series of K_{tg} values can be calculated after setting the initial χ value to zero.

The generated daily solar radiation can be calculated based on the definition of the clearness index value:

$$H_t = \frac{K_{tg}}{H_o} \quad (3-1-7)$$

where

H_t = daily solar radiation

H_o = extraterrestrial radiation (see Appendices B. Stella Equations).

Step 2. Generation of Hourly Clearness Index Values, k_h

Hourly values for solar radiation were generated from the daily values determined as indicated above. The equation for the generation of the hourly values reported by Knight et al. (1991) was adopted:

$$k_h = K_m - \frac{\sigma_i}{1.58} \ln \left[\frac{1}{0.5 \left(1 + \operatorname{erf} \left(\frac{\psi(i)}{\sqrt{2}} \right) \right)} - 1 \right] \quad (3-1-8)$$

where K_m is the hourly clearness index calculated using an expression which breaks down the daily values according to the sunset hour angle (h_s , degrees) and the hour angle (h , degrees) (Duffie and Beckman, 1991).

$$K_m = K_t (p + q \cos(h)) \quad (3-1-9)$$

where

$$p = 0.409 + 0.5016 \sin(h_s - 60) \quad (3-1-10)$$

$$q = 0.6609 - 0.4767 \sin(h_s - 60) \quad (3-1-11)$$

The standard deviation was estimated from (Knight et al., 1991)

$$\sigma_i = 0.1557 \sin\left(\frac{\pi K_{tg}}{0.933}\right) \quad (3-1-12)$$

And $\Psi(i)$ values follow an AR1 model that can be expressed as

$$\psi(i) = \Phi\psi(i-1) + \varepsilon \quad (3-1-13)$$

where

ψ = first order autoregressive term for hourly radiation

Φ = first order autocorrelation coefficient for k_i

ε = normally distributed random number with a mean of zero and a variance of $1-\Phi^2$

i = hour

The random numbers generated are based on ε , calculated with a Φ of 0.54 (Graham and Hollands, 1990). The initial value of Ψ is zero.

Similar to the daily solar radiation, the hourly solar radiation will be calculated by

$$H_h = \frac{k_h}{H_{ho}} \quad (3-1-14)$$

where

H_h = hourly solar radiation

H_{ho} = hourly extraterrestrial radiation

The solar radiation data in the PD/A CRSP database were measured using a photometer, in terms of the photosynthetically active radiation (PAR, in units of moles of photon/m²)

d). Photometers only measure the number of photons at wavelengths between 420 and 750 nm. For an energy balance model, the solar radiation input needs to be described in terms of energy (e.g. in units of MJ/m²d). Therefore, the *PAR* values have to be converted to total solar energy values. The task is made difficult by the fact that absorbance in the atmosphere is wavelength and atmospheric conditions dependent. Therefore, a straightforward universal conversion is not possible. Piedrahita and Teichert-Coddington (1992) developed a regression equation from side by side *PAR* and total energy measurements from the Honduras site. The solar radiation can be calculated as:

$$H_t = 6.37 * (PAR - 5.5958) \quad (3-1-15)$$

where

H_t = solar radiation, MJ/m²d

PAR = photosynthetically active radiation, $PAR > 0$, $\mu E/m^2 s$.

3.1.2. Air Temperature

Similar to the solar radiation generation model, the hourly air temperature values are generated in two steps. The first step is to generate daily values and then using the generated daily values to generate hourly values. The means and standard deviations of daily maximum and minimum were calculated from the PD/A CRSP data. The daily air temperature was assumed to follow a normal distribution. Therefore, the maximum or minimum air temperature are generated by:

$$T_{air}(t) = \mu_a + \sigma_a \chi_a(t) \quad (3-1-16)$$

Where,

t = Julian day

μ_a = the means of daily maximum or minimum air temperature

σ_a = the standard deviations of daily maximum or minimum air temperature

$$\chi_a(t) = \rho_a \chi_a(t-1) + \varepsilon_a \quad (3-1-17)$$

This equation is similar to Equation (3-1-2) except for the values which were calculated using the air temperature data. The means and standard deviations are calculated for each day of the year. The autocorrelation coefficient is calculated from the data for each location. The random variable ε_a is normally distributed with a mean of zero and a standard deviation of one.

Since the diurnal profiles of daily temperature for the three sites are similar to those of the sites which Ephrath and co-workers (1996) studied, the hourly air temperature is estimated using the two equations modified by Ephrath et al. (1996). The day-time (from sunrise to sunset) equation is expressed as:

$$T_{ad} = T_{amin} - \frac{T_{ak}}{2} + 0.5 * \sqrt{T_{ak}^2 + 4 * (T_{amax} - T_{amin}) * (1 + \frac{T_{amax} - T_{amin}}{T_k}) * T_k * \sin(\pi \frac{t_a - t_{high} + DI}{DI + 2P_{ad}})} \quad (3-1-18)$$

and the night time (from sunset to sunrise) equation can be expressed as:

$$T_{an} = \frac{T_{amin} - T_{as} * \exp(-\eta_a / \tau_a) + (T_{as} - T_{amin}) * \exp((-t_a - t_s) / \tau_a)}{1 - \exp(-\eta_a / \tau_a)} \quad (3-1-19)$$

where

T_{ad} = the day time temperature, °C

T_{amin} = the minimum air temperature, °C

T_{amax} = the maximum air temperature, °C

t_a = current time, h

t_{high} = the time of sun at the highest position, h

T_{an} = the night time temperature, °C

T_{ak} = 15°C, temperature increment parameter

Dl = day length, calculated, h

P_{ad} = delay parameter, h

T_{as} = temperature at sunset, °C

τ_a = Time coefficient, h

$\eta_a = 24 - Dl$; Night length, h

t_s = sunset time, h

The time coefficients and T_{ak} are calibrated based on the data. Since the maximum air temperature occurs later than the maximum solar height, the parameter P_{ad} is used to calibrate the delay. The parameters were calibrated using the hourly air temperature data for the Thailand site.

3.1.3. Wind Speed

As in the case of air temperature, very limited wind speed data are available for the PD/A CRSP sites. Therefore, a very simplistic model was developed for generating wind speed values. Wind speed is assumed to follow a normal distribution. The daily wind speed W_{sp} was generated by:

$$W_{sp}(t) = \mu_w + \sigma_w \chi_w(t) \quad (3-1-20)$$

where

μ_w = mean of daily wind speed

σ_w = standard deviation of daily wind speed

$$\chi_w(t) = \rho_w \chi_w(t-1) + \varepsilon_w \quad (3-1-21)$$

Similar to Equation 3-1-2, the random variable, χ_w is a first order autoregressive term for daily wind speed. ρ_w is an autocorrelation coefficient of wind speed, and ε_w is a normally distributed random number with a mean of zero and standard deviation of one. The means, standard deviations, and autocorrelation coefficients were calculated from the data.

From the data, the diurnal pattern of the wind speed shows similarities among the different locations. To simplify the estimation process, the hourly wind speed values W_{hr} are estimated by:

$$W_{hr} = W_{sp} (a_w + b_w \exp(0.5(t_w - c_w)/d_w)^2) \quad (3-1-22)$$

where

t_w = time, hr

a_w, b_w, c_w, d_w are parameters that are estimated for each location using curve fitting techniques (TableCurve™) (Table 3-3).

Table 3-3. Estimated parameters for wind speed curves

Locations	a_w	b_w	c_w	d_w
Thailand	1.098	0.89	21.32	2.04
Honduras	0.575	0.899	9.928	3.687
Rwanda	0.377	1.471	13.047	3.160

3.1.4. Wind Direction

There are only a few wind direction measurements available from the PD/A CRSP database. An equation with a normal distribution was used by dos Santos Neto and Piedrahita (1994) and was adapted in this model. The equation can be expressed as:

$$W_{wd} = \frac{\pi}{180} \left(\sigma_{wd} \frac{2}{s_{wd}} \left(\left(1 + \frac{s_{wd}}{6} \left(\varepsilon_{wd} - \frac{s_{wd}}{6} \right) \right) \right)^3 - 1 \right) + \mu_{wd} \quad (3-1-23)$$

Where

W_{wd} = wind direction

σ_{wd} = standard deviation of measured wind direction

ε_{wd} = random term generated based on a normal distribution with a mean of zero and standard deviation of one

μ_{wd} = mean of the historical data

s_{wd} = skewness coefficient.

3.2. Water Quality Model

The water quality model includes the simulations of water temperature and DO. The present model has been developed based on the structure of the model proposed by Losordo (1988) and modified by Culberson (1993). The detailed modeling approaches were discussed by Losordo (1988) and Culberson (1993). The model description here intends to avoid repeating the detailed modeling approach and to emphasize the modification of the model for long term simulations. Culberson (1993) showed that three volume elements and one sediment element are sufficient to simulate stratification of a one meter deep pond. The present model simulates the temperature and DO in the three water volume elements (surface, middle, and bottom layers) and one sediment volume element of a pond (Figure 3.2.1). The temperature and DO are calculated using the same approaches as in Losordo's and Culberson's models, in which energy and mass balances are applied on each element. The pond depth is maintained as a constant for an entire simulation and the simulation time step is one hour.

3.2.1. Water Temperature Model

Water temperature in a fish pond is determined by the heat transfer rates into and out of the water body (Figure 3.2.1). In general, water temperature distributions depend on the heat and momentum transfer across the water surface and the gravitational force acting on density differences in the water column. The heat transfer between the water surface and the environment is affected by a number of climate factors, such as solar radiation, air temperature, relative humidity, wind speed, and cloud cover. The net energy in the surface, middle, and bottom layers is expressed as (Culberson, 1993):

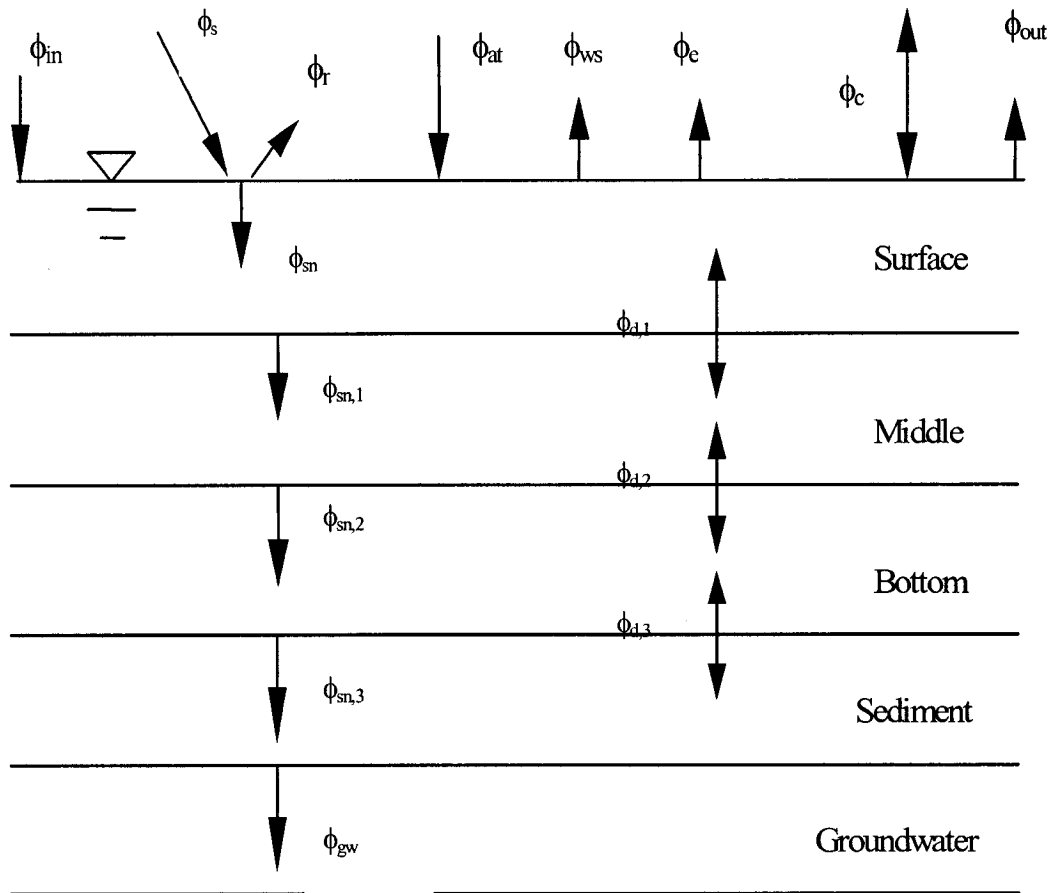


Figure 3.2.1. Water temperature model (Energy Balance)
All terms are as defined in the text.

Surface layer:

$$\phi_{surf} = \phi_{sn} - \phi_{sn,1} + \phi_{at} - \phi_{ws} - \phi_e \pm \phi_c \pm \phi_{d,1} + \phi_{in} - \phi_{out} \quad (3-2-1)$$

where

All of the heat flux terms are in units of kJ/m²hr.

ϕ_{surf} = net energy in the surface layer

ϕ_{sn} = solar radiation entering the surface layer

$\phi_{sn,1}$ = solar radiation leaving the surface layer

ϕ_{at} = atmospheric radiation

ϕ_{ws} = radiation emitted by the water

ϕ_e = evaporative heat

ϕ_c = sensible heat transfer

$\phi_{d,1}$ = effective heat diffusion between the surface and middle layers

ϕ_{in} = heat in influent water

ϕ_{out} = heat in effluent water

Middle layer:

$$\phi_{mid} = \phi_{sn,1} - \phi_{sn,2} \pm \phi_{d,1} \pm \phi_{d,2} \quad (3-2-2)$$

where

ϕ_{mid} = net heat in the middle layer

$\phi_{sn,2}$ = solar radiation leaving the middle layer

$\phi_{d,2}$ = effective heat diffusion between the middle and bottom layers

Bottom layer:

$$\phi_{bot} = \phi_{sn,2} - \phi_{sn,3} \pm \phi_{d,2} \pm \phi_{d,3} \quad (3-2-3)$$

where

ϕ_{bot} = net heat in the bottom layer

$\phi_{sn,3}$ = solar radiation leaving the bottom layer

$\phi_{d,3}$ = effective heat diffusion between the bottom and sediment layers

Sediments:

$$\phi_{sed} = \phi_{sn,3} \pm \phi_{d,3} - \phi_{gw} \quad (3-2-4)$$

ϕ_{gw} = heat loss from the sediment to the groundwater

In the energy balance equation, the positive terms are heat sources and negative terms are heat loss terms or sinks. Some terms may be either sources or sinks, depending on temperature differences causing the heat transfer.

3.2.1.1. Input Heat Sources

The heat sources include the solar radiation penetrating into each water layer

($\phi_{sn,1}$, $\phi_{sn,2}$, $\phi_{sn,3}$), the atmospheric radiation (ϕ_{at}) on the surface layer, the sensible heat transfer (ϕ_c), and the heat in the influent water, (ϕ_{in}).

3.2.1.1.1. Solar Radiation Penetration

Solar radiation is the major heat source for an aquaculture pond. The amount of short - wave solar radiation penetrating into the surface, middle, and bottom layers is dependent on incident radiation, water surface roughness, and water turbidity. The solar radiation penetrating the surface ϕ_{sn} can be estimated as (Losordo, 1988):

$$\phi_{sn} = \phi_s - \phi_r = \phi_s (1 - R_{ref}) \quad (3-2-5)$$

where

ϕ_s = the measured incident radiation or values generated using a stochastic model

ϕ_r = the reflected incident short-wave radiation

R_{ref} = the adjusted reflectivity that takes into account the effect of wind speed W_z at a height Z meters above the water surface. R_{ref} is estimated using the empirical equation (Losordo, 1988):

$$R_{ref} = R_s (1 - 0.08W_z) \quad (3-2-6)$$

where

R_s = the reflectivity of a smooth water surface under scattered clouds estimated as a function of solar altitude angle (Losordo, 1988),

$$R_s = 2.2 \left(\frac{180}{\pi} \lambda \right)^{-0.97} \quad (3-2-7)$$

The solar altitude (λ , radians) is calculated from the solar zenith angle, the latitude, the time of day, and the Julian day. It can be expressed as (Hsieh, 1986),

$$\lambda = 1.57 - \arcsin(\sin L \sin \delta + \cos L \cos \delta \cosh) \quad (3-2-8)$$

where

$$\delta = \frac{\pi}{180} (23.45 \sin(\frac{360}{365} (284 + \text{Julianday}))) \quad (3-2-9)$$

L = latitude (radians)

h = hour angle (radians), which can be calculated by

$$h = \frac{\pi}{180} (\pm \frac{1}{4} (\text{number of minutes from local solar noon}))$$

The solar radiation penetrating the middle or bottom layers can be estimated using the Lambert-Beer law (cited in Losordo, 1988):

$$\phi_{sn,i} = \phi_s (1 - R_{ref}) (1 - \beta) e^{(-\eta_{kt} z)} \quad (3-2-10)$$

where

$\phi_{sn,i}$ = the solar radiation penetrating the middle, bottom, or sediment layers, i (kJ/m²hr)

z = water depth, m

β = the fraction of incident solar radiation absorbed at the surface. (~ 0.03, fraction)

(Losordo, 1988)

η_{kt} = the effective light extinction coefficient at time t , 1/m

η_{kt} is affected by the light angle of incidence and the water turbidity. A common method to estimate the light extinction coefficient is to use the empirical function based on Secchi disk depth (SDD) (cited in Losordo, 1988).

$$\eta_{kt} = 1.7 / SDD \quad (3-2-11)$$

SDD measures the pond turbidity, which varies substantially from time to time due to changes in the concentration of phytoplankton, suspended organic matter, fish movements, etc. For a short term simulation, measured SDD values may be used (Losordo, 1988; Culberson, 1993). However, for a long term simulation, the SDD is a

variable which has to be modeled. SDD values can be estimated using a correlation between SDD and chlorophyll-a (Chla) (Almazan and Boyd, 1978; Lee et al., 1991b).

After analyzing several data sets from the PD/A CRSP database, a linear relationship between chlorophyll a and overall light extinction coefficient was found (Jamu et al., 1999). The overall light extinction coefficient is the sum of phytoplankton and non-phytoplankton coefficients, and can be expressed as,

$$\eta_{kt} = \eta_{kw} - \eta_{kc} Chla \quad (3-2-12)$$

where

η_{kw} = light extinction due to non-phytoplankton contribution, m^{-1}

η_{kc} = light extinction due to phytoplankton contribution, $(m (\mu g/L Chla))^{-1}$

$Chla$ = Chlorophyll a concentration, $\mu g/L$

The η_{kc} and η_{kw} can be estimated using regression equations based on the measured SDD and $Chla$ for a particular site. The η_{kc} is relatively constant (Jamu et al., 1999). The η_{kw} is affected by clay, organic matter, and other particles in the water.

3.2.1.1.2. Atmospheric Radiation

The heat radiation from the atmosphere has been taken into account in the energy balance (Equation 3-2-1). The atmospheric heat radiation is the sum of the long wave radiation emitted from water vapor and other atmospheric gases. The net atmospheric radiation equation used by Losordo (1988) is

$$\phi_{at} = (1 - r)e\sigma(T_{aK})^4 \quad (3-2-13)$$

where

r = the reflectance of the water surface to long wave radiation (~ 0.03 , decimal fraction)

e = the average emittance of the atmosphere (dimensionless); which can be estimated as:

$$e = 0.398 \times 10^{-5} (T_{aK})^{2.148} \quad (3-2-14)$$

σ = Stefan-Boltzman constant, $2.04 \times 10^{-7} (\text{kJ/m}^2 \text{ hr K}^4)$

T_{aK} = the absolute air temperature two meters above the water surface (K)

3.2.1.1.3. Sensible Heat Transfer

Sensible heat transfer is the heat transfer between the water surface and air through conduction and convection. The sensible heat term can be a heat source or heat sink depending on the temperature difference between the water surface and air. For a fish pond, the sensible heat transfer rate is expressed as (Losordo, 1988)

$$\phi_c = 1.57 W_2 (T_{surf} - T_{ac}) \quad (3-2-15)$$

where

W_2 = the wind speed at two meters above the water surface, km/hr

T_{surf} = the water surface temperature, °C

T_{ac} = the air temperature, °C

3.2.1.1.4. Water Inflow

Energy in inflow water can be calculated by

$$\phi_{in} = T_{in} Q_{in} c_{pw} \rho_w / A \quad (3-2-16)$$

where

T_{in} = water temperature of inflow water, °C

Q_{in} = inflow rate, m³/hr

c_{pw} = heat capacity of water, 4.1816 kJ/(°C kg)

ρ_w = water density, kg/m³, calculated by (Spain, 1982, cited in Culberson, 1993)

$$\rho_w = ((0.99987 + (0.69 \times 10^{-5}) \times T_{surf}) - (8.89 \times 10^{-6}) \times T_{surf}^2 + (7.4 \times 10^{-8}) \times T_{surf}^3) \times 1000 \quad (3-2-17)$$

A = surface area, m²

It is assumed that all influent water goes to the surface layer and all effluent water comes from the surface layer, with no direct energy changes in the other two layers.

3.2.1.2. Heat Loss

Heat losses from the pond water include water surface radiation, evaporative heat, and heat losses to the sediment and ground water. As indicated earlier, sensible heat may be a sink if the surface water temperature is higher than the air temperature.

3.2.1.2.1. Water Surface Radiation

The long-wave back radiation emitted from the water surface to the atmosphere depends on the water surface temperature and the water emissivity. The back radiation from the water surface can be estimated by (Losordo, 1988):

$$\phi_{ws} = \varepsilon_w \sigma (T_{wK})^4 \quad (3-2-18)$$

where

ε_w = the emissivity of the water surface (the ratio of actual radiation to the ideal black body), ~0.97

T_{wK} = the absolute water surface temperature, K

3.2.1.2.2. Evaporative Heat

Heat loss from water evaporation is due to the heat required to evaporate water from the pond surface. Many factors influence the evaporation rate, such as wind speed, air temperature, surface water temperature, atmospheric pressure, vapor pressure, and relative humidity.

Values for most of these factors cannot be obtained directly. Therefore an empirical equation as a function of wind speed and vapor pressure was used by Losordo (1988) and Culberson (1993),

$$\phi_e = NW_2(e_s - e_a) \quad (3-2-19)$$

where

$$N = \text{empirical coefficient, } 5.06 \frac{\text{kJ}}{\text{m}^2 \text{ km mmHg}}$$

e_s = saturated vapor pressure at T_{wK} , mmHg

e_a = vapor pressure in the overlaying air, mmHg

and e_s and e_a can be estimated as:

$$e_s = 25.374 \exp(17.62 - 5271/T_{wK}) \quad (3-2-20)$$

$$e_a = Rh 25.374 \exp(17.62 - 5271/T_{aK}) \quad (3-2-21)$$

where

Rh = relative humidity 2.0 m above the water surface (fraction)

T_{aK} = air temperature, K

For those locations for which Rh values are not available, a substitute equation can be used (Culberson, 1993).

$$e_a = 610.78 \exp[17.2694(T_d - 273.16)/(T_d - 35.86)] \quad (3-2-22)$$

where

T_d = dew-point temperature, K

Because the dew-point temperature T_d is not recorded in the PD/A CRSP database and is rarely available for pond sites, the daily average dew-point temperature can be estimated by subtracting 2 °C from the morning minimum dry-bulb temperature (Culberson, 1993). Culberson (1993) pointed out that accuracy in the estimation of T_d is critical because the heat loss due to evaporation may be as high as one third of the total energy loss from the water column.

3.2.1.2.3. Heat Loss to the Sediment and Groundwater

The heat loss by conduction from the water column to the sediment can be simulated as a function of thermal conductivity and the water temperature difference between the bottom volume element and the sediment element. The equation is expressed as (Losordo, 1988):

$$\phi_{sed} = K_{sed} \left(\frac{T_{sed} - T_{bot}}{Z_{sb}} \right) \quad (3-2-23)$$

where

K_{sed} = thermal conductivity coefficient for the sediment, $\sim 2.53 \frac{kJ}{mhr^\circ C}$

T_{bot} = bottom layer temperature, °C

T_{sed} = sediment temperature, °C

Z_{sb} = distance between the centers of the bottom and sediment elements.

The sediment element is assumed to be 20 cm deep and have the same density as water.

The heat loss from the sediment to the groundwater was included in Losordo's (1988) and Culberson's (1993) models. The simulation results from Culberson's model show that the heat loss from the sediment to the groundwater is only 2% of the total heat loss from the fish water column in a fish pond at a Rwanda site. However, the heat sink to the groundwater remains in the present model (Losordo, 1988).

$$\phi_{gw} = k_e \left(\frac{T_{sed} - T_{gw}}{Z_{sg}} \right) \quad (3-2-24)$$

where

k_e = thermal conductivity coefficient for the earth, $\sim 2.53 \frac{kJ}{mhr^\circ C}$ (Culberson, 1993)

T_{gw} = groundwater temperature, °C

Z_{sg} = depth between the sediment and ground

The distance between the sediment and the groundwater is assumed to be 5.0 meters. The groundwater temperature is given.

3.2.1.2.4. Heat Loss from the Effluent

The heat losses due to the effluent can be estimated using a similar equation to that used for the influent:

$$\phi_{out} = T_{out} Q_{out} c_{pw} \rho_w / A \quad (3-2-25)$$

where

T_{out} = water temperature in the effluent water, which is the water surface temperature, °C

Q_{out} = effluent flow rate, m³/hr

3.2.1.3. Heat Transfer within the Water Column

The heat transfer rate between two adjacent volume elements in the water column is dependent on molecular diffusion, effective diffusion (turbulent diffusivity), and convective mixing (caused by buoyant instability) (Jørgensen and Gromiec, 1989). The effective diffusion term often includes the effect of molecular diffusion.

3.2.1.3.1. Effective Diffusion

Heat transfer by diffusion was described by Losordo (1988) as:

$$\phi_{d,i} = \rho_w c_{pw} E_{z,z} (\Delta T / \Delta Z) \quad (3-2-26)$$

where

$\phi_{d,i}$ = heat transfer rate between adjacent volume elements, kJ/hr m²

$E_{z,z}$ = effective diffusion coefficient at depth z, m²/hr

$\Delta T / \Delta Z$ = temperature gradient between the adjacent volume elements, K/m

The effective diffusion coefficient $E_{z,z}$ can be estimated from a neutrally buoyant diffusion coefficient, $E_{\theta,z}$ (diffusion if the water column is at neutral buoyancy with no density gradients) and a Richardson number, R_z (Culberson, 1993).

$$E_{z,z} = E_{\theta,z} / (1 + 0.05 R_z) \quad (3-2-27)$$

The neutrally buoyant diffusion coefficient is a function of wind shear stress, drift velocity and a decay coefficient (Culberson, 1993).

$$E_{\theta,z} = \left[\frac{\tau_o}{\rho_w} / (\mu_s k^*) \right] \exp(-k^* z) / 3600 \quad (3-2-28)$$

where

$$\tau_o = \rho_a C_z (W_{vz})^2 \quad \text{wind shear stress, N/m}^2 \quad (3-2-29)$$

$$\mu_s = 30 \left(\frac{\tau_o}{\rho_w} \right)^{0.5} \quad \text{drift velocity, m/s} \quad (3-2-30)$$

$$k^* = 6 (A_{ws})^{-1.84} \quad \text{decay coefficient, m}^{-1} \quad (3-2-31)$$

where

$$\rho_a = \text{air density (kg/m}^3\text{)}$$

C_z = the coefficient of aerodynamic resistance, 0.001 (Losordo, 1988)

W_{vz} = wind vector magnitude at height $z = 10$ meters above the water surface (m/s)

A_{ws} = wind shear area

The Richardson number represents the ratio of buoyancy and shear forces, and can be calculated as (Losordo, 1988):

$$R_z = \left[\frac{(a_v \times g \times z^2)}{(\tau_o / \rho_w)} \right] \left(\frac{\Delta T}{\Delta Z} \right) \quad (3-2-32)$$

where

a_v = coefficient of water expansion which is estimated by

$$a_v = 1.5 \times 10^{-5} (T_{avK} - 277) - 2.0 \times 10^{-7} (T_{avK} - 277)^2, \text{ 1/K} \quad (3-2-33)$$

g = gravitational acceleration constant, 9.8 m/s^2

z = height at which the Richardson number is used, m

T_{avK} = average temperature of the two adjacent volume elements, K

3.2.1.3.2. Convective Mixing

Convective mixing accounts for the effect of mixing due to buoyancy instability when the density of the upper water layers is higher than that of lower layers. Since convective mixing is much stronger than turbulent diffusion, a maximum effective diffusion coefficient, E_{max} , is used to simulate convective mixing (Losordo, 1988).

If the temperature in a volume element is higher than in the elements above it, then convective mixing occurs and the effective diffusion coefficient is set to E_{max} . The value of E_{max} has to be adjusted based on the numerical stability of the model. Values between 0.018 and 21.02 m²/hr were found from Lake Ontario by Chapra and Reckow (1983). Losordo (1988) and Culberson (1993) used 0.06 m²/hr for fish pond models.

3.2.1.4. Temperature Calculation

A detailed calculation procedure is explained by Losordo (1988). The temperature for each volume element is calculated as

$$T_{i,t} = T_{i,t-\Delta t} + \Delta T_{i,t-\Delta t} \quad (3-2-34)$$

where

i = the volume elements, from 1 to 3

Δt = simulation time step

$T_{i,t-\Delta t}$ = temperature of water layer i at the previous time step, °C

$$\Delta T_{i,t-\Delta t} = \frac{\phi_i A}{(\rho_w c_{pw} V_i)} \Delta t \quad (3-2-35)$$

ϕ_i = net heat flux for the volume element calculated from equations 3-2-1 through 3-2-4

V_i = volume of water layer i , m³

The initial temperature for each element is given. The net heat flux, ϕ_i , is set to zero at the beginning of the simulation.

3.2.2. Dissolved Oxygen Model

The DO model has a structure similar to that of the temperature model. There are three volume elements. Mass balances for each volume element are carried out in terms of rates of oxygen input, output, production, and consumption. The input terms include reaeration at the surface layer and diffusion between adjacent elements. The production term is due to photosynthesis. The oxygen consumption terms include phytoplankton respiration, fish respiration, organic oxidation, nitrification, and sediment respiration. The present model is based on the structure of a previous model (Culberson, 1993). The model has been modified for long term simulations. The major changes in the DO model are: (1) the separation of the water column oxygen consumption term into terms for organic matter oxidation and nitrification; (2) the combination of phytoplankton consumption in the dark and light period; (3) using a dynamic carbon to chlorophyll a ratio; and (4) including the effect of nitrogen on phytoplankton growth.

The oxygen mass balance at each volume element is shown in Figure 3.2.2. The equations for the three volume elements can be expressed as (after Culberson, 1993):

Surface layer:

$$M_{surf} = M_{phy,1} \pm M_{d,1} \pm M_{d,2} - M_{fish} - M_{pr} - M_{nr} - M_{og} + M_{in} - M_{out} \quad (3-2-36)$$

Middle layer:

$$M_{mid} = M_{phy,2} \pm M_{d,2} \pm M_{d,3} - M_{fish} - M_{pr} - M_{nr} - M_{og} \quad (3-2-37)$$

Bottom layer:

$$M_{bot} = M_{phy,3} \pm M_{d,3} - M_{fish} - M_{pr} - M_{nr} - M_{og} - M_{sed} \quad (3-2-38)$$

where

All terms are in units of mg O₂/hr.

M_{surf} , M_{mid} , M_{bot} = DO change rates in the surface, middle, and bottom volume elements,
respectively

$M_{phy,1}$, $M_{phy,2}$, $M_{phy,3}$ = oxygen production rate due to photosynthesis in surface, middle,
and bottom elements, respectively

$M_{d,1}$ = reaeration rate at the water surface

$M_{d,2}$, $M_{d,3}$ = oxygen diffusion rate between the surface layer and middle layer, and
between the middle layer and bottom layer

M_{fish} = fish respiration rate

M_{pr} = phytoplankton respiration rate

M_{nr} = oxygen consumption rate due to nitrification

M_{og} = oxygen consumption rate due to organic matter oxidation

M_{sed} = DO consumption rate by the sediment

M_{in} = oxygen transfer rate with influent water

M_{out} = oxygen transfer rate with effluent water

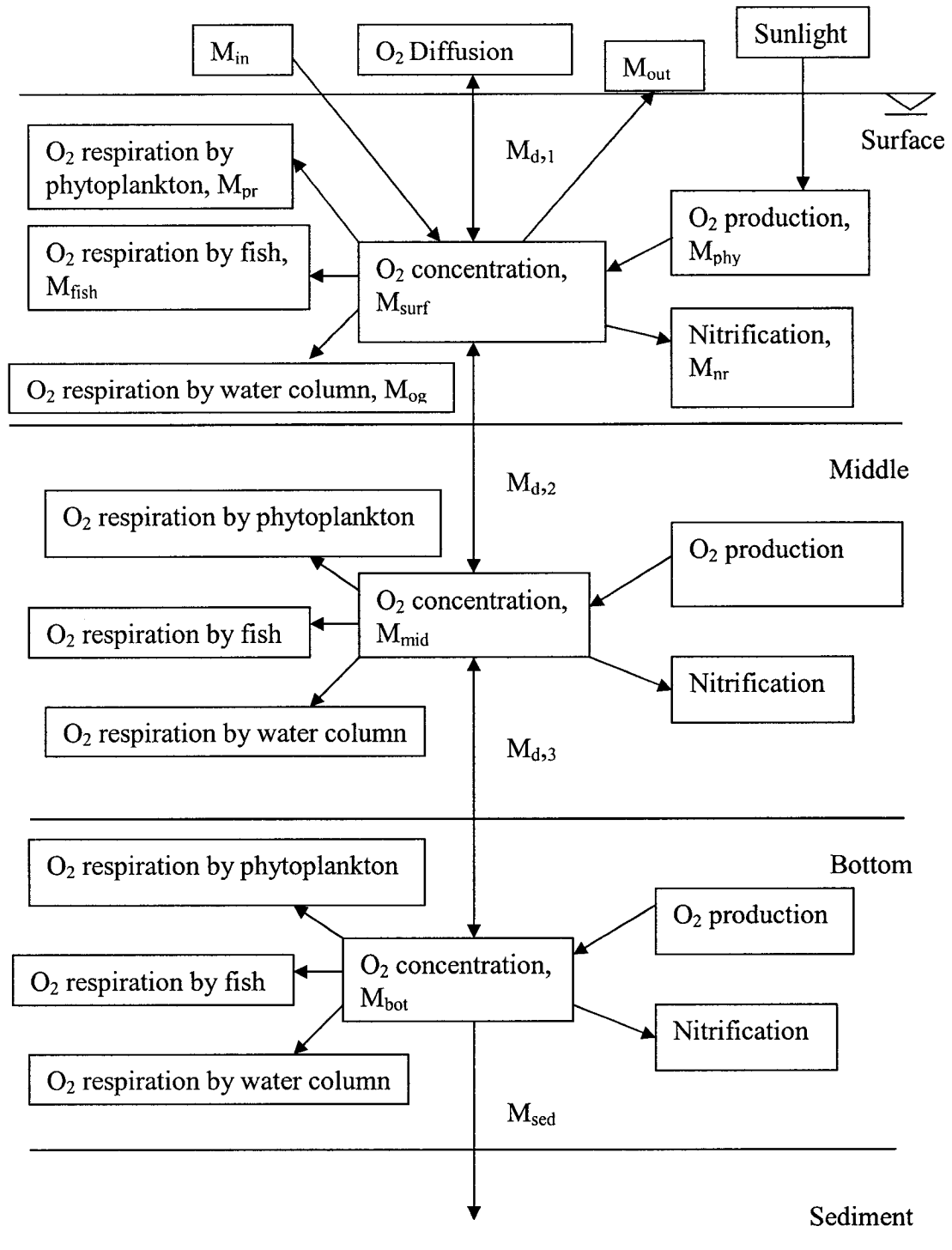


Figure 3.2.2. Schematic diagram of the dissolved oxygen model

All terms in equations 3-2-36 to 3-2-38 are explained in sections: source inputs ($M_{phy,i}$, $M_{d,1}$), oxygen consumptions (M_{pr} , M_{fish} , M_{og} , M_{nr} , M_{sed}), oxygen diffusion between adjacent elements ($M_{d,2}$, $M_{d,3}$), and oxygen in the water influent and effluent (M_{in} , M_{out}).

3.2.2.1. Input Sources

The input sources for the whole water column including photosynthesis and surface water reaeration are described below.

3.2.2.1.1. Photosynthesis

The oxygen production rate through photosynthesis depends on the light intensity, temperature, nutrient concentration, and concentration of chlorophyll-a (Chla). The photosynthetic oxygen production rate can be expressed as (Lee et al., 1991a):

$$M_{phy,i} = P_{max} f(I) f(T) f(N) Chla V_i \quad (i = 1, 2, 3) \quad (3-2-39)$$

where

P_{max} is the maximum oxygen production rate due to photosynthesis and can be calculated based on the maximum phytoplankton growth rate at light saturation and the ratio of carbon to Chlorophyll a ($CChla$, mg C/mg Chla) (Giovannini, 1994):

$$P_{max} = \mu_{max} CChla \text{ (mg O}_2\text{/mg Chla /hr)} \quad (3-2-40)$$

where μ_{max} is the maximum phytoplankton growth rate, mg O₂/mg C/hr and can be estimated using an equation developed by Giovannini (1994):

$$\mu_{max} = (((10^{(0.0275 * T_{opt} - 0.23)}) / 12)) * 2.67 \quad (3-2-41)$$

where

T_{opt} = the optimal temperature for phytoplankton growth, °C

The estimation of $CChla$ is described in a latter part of this section.

$f(I)$, $f(T)$, and $f(N)$ are functions quantifying the effect on photosynthesis of light, temperature, and nitrogen, respectively. They are described below.

The effect of light on photosynthesis is described using Steele's equation (Steele, 1962)

$$f(I) = \frac{I}{I_{max}} \exp\left(1 - \frac{I}{I_{max}}\right) \quad (\text{unitless}) \quad (3-2-42)$$

where

I = light intensity, $\mu\text{mole}/\text{m}^2/\text{s}$

I_{max} = saturated light intensity, $\mu\text{mole}/\text{m}^2/\text{s}$

The equation describes the effect of light intensity on photosynthetic rate. When light intensity is equal to or larger than the saturated light intensity photo-inhibition will occur and photosynthesis will decrease. The estimation of I_{max} will be described below.

The temperature effect factor can be described as (Lee et al., 1991b)

$$f(T) = 1.066^{(T_{ave}-20)} \quad (\text{unitless}) \quad (3-2-43)$$

where T_{ave} is the average temperature of the three layers, °C

The nitrogen limitation factor is based on the assumption that the nitrogen uptake rate by phytoplankton is limited by the concentration of total ammonia nitrogen (TAN) and a half-saturation constant for TAN (Thomann and Mueller, 1987 and described in Lee et al., 1991b):

$$f(N) = \frac{N_{Am}}{K_N + N_{Am}} \quad (\text{unitless}) \quad (3-2-44)$$

where

K_N = half saturation constant for TAN, $\mu\text{g/L}$

N_{Am} = TAN concentration, $\mu\text{g/L}$

The maximum specific growth rate, μ_{max} is obtained empirically. The CChla ratio varies from 12.5 to 50 (g carbon/g Chla; Reynolds, 1984) due to the effects of light intensity, temperature, nutrients, etc. The estimation of CChla is based on the assumption that the initial slope of the photosynthetic rate vs. light intensity curve is constant. The ratio of carbon to Chla was found to be almost constant during 24 hours under a light intensity between 15 and 1500 $\mu\text{mole photons/m}^2/\text{s}$ (Cosper, 1982). The photosynthetic production rate can be described in terms of carbon, based on CO_2 fixed in algal cells using the stoichiometric mass equivalent of oxygen to carbon in CO_2 (2.67 mg $\text{O}_2/\text{mg C}$, Lee, et al., 1991b):

$$\frac{M_{phy}}{(2.67 * Chla)V_i} = \frac{P_{max} f(I)f(T)f(N)}{2.67} \quad (3-2-45)$$

Let

$$Phyt = \frac{M_{phy}}{(2.67 * Chla)V_i} \quad (3-2-46)$$

V_i = water volume for layer i (m^3)

For small I, the slope of the photosynthesis rate vs. light intensity curve, α is estimated by

$$\alpha = \left. \frac{d(Phyt)}{dI} \right|_{I=0} \quad (3-2-47)$$

where α is in units of $(\text{mg C}/(\text{mg Chla hr})) / (\mu\text{mole}/\text{m}^2 \text{ s})$

Substituting Equations 3-2-45 and 3-2-46 into 3-2-47, and then rearranging,

$$\alpha = \frac{d(Phyt)}{dI} \Big|_{I=0} = \frac{\mu_{\max} CChla}{2.67} \frac{e}{I_{\max}} f(T)f(N) \quad (3-2-48)$$

therefore

$$CChla = \frac{2.67\alpha I_{\max}}{\mu_{\max}} \frac{1}{e f(T)f(N)} \quad (3-2-49)$$

To simplify the equation, the effect of nitrogen was assumed to be minor, so the equation is reduced to:

$$CChla = \frac{2.67\alpha I_{\max}}{\mu_{\max}} \frac{1}{e f(T)} \quad (3-2-50)$$

The ratio of carbon to Chla is directly proportional to I_{\max} and is inversely proportional to μ_{\max} and $f(T)$. The value of α can be obtained from local data or inferred from previous data. In the present model, the value of α is inferred from Culberson's model. It is difficult to determine the saturated light intensity I_{\max} for a long term simulation because the light-limited photosynthetic efficiency is not constant and because of adaptation of phytoplankton to the prevalent light regime. The photosynthetic capacity has been found to be affected by the cell's recent light history (Reynold, 1984). The present model takes into account the past history of light intensity to which phytoplankton have been exposed.

I_{\max} can be determined from the previous three days' light intensity (Lee et al., 1991b),

$$I_{\max,i} = 0.7I_{\max,i-1} + 0.2I_{\max,i-2} + 0.1I_{\max,i-3} \quad (3-2-51)$$

where

$I_{\max i-1}$, $I_{\max i-2}$, $I_{\max i-3}$ are the maximum light intensities on one day, two days, and three days before day i , respectively. At $i=1$, $I_{\max,i-1}$ is given.

Although the effect of nitrogen on the carbon to chlorophyll a ratio was assumed to be small, its impact on photosynthetic rate is included in the model. The input TAN sources are fertilizers, excretion by fish, and the decay of detritus and dead phytoplankton. The nitrogen release rate from the fertilizers and detritus is estimated based on the organic matter decay rate. The nitrogen excreted by fish is assumed to be proportional to the total uptake of food. The half-saturation constant, K_N is in the range of 10 to 20 $\mu\text{g/L}$ (Lee et al., 1991b).

$Chla$ is a variable obtained using a mass balance (see Section Phytoplankton Model).

3.2.2.1.2. Reaeration

Water surface reaeration can be either a source or a sink depending on the DO difference between the surface water and the air. A first order function is used to predict the reaeration rate (Culberson, 1993):

$$M_{d,1} = K_{od} (C_s - DO_{surf}) * 1000 * A \quad (3-2-52)$$

where

K_{od} = oxygen transfer coefficient, m/hr. It can be determined by (Banks and Herrera, 1977):

$$K_{od} = 0.0036(8.43W_{2s})^{0.5} - 3.67W_{2s} + 0.43(W_{2s})^2 \quad (3-2-53)$$

W_{2s} = wind speed at two meter above the water surface, m/s

C_s = saturated DO in water at a given elevation and temperature, mg/L. It can be calculated by (Culberson, 1993):

$$C_s = (14.625 - 0.41022T_{surf} + 0.007991(T_{surf})^2 - 0.0000778(T_{surf})^3) (1 - 0.0001E) \quad (3-2-54)$$

E = site elevation, m

DO_{surf} = oxygen concentration for the surface layer, mg/L.

3.2.2.2. Oxygen Consumption

Oxygen consumption in the water column is due to phytoplankton respiration, fish respiration, organic matter oxidation, nitrification, sediment respiration, and DO in the water effluent.

3.2.2.2.1. Phytoplankton Respiration

Oxygen consumption by phytoplankton can be divided into two parts: one is the respiration due to photosynthesis (light respiration) and the other is the respiration due to maintenance (dark respiration) (Losordo, 1988). Because the light respiration is related to the oxygen production rate, it can be estimated in proportion to the photosynthetic rate. The light respiration rate has been estimated using 10% of the primary production rate delayed by 3 hours (Culberson, 1993). This simple model provides satisfactory results. However, Giovannini (1994) pointed out that the simple model might not be true for all fish ponds and the use of this simple model for a long term simulation may be limited. The phytoplankton respiration during the night time hours is included in the water column respiration term (Losordo, 1988; Culberson, 1993).

In the present model, the light and dark respiration during the light time hours are simulated based on the Chla which is simulated dynamically. The respiration is calculated based on the temperature and on the concentration of chlorophyll a:

$$M_{pr} = K_{r20} f(T) \frac{Chla}{K_{chla} + Chla} \quad (3-2-55)$$

where

K_{r20} = maximum phytoplankton respiration rate at 20 °C, mg O₂/hr

K_{Chla} = half-saturation respiration constant, mg/m³ Chla

3.2.2.2.2. Fish Respiration

Fish respiration rate for tilapia was calculated using the regression equation developed by Boyd (1979) for estimating channel catfish respiration. The equation has been found to provide satisfactory estimations for tilapia (Culberson, 1993). The equation is a function of water temperature and fish mass (Culberson, 1993).

$$M_{fish} = 10^x W_f Fish_{pop} \quad (3-2-56)$$

where

$$x = -0.999 - 9.57 \times 10^{-4} \times W_f + 6.0 \times 10^{-7} \times W_f^2 + 3.27 \times 10^{-2} \times T_{ave} - 8.7 \times 10^{-6} \times T_{ave}^2 + 3.0 \times 10^{-7} \times W_f \times T_{ave} \quad (3-2-57)$$

W_f = average fish mass, g/fish

$Fish_{pop}$ = total number of fish

T_{ave} = average of T_{surf} , T_{mid} , and T_{bot} , °C.

3.2.2.2.3. Organic Matter Oxidation

Suspended organic matter consumes oxygen. The organic matter is composed of fertilizers (chicken manure and fresh cut grass), detritus, and fish feces. Mass balances of organic matter are described in Section 3.2.5. The oxygen consumption for all types of organic matter due to oxidation is calculated by:

$$M_{og} = F_{og} \left(\sum_{i=1}^m OM_{decay,i} \right) \quad (3-2-58)$$

where

F_{og} = oxygen consumption due to organic matter decomposition, mg O₂/mg OM

$OM_{decay,i}$ = organic matter decay rate estimated from Equation (3-2-85), mg OM/hr

m = number of organic matter sources included in the model: $m=4$ in the model. It includes chicken manure, fresh cut grass, fish feces, and detritus.

3.2.2.2.4. Nitrification

Ammonia concentration represents the total ammonia nitrogen (TAN) from fertilizers and fish wastes. Nitrification is a two step process where ammonia is oxidized to nitrite and then to nitrate. The rate of nitrification is sensitive to pH and temperature (Boyd, 1979).

Although pH in a pond varies over time, the model uses a constant pH value because modeling pH fluctuations was beyond the scope of this work. A simple first order function of TAN was used for simulating nitrification rate. The equation can be expressed as (Lee et al., 1991b):

$$M_{nr} = 4.57k_{nr}N_{Am} / 1000 \quad (3-2-59)$$

where

4.57 = stoichiometric coefficient for oxygen consumption in nitrification, mg O₂/mg N,

$$k_{nr} = 0.1(1.08)^{(T-20)} \quad (3-2-60)$$

k_{nr} = nitrification rate, 1/hr

3.2.2.2.5. Sediment Respiration

Although there are many factors affecting sediment respiration, sediment respiration is described by a simple function which includes the influence of temperature (Jamu, 1998).

The model is expressed as (Culberson, 1993):

$$M_{sed} = K_{sed} \theta^{(T-T_m)} \quad (3-2-61)$$

where

K_{sed} = sediment respiration rate at reference temperature, T_m, mg O₂/ hr

θ = temperature correction factor, 1.065 (Culberson, 1993)

3.2.2.3. Oxygen Diffusion between Adjacent Elements

The process of oxygen diffusion between adjacent water layers is analogous to that for thermal energy. Effective diffusion is calculated as (Losordo, 1988):

$$M_{d,z} = E_{z,z} A \frac{\Delta DO}{\Delta Z} 1000 \quad (3-2-62)$$

where

$E_{z,z}$ = effective diffusion coefficient at depth z (see Equation 3-2-27), m²/hr

ΔDO = oxygen concentration difference between adjacent layer, mg / L

ΔZ = depth difference between adjacent layers, m

3.2.2.4. Oxygen in the Water Influent and Effluent

The oxygen input to the surface layer is calculated as

$$M_{in} = Q_{in} DO_{in} 1000 \quad (3-2-63)$$

where

DO_{in} = DO concentration in the influent water (mg/L)

The oxygen output in the effluent water can be calculated by

$$M_{out} = Q_{out} DO_{surf} 1000 \quad (3-2-64)$$

The effluent concentration is assumed to be same as the concentration of the surface layer, DO_{surf} , Q_{in} , Q_{out} , and DO_{in} are given.

3.2.2.5. Dissolved Oxygen Calculation

Similar to the temperature model, the DO for each layer at any time is calculated by

$$DO_{i,t} = DO_{i,t-\Delta t} + \frac{\Delta M_{neti}}{V_i} \quad (3-2-65)$$

where

$DO_{i,t}$ = DO in layer i at time t

ΔM_{neti} = the net change of DO mass in layer i between time t and $t-\Delta t$, calculated from equations 3-2-36, 37, or 38 multiplied by Δt .

3.2.3. Phytoplankton Model

Phytoplankton concentration affects water temperature, DO, and food availability. As described early, phytoplankton is modeled in terms of chlorophyll a (Chla). Because

there are no data for the distributions of chlorophyll-a concentration in the water column, the distribution of chlorophyll-a is assumed to be uniform. The production term is estimated from the primary production rate. The consumption terms include the rates of fish grazing, sinking to the sediment, and non-predatory mortality. The model can be described as:

$$Chla_{net} = Chla_{prod} - Chla_{graze} - Chla_{dead} - Chla_{sink} + Chla_{in} - Chla_{out} \quad (3-2-66)$$

where

All terms are in units of mg Chla/hr.

$Chla_{net}$ = the net growth rate of chlorophyll in the water column

$Chla_{prod}$ = production rate

$Chla_{graze}$ = grazing by fish

$Chla_{dead}$ = non-predatory mortality rate

$Chla_{sink}$ = sinking to sediment

$Chla_{in}$ = in the inflow water, assumed as zero

$Chla_{out}$ = in the effluent water

3.2.3.1. Chlorophyll a Production

The production rate is calculated based on the primary production rate

$$Chla_{prod} = \frac{\sum_{i=1}^3 M_{phy,i}}{F_{co2} CChla} \quad (3-2-67)$$

where

$M_{phy,i}$ = photosynthetic rate obtained from Equation 3-2-39, mg O₂/ hr

F_{CO_2} = stoichiometric equivalent factor, 2.67 mg O₂/mg C

C_{Chla} = ratio of carbon to Chla, from Equation 3-2-50, mg C/mg Chla

3.2.3.2. Chlorophyll a Consumption

All consumption terms are described using a first order function proportional to the concentration of chlorophyll-a. The consumption rates are estimated from Lee et al. (1991a). The Chla uptake rate by fish is dependent on the grazing coefficient, fish population, and the ratio of Chla to phytoplankton dry weight. The equation can be expressed as:

$$Chla_{graze} = R_{graze} Fish_{pop} F_{cell} \times 1000 \quad (3-2-68)$$

where

R_{graze} = fish grazing coefficient that is calculated from Equation 3-3-2 (Fish growth model), $\mu\text{g dry weight}/(\text{hr fish})$

$Fish_{pop}$ = fish population, fish

F_{cell} = ratio of Chla to cell dry weight, range can be 0.005 to 0.012 $\mu\text{g Chla}/\mu\text{g dry weight}$ (Reynolds, 1984)

Phytoplankton death may cause significant population reduction. A variety of reasons may cause phytoplankton death, such as inadequate light and nutrients, exposure to toxic substances, infection by fungi, bacteria, and viruses (Boyd, 1979). To simplify the model, a first order equation can be used (Lee et al., 1991b):

$$Chla_{dead} = K_{dead} Chla V \quad (3-2-69)$$

where

K_{dead} = death rate, 1/hr

Some phytoplankton particles will sink to the sediment because their density is higher than that of water. The settling rate is a species and site specific variable. Since no data are available from the CRSP database on sinking rates, it was estimated using a simple zeroth order model (Losordo, 1988).

$$Chla_{sink} = K_{sink} Chla V \quad (3-2-70)$$

where

K_{sink} = settling rate, 1/hr

The effluent water will remove chlorophyll a from the pond, which was incorporated into the model as:

$$Chla_{out} = Q_{out} Chla \quad (3-2-71)$$

3.2.3.3. Chlorophyll a Calculation

The Chla at time t can be calculated by

$$Chla_t = Chla_{t-\Delta t} + \frac{Chla_{net}}{V} \Delta t \quad (3-2-72)$$

3.2.4. Total Ammonia Nitrogen Model

The nitrogen model is based on a mass balance of total ammonia nitrogen (TAN) in the water column. The nitrogen in the pond is assumed to be completely mixed. The

nitrogen sources include applied inorganic fertilizers, mineralization of organic nitrogen, and excretion by fish.

The mass balance can be expressed as:

$$N_{net} = N_{orgn} + N_{add} + N_{fish} + N_{sed} + N_{in} - N_{phy} - N_{nitr} - N_{leach} - N_{out} \quad (3-2-73)$$

where

All terms are in unit of mg/hr

N_{net} = total ammonia nitrogen accumulation rate in the water column

N_{orgn} = TAN production due to mineralization

N_{add} = TAN application rate through fertilization

N_{fish} = TAN excretion by fish

N_{sed} = TAN production by diffusion from sediments

N_{in} = TAN addition in the influent water

N_{phy} = TAN uptake by phytoplankton

N_{nitr} = nitrification rate

N_{leach} = TAN leaching to lower sediment

N_{out} = TAN removed in the effluent water

Organic matter decomposition rate affects the concentration of TAN. The TAN production due to organic mineralization is estimated by (Jamu, 1998).

$$N_{org} = F_n \left(\sum_{i=1}^m OM_{decay,i} \right) \quad (3-2-74)$$

where

F_n = fraction of nitrogen in organic matter, mg organic N/mg OM

The amount of ammonia nitrogen added through fertilization is estimated based on nitrogen content of the fertilizer. For urea, the equation is expressed as:

$$N_{add} = F_{add} U_{add} \quad (3-2-75)$$

where

F_{add} = fraction of ammonia nitrogen in the fertilizer, mg N/mg urea

U_{add} = added amount of urea, mg urea/hr

TAN excretion rate by fish is estimated based on the feed intake. The equation is expressed as:

$$N_{fish} = K_{fishn} R_{fish} \quad (3-2-76)$$

where

K_{fishn} = fraction of feed intake excreted as TAN, mg N/g feed

R_{fish} = feed intake rate, g feed/hr

The nitrogen diffusion from the sediment is affected by the sediment temperature.

$$N_{sed} = R_{Nsed} \theta^{(T_{sed} - T_{sedref})} \quad (3-2-77)$$

where

R_{Nsed} = the diffusion rate from the sediment to the water column, mg N/hr (Shroeder, 1987)

θ = temperature coefficient for sediment diffusion, 1.024

T_{sed} = sediment temperature, °C

T_{sedref} = sediment diffusion reference temperature, °C

The diffusion rate R_{Nsed} is assumed to be a constant (Jamu, 1998). The sediment temperature is simulated and the sediment diffusion reference temperature is a constant but varies with location. It was assumed to be the initial water temperature in the current model.

Leaching of TAN in the water column to the sediment depends on the concentration of TAN in the water column and the transfer rate. The equation can be expressed as:

$$N_{leach} = K_{leach} N_{Am} V \quad (3-2-78)$$

where

K_{leach} = TAN leaching rate calculated based on infiltration rate and the depth of the sediment, 1/hr

The nitrification rate uses a first order equation as:

$$N_{nitr} = k_{nr} N_{Am} V \quad (3-2-79)$$

The rate of nitrogen uptake by phytoplankton depends on the phytoplankton growth rate.

It is expressed as

$$N_{phyt} = Chla_{prod} F_{phyt} \quad (3-2-80)$$

where

$Chla_{prod}$ = *Chla* production rate (see Equation (3-2-67)), mg *Chla*/hr

F_{phyt} = mg N/mg *Chla*

The nitrogen from the influent added in to the pond is calculated using

$$N_{in} = Q_{in} N_{influ} \times 1000 \quad (3-2-81)$$

where

N_{influ} = TAN concentration in the influent, mg/L

The nitrogen loss to the effluent is expressed as:

$$N_{out} = Q_{out} N_{Am} \times 1000 \quad (3-2-82)$$

The ammonia nitrogen in the pond at time t can be calculated by

$$N_{Am,t} / 1000 = N_{Am,t-\Delta t} / 1000 + N_{net} \Delta t \quad (3-2-83)$$

3.2.5. Organic Matter Model

Three major types of organic matter are modeled: fertilizer (chicken manure and fresh grass), detritus (dead phytoplankton), and fish feces. The organic matter distributions in the water column are assumed to be uniform with no re-suspension from the sediment.

The decay rate varies with the chemical composition of organic matter and environmental variables. The oxidation of each of the types of organic matter was calculated using different oxidation rates by Jamu (1998). In the present model, the decay rate for each organic matter was obtained based on the content and decomposition rates of carbohydrates, protein, and cellulose. The decomposition rate for each organic matter

type is assumed to follow a first order function with a constant decay coefficient. The effect of water temperature on reaction rate is included in the model.

Organic matter can be estimated by

$$OM_{net,i} = OM_{in,i} - OM_{decay,i} - OM_{fish,i} - OM_{sed,i} \quad (3-2-84)$$

where

$OM_{net,i}$ = net organic matter i accumulation rate. It can be chicken manure, cut grass, fish feces, or detritus.

$OM_{in,i}$ = organic matter i input.

$OM_{decay,i}$ = decomposition rate of organic matter i , described as

$$OM_{decay,i} = (k_{carbon}R_{carbon} + k_{cp}R_{cp} + k_{cellu}R_{cellu})OM_{i,t} \quad (3-2-85)$$

where

k_{carbon} , k_{cp} , k_{cellu} = the decay rate for carbohydrate, crude protein, and cellulose, respectively.

R_{carbon} , R_{cp} , R_{cellu} = the fraction of carbohydrate, crude protein, and cellulose in organic matter i ,

$OM_{i,t}$ = organic matter i content at time t (see Equation 3-2-88)

$OM_{fish,i}$ = organic matter grazed by fish.

$$OM_{fish} = R_{fishtaken} OM_{i,t} \quad (3-2-86)$$

where

$R_{fishtaken,i}$ is the fraction of fish food taken from organic matter directly

$OM_{sed,i}$ = organic matter that sinks to the sediment

$$OM_{sed,i} = k_{orgset,i} OM_{i,t} \quad (3-2-87)$$

k_{orgset} is the sink rate of organic matter. The same sink rate was used for fertilizer and fish feces.

All terms are in units of mg OM/hr

The inputs of chicken manure and cut grass are applied as fertilizers. The detritus input is calculated from the dead phytoplankton (see equation 3-2-69). The fish feces input is calculated based on the efficiency of food assimilation, b (see equation 3-3-1), the amount of food taken by fish, and the number of fish.

The organic matter content can be calculated by

$$OM_{i,t} = OM_{i,t-\Delta t} + OM_{net,i} \Delta t \quad (3-2-88)$$

3.3. Fish Growth Model

Fish growth rate is affected by environmental and physical factors, such as water quality, fish stocking density, food availability, and food quality. Several researchers have developed fish growth models using the CRSP database (Liu and Chang, 1992; Nath, 1996; Jamu and Piedrahita, 1996). The model developed by Liu and Chang (1992) evaluated the effects of fertilization, stocking density, and spawning on tilapia growth. Their model was modified by Nath (1996) by adding more variables, such as photoperiod, water temperature, DO, unionized ammonia, and food supply. Jamu and Piedrahita (1996) modified the model by including factors to account for multiple food resources and food qualities. The current model is focused on the effects of the water quality on fish growth over a full growing season. The variables considered to have an impact on

fish growth include water temperature, DO, unionized ammonia, and the concentration of three types of food sources (phytoplankton, non-phytoplankton, and supplied feed). Fish population is estimated based on an assumption of no reproduction. The mortality rate is estimated based on the data obtained from the PD/A CRSP database. The simulated fish growth rate is based on the average weight of an individual fish.

The structure of the model is adapted from the one developed by Jamu and Piedrahita (1996) and is based on bio-energetic principles. Fish growth is estimated based on the energy difference between the inputs and outputs in a fish body. The energy input comes from food intake; the energy outputs account for the energy consumption through food assimilation and metabolism. The model is based on the assumption that the composition of feed and fish are the same, and the equation is expressed as (Nath, 1996):

$$\frac{dW_f}{dt} = b(1 - a)R - kW_f^n \quad (3-3-1)$$

where

W_f = fish mass, g

b = average feed assimilation efficiency, unitless

a = fraction of feed assimilated which is used for feeding catabolism, 0 to 1, unitless

R = feed uptake rate, in terms of fish mass, g/hr

$$R = h\lambda_f\eta_f f(Temp)f(DO)f(NH_3)W^m \quad (3-3-2)$$

h = coefficient for food consumption, g^{1-m}/hr

λ_f = relative feeding level, 0 to 1, unitless

η_f = feed preference factor, 0 to 1, unitless

$f(Temp)$ = factor for temperature effects on feed intake, 0 to 1, unitless

$f(DO)$ = factor for DO effects on feed intake, 0 to 1, unitless

$f(NH_3)$ = factor for unionized ammonia effects on feed intake, 0 to 1, unitless

m = exponent of anabolism, unitless

k = coefficient of catabolism, g^{1-n}/hr

n = exponent of catabolism, unitless

The parameter a represents the energy used for feeding. The parameter b accounts for the efficiency of the nutrient digestion by fish. The parameter h is the coefficient of food consumption under optimal condition (Nath, 1996). The values of these three parameters depend on the food type and on fish species and size. The overall energy losses in the model include fish excretion, urinary waste, heat increase, and catabolism of fasting fish. These losses are all accounted for by the catabolism term in Equation 3-3-1.

The equations for estimating the effects of water temperature, DO, unionized ammonia, and food availability are described below.

3.3.1. Water Temperature Effects

Water temperature affects the food intake (Brett et al., 1969). Caulton (1978) described the relationship between temperature and feed intake for tilapias. Food intake rate reaches the maximum value when the temperature is in an optimal range. If the temperature is outside the optimal range, the food intake rate decreases. Food intake

stops when the temperature is outside the limit range. The temperature factor (from 0 to 1) can be described as (Svirezhev and co-workers, 1984):

$$\begin{aligned} f(Temp) &= \exp\{-4.6[(T_{optf}-T)/(T_{optf}-T_{min})]^4\} & \text{if } T < T_{optf} \\ &= \exp\{-4.6[(T-T_{optf})/(T_{max}-T_{optf})]^4\} & \text{if } T \geq T_{optf} \end{aligned} \quad (3-3-3)$$

where

T_{min} = below this temperature fish stop eating, °C

T_{max} = above this temperature fish stop eating, °C

T_{optf} = optimum temperature for fish taking food, °C

The values of the optimal and limit temperatures vary with species. Nath (1996)

suggested that $T_{min} = 15^\circ\text{C}$, $T_{max} = 40^\circ\text{C}$, and $T_{optf} = 33^\circ\text{C}$ (range is 30 to 36°C) for tilapia.

The catabolism term is also affected by temperature. The effect is described as (Nath, 1996):

$$k = k_{min} \exp[s(T - T_{min})] \quad (3-3-4)$$

where

k_{min} = coefficient of fasting catabolism at T_{min} , g^{1-n}/hr

s = a constant

The k_{min} and s can be determined through model calibration and $k_{min} = 0.025$ and $s = 0.015$ were found suitable for tilapia in the model developed by Nath (1996). The range of k was 0.0319 to 0.0468 from an earlier published model (Liu and Chang, 1992). In early models, fish growth was simulated on a daily basis (Nath, 1996; Liu and Chang, 1992).

3.3.2. Dissolved Oxygen Effects

The effect of DO on fish growth is described in three stages. When DO is below the minimum limit level, DO_{min} , fish feeding stops. When DO is above a critical level, DO_{crit} , DO has no effect on feeding. When DO is between DO_{min} and DO_{crit} , feeding is affected by DO (Nath, 1996):

$$f(DO) = \frac{(DO - DO_{min})}{(DO_{crit} - DO_{min})} \quad (3-3-5)$$

if $DO > DO_{crit}$ then $f(DO) = 1.0$

if $DO < DO_{min}$ then $f(DO) = 0.0$

3.3.3. Un-ionized Ammonia Effects

Un-ionized ammonia, NH_3 , is toxic to fish (Boyd, 1979). The effect of un-ionized ammonia can be simulated using an equation similar to that for DO (Nath, 1996). When NH_3 is higher than NH_{3max} , then the fish stop feeding. When NH_3 is lower than the critical value, NH_{3crit} , then there is no effect on feeding. When the concentration of NH_3 is higher than the critical value, NH_{3crit} and lower than a maximum value, NH_{3max} , then food intake will decrease as the concentration of NH_3 increases. The function can be described as (Nath, 1996):

$$f(NH_3) = \frac{(NH_{3max} - NH_3)}{(NH_{3max} - NH_{3crit})} \quad (3-3-6)$$

where

NH_3 = un-ionized ammonia concentration, $\mu\text{g/L}$

if $NH_3 \leq NH_{3crit}$ then $f(NH_3) = 1.0$

if $NH_3 \geq NH_{3max}$ then $f(NH_3) = 0.0$

$$NH_3 = \frac{1}{10^{(pKa-pH)} + 1} N_{Am} \quad (3-3-7)$$

where pKa is estimated by (Emerson et al, 1975)

$$pKa = 0.09018 + \frac{2729.92}{T_{ave} + 273} \quad (3-3-8)$$

pH is a constant in the model.

3.3.4. Food Supply Effects

The fish growth rate is dependent on the amount of food and the quality of food available.

There are many types of food for fish but the model includes two major types of food:

artificial (or introduced in a feed or fertilizer) and natural food (produced within the pond). The model assumes that the fish takes the most favorable food first. If the supply is not sufficient, then the fish switches to the substitute feed source. For tilapia, the preferred food is natural food (Jamu, 1998). If the available natural food is not sufficient to meet the food demand, then the fish will consume artificial food. Two types of natural food are included in the model: phytoplankton and the other organic matters (chicken manure, fresh cut grass, and dead phytoplankton). The phytoplankton is assumed to be preferred by tilapia over the other organic matters (Jamu, 1998).

The phytoplankton uptake coefficient can be calculated as:

$$\eta_{phy} = \frac{Chla}{K_{uptakeChla} + Chla} \quad (3-3-9)$$

where

η_{phy} = coefficient of phytoplankton uptake by fish, unitless

$Chla$ = concentration of Chla, $\mu\text{g/L}$

$K_{uptakeChla}$ = half saturation constant for phytoplankton uptake, $\mu\text{g/L}$

The organic matter uptake coefficient is calculated as (Jamu, 1998):

$$\eta_{Org} = (1 - \eta_{phy}) \frac{OM_{tot} / V}{K_{uptakeOrg} + OM_{tot} / V} \quad (3-3-10)$$

where

η_{Org} = coefficient of organic matter uptake, unitless

OM_{tot} = concentration of all types of organic matter, mg.

where

$$OM_{tot} = \sum_i^m OM_{i,t} \quad (3-3-11)$$

The concentration of all types of organic matter is the sum of chicken manure, fresh cut grass, and dead phytoplankton. Mass balances for all three types of organic matter are described in Section 3-2-5.

$K_{uptakeOrg}$ = half saturation constant for organic matter uptake, mg/m^3

Similar to the coefficient of detritus uptake, the artificial feed uptake coefficient can be calculated as (Jamu, 1998):

$$\eta_{artf} = (1 - \eta_{phy} - \eta_{detri}) \frac{Artf}{K_{uptakeartf} + Artf} \quad (3-3-12)$$

where

η_{artf} = coefficient of artificial food uptake, unitless

$Artf$ = concentration of artificial food, $\mu\text{g/L}$.

$K_{\text{uptakeartf}}$ = half saturation constant for artificial food, $\mu\text{g/L}$

The feed preference factor, η_f can be calculated based on the uptake coefficients from Equations (3-3-9 through 3-3-12)

$$\eta_f = \eta_{phy} + \eta_{Org} + \eta_{artf} \quad (3-3-13)$$

The relative feeding level, λ_f is a dimensionless parameter that represents the carrying capacity of the pond. If the fish biomass is less than the critical standing stock, the relative feeding level, λ_f is one, otherwise, the relative feeding level, λ_f can be calculated using (Bolte et al., 1994):

$$\lambda_f = \frac{\text{CriticalStandStock}}{\text{TotalFishBiomass}} \quad (3-3-14)$$

The critical standing stock depends on the pond management and environmental conditions and can be estimated using the guidelines provided by Balarin and Haller (1982).

3.3.5. Fish Population

The fish population is estimated using a very simple logistic equation (Pearl and Reed, 1920, cited in Jamu, 1998). The assumptions of the model include no reproduction, no harvest, and no additional stocking during the culture period. Under these assumptions, the fish population is reduced only by mortality rate, which was estimated using the data from the CRSP PD/A database. The equation can be expressed as (Pearl and Reed, 1920):

$$\frac{dfish_{pop}}{dt} = -k_{fnum} \frac{(fish_{numallowed} - fish_{pop})}{fish_{numallowed}} fish_{pop} \quad (3-3-15)$$

where

k_{fnum} = mortality rate, 1/hr

$fish_{numallowed}$ = the management allowable fish population, number of fish

$fish_{pop}$ = the fish population, number of fish

The management allowable fish is estimated from the recorded data at fish harvest.

Fish

4. Results: Model Calibration and Validation

The process of model development includes verification, calibration, and validation steps (Jørgensen and Gromiec, 1989). Verification consists of demonstrating the accuracy of mathematical hypotheses and the logical interrelationship among state variables (Leohle, 1997). Calibration consists of tuning the coefficients or parameters to obtain the best possible agreement between the simulated and observed data (Leohle, 1997). Validation consists of further checking the model using different sets of data to demonstrate the credibility of the model and to provide a way of determining the magnitude of expected errors in simulations (Tanji, 1981).

The probability functions in the weather generation component have been verified by many researchers (Liu and Jordan, 1960; Graham et al., 1988; Graham and Hollands, 1990; Knight et al., 1991). The equations describing the interrelationships among the state variables in the water quality models have been verified by previous modelers, especially by Losordo (1988) and Culberson (1993).

The model calibration and validation processes were carried out using data from different treatments at three PD/A CRSP sites. The site characteristics of the three locations have been listed in Table 3-1 (Section 3.1.1.). The experiments and treatments used for model testing are listed in Table 4-1. The experiments were designed to compare the responses of physical, chemical, and biological factors in fish ponds under different fertilization regimes. At each location, there were at least three fertilization rates. Each treatment had

three to four replications. One treatment was used for model calibration and the others were used as model validation for each location.

Table 4-1. Selected ponds and treatments used for model calibration and validation (PD/A CRSP, 1987, 1988, 1989)

	Thailand (C404)*	Rwanda (H403)*	Honduras (F3d)*
Starting Julian Day	279	125	38
Treatment 1**	100 CM+24.3UR***	100 CM+400 GR	500 CM
Treatment 2	44 CM+10.8UR	150 CM+600 GR	250 CM
Treatment 3	200 CM+48.6UR	200 CM+800 GR	125 CM
Treatment 4		100 CM+400 GR +28.6 UR	1000 CM
Replications (# of ponds)	4	3	3

* C404, H403, and F3d are the CRSP data file names.

** Treatments used for model calibration

*** CM is Chicken Manure, UR is Urea, GR is Grass. The numbers indicate the treatment rates in units of kg/ha/wk

During model validation, only the changes of the values of pond inputs and initial water quality values are allowed. Because stochastic weather variables are generated and used in the model, the probability distributions of the simulation results were calculated and compared to the observations for the sites. For cases in which sufficient data were not available to obtain probability distributions, the means and standard deviations of the simulated values were compared to the measured data. Since the Monte Carlo method was used in the model, the simulation results were obtained after running the model 20 times for each treatment. The simulation length was one growing season (150 days).

4.1. Solar Radiation

The solar radiation model was designed for generating the hourly solar radiation values starting at any day of a given year (using Julian day, from 1 to 365) and can continue generating values as long as the computer memory allows. Since solar radiation values are inputs to the water quality model, the model was calibrated and validated independent of the water quality model. During model calibration, the simulation time step was set to 0.25 hour. The model calibration and validation process included the calculation of average monthly clearness indices \bar{K}_t at different locations, the comparison of the simulated and measured daily cumulative frequency distribution (CFD) curves, the demonstration of the effect of the autocorrelation coefficient ρ and the comparison of the simulated and measured hourly solar radiation values at different locations and different months.

Obtaining accurate average monthly clearness indices \bar{K}_t and the CFD function is crucial for the solar radiation model development. The calculated \bar{K}_t values for the three selected PD/A CRSP sites are listed in Table 4-2. The \bar{K}_t values range from 0.356 to 0.654. The lowest value is for the Rwanda site, and the highest value is for the Honduras site. The two highest \bar{K}_t values for the Rwanda site are close to the lowest \bar{K}_t value for the Thailand site. The data from the Thailand site show that the \bar{K}_t values are lower from May to September than from October to April. At the Thailand site, the wet season occurs from May to September resulting in a higher cloud cover than during October to April. The \bar{K}_t values at the Rwanda site show less variation than for Thailand and no

clear seasonal pattern. The highest \bar{K}_t value is in June and the lowest value is in October. The \bar{K}_t values at the Honduras site are higher than for the other two sites. The Honduras site is relatively dry and the cloud cover is lower than at the other two sites. The values from January to March are higher than during the other months.

Table 4-2. Summary of monthly average clearness index values \bar{K}_t calculated from data in the PD/A CRSP database

Months	Thailand	Rwanda	Honduras
January	0.548	0.374	0.654
February	0.550	0.434	0.624
March	0.520	0.400	0.601
April	0.540	0.366	0.562
May	0.480	0.386	0.521
June	0.478	0.455	0.535
July	0.479	0.416	0.529
August	0.444	0.378	0.538
September	0.472	0.369	0.541
October	0.505	0.356	0.532
November	0.590	0.362	0.514
December	0.624	0.372	0.523
Average	0.519	0.389	0.556
Maximum	0.624	0.455	0.654
Minimum	0.444	0.356	0.514
Standard Deviation	0.053	0.031	0.045

Using the parameters listed in Table 3-2 (in Chapter 3.1.1), the cumulative frequency distribution (CFD) curves are obtained after running the model 20 times for each site.

The CFD curves of K_t for January, August, and December are shown in Figure 4.1.1 for the Thailand site as an example of the month to month differences observed. Two CFD curves for the Thailand and Honduras sites with the same \bar{K}_t (0.624) are shown in Figure

4.1.2 illustrating that the \bar{K}_t values alone cannot determine the CFD curves, and the CFD must be calculated based on site data, making it location-dependent.

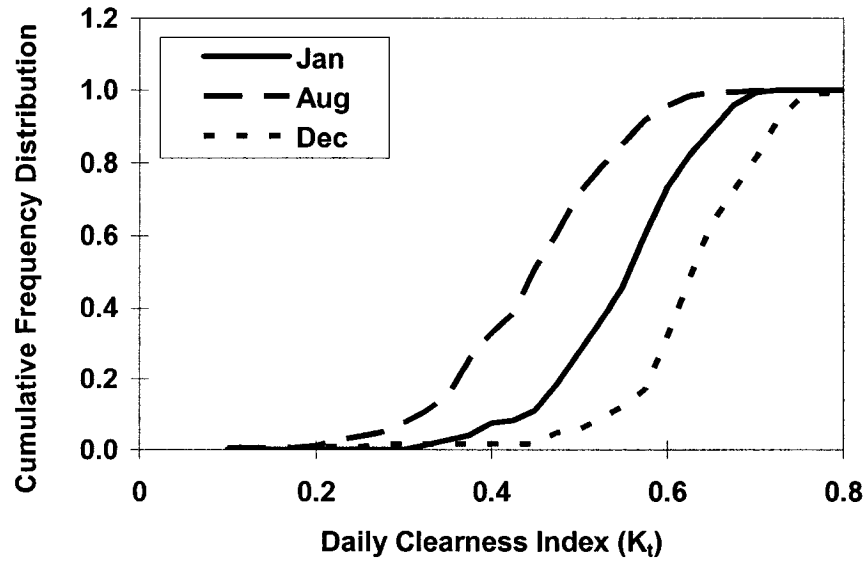


Figure 4.1.1. Calculated CFD for three different months for the Thailand site

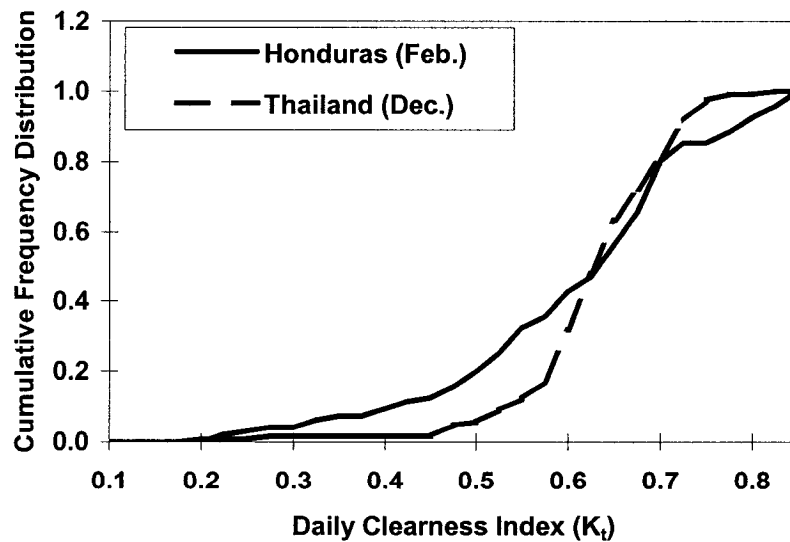


Figure 4.1.2. Comparison of CFD curves with same \bar{K}_t values for the Thailand and Honduras sites

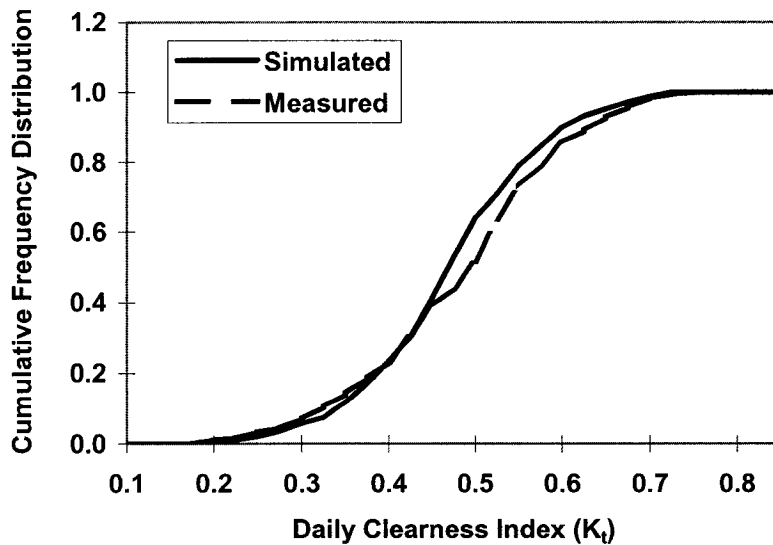


Figure 4.1.3a. Generated and measured CFD curves for May for the Thailand site

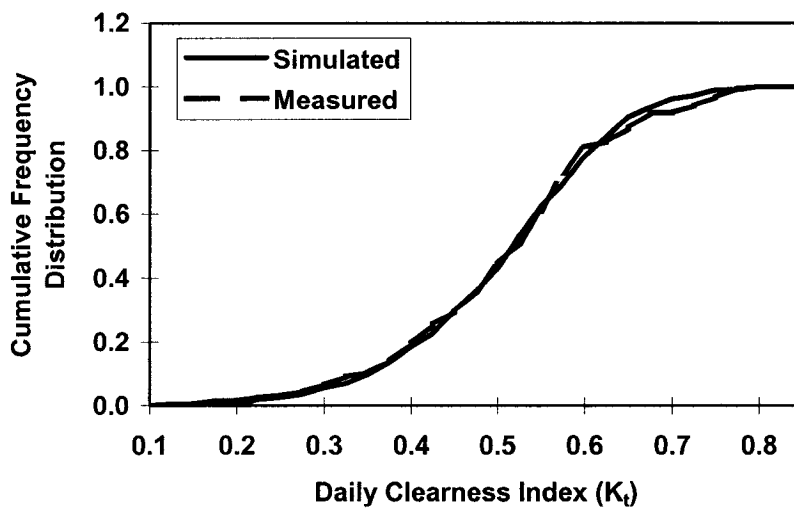


Figure 4.1.3b. Generated and measured CFD curves for October for the Thailand site

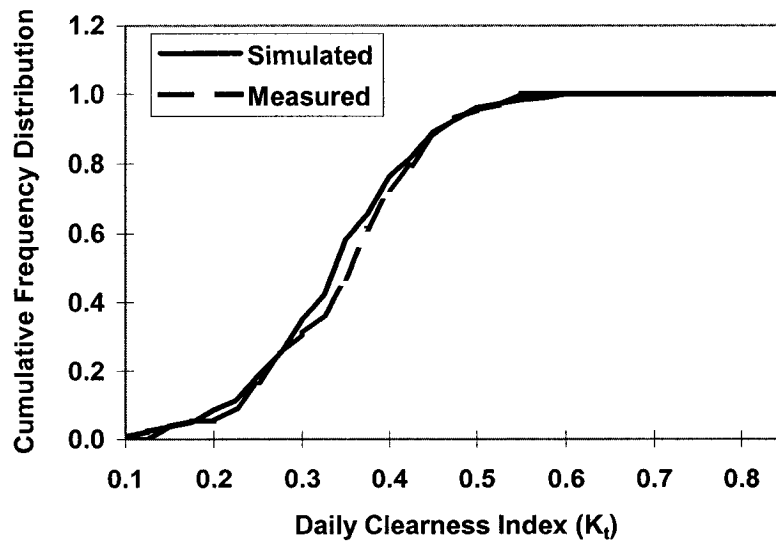


Figure 4.1.4a. Generated and measured CFD curves for September for the Rwanda site.

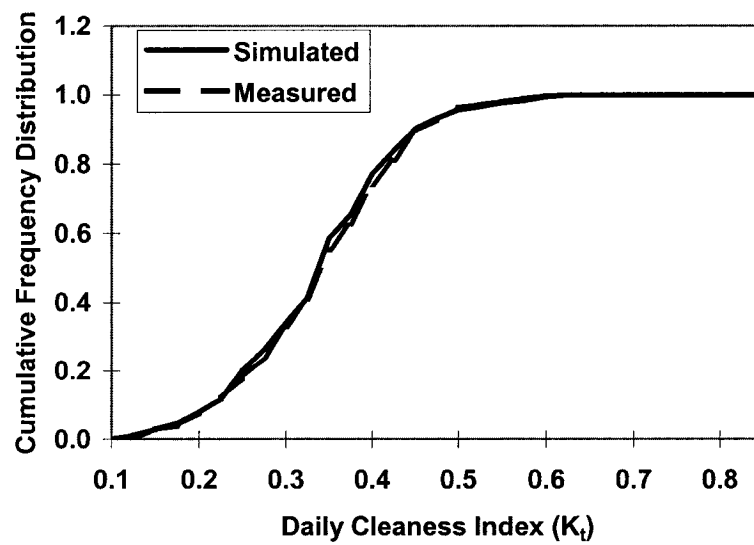


Figure 4.1.4b. Generated and measured CFD curves for January for the Rwanda site.

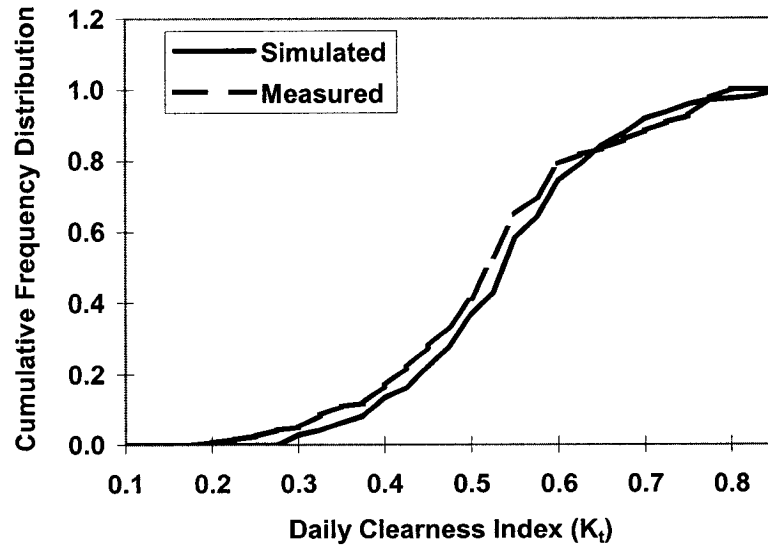


Figure 4.1.5a. Generated and measured CFD curves for August for the Honduras site

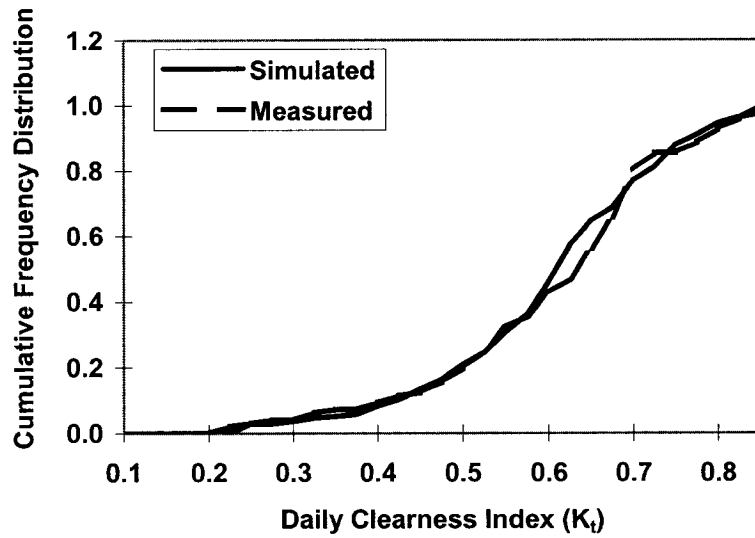


Figure 4.1.5b. Generated and measured CFD curves for February for the Honduras site

The outputs from the model include calculated daily and hourly clearness index values from which daily and hourly solar radiation estimates are made. The CFDs of the generated daily clearness index values were compared to those of the measured data for two random selected months (one for each half year) at each location. The sample comparisons of the simulated and measured CFD for the sites in Thailand, Rwanda, and Honduras are shown in Figures 4.1.3 to 4.1.5. For the Thailand site, the generated and measured CFD curves have good agreement for May and October (Figures IV1.3a and 4.1.3b). The comparisons of simulated and measured CFD at the Rwanda site show the best agreement among the three sites (Figures 4.1.4a and 4b). The differences between the generated and measured CFDs are mainly due to curve smoothing. Figures 4.1.5a and 5b show the comparison of the generated CFD to the measured CFD for August and February for the Honduras site. The CFD of the generated values in August is slightly lower than that of the measured values (Figure 4.1.5a). Figure 4.1.5b shows good agreement between the simulated and measured values. The comparisons of the simulations and measurement suggest that Equation 3-1-6 can be used for the generation of clearness indices.

The range of values for the lag one autocorrelation coefficient, ρ , reported by previous researchers for various locations in North America is between 0.15 and 0.35 (Knight et al., 1991). The values calculated for the Thailand, Rwanda, and Honduras sites are 0.52, 0.29, and 0.76, respectively. The value of ρ suggested by Graham and co-workers (1988) was 0.29. Since Figure 4.1.5b shows a good match for the generated CFD curve for February for the Honduras site and the Honduras site has the highest ρ value, the

simulated CFD curves using $\rho = 0.29$ and $\rho = 0.76$ were compared for the Honduras site in February (Figure 4.1.6). The similarity between the two curves suggests that the influence of the autocorrelation coefficient on the generation of daily clearness index values is weak. Since the difference in the ρ values does not appear to have a significant effect on the generated CFD curves, and since Graham and co-workers (1988) used a more extensive and complete data set than the one used here, their recommended value of $\rho = 0.29$ (Graham et al., 1988) was used in the model to generate daily solar radiation values for the three locations.

The PD/A CRSP data set includes only a few days for which solar radiation values were recorded at intervals of less than one day: three days for Rwanda, six days for Honduras, and 36 days for Thailand, of which 30 days is a continuous 30 day record with readings obtained at five minute intervals. Given the limited data available on measured hourly values from the PD/A CRSP database, no CFD of hourly clearness index curves could be calculated. However, the data were used to test the model by comparing measured and generated hourly solar radiation values. All comparisons gave good agreement as illustrated in Figure 4.1.7 for the Thailand site. The comparison includes the measured data and generated values for Julian days 280 to 287. The hourly values were obtained from data collected at five-minute intervals in 1996. The mean, maximum, and minimum of the generated solar radiation values were obtained after 20 runs of the model. The Rwanda site has diurnal measured solar radiation for only three days. Figure 4.1.8 shows the comparison of the simulated and observed hourly solar radiation values at the Rwanda site. The measured solar radiation values are a little lower than the simulations for early

mornings and evenings. Figure 4.1.9 shows the simulated and observed hourly solar radiation values for the Honduras site. The simulated average values are lower than the observations for most days except for Julian day 144.

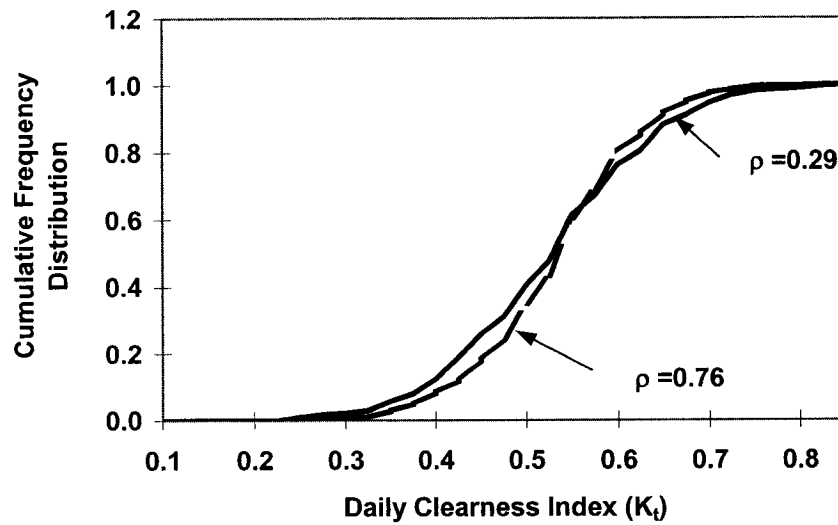


Figure 4.1.6. Comparison of CFD curves generated using two different ρ values

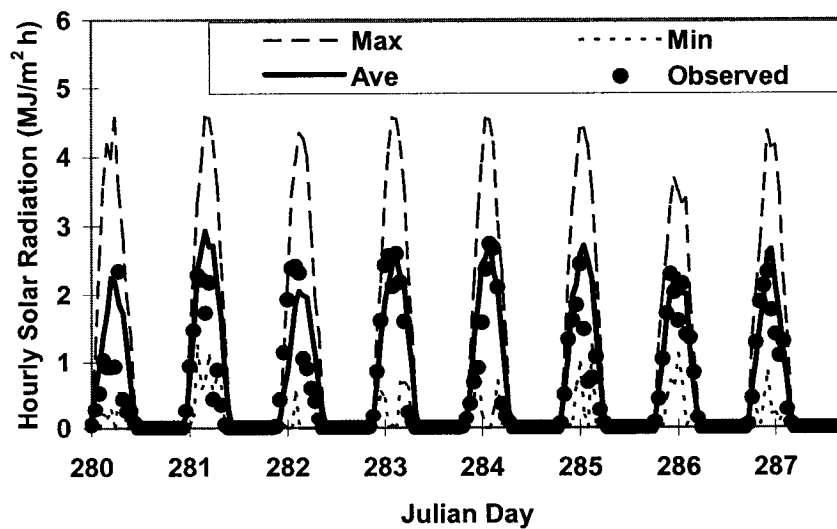


Figure 4.1.7. Comparison of hourly solar radiation for the Thailand site

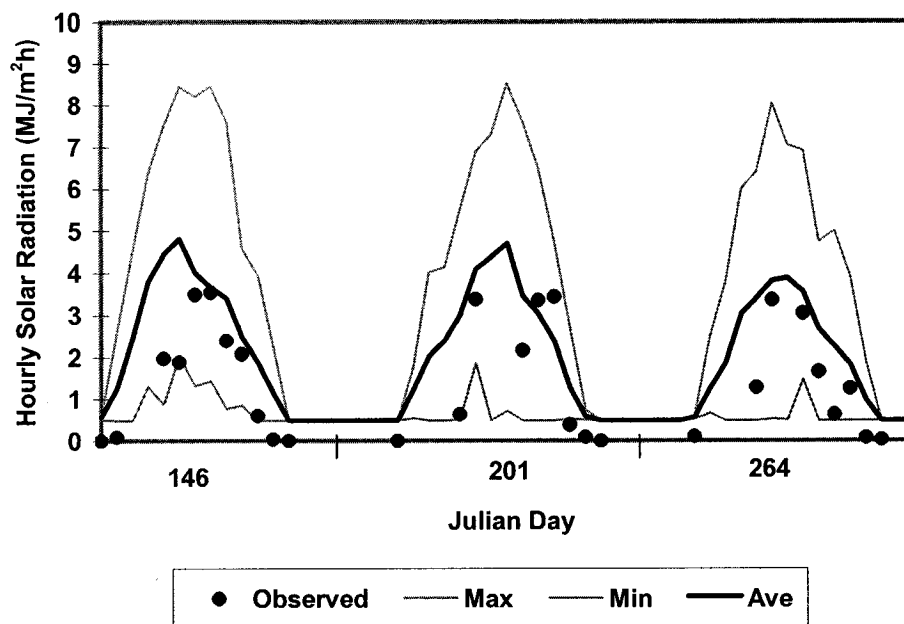


Figure 4.1.8. Comparison of hourly solar radiation for the Rwanda site

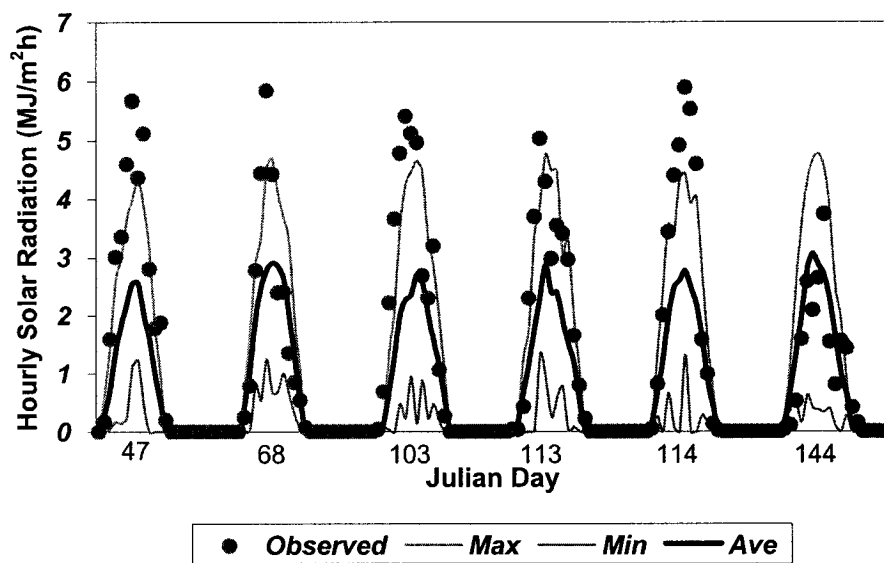


Figure 4.1.9. Comparison of hourly solar radiation for the Honduras site

4.2. Water Quality Simulation Results

The simulated state variables in the water quality model include water temperature, DO, chlorophyll a (Chla), and total ammonia nitrogen (TAN). The simulated results, except for TAN, are compared graphically. In order to provide information for risk assessment, the simulated results are also presented in the format of frequency distributions.

Frequency distributions obtained from the simulations are compared to the frequency distributions calculated from the measurements for the three sites.

The initial water quality inputs include water temperature, DO, TAN, and Chla. The measured initial water quality data have high variations among the replicate ponds, especially for Chla (Table 4-3). Having such a high variation among replicates, it was decided to use initial values generated from a normal distribution using the averages and standard deviations from all ponds at each site. The use of randomly generated initial values allows the model to be started at anytime of the year.

Table 4-3. Initial water quality input values
(numbers in parentheses represent standard deviations)

Input Parameters	Thailand	Rwanda	Honduras	Description
Tsurf, Tmid, Tbot (°C)	25.3 (±0.3)	20.8 (±0.3)	25.4 (±2.0)	Temperature for three layers*
DOsurf, DOmid, DObot (mg/L)	5.2 (±1.3)	3.7 (±2.3)	0.8 (±1.1)	DO for three layers*
TAN (µg/L)	57 (±33.5)	33 (±27.8)	20 (±13.3)	Total ammonia nitrogen
Chla (µg/L)	34 (±16)	1000 (±570)	150 (±120)	Chlorophyll a

* the initial values were taken when the ponds were de-stratified (at 6 am)

The parameters and coefficients needed to run the models were determined using values from the literatures as guidelines, or using mathematical or statistical methods. The site specific parameters include the slope of the photosynthetic rate versus light intensity (PI) curve, the non-phytoplankton light extinction coefficient, the chlorophyll a content, and the water column respiration rate (see Table 4-4). The initial slopes of PI curves were used to determine the photosynthetic efficiency for each location. The slope is regulated mainly by the content of chlorophyll a pigment and solar radiation. Under low radiation, the PI slope does not change rapidly as solar radiation increases even at high pigment content, but photosynthetic efficiencies are higher than those under high light intensity (Reynolds, 1984). Ultimately, the calibrated slopes of PI curves provide a measurement of photosynthetic efficiency at low solar radiation.

The light extinction coefficient is one of the most important parameters for the estimation of Chla concentration. The light extinction coefficient was calculated using non-phytoplankton, η_{kw} , and phytoplankton, η_{kc} , light extinction coefficients (Table 4-4).

The calibrated η_{kw} and η_{kc} are similar to the values presented by Jamu et al. (1999). The η_{kw} values indicated that the ponds for the Honduras site had higher background turbidity than the other two sites. The η_{kc} values were approximately the same for the three sites.

The calibrated η_{kc} value does not reflect the composition of phytoplankton.

Table 4-4. Site specific calibrated parameters for water quality models

Parameters	Calibrated range	Thailand	Rwanda	Honduras
Slope of PI curve mg C/(mg Chla ($\mu\text{mol hr/m}^2/\text{s}$))	0.03 to 0.08 ^a	0.05	0.04	0.04
Phytoplankton light extinction coefficient ($\text{m}^{-1}(\text{mg.m}^{-3})^{-1}$)	0.009 to 0.02 ^b	0.015	0.013	0.013
Non-phytoplankton light extinction coefficient (m^{-1})	Ranges are showed in parentheses	3.57 (1.88 to 5.25) ^b	2.89 (2.89 to 5.23) ^b	7.67 (6.12 to 10.84) ^b
Water column O ₂ respiration rate ($\text{mgO}_2/\text{m}^2/\text{hr}$)	50 to 100 ^c	100	100	50
Oxygen consumption in organic matter oxidation (mgO_2/mgOM)	1.08 to 3.00 ^d	3.00	3.00	3.00
Chla content in phytoplankton ((mg/L Chla) / (mg/L dry cell))	0.005 to 0.02 ^e	0.010	0.012	0.010
Half saturation constant for nitrogen uptake by phytoplankton, K _n ($\mu\text{g N/L}$)	4 to 10 ^f	5	5	5
Sediment respiration constant, ($\text{mgO}_2/(\text{m}^2 \text{ hr})$)	0.005 to 0.010 ^g	0.007	0.007	0.007

a. Lee et al., 1991b

b. Jamu et al., 1999

c. Losordo, 1988

d. Jørgensen and Gromiec, 1989; Schroeder, 1987

e. Reynolds, 1984

f. Lee et al., 1991b; PD/A CRSP, 1988

g. Jamu, 1998

Water column respiration rate is a site specific parameter. The water column respiration rate excluded phytoplankton respiration and nitrification rates. The major oxygen consumption included in this term may be by zooplankton and suspended bacteria. The same water column respiration rates were obtained for the Thailand and Rwanda sites and they were twice the rate for the Honduras site (Table 4-4). It is difficult to determine the

accuracy of the values because the population of zooplankton and concentration of suspended bacteria were not available. In addition, the respiration rate is probably not a fixed value over a fish growing season.

The organic matter decomposition rate in water depends on bacterial populations, nutrients, and suspended organic matter concentrations. The oxygen consumption rate by organic decomposition depends on an oxygen consumption stoichiometric ratio.

Literature values for this parameter range from 1.08 to 3 mgO₂/mg OM (Jørgensen and Gromiec, 1976; Schroeder, 1987). The calibrated parameter value was 3 mgO₂/mg OM which is similar to the value calibrated by Jamu (1998).

The phytoplankton grazed by fish were estimated based on cell dry weight. Therefore, the chlorophyll a content had to be converted to cell dry weight. The range of average chlorophyll a content in various freshwater phytoplankton is 0.5% to 2% of dry weight (Reynolds, 1984). The calibrated ratio of chlorophyll a to cell dry weight was 0.01 for the Thailand and Honduras sites and 0.012 for the Rwanda site (Table 4-4).

Phytoplankton growth depends on many factors including water temperature, nitrogen concentration, and phytoplankton species. Nutrient uptake by phytoplankton was regulated by a half-saturation constant K_n . The calibrated K_n value was the same for the three sites and within the reported range of 20 to 90 µg/L (Lee et al., 1991b; Jørgensen and Gromiec, 1989).

The calibrated value for the sediment respiration rate was $0.007 \text{ mg O}_2/\text{m}^2 \text{ hr}$ (Table 4-4). This value corresponds to that used by Culberson in his model (1993).

4.2.1. Thailand Site

The selected Experiment (C404, PD/A CRSP, 1987, 1988) at the Thailand site was designed for testing the effects of different fertilization rates on fish growth and water quality. The application rates of chicken manure were 44, 100, and 200 kg/ha/week combined with urea application rates of 10.8, 24.3, and 48.6 kg/ha/week, respectively, to maintain a C: N ratio of 5:1 (Table 4-1). Treatment 1 (100 kg/ha/wk CM) was used for model calibration. Treatments 2 (44 kg/ha/wk CM) and 3 (200 kg/ha/wk CM) were used for model validation. The simulations were started on Julian day 279 for a period of 150 days. All pond initial conditions were as listed in Table 4-3. The simulation results are compared with the measured values from four replicate ponds (C01, C04, C05, and C10 for Treatment 1; B01, B07, B11, and B12 for Treatment 2; and A06, A08, A09, and A14 for Treatment 3).

Diurnal water temperature and DO measurements were collected every two weeks. The samples were collected approximately at 600, 1000, 1400, 1600, 1800, and 2300 hours. The simulated maximum, minimum, and average corresponding to the sampling days are presented for comparisons with the data.

4.2.1.1. Calibration Run (Treatment 1: 100 kg/ha/wk chicken manure and 24.3 kg/ha/wk urea)

Figures 4.2.1.1 to 4.2.1.3 show the water temperature at the three layers. The simulated water temperatures cover most of the observed data but the average values are higher than most of the observations at the surface and middle layers. The bottom layer simulations have better agreement to the observations than the two upper layers. The difference between the average simulations and measurements could be reduced by adjusting the effective diffusion coefficient (see Equation 3-2-27), but the reduction of the effective diffusion coefficient would result in an increase in the differences for the DO simulations. The effective diffusion coefficients were determined to obtain the best possible fit for both temperature and DO simulations.

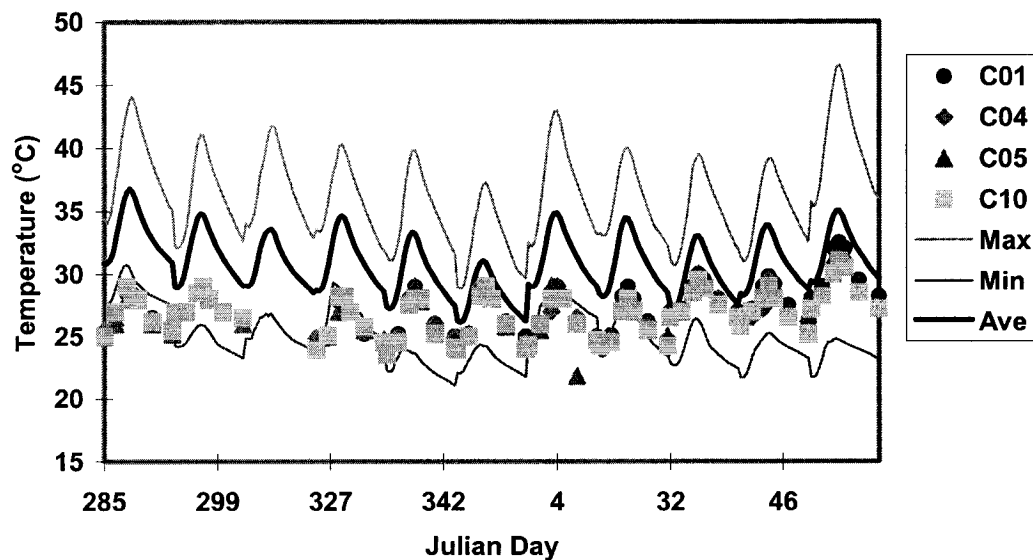


Figure 4.2.1.1. Temperature of the surface layer for Treatment 1 for the Thailand site

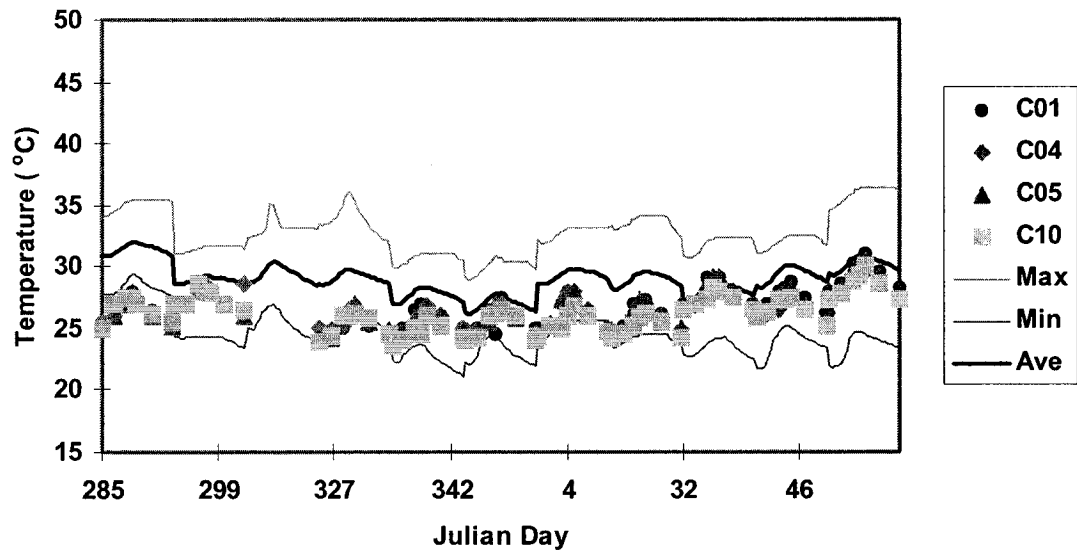


Figure 4.2.1.2. Temperature of middle layer for Treatment 1 for the Thailand site

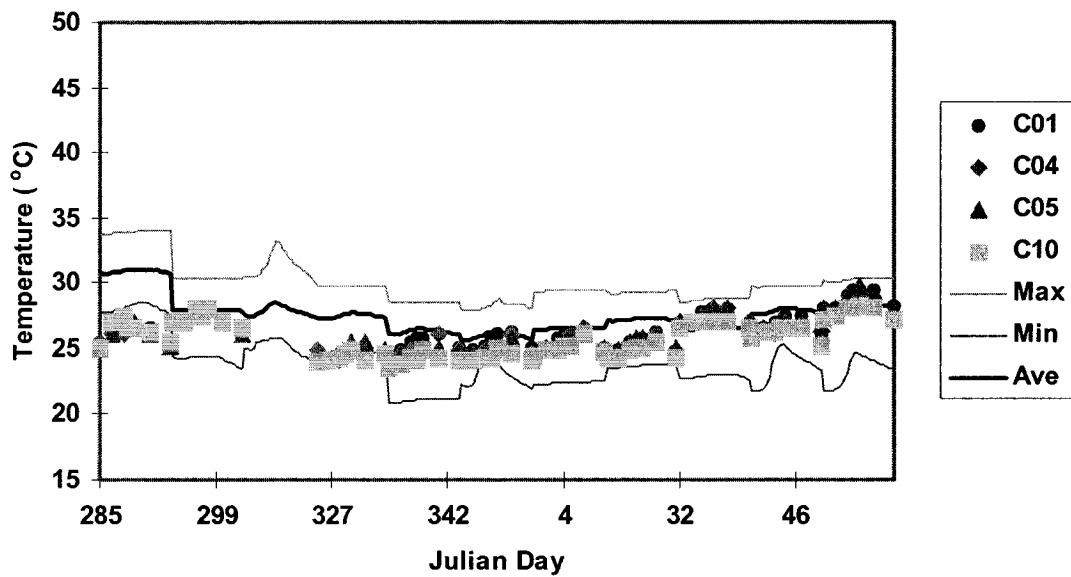


Figure 4.2.1.3. Temperature of bottom layer for Treatment 1 for the Thailand site

Figures 4.2.1.4 to 4.2.1.6 show the simulated and measured DO for the three layers. For the surface layer, the simulated DO values are close to the observations on the three diel sampling days (Julian days 285, 299, and 313). During the later part of the culture season the simulated maximum DO values are much lower than the observations. A similar trend occurs at the middle and bottom layers. The simulated DO for the middle and bottom layers are about 10 mg/L lower than the measurements for the three sampling days. It is unusual to have such highly supersaturated DO at the beginning of a fish culture season while Chla was under 100 µg/L. On the second sampling day (two weeks later), the simulated DO are closer to the measured values for the surface layer.

It was difficult to calibrate the DO model because the simulation has good agreement for the surface layer on the first sampling day but not for the middle and bottom layers. In addition, the differences among DO measurements for the replicate ponds increased substantially towards the end of the experiment. On the last sampling day, the measured difference of DO between two replicate ponds was up to 15 mg/L. The calibrated results indicate that the model is missing some important factors which affect DO in the ponds.

Chla is a crucial variable affecting DO concentration in ponds. Figure 4.2.1.7 shows the simulated and measured Chla. The simulation curves show a different trend from the measured Chla. The simulated Chla are higher than the observations in the first three months and lower than some of the observations in the last two months. At the end of the season, the maximum measured Chla was over 800 µg/L in Pond C10 while Chla in Pond C01 was almost zero. The simulated Chla are close to the measured Chla in pond C05.

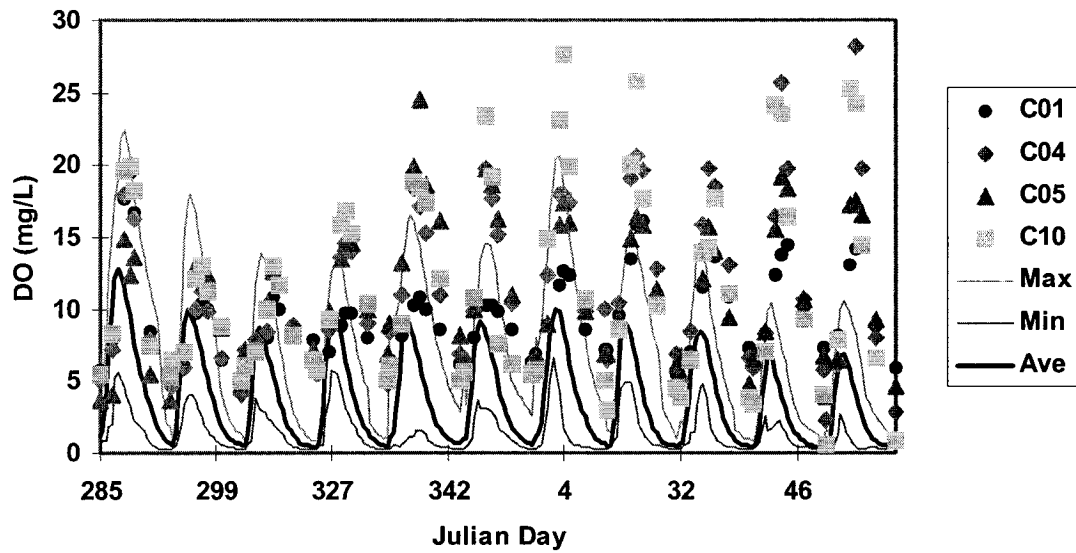


Figure 4.2.1.4. Surface layer DO for Treatment 1 for the Thailand site

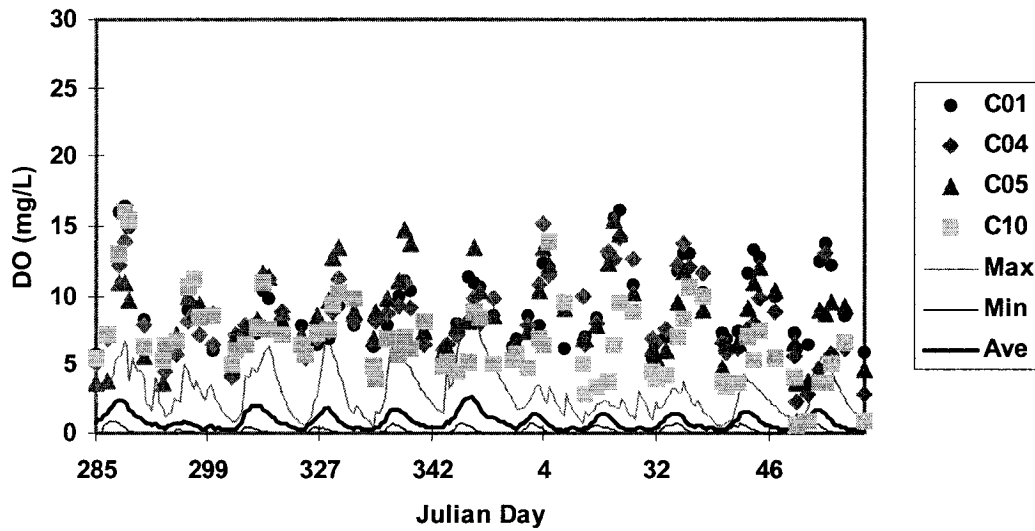


Figure 4.2.1.5. Middle layer DO for Treatment 1 for the Thailand site

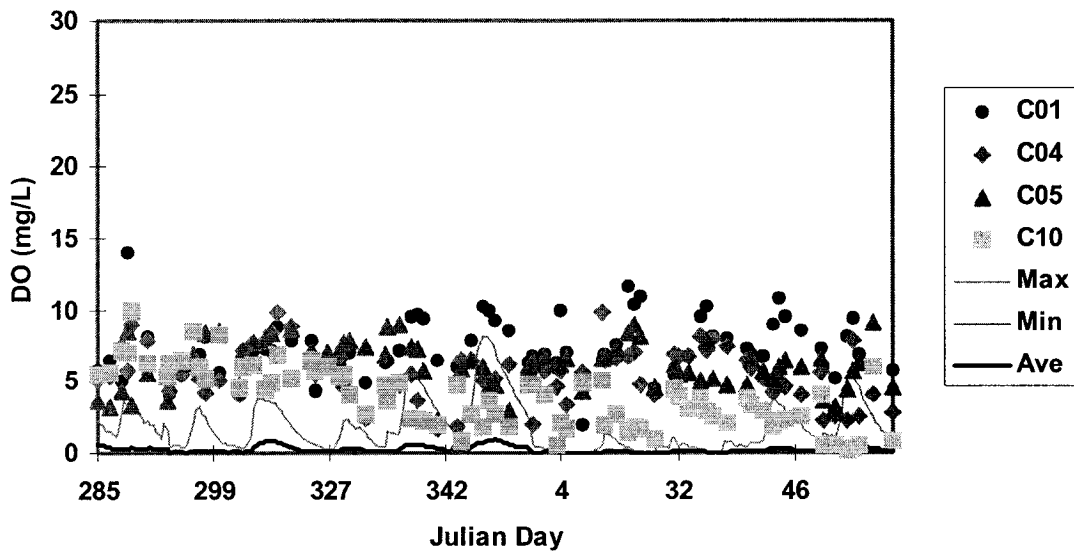


Figure 4.2.1.6. Bottom layer DO for Treatment 1 for the Thailand site

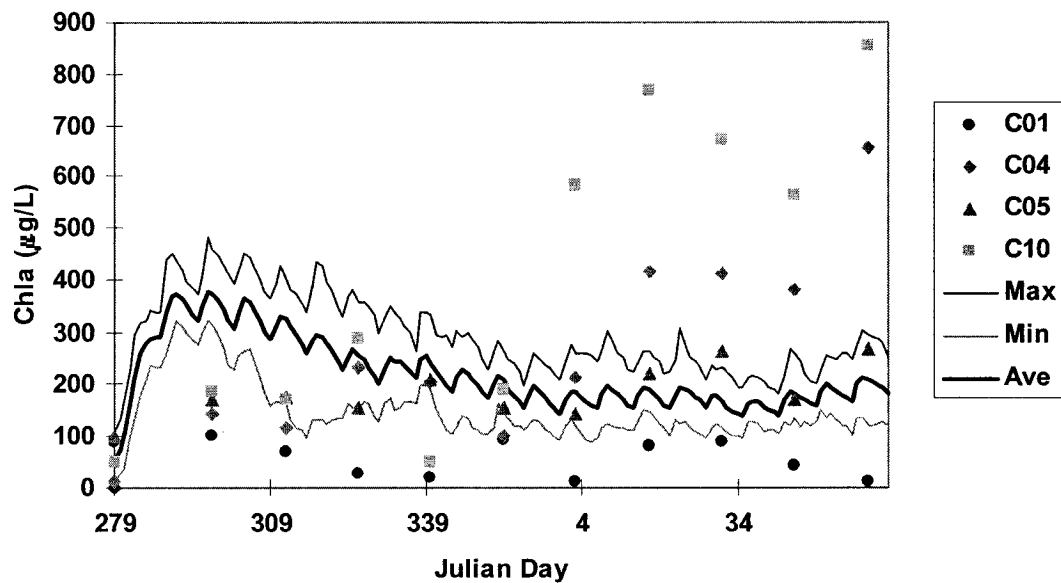


Figure 4.2.1.7. Chlorophyll a for Treatment 1 for the Thailand site

4.2.1.2. Validation Run (Treatment 2: 44 kg/ha/wk chicken manure and 10.8 kg/ha/wk urea)

Figures 4.2.1.8 to 4.2.1.10 show the comparisons of the simulated and measured water temperature in Treatment 2 for the three layers. The simulated water temperatures cover the observed data for all three layers but the simulated average values are higher than the observations. Agreement between simulated and measured values improved towards the end of the simulation period.

The comparisons of the simulated and measured DO for the three layers are shown in Figures 4.2.1.11 to 4.2.1.13. The simulated DO are lower than the observations except for Julian day 285 for the surface layer. For the middle and bottom layers, the simulations are much lower than the observations. The measured DO values were between 2.2 mg/L and 14 mg/L and the simulations are from 0 to 8 mg/L for the middle layer. The simulated DO showed a similar pattern to that of the observations, but the simulated range was much lower.

Figure 4.2.1.14 shows the simulated and measured Chla. Although the range of the simulations is very wide and is similar to that of the observations, the trends of the simulations and observations are different. The largest difference between the measured and observed Chla is about 350 $\mu\text{g/L}$ at the beginning of the simulation. The simulated Chla increase faster than the observations at the beginning of the culture season. At the end of the simulation, the simulations and the observations show better agreement but a number of measured values were outside the simulated range.

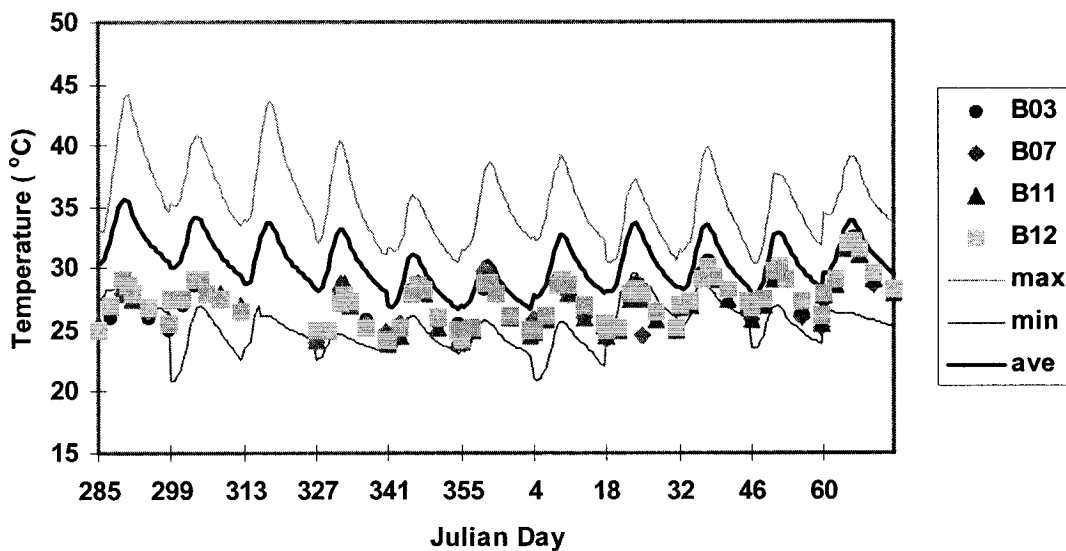


Figure 4.2.1.8. Temperature of surface layer for Treatment 2 for the Thailand site

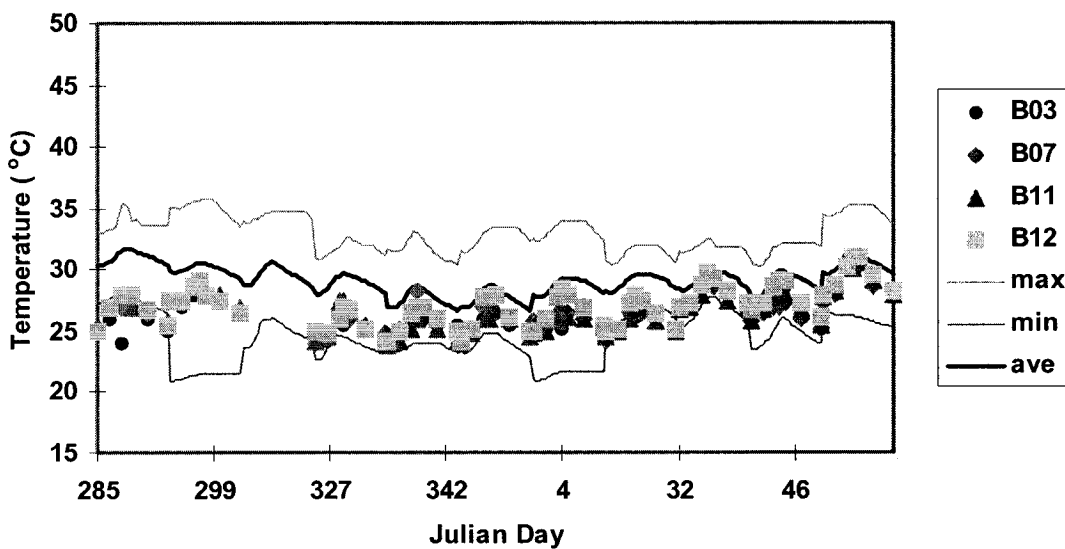


Figure 4.2.1.9. Temperature of middle layer for Treatment 2 for the Thailand site

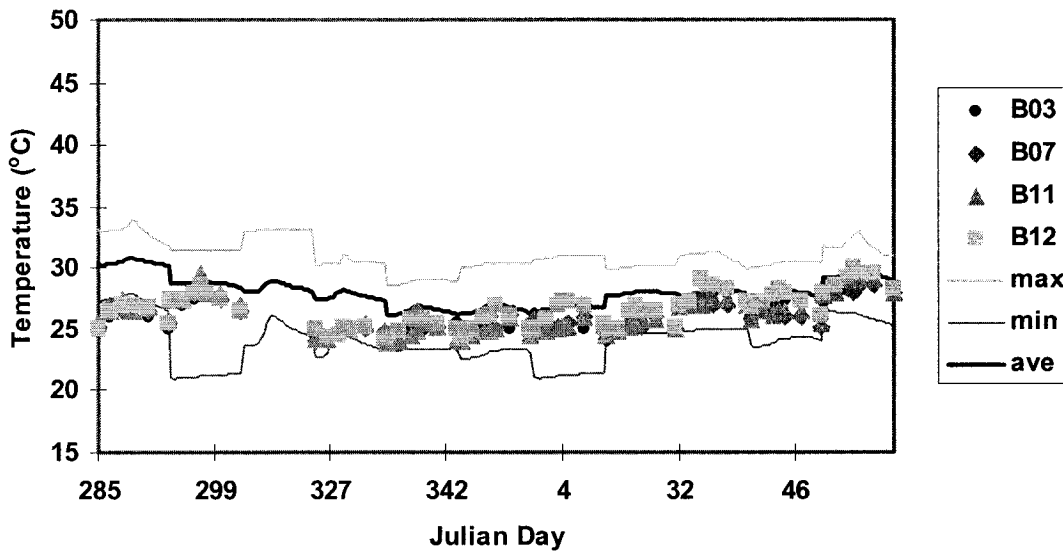


Figure 4.2.1.10. Temperature of bottom layer for Treatment 2 for the Thailand site

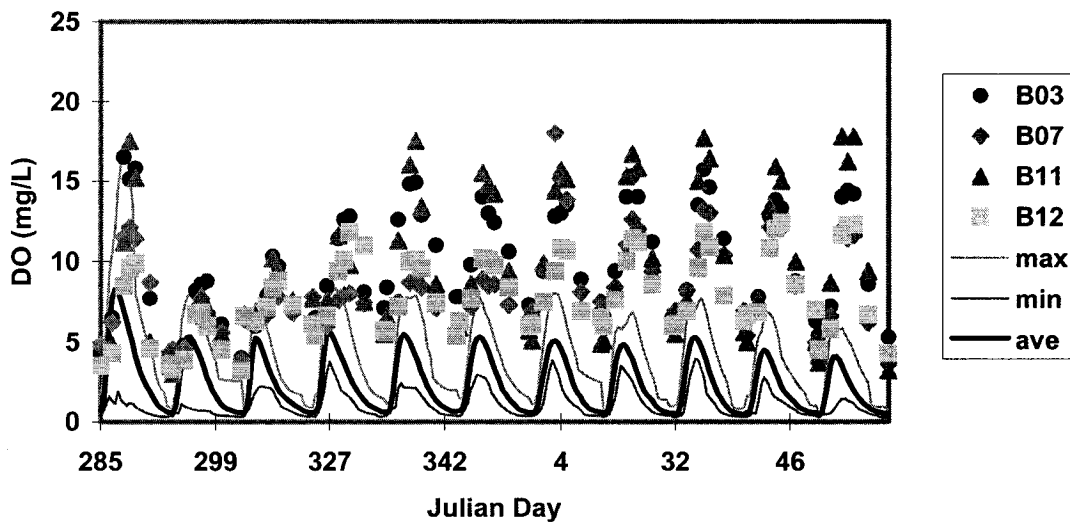


Figure 4.2.1.11. Surface layer DO for Treatment 2 for the Thailand site

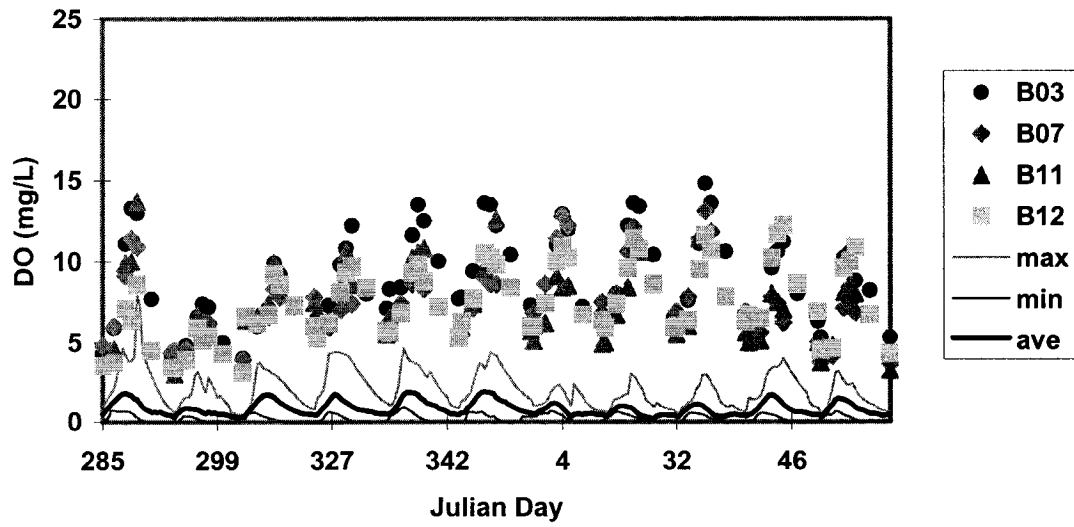


Figure 4.2.1.12. Middle layer DO for Treatment 2 for the Thailand site

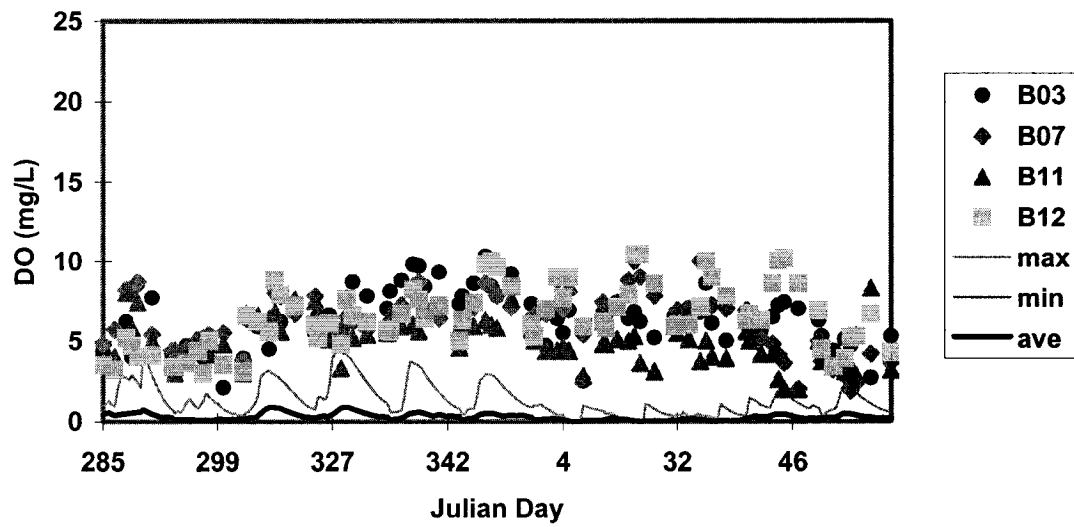


Figure 4.2.1.13. Bottom layer DO for Treatment 2 for the Thailand site

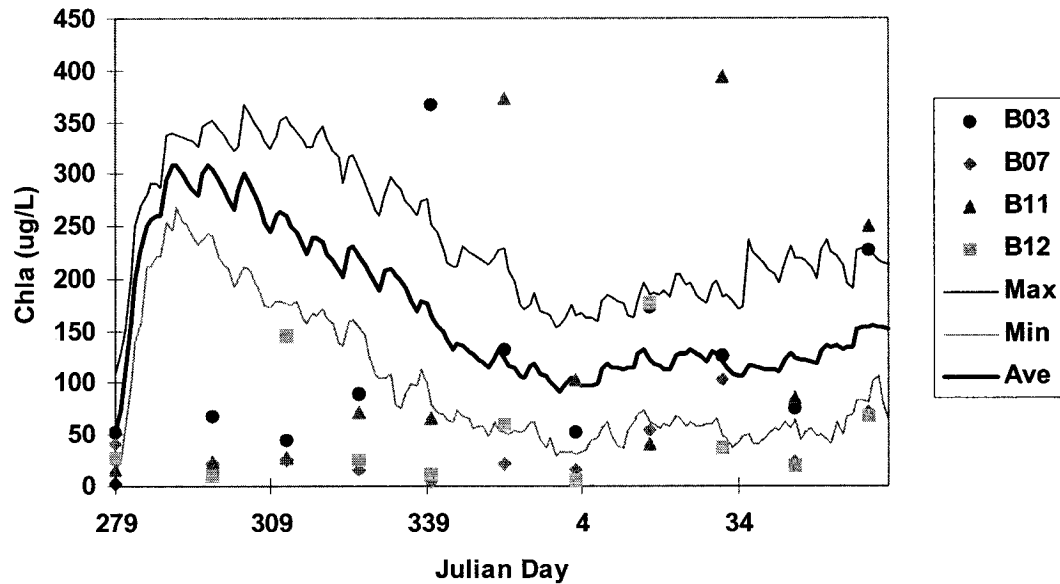


Figure 4.2.1.14. Chlorophyll a for Treatment 2 for the Thailand site

4.2.1.3. Validation Run (Treatment 3: 200 kg/ha/wk chicken manure and 48.6 kg/ha/wk urea)

Figures 4.2.1.15 to 4.2.1.17 show the water temperature for the three layers under Treatment 3. The simulated average water temperatures are higher than the observations for the surface layer. For the middle and bottom layers, the simulations are close to the observations at the end of the simulation.

Figures 4.1.18 to 4.1.20 show the simulated and observed DO for the surface, middle, and bottom layers, respectively. For the surface layer, the simulations are much better than the simulations in Treatments 1 and 2. The simulations cover most of observations

except for the last two sampling days. For the middle and bottom layers, many observations were beyond the simulated ranges, especially for the second half of the simulations.

Figure 4.2.1.21 shows that the pattern of the simulated Chla is different from that of the observations. At the beginning, the simulated Chla is higher than measured values, but this pattern is reversed towards the end of the simulation. As in the case of Treatments 1 and 2, there are large variations among replicates.

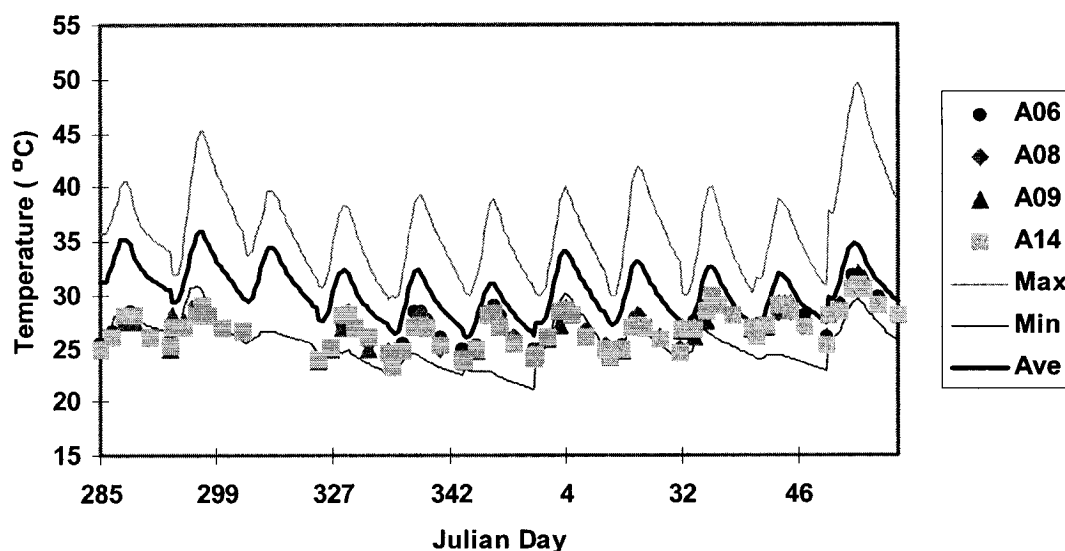


Figure 4.2.1.15. Temperature of surface layer for Treatment 3 for the Thailand site

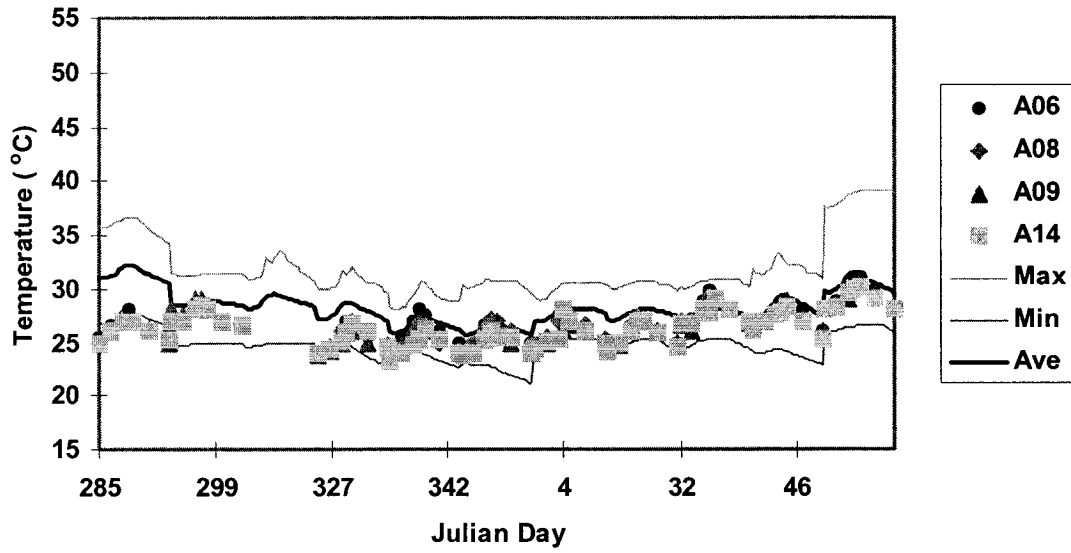


Figure 4.2.1.16. Temperature of middle layer for Treatment 3 for the Thailand site

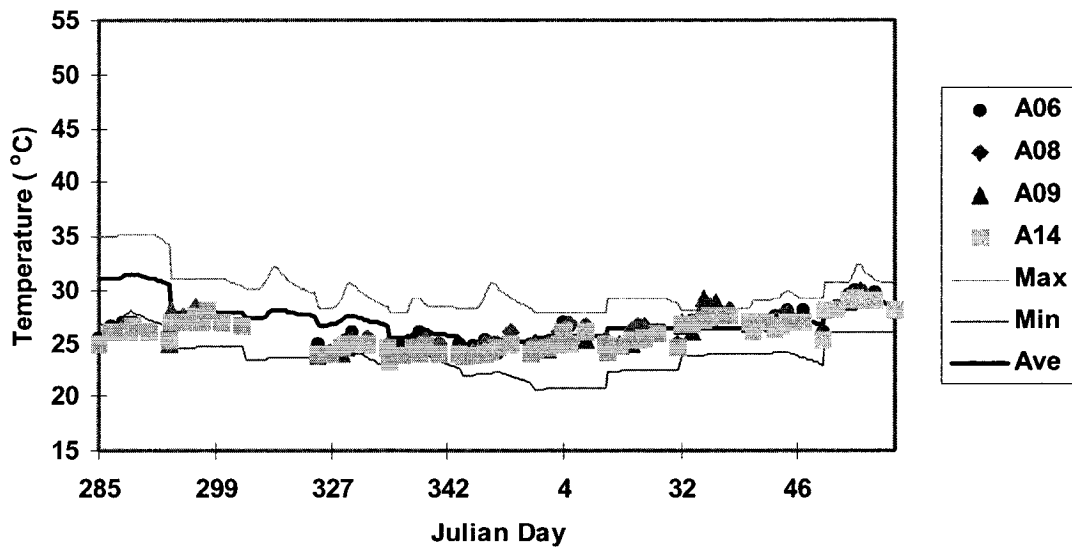


Figure 4.2.1.17. Temperature of bottom layer for Treatment 3 for the Thailand site

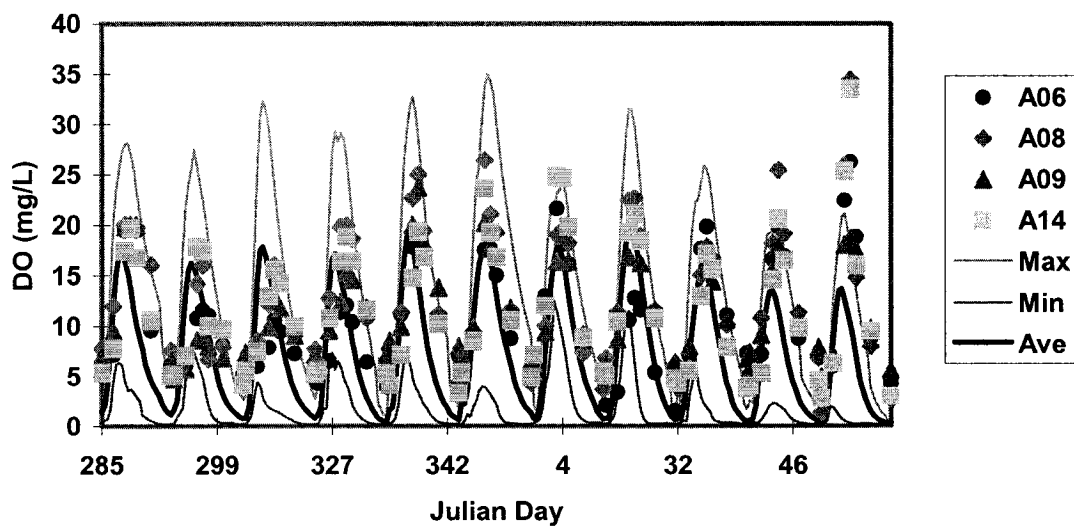


Figure 4.2.1.18. Surface layer DO for Treatment 3 for the Thailand site

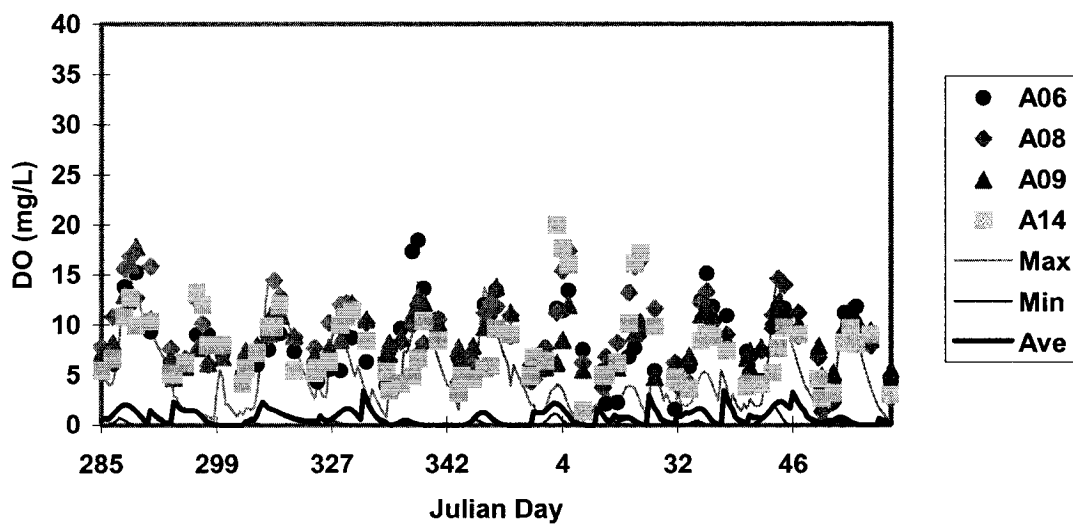


Figure 4.2.1.19. Middle layer DO for Treatment 3 for the Thailand site

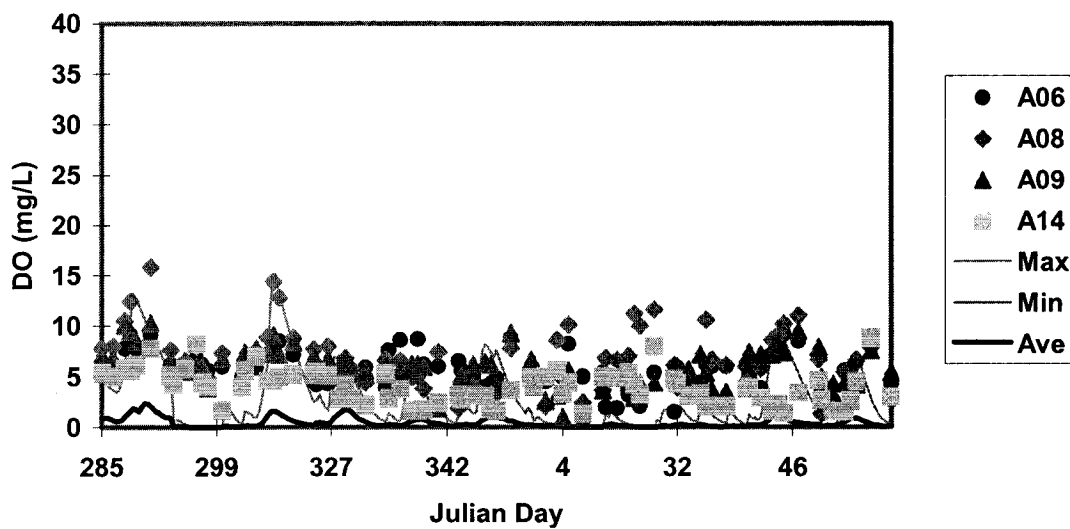


Figure 4.2.1.20. Bottom layer DO for Treatment 3 for the Thailand site

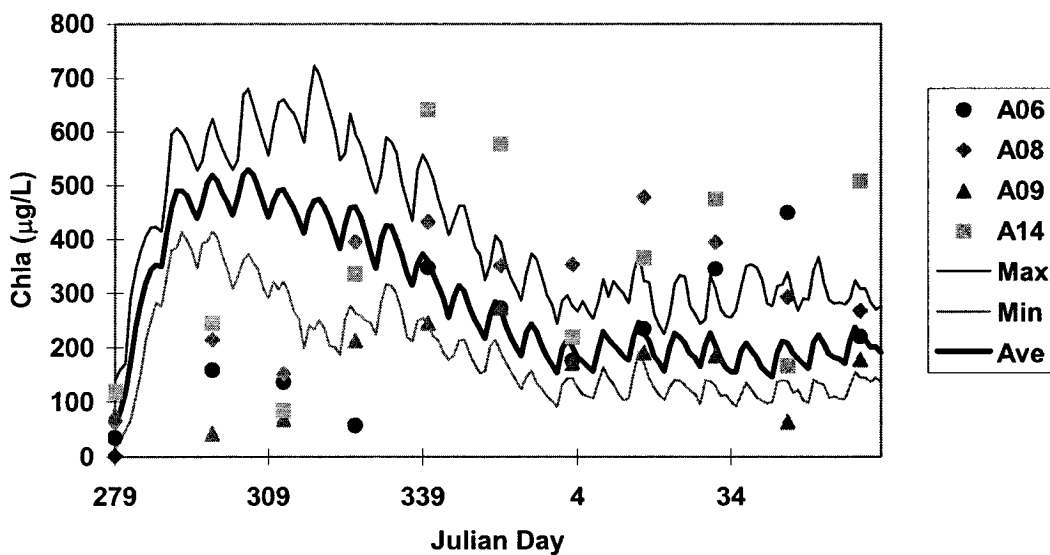


Figure 4.2.1.21. Chlorophyll a for Treatment 3 for the Thailand site

4.2.1.4. Frequency Distributions

The simulated water temperature and DO are presented as frequency distributions at different time periods. Frequency distributions are presented between 15 and 33°C with intervals of 2°C and DO from 0.5 to 19.5 mg/L with intervals of 1 mg/L. Figures 4.2.1.22 to 4.2.1.27 show the frequency distributions of water temperature and DO for the three layers. The frequencies are shown for six time periods, 6:00, 10:00, 14:00, 18:00, and 22:00. The distributions show that the probability of having a temperature below 21°C at the surface layer is almost zero during all time periods. The highest frequency for surface temperature over 33°C occurs at 14:00 and 18:00, while lower frequencies of surface temperatures over 33°C are at 6:00 and 10:00. (Figure 4.2.1.22). For the middle layer, the temperature distributions are more uniform than for the surface layer. The temperature distribution for the bottom layer is more uniform than the middle layer's.

The distributions show that the probability of having DO below 1.5 mg/L for the three layers is the highest at 6:00, especially for the bottom layers (Figures 4.2.1.25 to 4.2.1.27). The frequency distributions show a probability of having DO over 19 mg/L for the surface layer but there is zero probability for the middle and bottom layers.

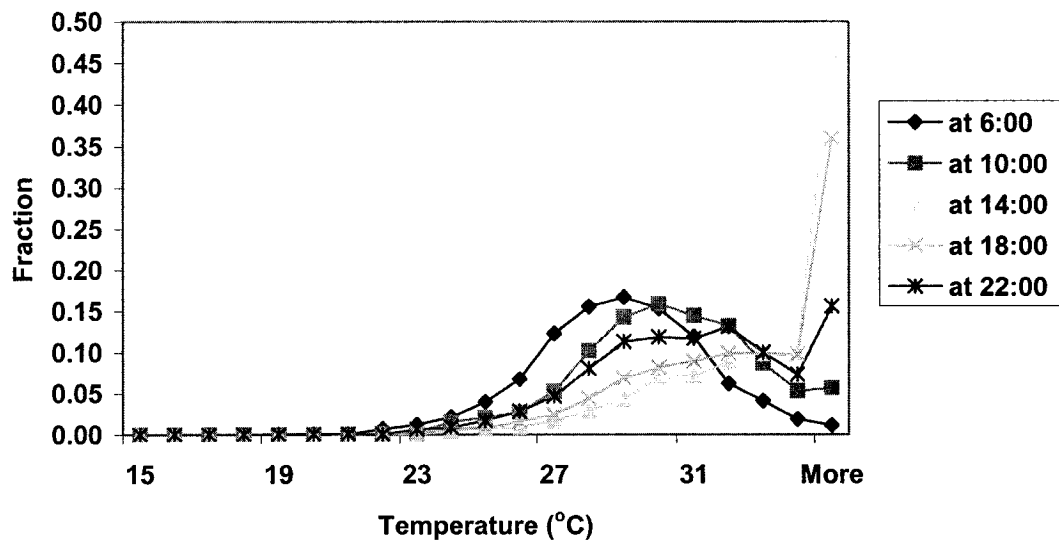


Figure 4.2.1.22. Frequency distributions for surface layer temperature (Treatment 1, Thailand site)

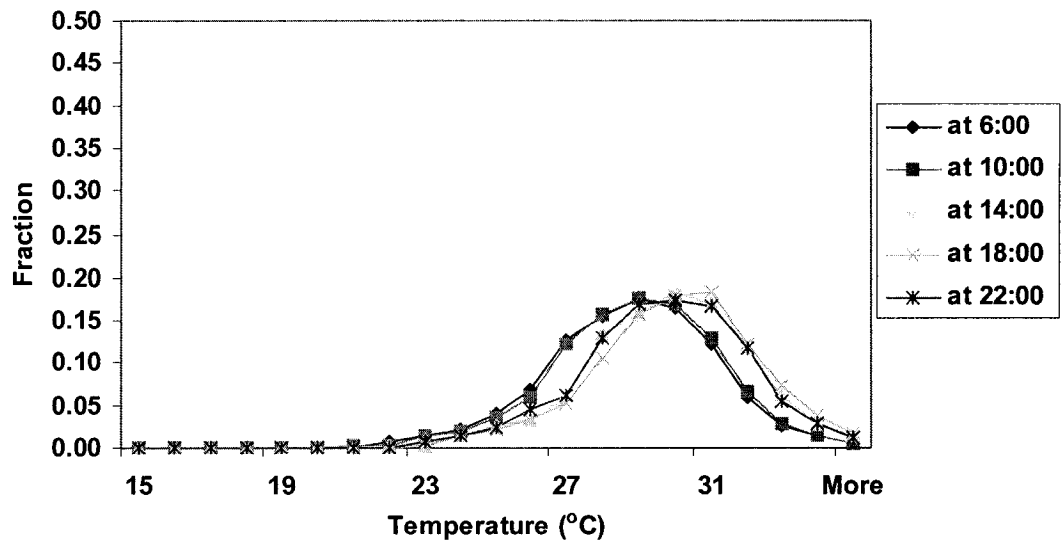


Figure 4.2.1.23. Frequency distributions for middle layer temperature (Treatment 1, Thailand site)

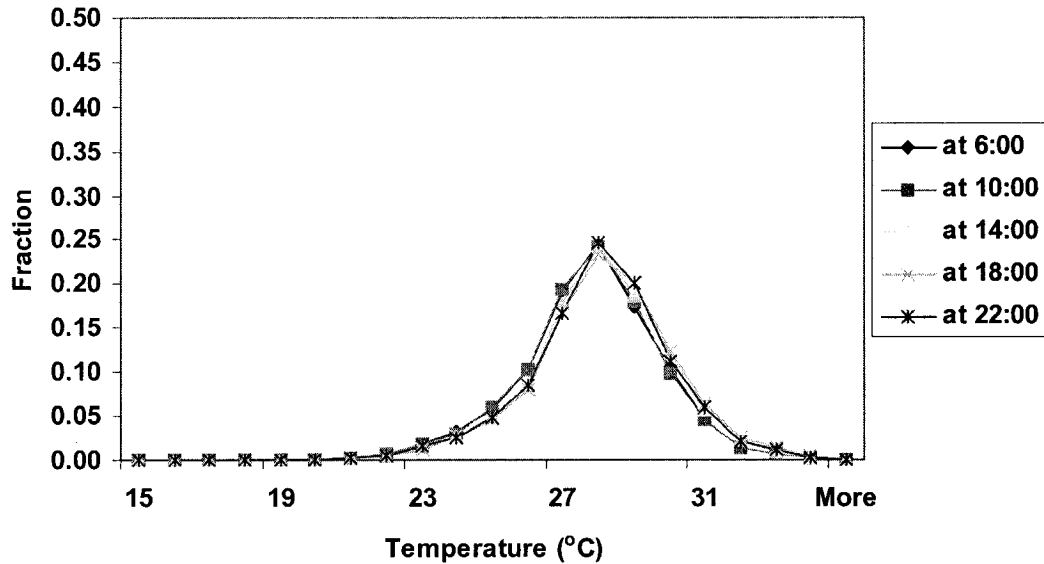


Figure 4.2.1.24. Frequency distributions for bottom layer temperature (Treatment 1, Thailand site)

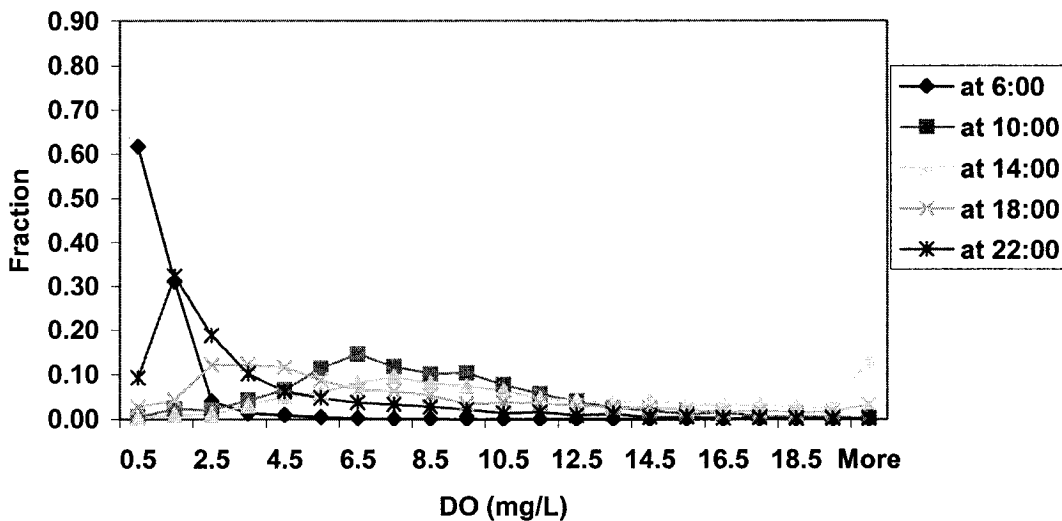


Figure 4.2.1.25. Frequency distributions for surface layer DO (Treatment 1, Thailand site)

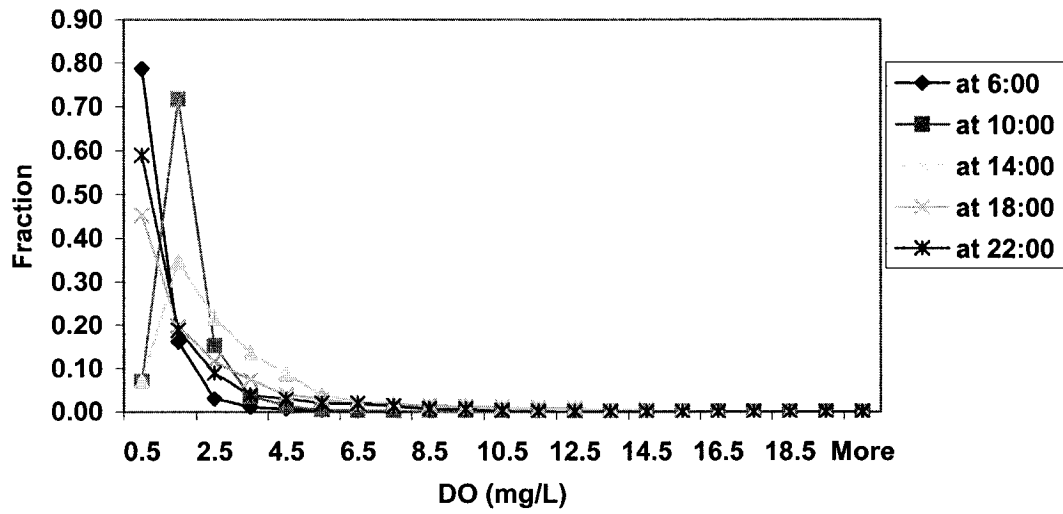


Figure 4.2.1.26. Frequency distributions for middle layer DO (Treatment 1, Thailand site)

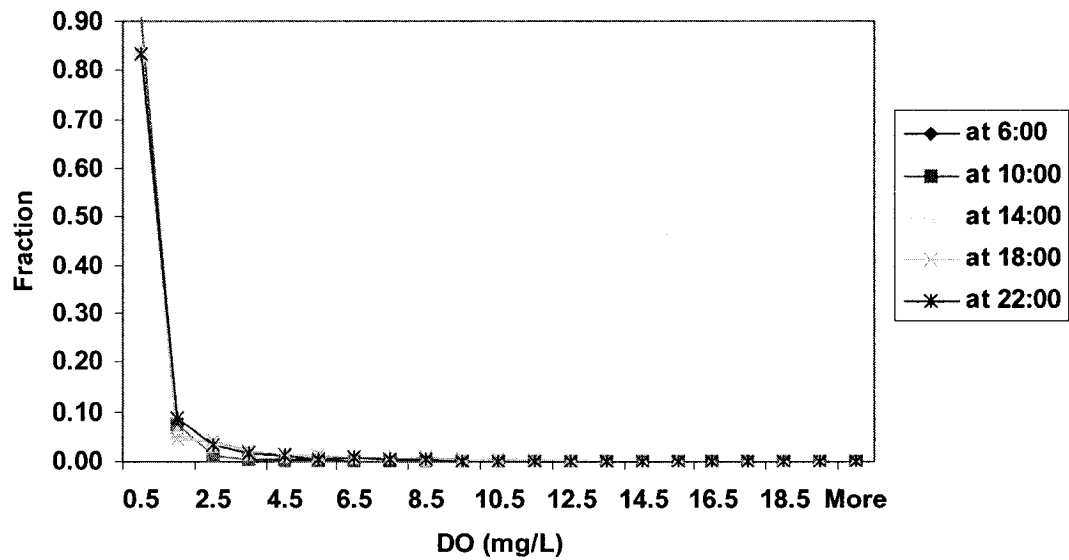


Figure 4.2.1.27. Frequency distributions for bottom layer DO (Treatment 1, Thailand site)

4.2.2. Rwanda Site

The selected experiment (H403) from the Rwanda site was designed to determine the effect of fertilization on water quality and fish growth. Four treatments were used for the model calibration and validation (Table 4-2). In Treatments 1, 2, and 3, a mixture of chicken manure and fresh cut grass was applied at the rates of 500, 750, and 1000 kg/ha/wk, respectively. The mixture ratio was 20:80 for the chicken manure and fresh cut grass on a dry weight basis. The ponds in Treatment 4 received the same amount of mixture as in Treatment 1 with additional urea to double the amount of total nitrogen added with respect to Treatment 1. The model simulation starts on Julian day 125 for a period of 150 days. The initial input values are listed in Table 4-3. The simulated water temperature, DO, and Chla for the three layers are compared to the observations on the diurnal sampling days (Julian day 146, 201, and 264). The frequency distributions of the water temperature and DO at the three layers are also presented.

4.2.2.1. Calibration Run (Treatment 1: 100 kg/ha/wk chicken manure and 400 kg/ha/wk grass)

Figures 4.2.2.1 to 4.2.2.3 display good agreement between the simulations and observations for the surface, middle, and bottom layers. Figures 4.2.2.4 to 4.2.2.6 illustrate the simulated and observed DO for the three layers. The simulated DO had good agreement with measurements for the surface layer. However, the simulated DO were lower than the observations on Julian days 146 and 264 for the middle and bottom layers. On Julian day 201, the simulations agreed with most of the data for the middle and bottom layers. Figure 4.2.2.7 shows the comparison of the simulated and observed

chlorophyll a. The simulations missed the peak values of pond C03 and D07. In general, the model simulation is close to the measured Chla from pond C07.

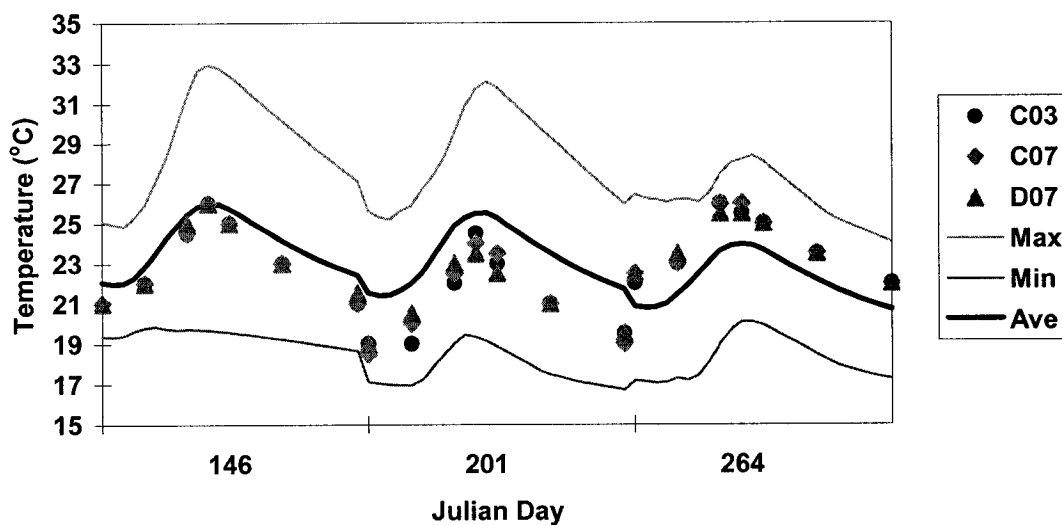


Figure 4.2.2.1. Temperature of surface layer for Treatment 1 for the Rwanda site

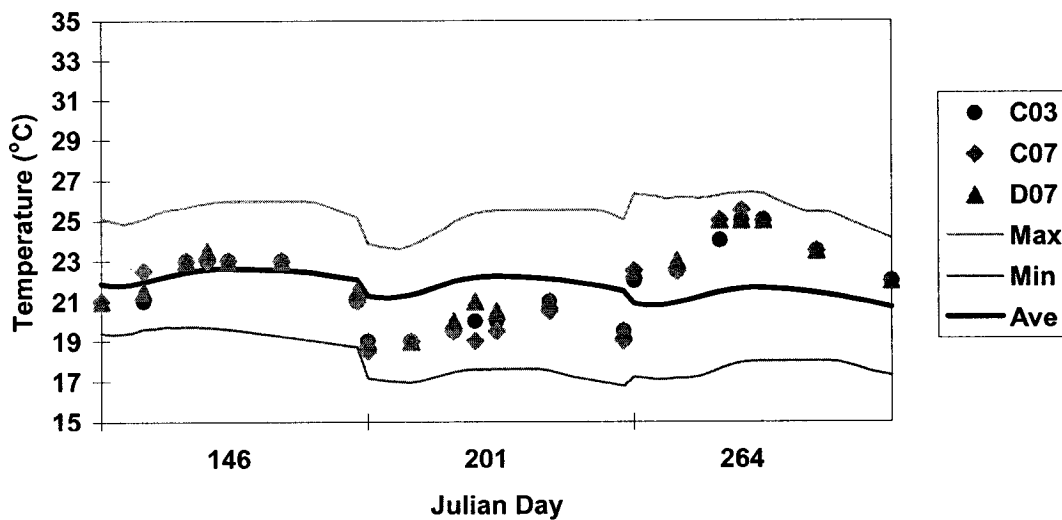


Figure 4.2.2.2. Temperature of middle layer for Treatment 1 for the Rwanda Site

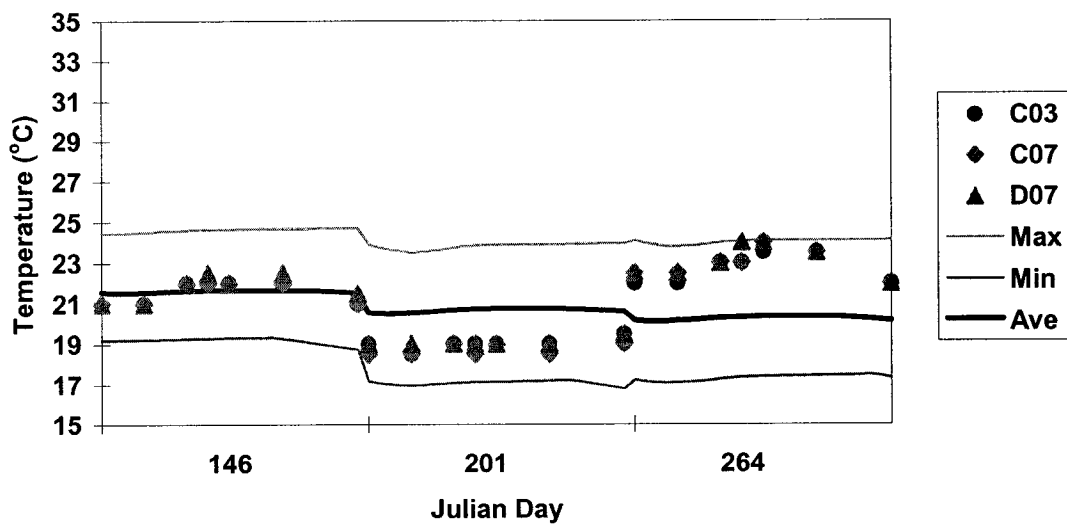


Figure 4.2.2.3. Temperature of bottom layer for Treatment 1 for the Rwanda site

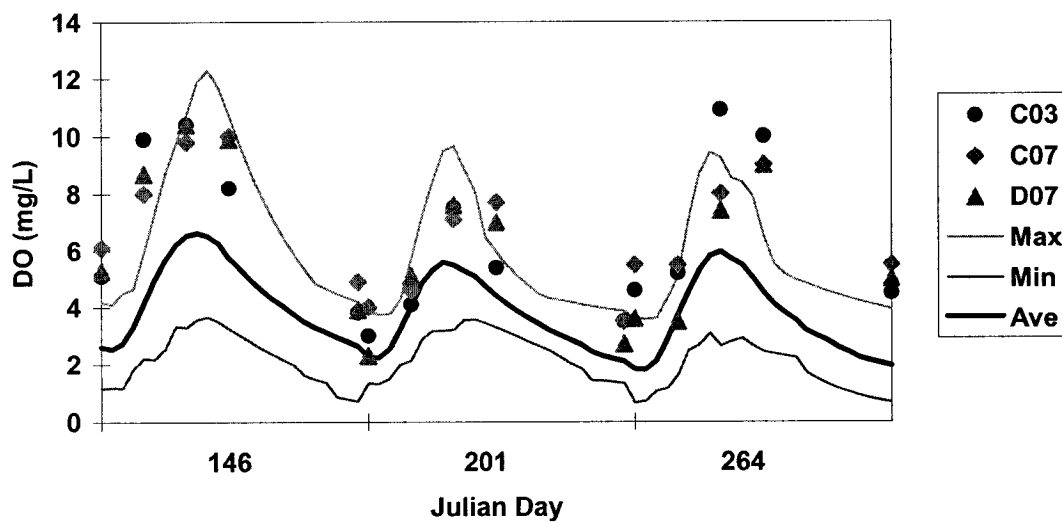


Figure 4.2.2.4. Surface layer DO for Treatment 1 for the Rwanda site

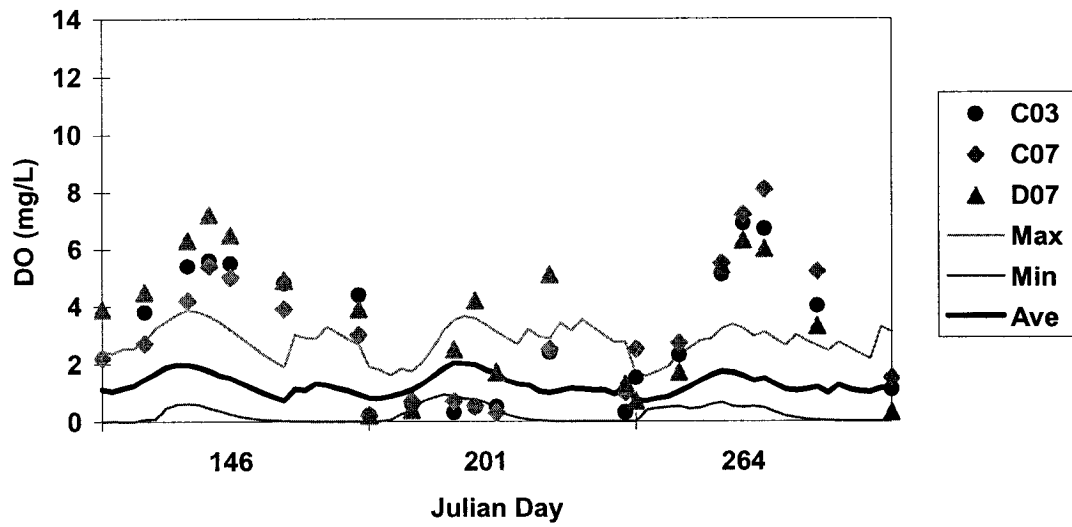


Figure 4.2.2.5. Middle layer DO for Treatment 1 for the Rwanda site

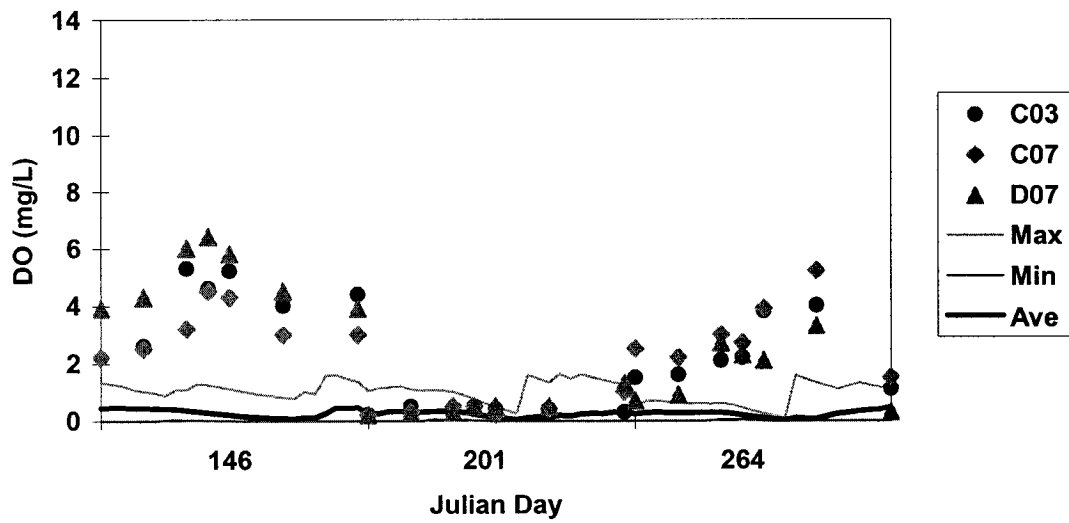


Figure 4.2.2.6. Bottom layer DO for Treatment 1 for the Rwanda site

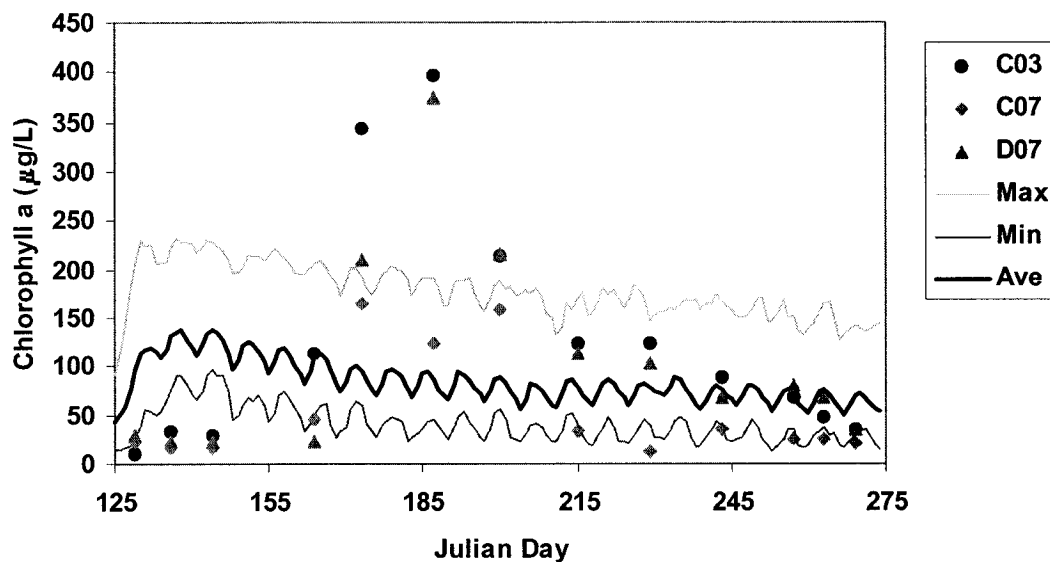


Figure 4.2.2.7. Chlorophyll a for Treatment 1 for the Rwanda site

4.2.2.2. Validation Run (Treatment 2: 150 kg/ha/wk chicken manure and 600 kg/ha/wk grass)

Treatment 2 simulations are closer to the corresponding measured values than Treatment 1. Most of the measured temperature values for the three layers are within the range of the simulated values (Figures 4.2.2.8 to 4.2.2.10). Only a couple of data points are below the simulated minimum values on Julian day 201 for the bottom layer.

Figures 4.2.2.11 to 4.2.2.13 show the simulated and observed DO for the three layers.

The simulated average DO values are slightly higher than the data for the surface layer.

For the middle layer, the maximum simulated DO values are below most of the data for pond #D11 but higher than data for the other two ponds. For the bottom layer, the observed DO values are higher than the simulations on Julian day 146 but within the simulation ranges on the other two days. The highest observed DO at the bottom layer was 4.5 mg/L but the simulated maximum DO was about 2 mg/L for the bottom layer.

The simulated Chla trend also is different from the observations (Figure 4.2.2.14). The best agreement between simulated and measured value is obtained at the end of the simulation period, when there are only a few data points outside of the maximum range. There were large differences between data from replicate ponds on Julian day 263, when the values were 343 $\mu\text{g/L}$ and 124 $\mu\text{g/L}$ from ponds D11 and C06, respectively.

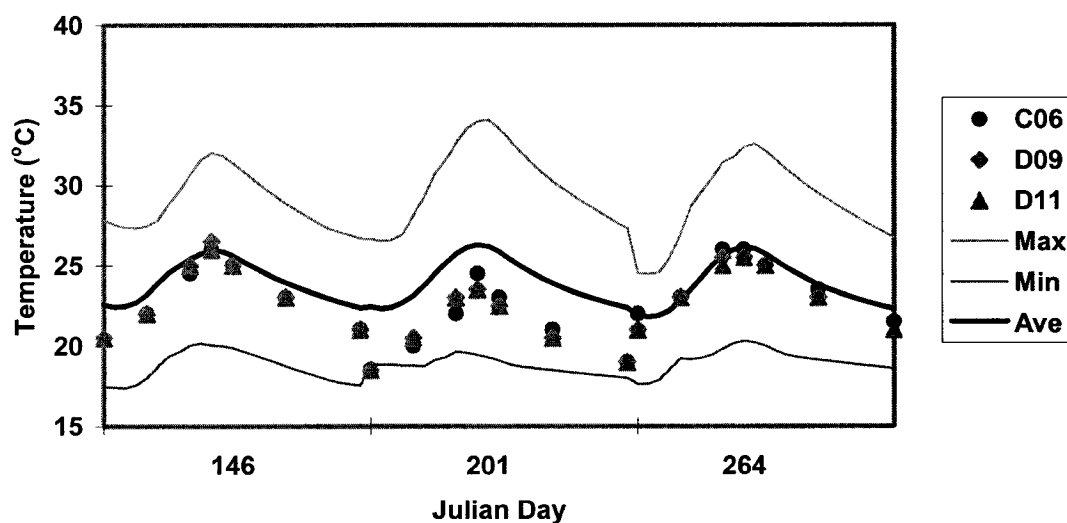


Figure 4.2.2.8. Temperature of surface layer for Treatment 2 for the Rwanda site

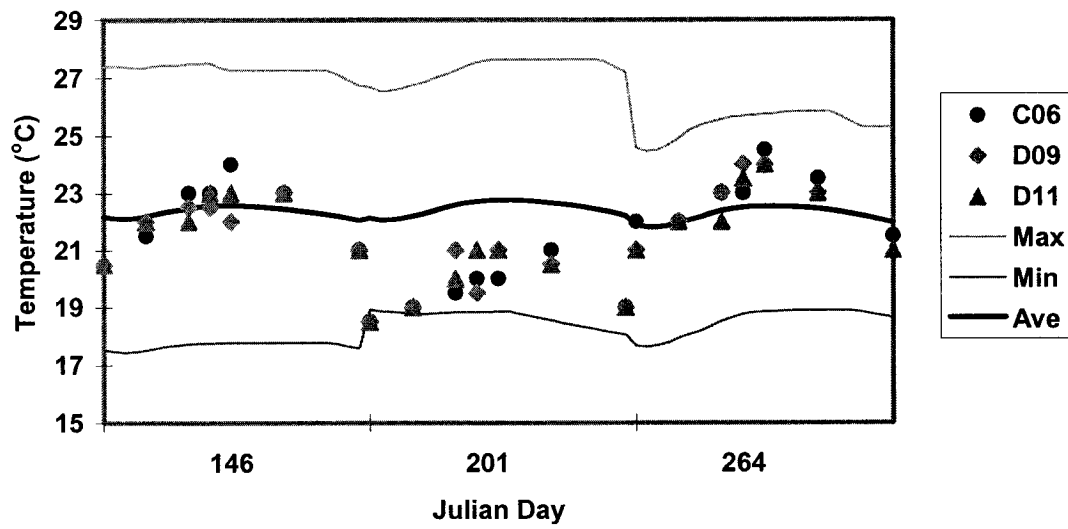


Figure 4.2.2.9. Temperature of middle layer for Treatment 2 for the Rwanda site

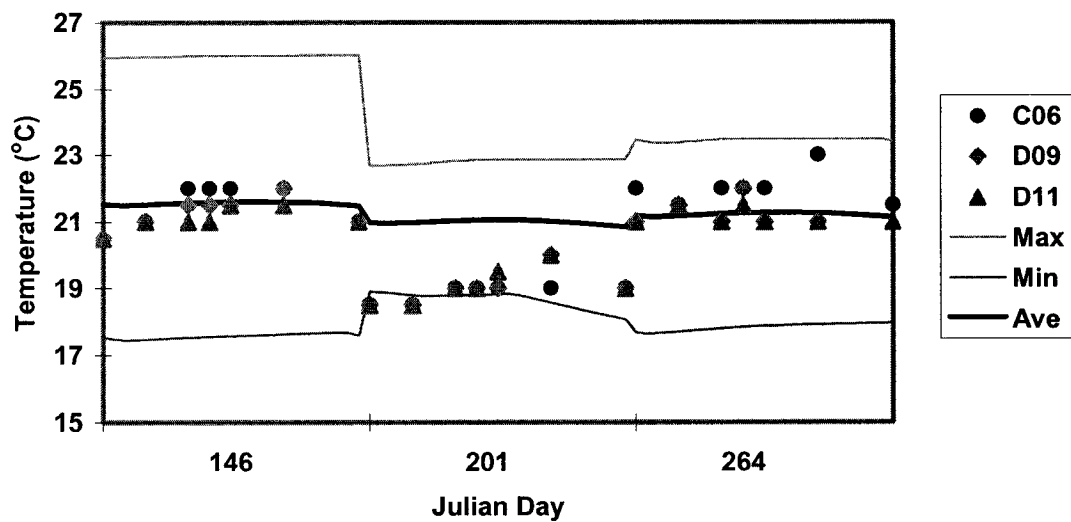


Figure 4.2.2.10. Temperature of bottom layer for Treatment 2 for the Rwanda site

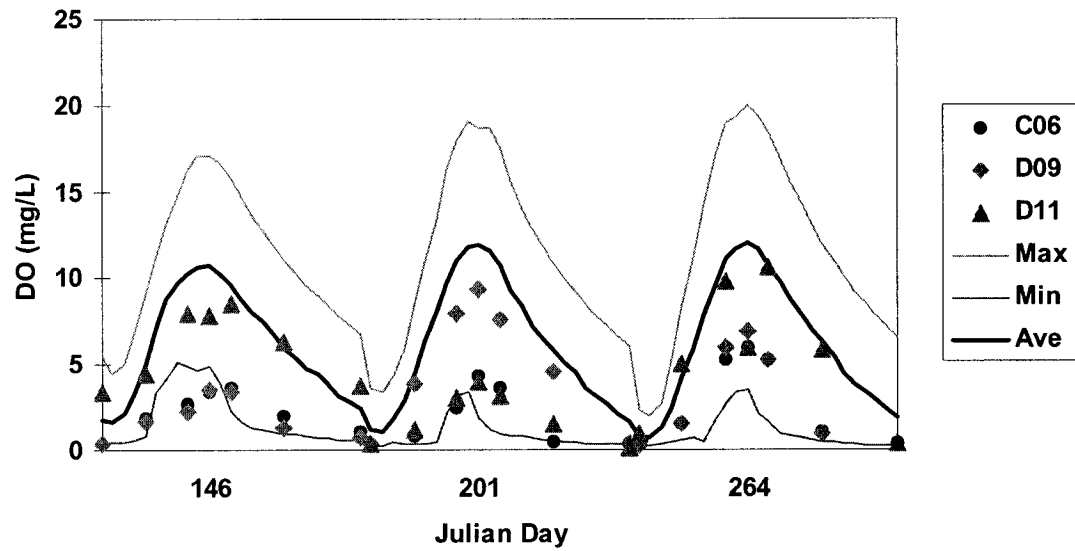


Figure 4.2.2.11. Surface layer DO for Treatment 2 for the Rwanda site

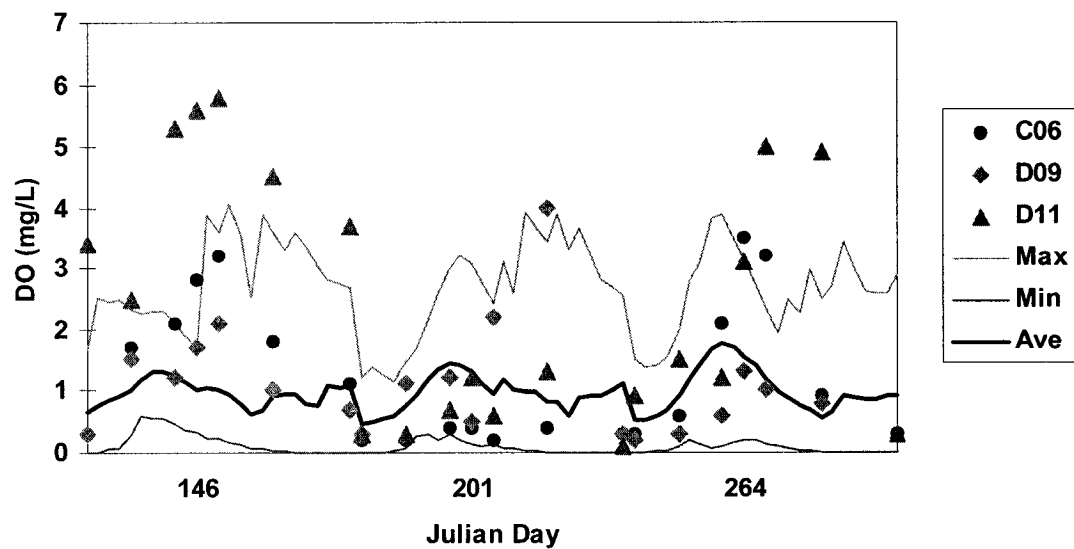


Figure 4.2.2.12. Middle layer DO for Treatment 2 for the Rwanda site

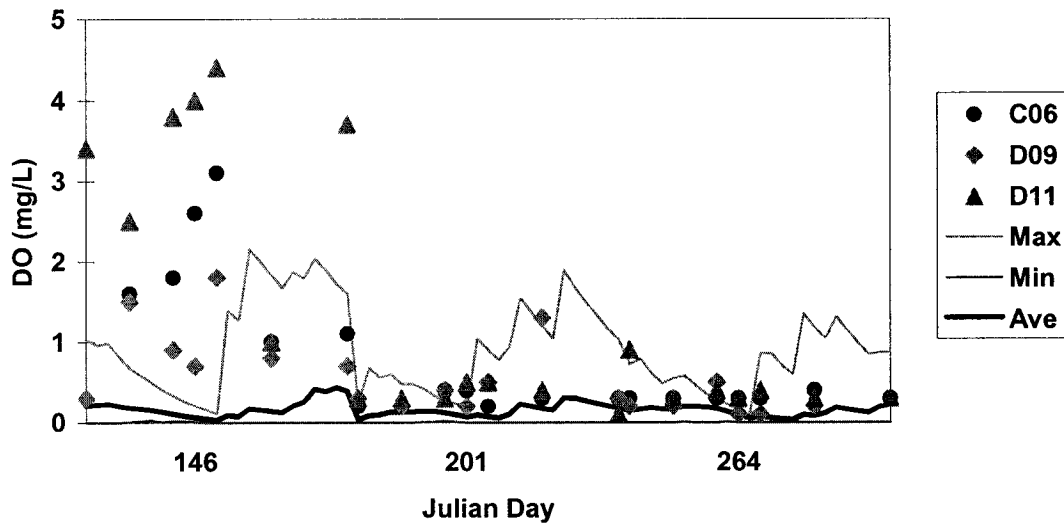


Figure 4.2.2.13. Bottom layer DO for Treatment 2 for the Rwanda site

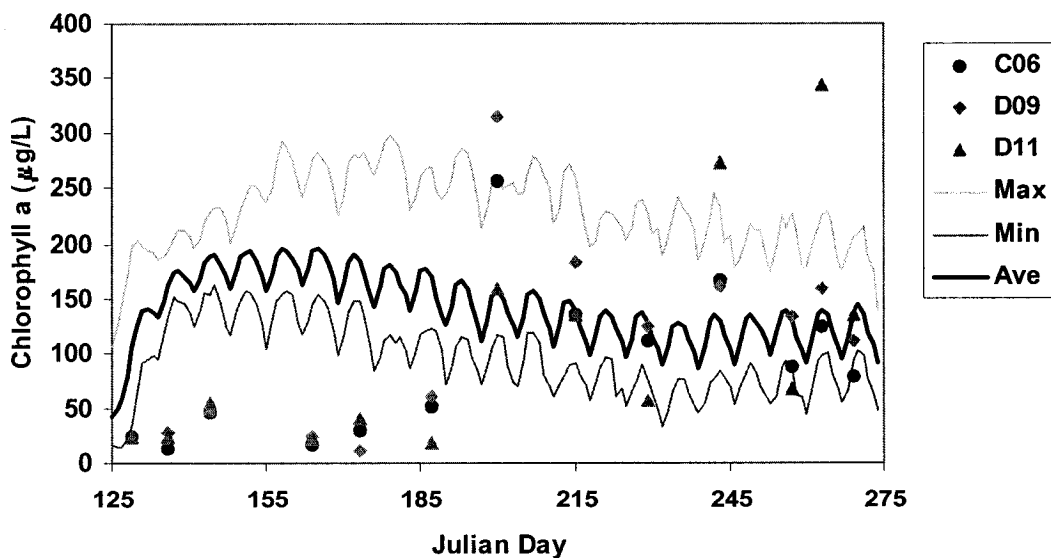


Figure 4.2.2.14. Chlorophyll a for Treatment 2 for the Rwanda site

4.2.2.3. Validation Run (Treatment 3: 200 kg/ha/wk chicken manure and 800 kg/ha/wk grass)

The measured water temperatures are within the range of the simulated values for the surface layer (Figure 4.2.2.15). For the middle layer, the simulated values cover most of the data (Figure 4.2.2.16) with a few data points outside of the simulated range on Julian day 264. For the bottom layer, on Julian day 146 and 201, the simulated values cover the data but the data on Julian 264 are higher than the maximum simulated values (Figure 4.2.2.17).

Figures 4.2.2.18 to 4.2.2.20 show the simulated and observed DO for the three layers. The simulated DO cover most of the observations for the surface layer. The simulated DO values for the middle and bottom layers are lower than the measured data for all three days especially for day 264 on the bottom layer. The simulations show no clear diurnal profile for the bottom layer.

The simulated Chl_a concentration trend was different from the observations for the first two months but very close to the observations at the end of the simulation period (Figure 4.2.2.21). The simulations did not catch the peak value (about 700 µg/L for Pond D01). Overall, the concentrations are stable.

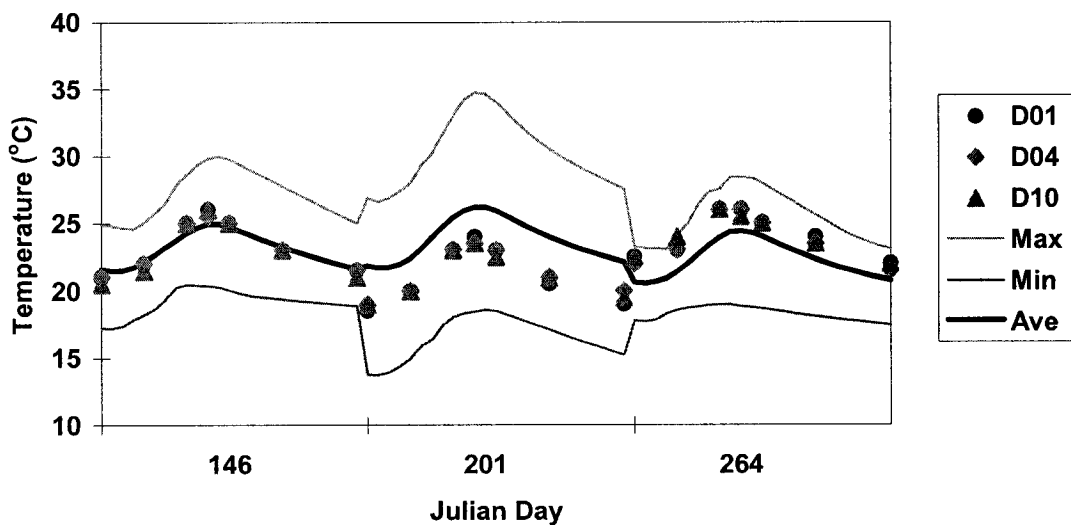


Figure 4.2.2.15 Temperature of surface layer for Treatment 3 for the Rwanda site

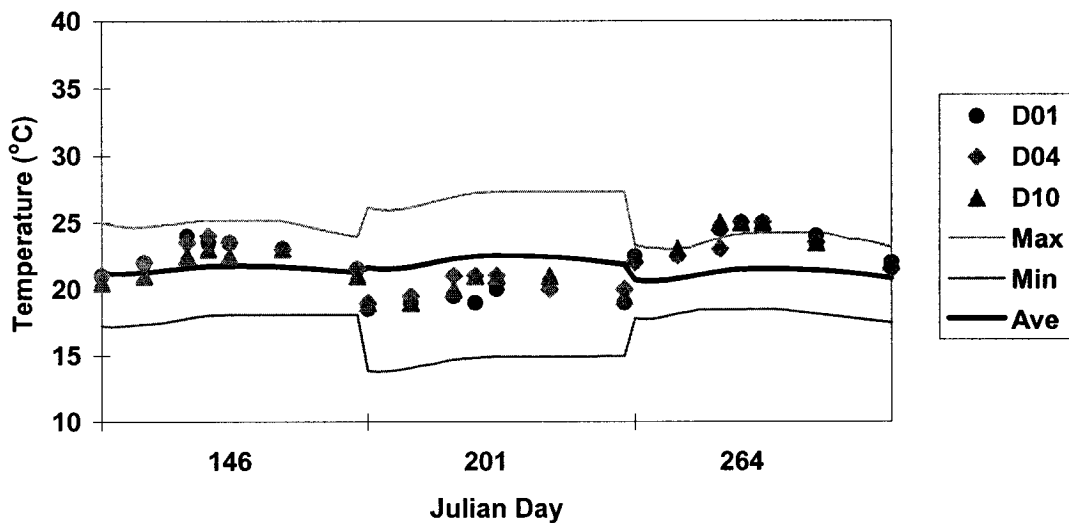


Figure 4.2.2.16. Temperature of middle layer for Treatment 3 for the Rwanda site

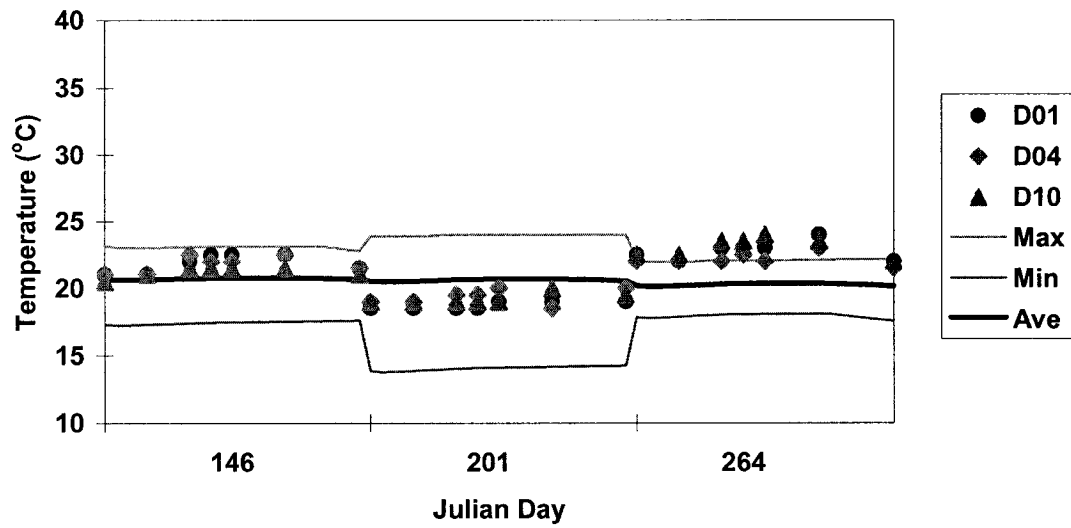


Figure 4.2.2.17. Temperature of bottom layer for Treatment 3 for the Rwanda site

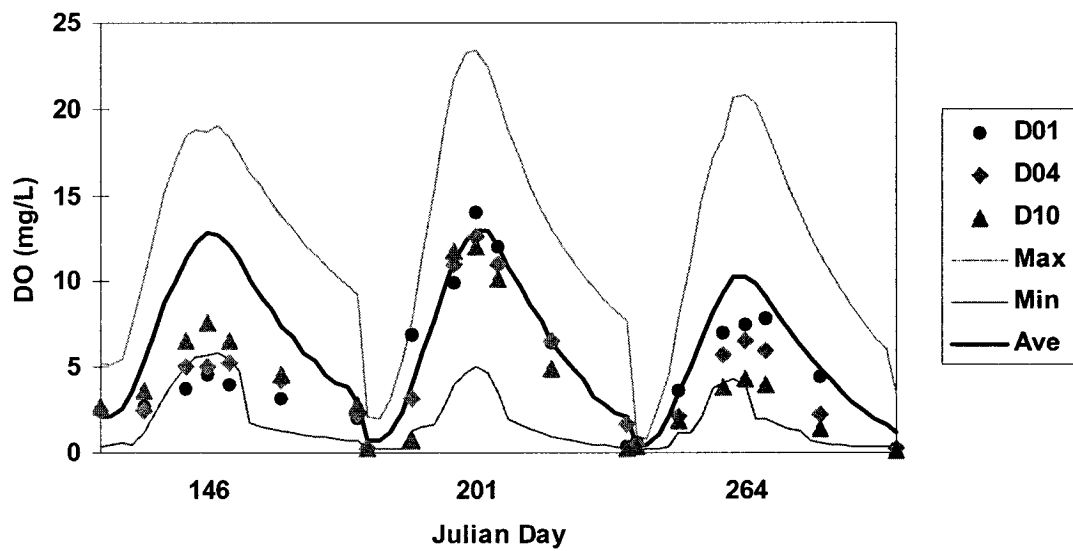


Figure 4.2.2.18. Surface layer DO for Treatment 3 for the Rwanda site

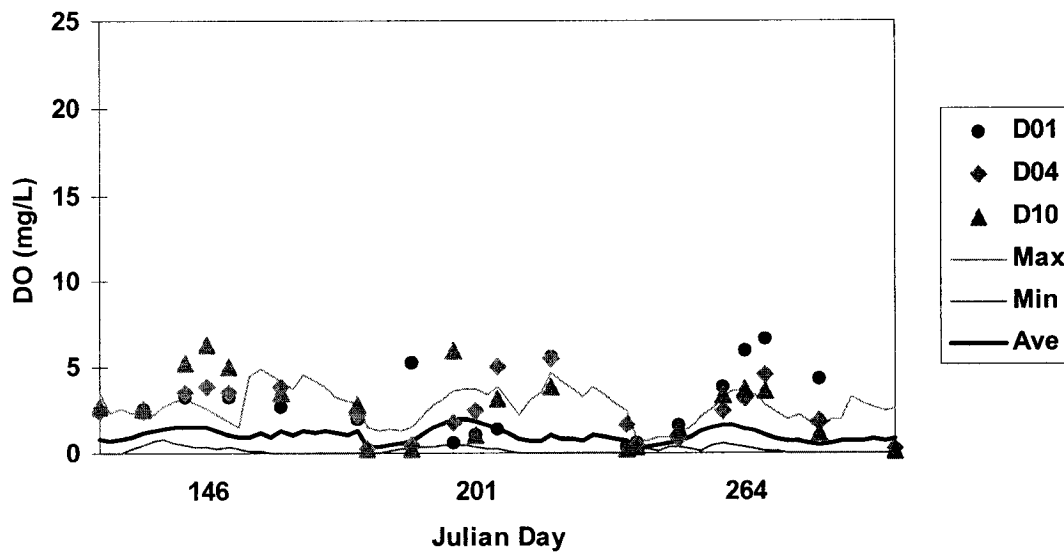


Figure 4.2.2.19. Middle layer DO for Treatment 3 for the Rwanda site

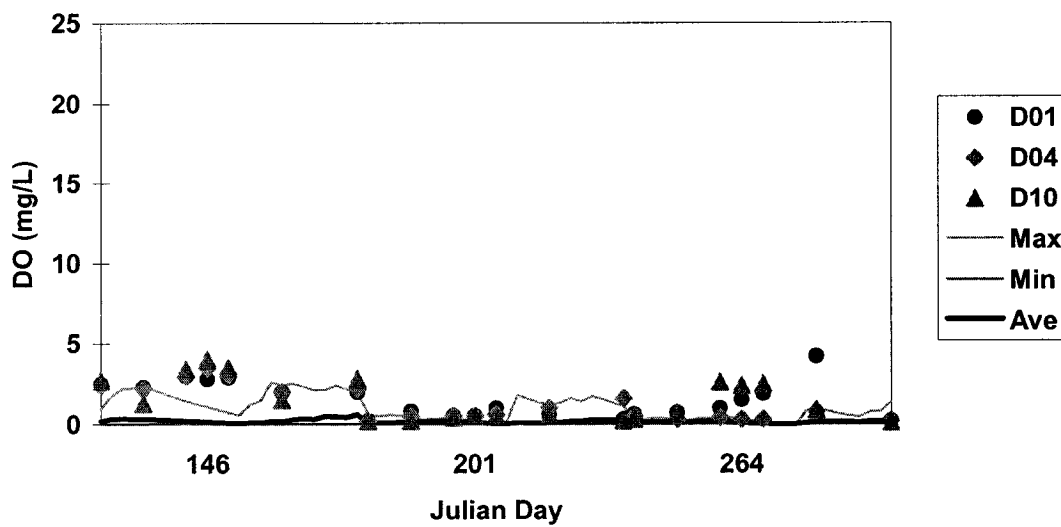


Figure 4.2.2.20a. Bottom layer DO for Treatment 3 for the Rwanda site

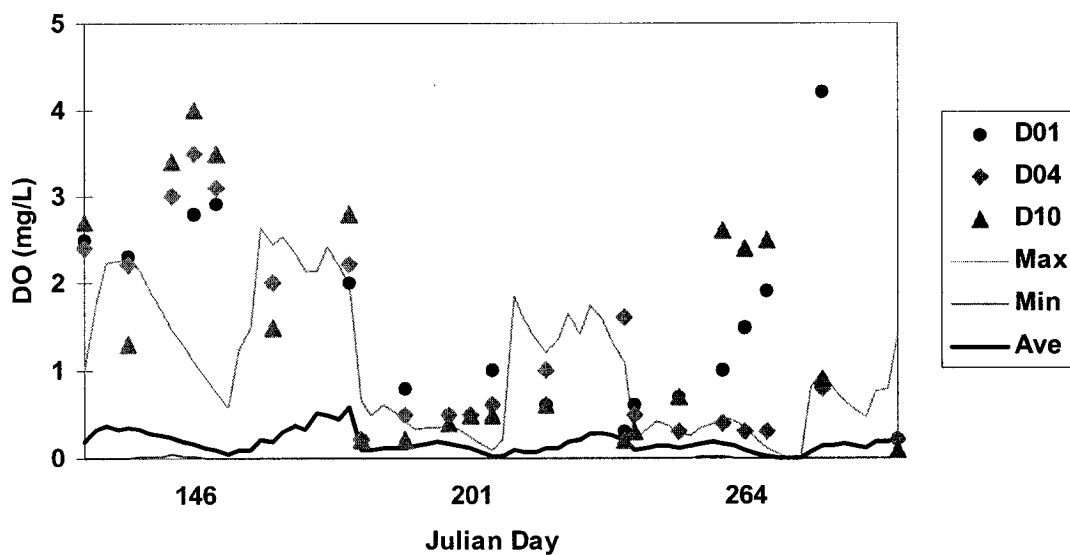


Figure 4.2.2.20b. Bottom layer DO for Treatment 3 for the Rwanda site (extended y-axis scale)

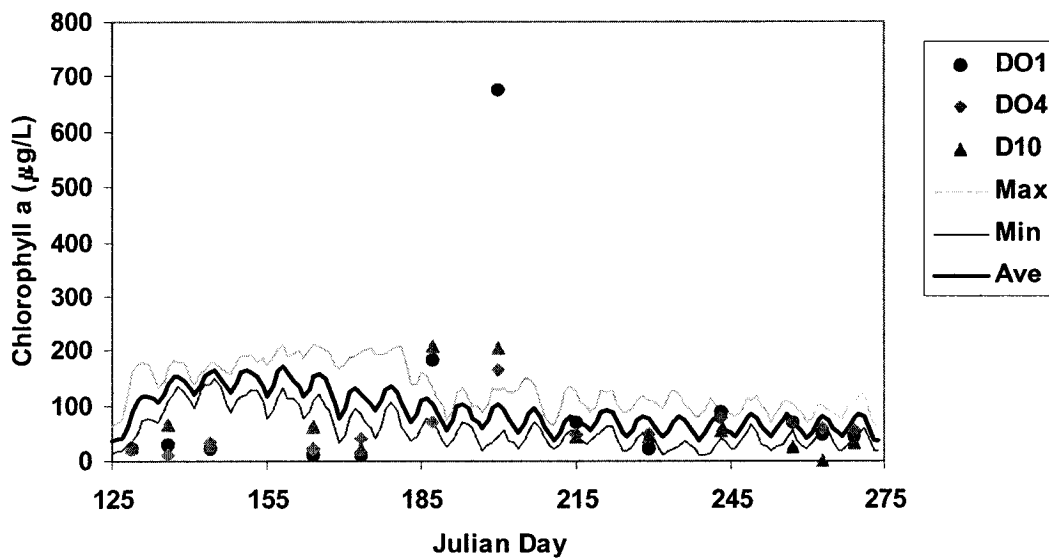


Figure 4.2.2.21. Chlorophyll a for Treatment 3 for the Rwanda site

4.2.2.4. Validation Run (Treatment 4: 100 kg/ha/wk chicken manure, 400 kg/ha/wk grass, and 28.6 kg/ha/wk urea)

Figures 4.2.2.22 to 4.2.2.24 show the simulated and observed water temperatures for the three layers. The simulations cover the measured data for the surface layer. For the middle and bottom layers, only a few observations are higher than the maximum simulations on Julian day 264.

The simulated DO values on Julian day 146 cover most observations for the surface layer even though the data for pond C08 are much lower than for the other two ponds (Figure 4.2.2.25). For the middle and bottom layers, the simulations are lower than the observations on Julian day 146 but cover most data for Julian day 201 and part of the data for Julian day 264 (Figures 4.2.2.26 to 4.2.2.27). The data had high variability for the middle and bottom layers.

The simulated Chl_a values were lower than the measured values for pond C05 and failed to capture the peak value of pond D06 on Julian day 200 (Figure 4.2.2.28). The simulation curves show much less variation than the observations.

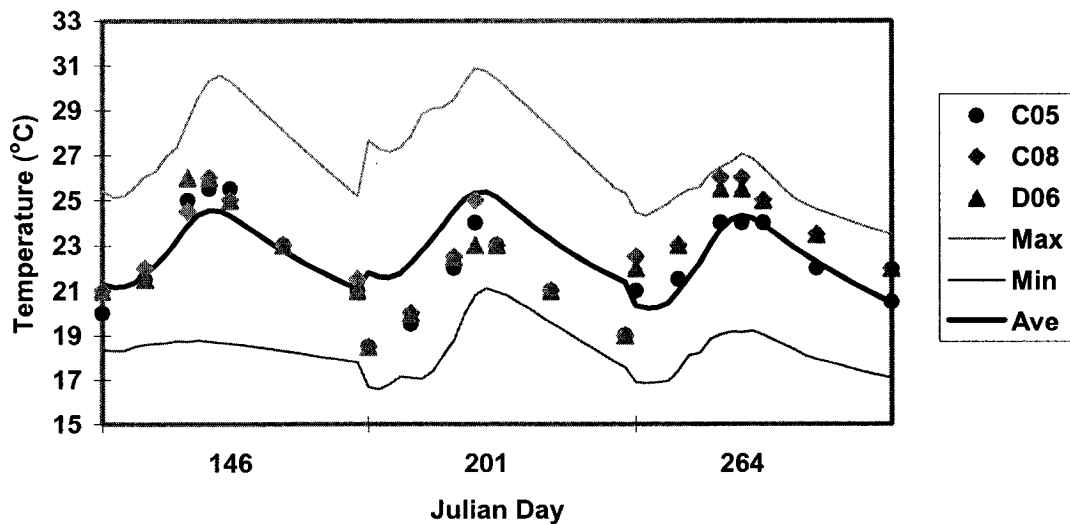


Figure 4.2.2.22. Temperature of surface layer for Treatment 4 for the Rwanda site

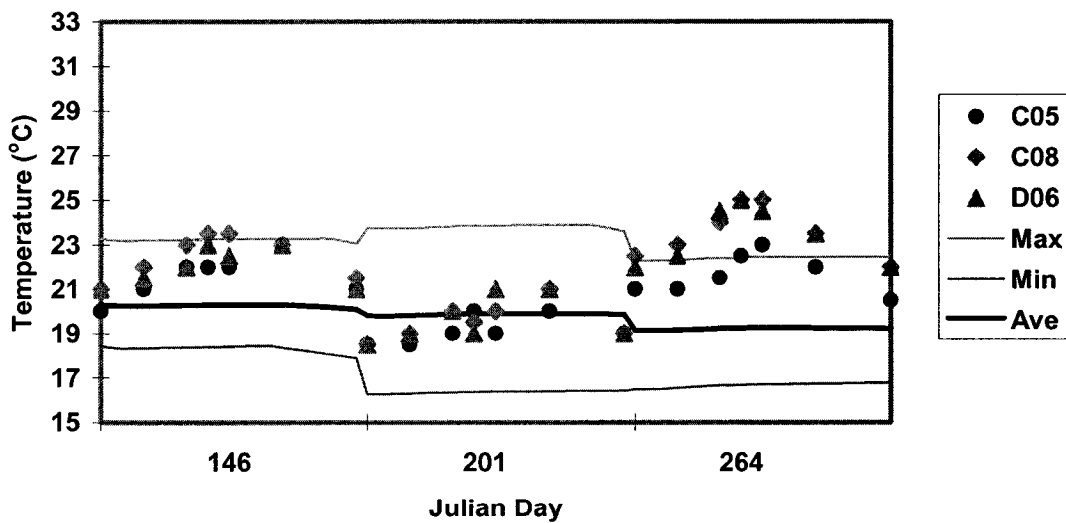


Figure 4.2.2.23. Temperature of middle layer for Treatment 4 for the Rwanda site

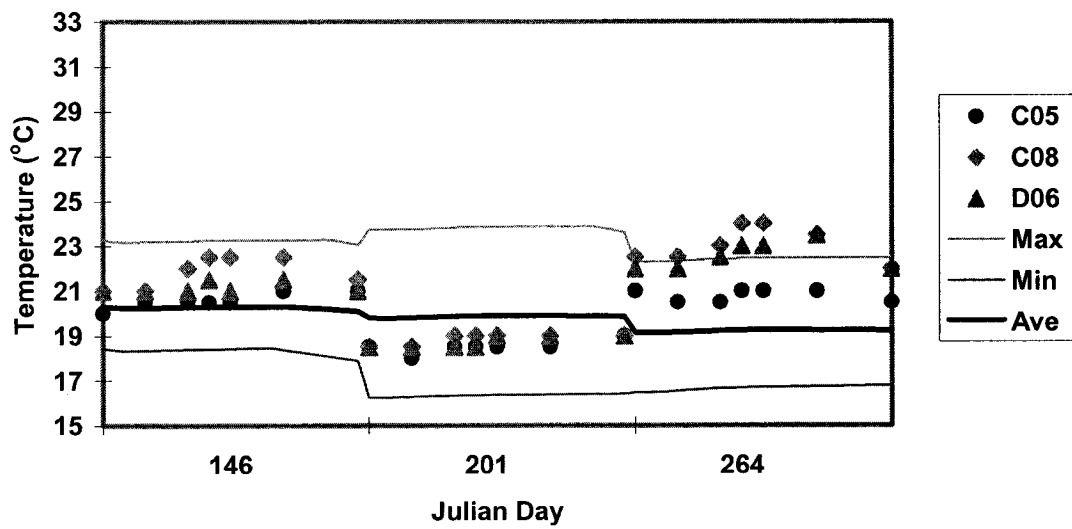


Figure 4.2.2.24. Temperature of bottom layer for Treatment 4 for the Rwanda site

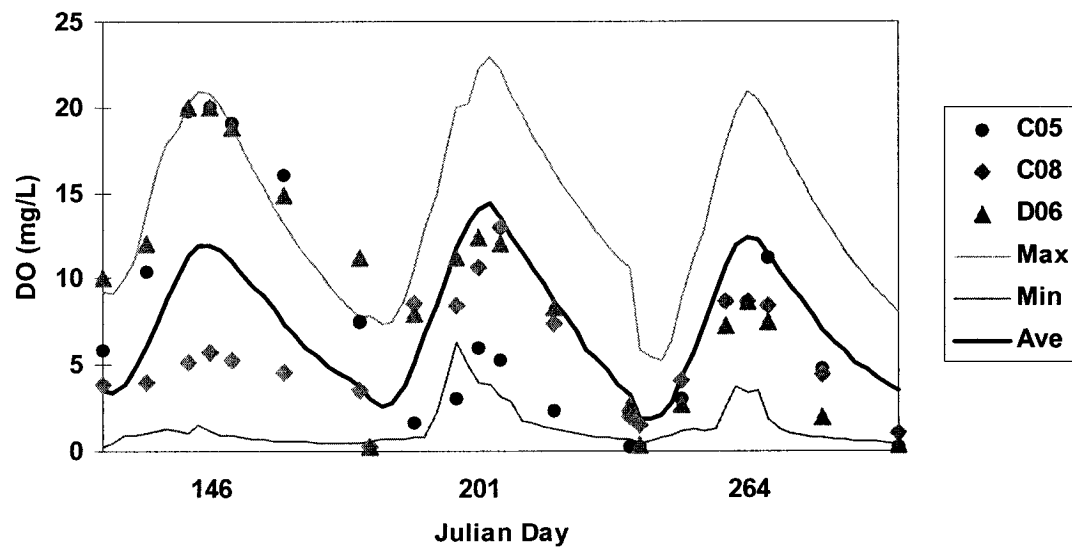


Figure 4.2.2.25. Surface layer DO for Treatment 4 for the Rwanda site

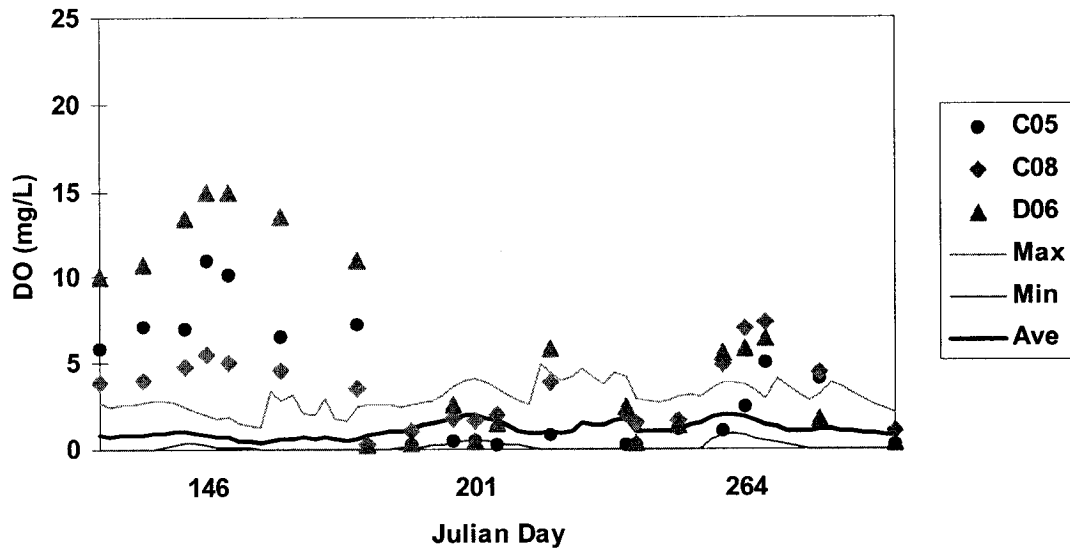


Figure 4.2.2.26. Middle layer DO for Treatment 4 for the Rwanda site

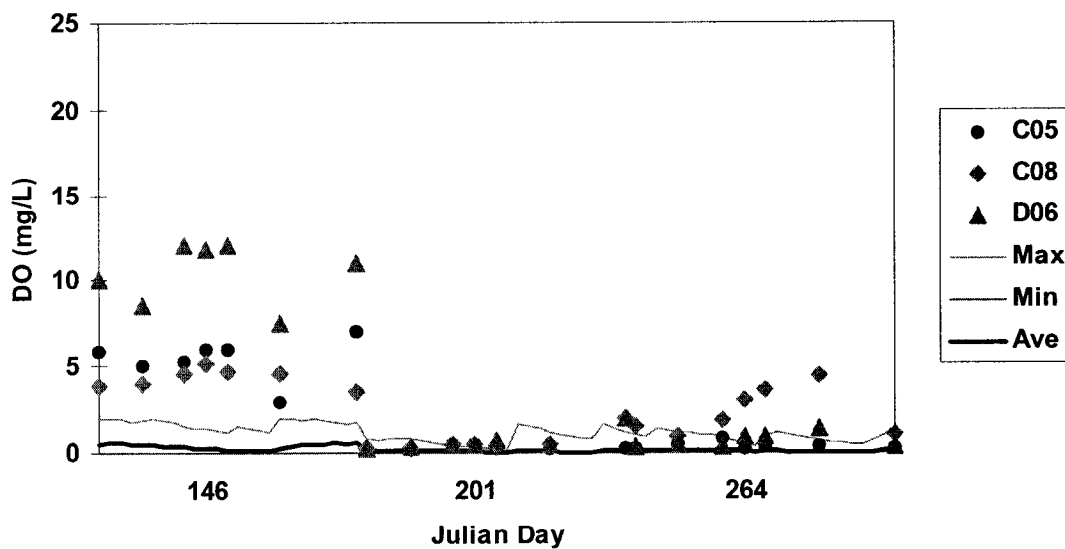


Figure 4.2.2.27a. Bottom layer DO for Treatment 4 for the Rwanda site

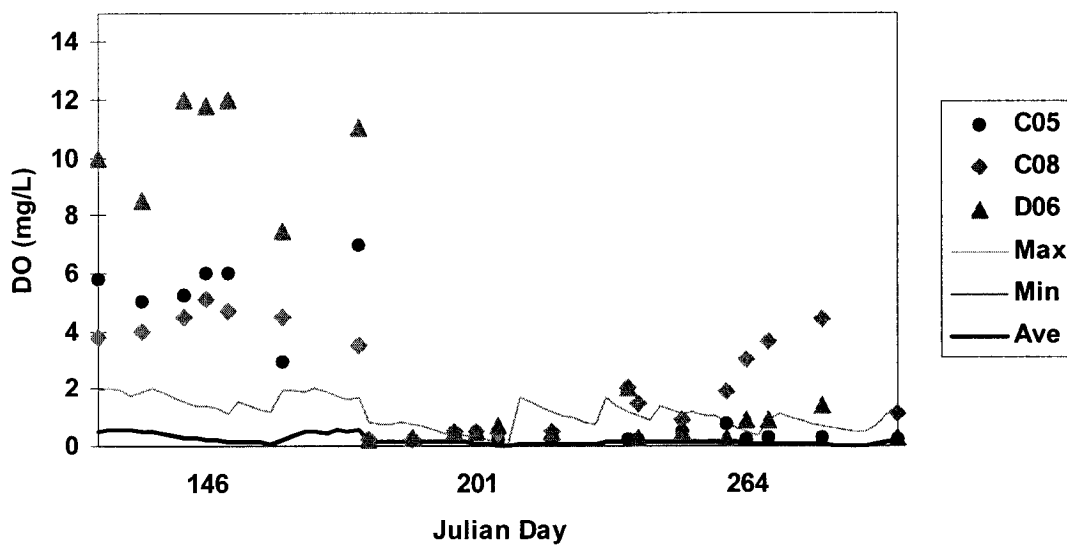


Figure 4.2.2.27b. Bottom layer DO for Treatment 4 for the Rwanda site (extended y-axis scale)

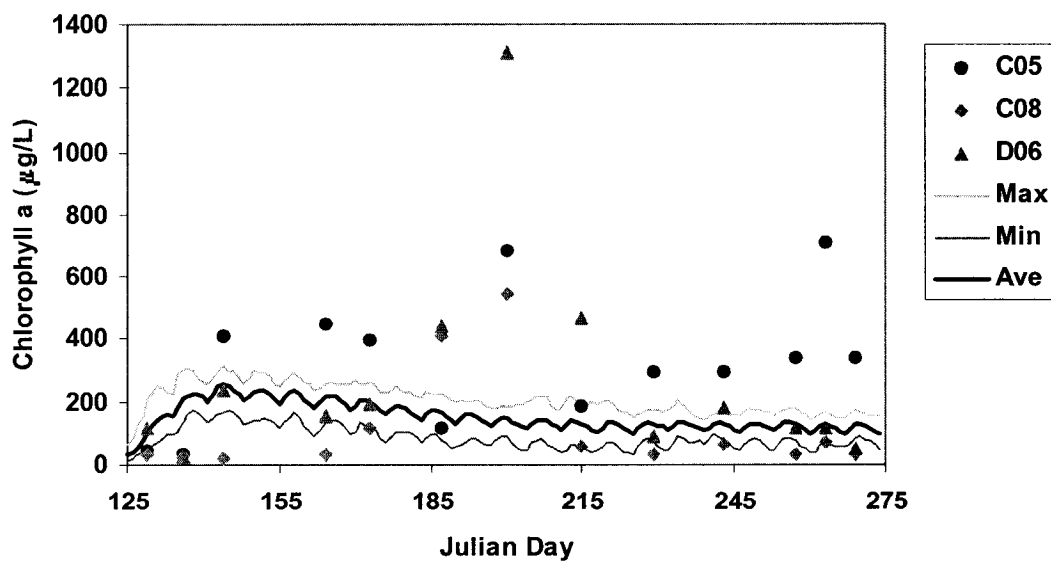


Figure 4.2.2.28. Chlorophyll a for Treatment 4 for the Rwanda

4.2.2.5. Frequency Distributions

The frequency distributions of water temperature for the surface layer are shown in Figure 4.2.2.29. The water temperatures between 21 and 23°C had the highest frequency at 6:00 and 10:00. In the afternoon, the highest frequency shifted to around 25°C. The chances of having temperature below 15°C and above 33°C are negligible. For the middle layer, the frequency distribution curves are the same for 6:00 and 10:00 (Figure IV2.2.30). The highest frequencies are for temperatures around 24°C. There were only minor differences between mornings and afternoons. For the bottom layer, the frequency distribution curves are almost the same for all times of the day (Figure 4.2.2.31).

Figure 4.2.2.32 shows the frequency distributions of DO at the surface layer. At 6:00 there is a very high probability of having a DO under 0.5 mg/L. At 10:00, the DO is most likely to be between 3.5 and 4.5 mg/L. At 14:00, the probability of having DO below 0.5 is very small. For the middle and bottom layers, there is a high probability of having very low DO values at all times of the day. This is particularly noticeable for the bottom layer, which according to the simulations is not suitable for fish culture at any time of the day.

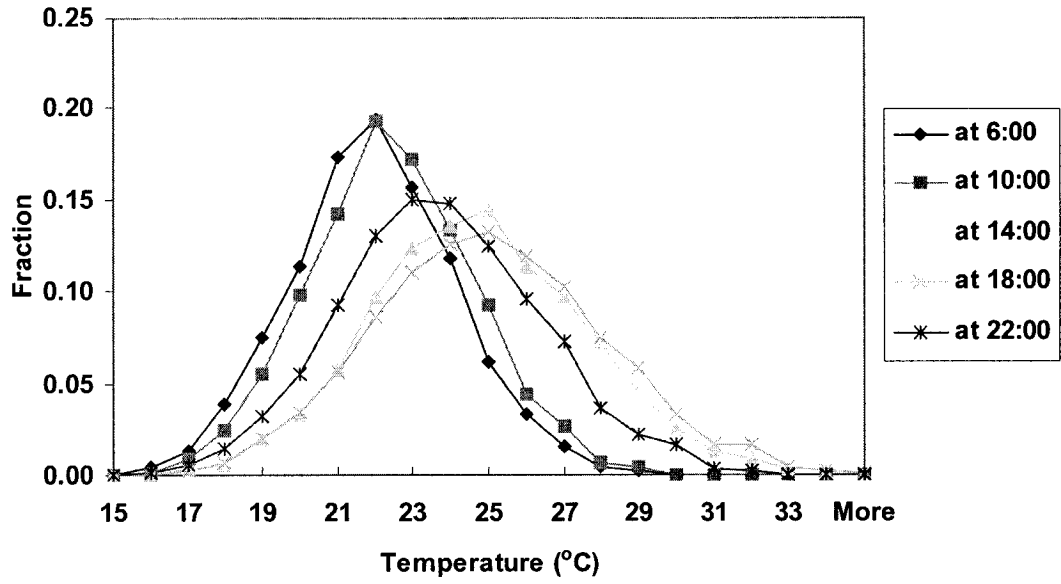


Figure 4.2.2.29. Frequency distributions for surface layer temperature (Treatment 1, Rwanda)

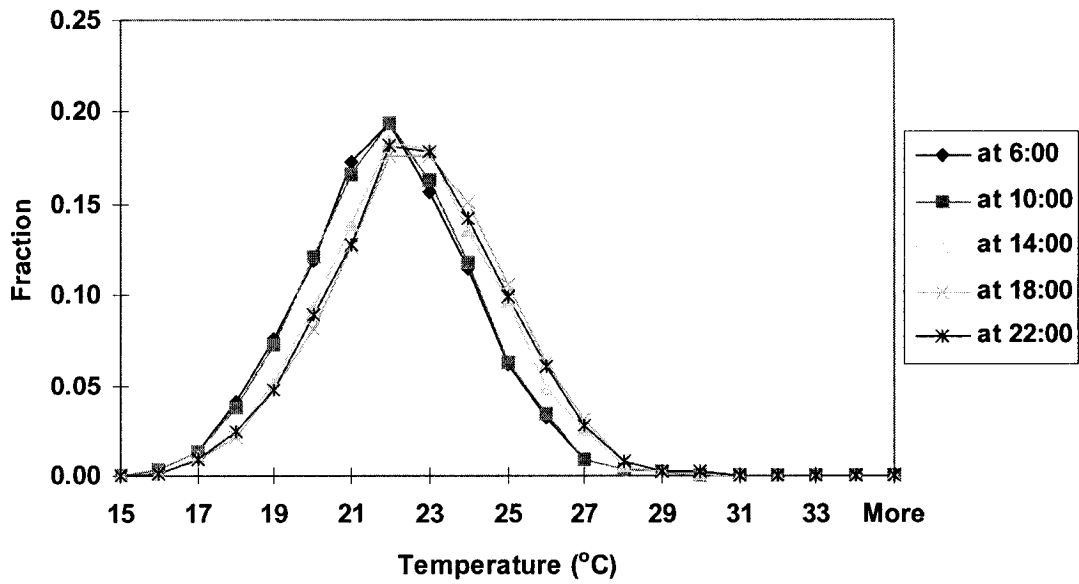


Figure 4.2.2.30. Frequency distributions for middle layer temperature (Treatment 1, Rwanda)

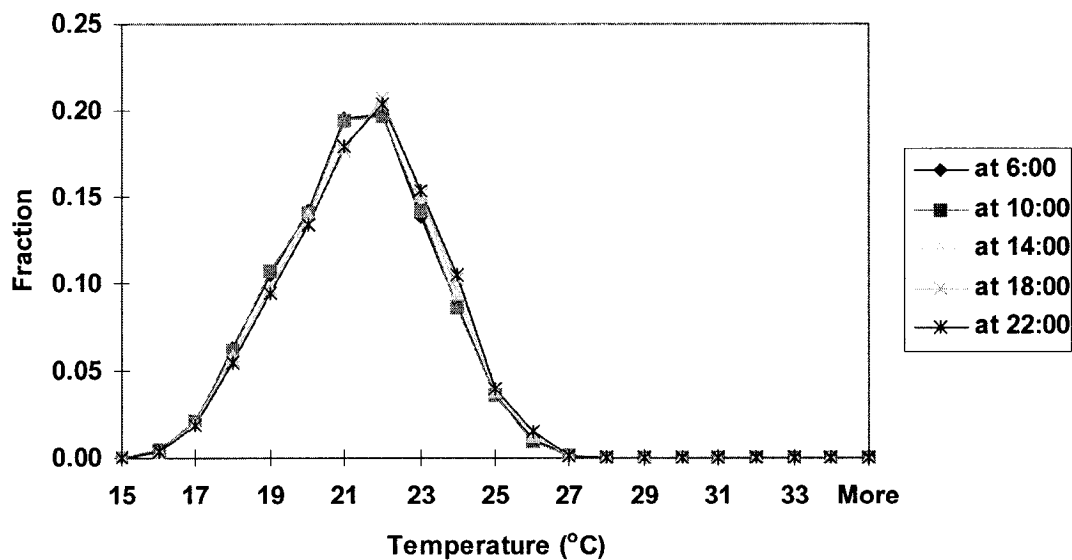


Figure 4.2.2.31. Frequency distributions for bottom layer temperature (Treatment 1, Rwanda)

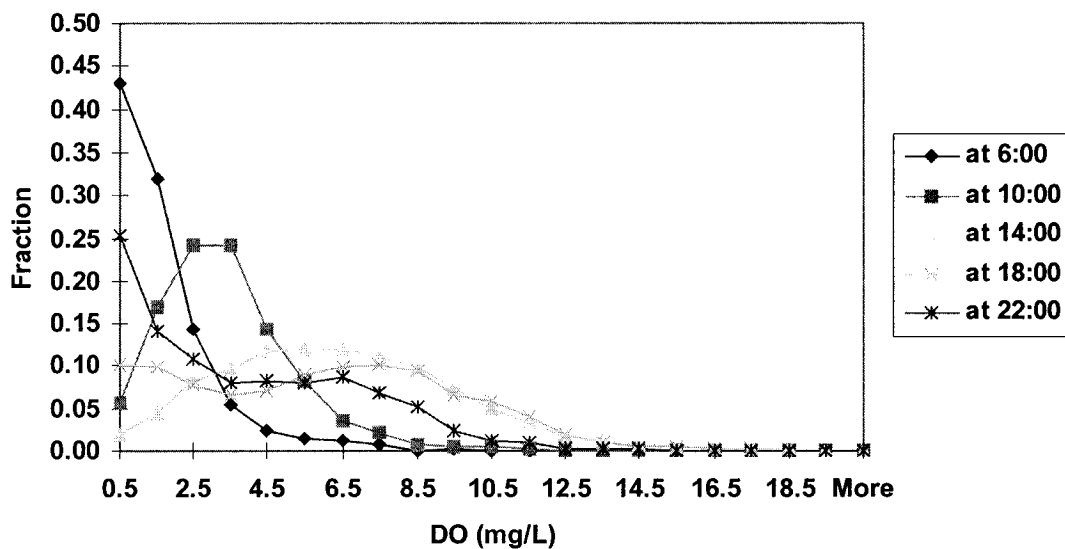


Figure 4.2.2.32. Frequency distributions for surface layer DO (Treatment 1, Rwanda)

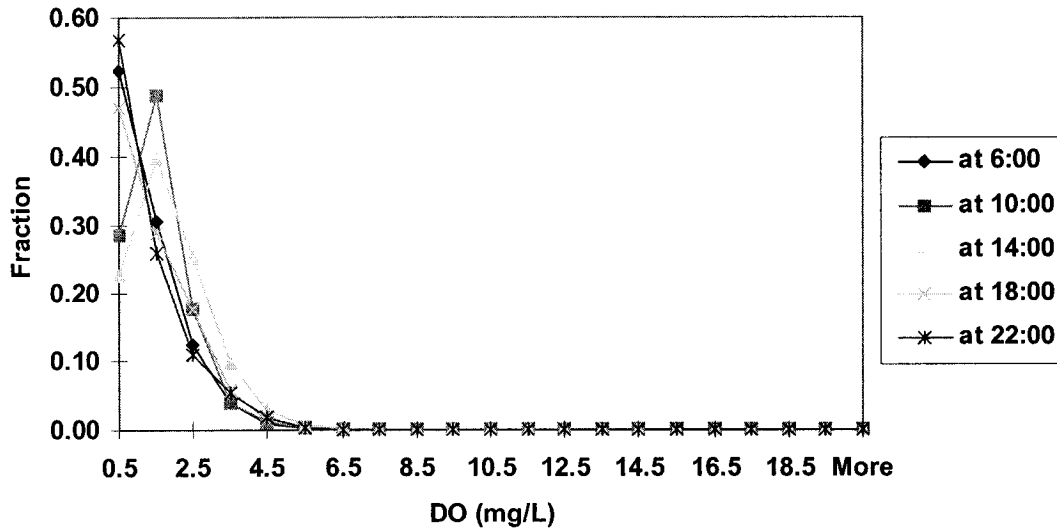


Figure 4.2.2.33. Frequency distributions for middle layer DO (Treatment 1, Rwanda)

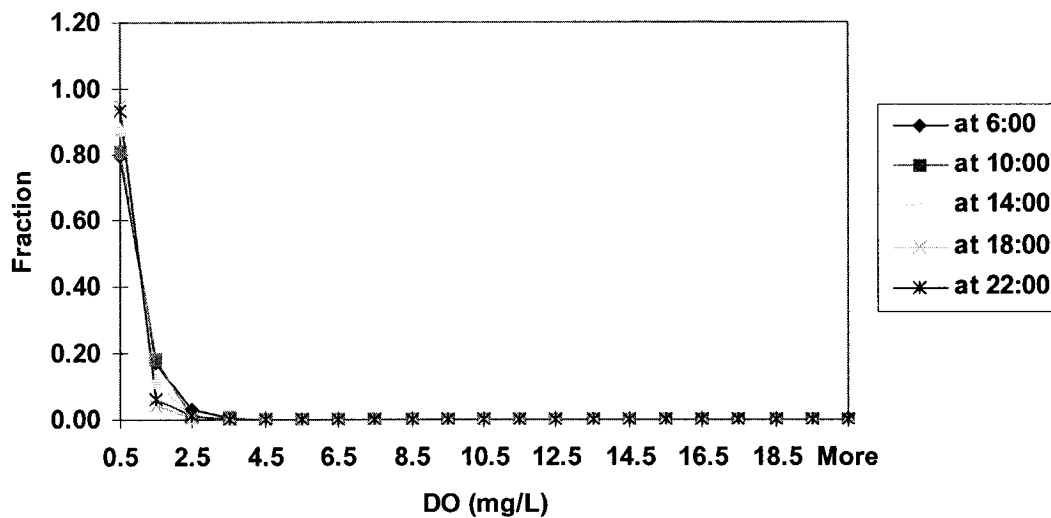


Figure 4.2.2.34. Frequency distributions for bottom layer DO (Treatment 1, Rwanda)

4.2.3. Honduras Site

The experiment (F3d) selected for the Honduras site was designed to evaluate the effect of chicken manure application rate on fish growth. Four fertilization rates were used for the model calibration and validation (Table 4-2). The model calibration procedure for the Honduras site is similar to that used for the Rwanda site, in which only specific location-related parameters are adjusted. Treatment 1 was 500 kg/ha/week chicken manure (dry weight). Treatments 2 to 4 were 250, 125, and 1000 kg/ha/wk chicken manure (dry weight), respectively. Three ponds were used for each treatment. The model simulations start on Julian day 38 and run for a period of 150 days. The initial conditions are listed in Table 4-3. A total of 11 days of diel data including water temperature, DO, and Chla are compared to the simulations.

4.2.3.1. Calibration Run (Treatment 1: 500 kg/ha/wk chicken manure)

Figures 4.2.3.1 to 4.2.3.3 show good agreement between simulated and measured values for the three layers. Although there were several measured points out of the simulated range, the model captured the temperature trend and ranges.

The measured DO values are around the average of simulated values and no data are out of the simulation ranges for the surface layer but the differences between the simulated maximum and minimum values are over 20 mg/L for some days (Figure 4.2.3.4). For the middle layer, the simulated and measured DO had good agreement (Figure 4.2.3.5). For the bottom layer, the simulated DO values are higher than the measured DO except for Julian days 47 and 117 (Figure 4.2.3.6).

Figure 4.2.3.7 illustrates the simulated and observed Chla. The trend of the simulation is similar to that of the observations. Some data are within the ranges of the simulations but most data are below the simulated minimum range.

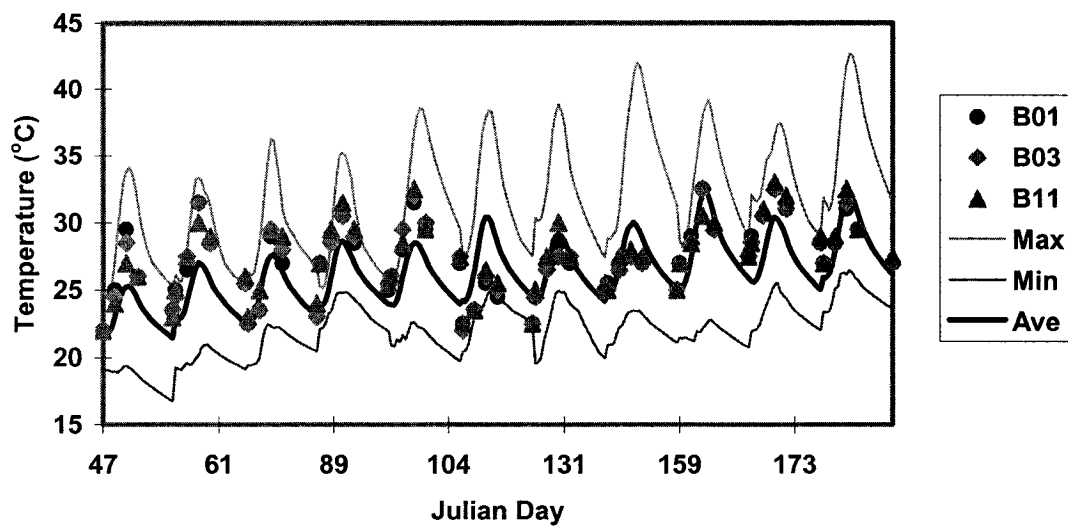


Figure 4.2.3.1. Temperature of surface layer for Treatment 1 for the Honduras site

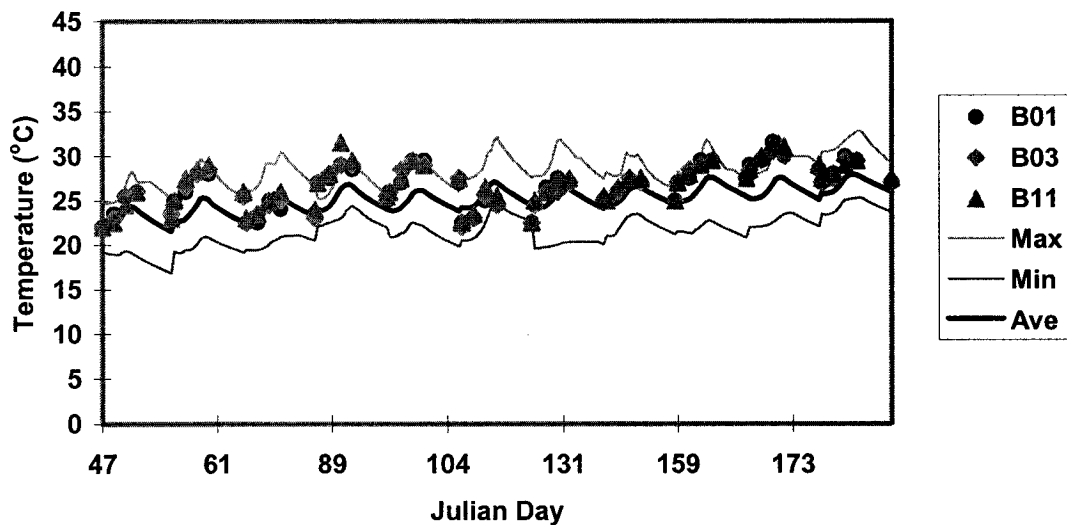


Figure 4.2.3.2. Temperature of middle layer for Treatment 1 for the Honduras site

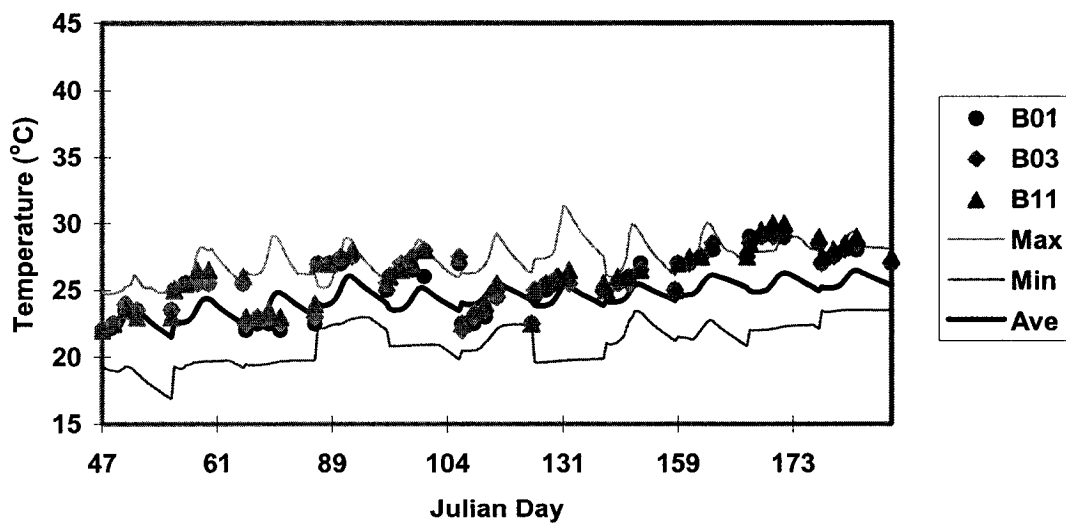


Figure 4.2.3.3. Temperature of bottom layer for Treatment 1 for the Honduras site

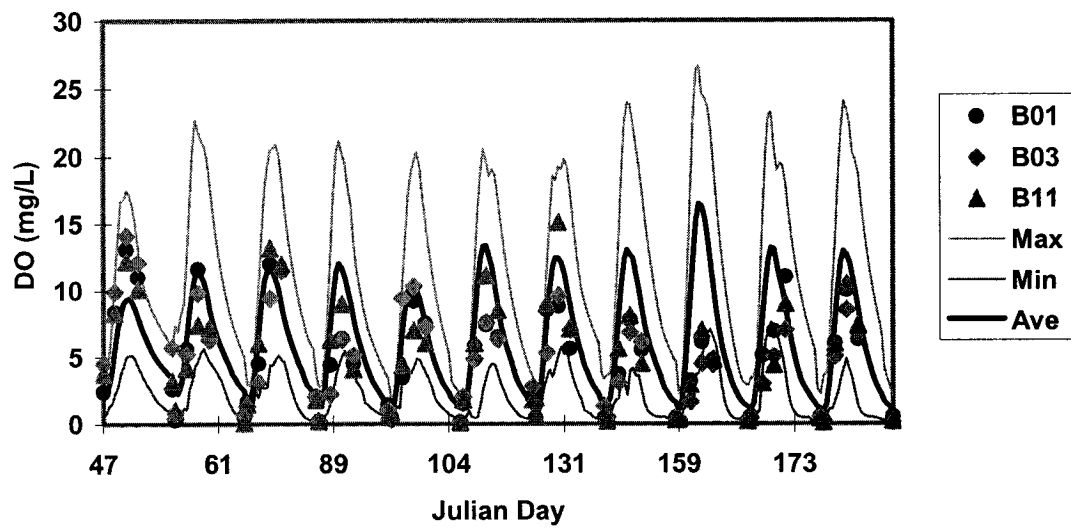


Figure 4.2.3.4. Surface layer DO for Treatment 1 for the Honduras site

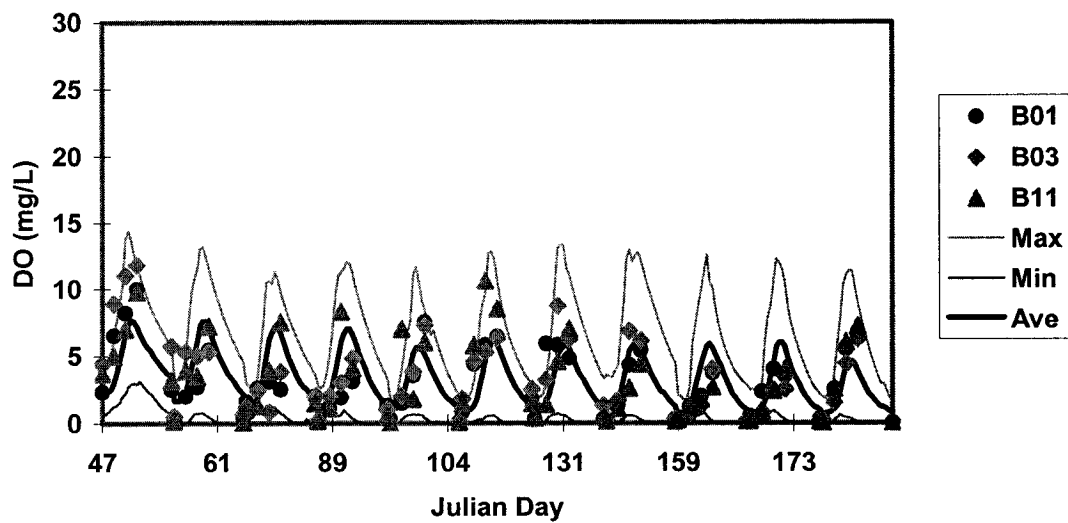


Figure 4.2.3.5. Middle layer DO for Treatment 1 for the Honduras site

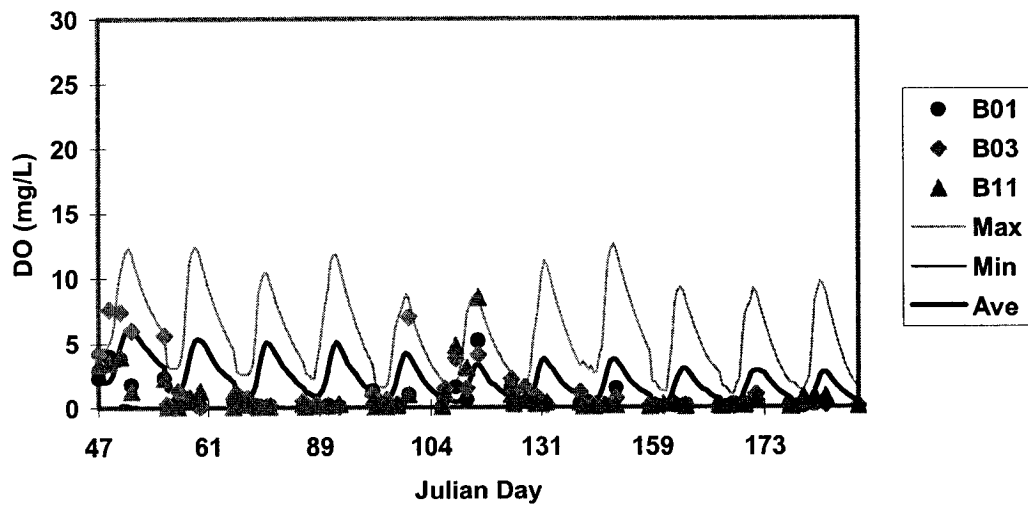


Figure 4.2.3.6. Bottom layer DO for Treatment 1 for the Honduras site

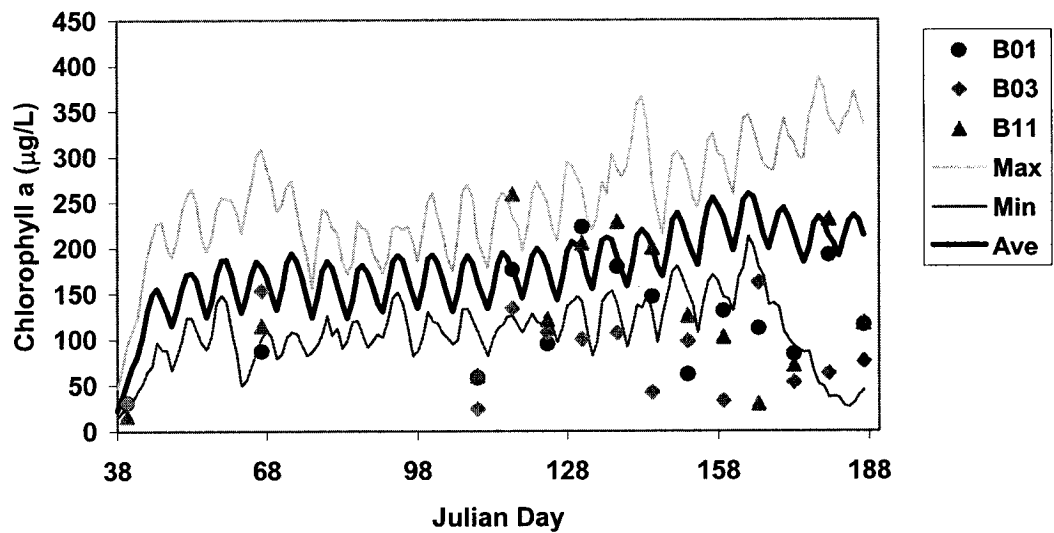


Figure 4.2.3.7. Chlorophyll a for Treatment 1 for the Honduras site

4.2.3.2. Validation Run (Treatment 2: 250 kg/ha/wk chicken manure)

The simulated water temperatures cover most of the measured data for the three layers (Figures 4.2.3.8 to 4.2.3.10). The trend of the simulations is similar to that of the observations.

Figures 4. 2.3.11 to 4.2.3.13 display the simulated and measured DO for the three layers. There are almost no observed data outside of the simulation ranges for the surface layer. For the middle layer, the simulations are a little lower than the observations for some days but the simulated ranges are close to the measured ranges. For the bottom layer, a couple of the observed points are higher than the simulation range.

The simulated and observed Chla are shown in Figure 4.2.3.14. Although several measured points are below the simulated minimum values, the simulated maximum values cover most of the observations. The measured data from pond B07 were higher than those for the other two ponds.

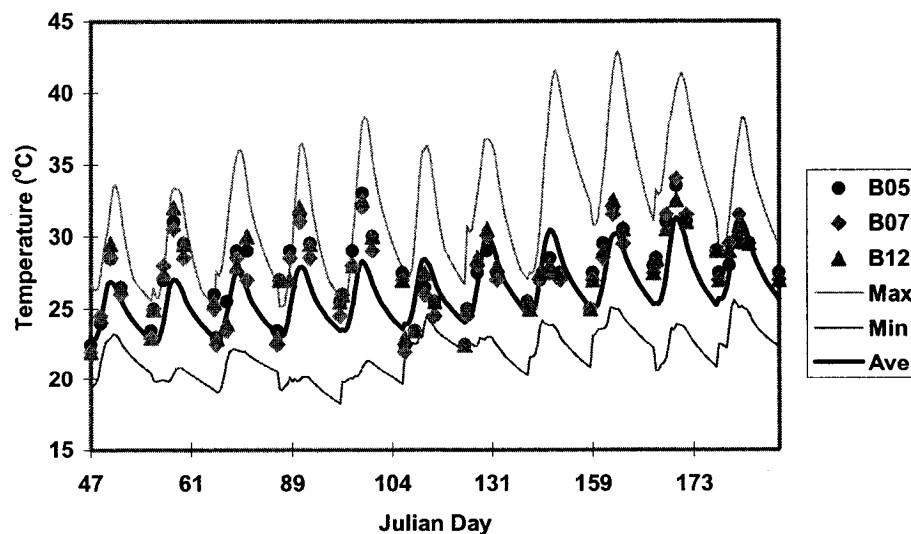


Figure 4.2.3.8. Temperature of surface layer for Treatment 2 for the Honduras site

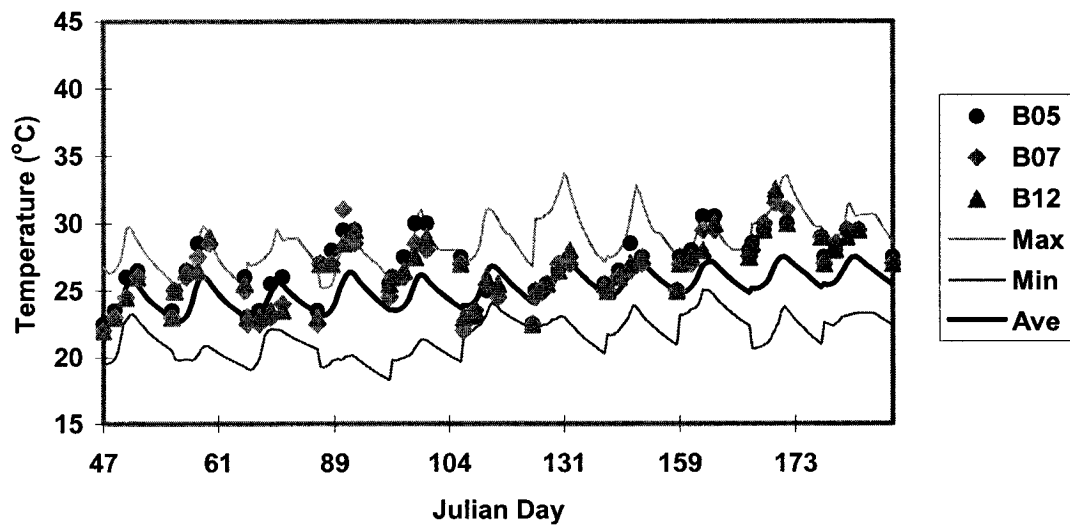


Figure 4.2.3.9. Temperature of middle layer for Treatment 2 for the Honduras site

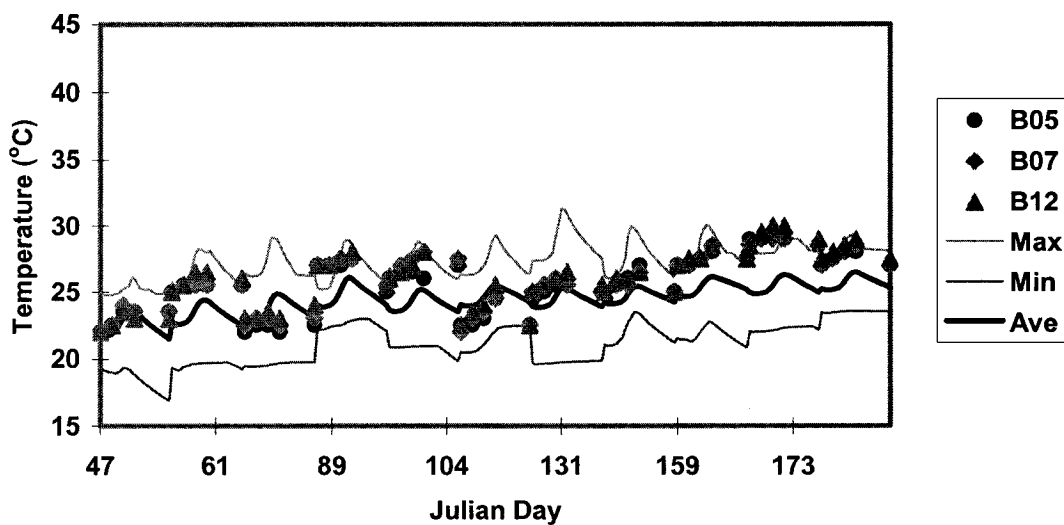


Figure 4.2.3.10. Temperature of Bottom layer for Treatment 2 for the Honduras site

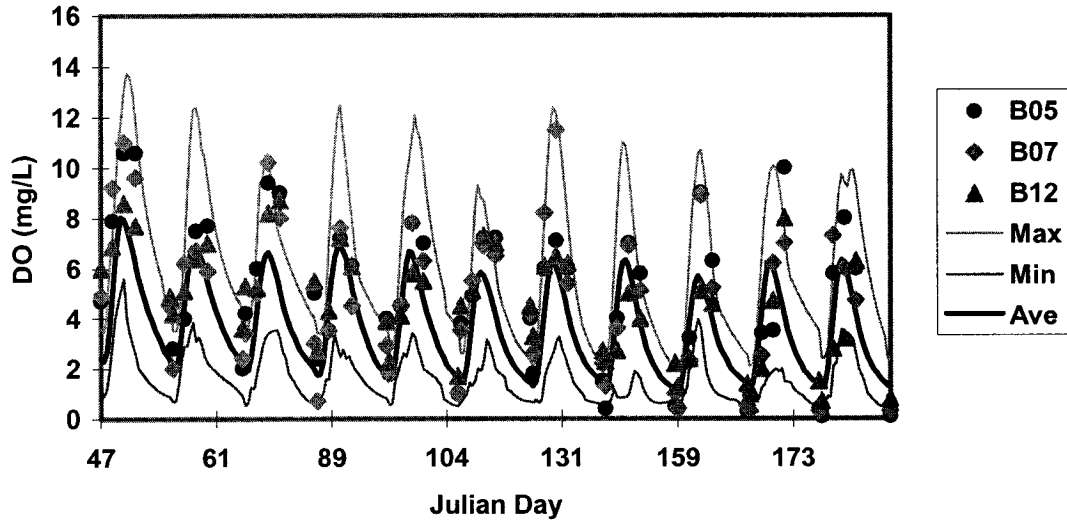


Figure 4.2.3.11. Surface layer DO for Treatment 2 for the Honduras site

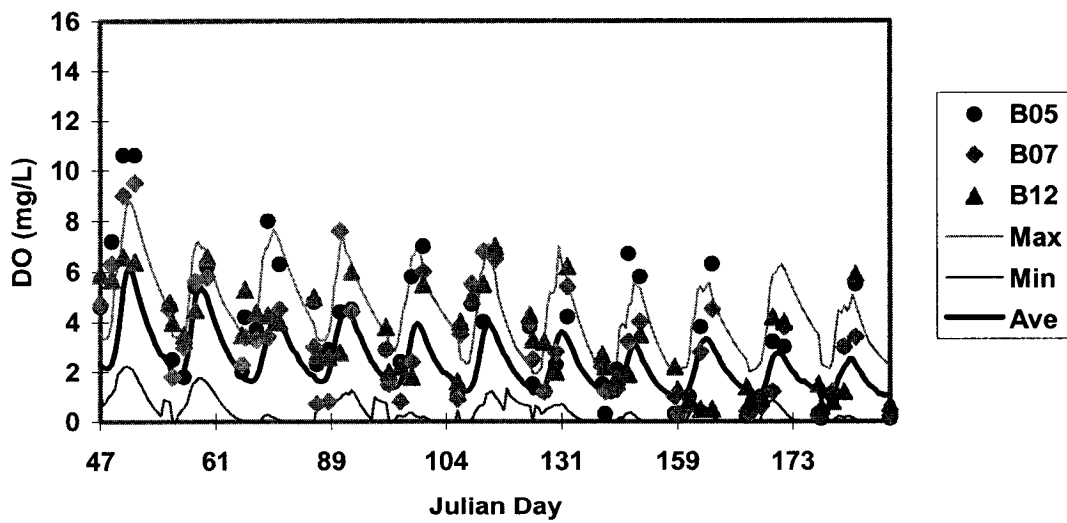


Figure 4.2.3.12. Middle layer DO for Treatment 2 for the Honduras site

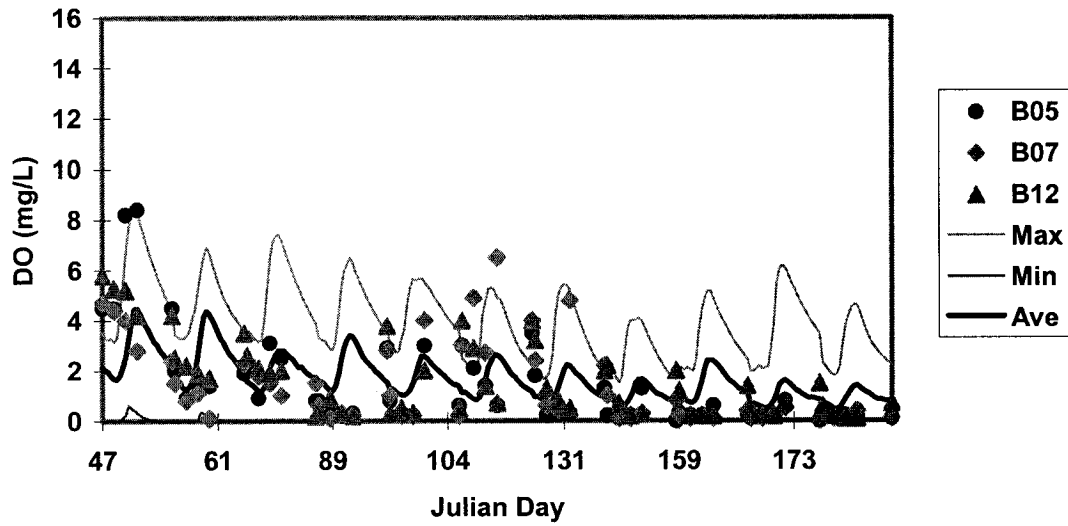


Figure 4.2.3.13. Bottom layer DO for Treatment 2 for the Honduras site

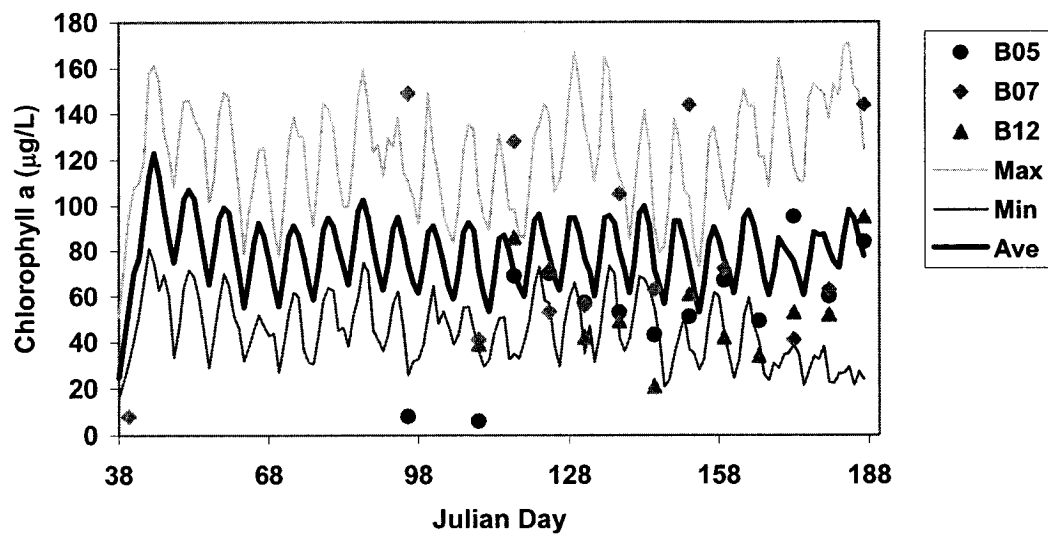


Figure 4.2.3.14. Chlorophyll a for Treatment 2 for the Honduras site

4.2.2.3. Validation Run (Treatment 3: 125 kg/ha/wk chicken manure)

Figures 4.2.3.15 to 4.2.3.17 show the simulated and observed water temperatures for the three layers. The simulated water temperature ranges cover the observations for the surface and middle layers, but there are a few observed data beyond the simulated water temperature range for the bottom layer.

The comparisons of DO show that the simulations are below several observations for the surface layer (Figure 4.2.3.18). The simulated DO values for the middle layer are lower than the observations on several days (Figure 4.2.3.19). For the bottom layer, the simulations cover most of the observations and also have a similar trend to that of the observations (Figure 4.2.3.20).

Figure 4.2.3.21 shows good agreement between simulations and observations. Since there were no measured data between days one and 98, the trend of Chla is unknown during this period but the trend of the simulations is similar to that of the observations during the later part of the simulation period.

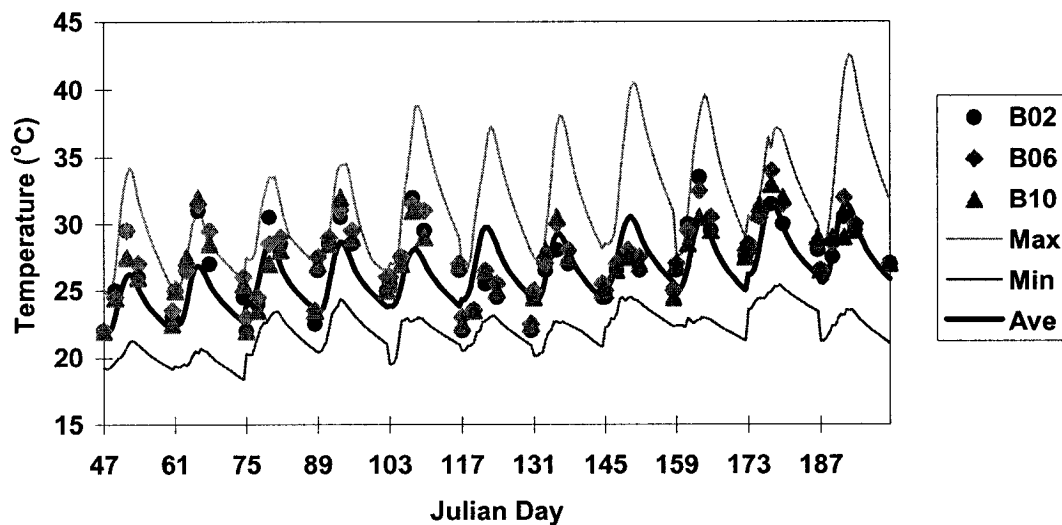


Figure 4.2.3.15. Temperature of surface layer for Treatment 3 for the Honduras site

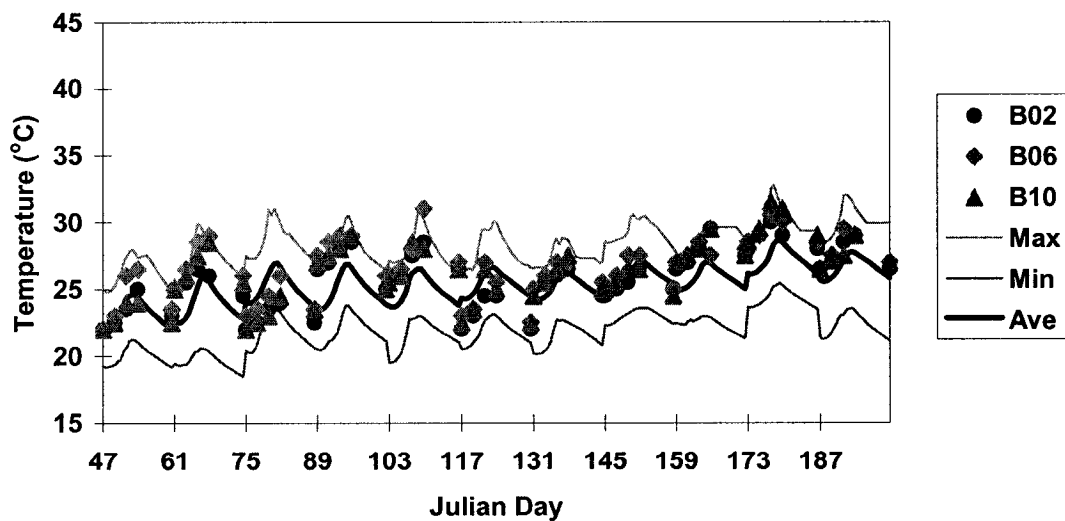


Figure 4.2.3.16. Temperature of middle layer for Treatment 3 for the Honduras site

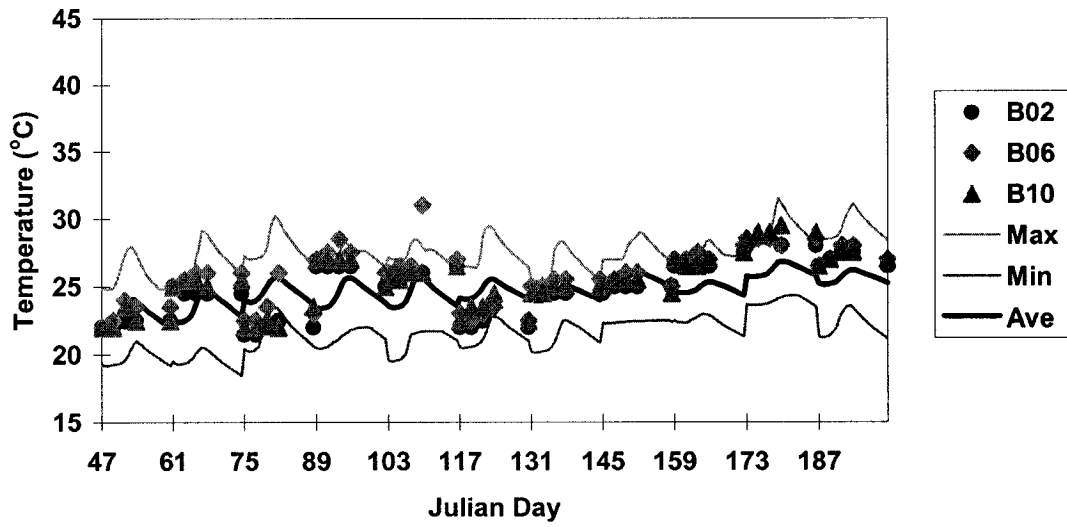


Figure 4.2.3.17. Temperature of bottom layer for Treatment 3 for the Honduras site

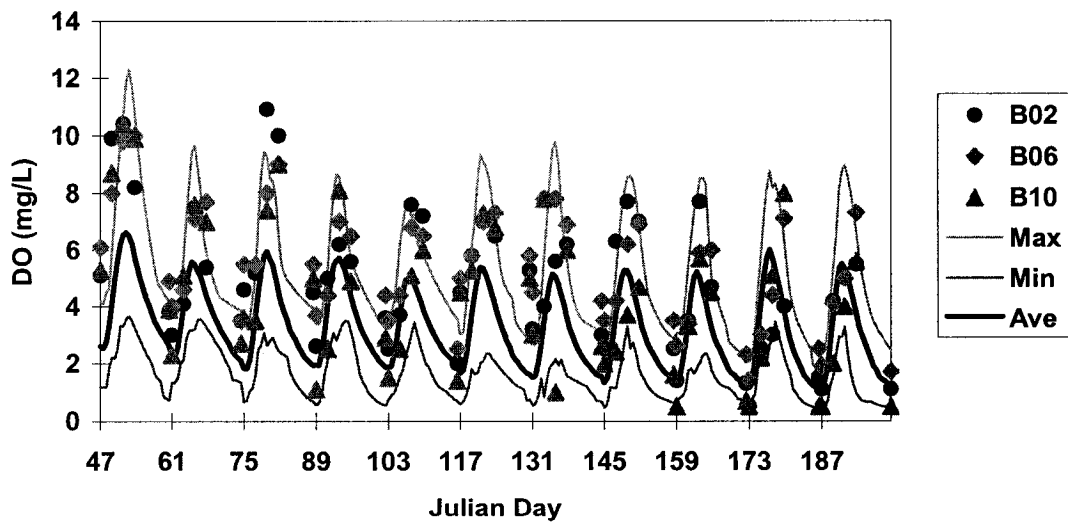


Figure 4.2.3.18. Surface layer DO for Treatment 3 for the Honduras site

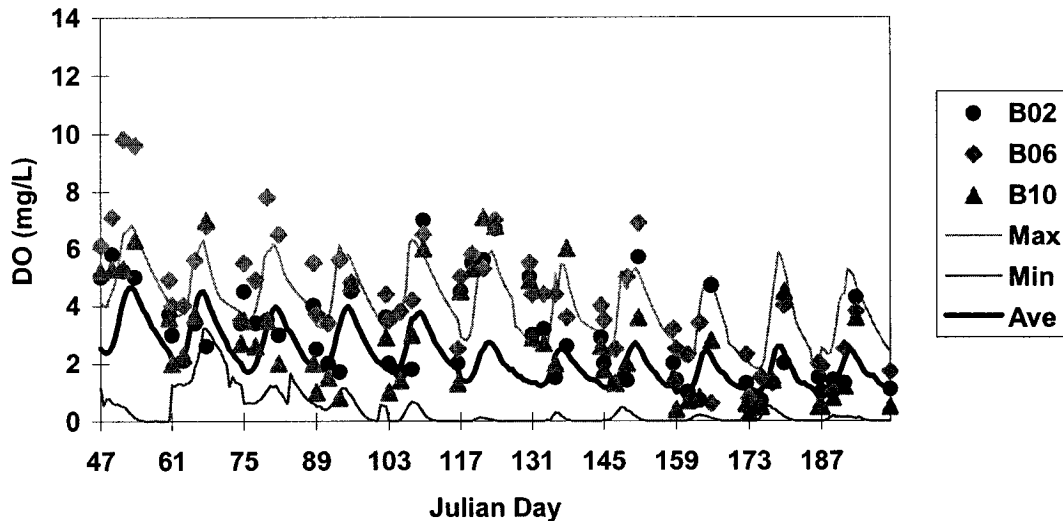


Figure 4.2.3.19. Middle layer DO for Treatment 3 for the Honduras site

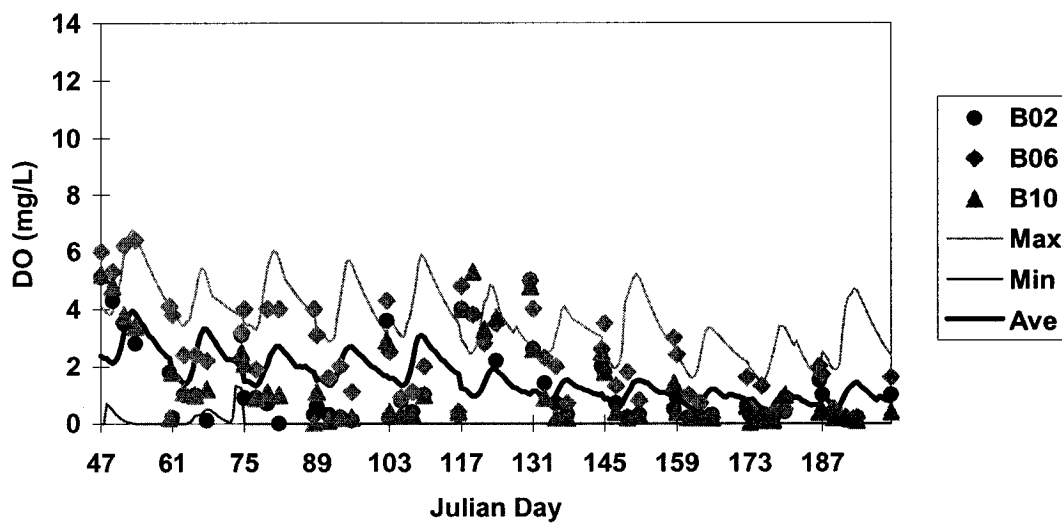


Figure 4.2.3.20. Bottom layer DO for Treatment 3 for the Honduras site

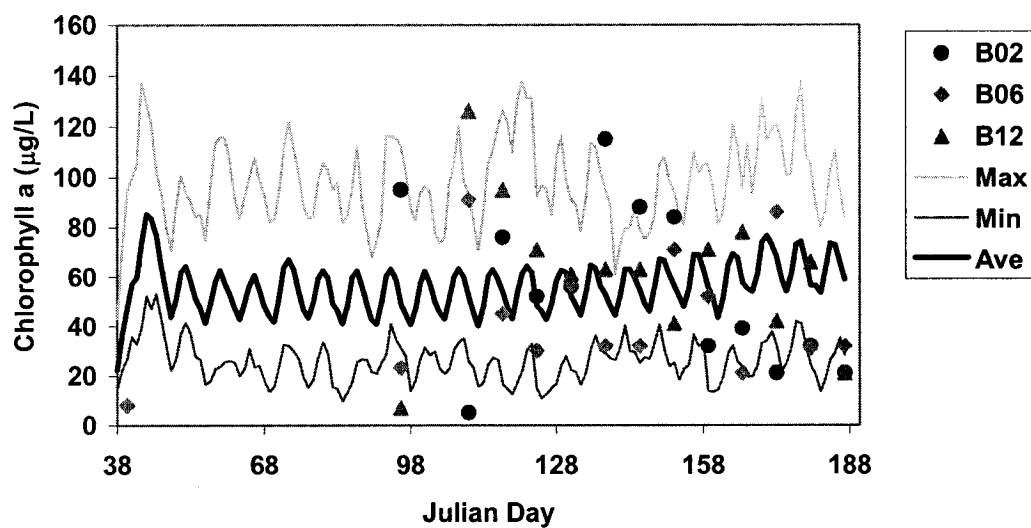


Figure 4.2.3.21. Chlorophyll a for Treatment 3 for the Honduras site

4.2.3.4. Validation Run (Treatment 4: 1000 kg/ha/wk chicken manure)

Figures 4.2.3.22 to 4.2.3.24 show the simulations and observations for the three layers under the highest fertilization rate used. Similar to the other treatments, the ranges of the simulated values cover most of the data for the surface layer but less for the middle and bottom layers.

Figures 4.2.3.25 to 4.2.3.27 show the simulated and measured DO for the three layers.

The simulated average values are much higher than the data for the surface layer for most days except for the first sampling day. For the middle layer, most of the data are around the average values. For the bottom layer, the data are much lower than the average simulated values for most days.

Figure 4.2.3.28 shows the simulated and observed Chla. The trend and ranges of the simulations are similar to those of the observations. Once again, large differences among replicate ponds were noted in the data.

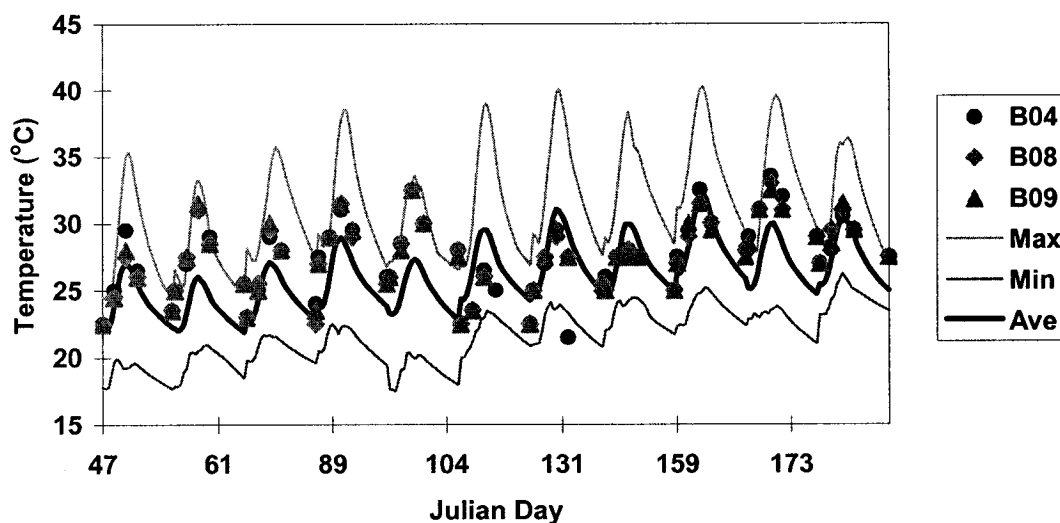


Figure 4.2.3.22. Temperature of surface layer for Treatment 4 for the Honduras site

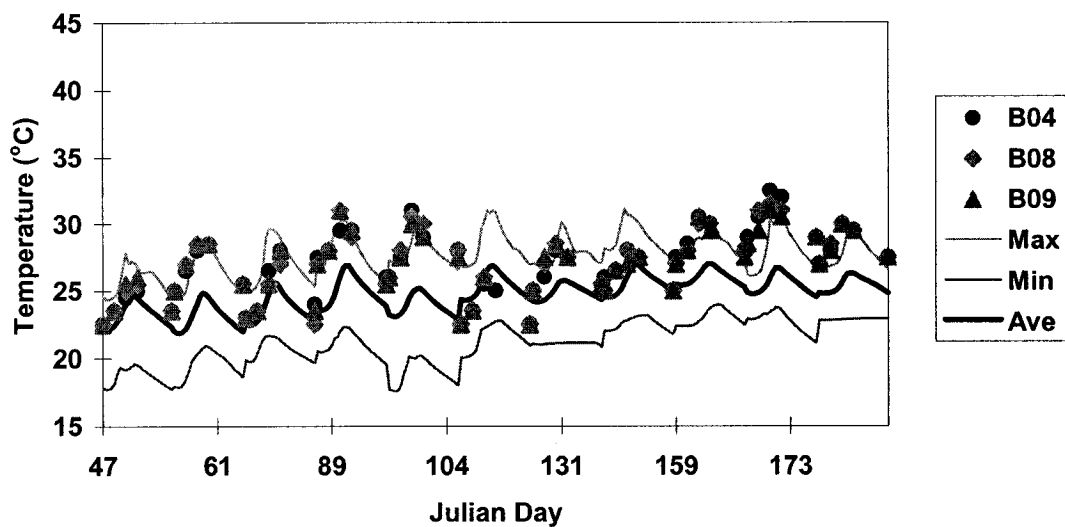


Figure 4.2.3.23. Temperature of middle layer for Treatment 4 for the Honduras site

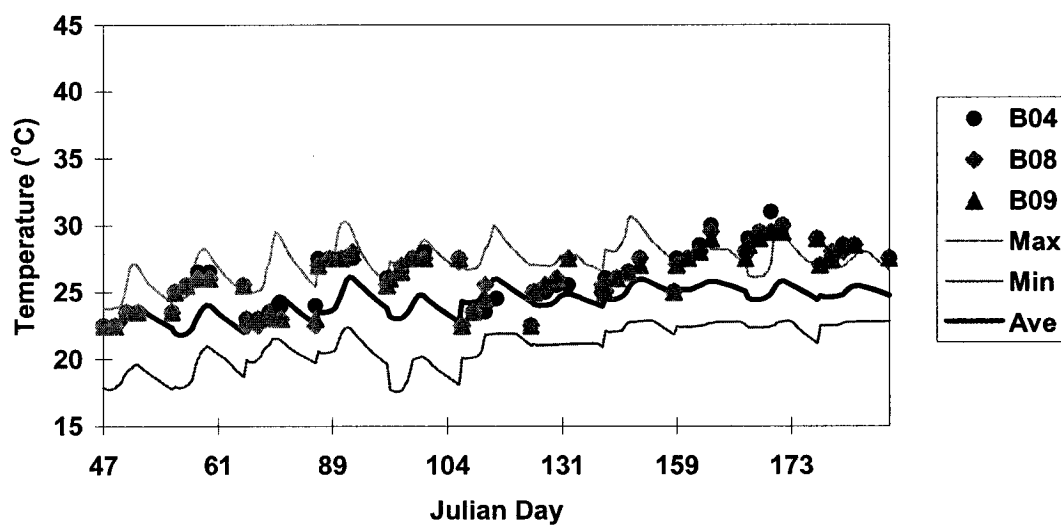


Figure 4.2.3.24. Temperature of bottom layer for Treatment 4 for the Honduras site

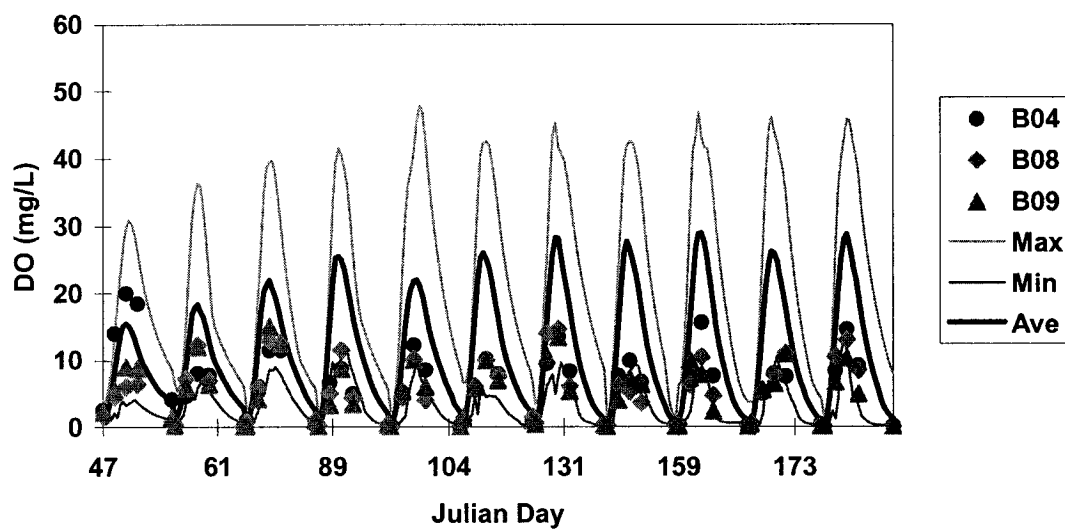


Figure 4.2.3.25. Surface layer DO for Treatment 4 for the Honduras site

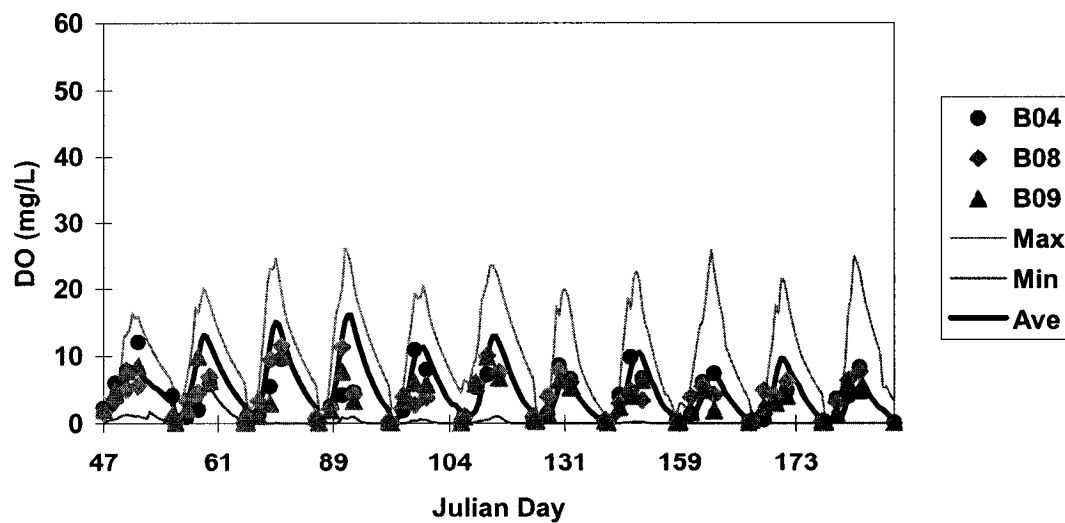


Figure 4.2.3.26. Middle layer DO for Treatment 4 for the Honduras site

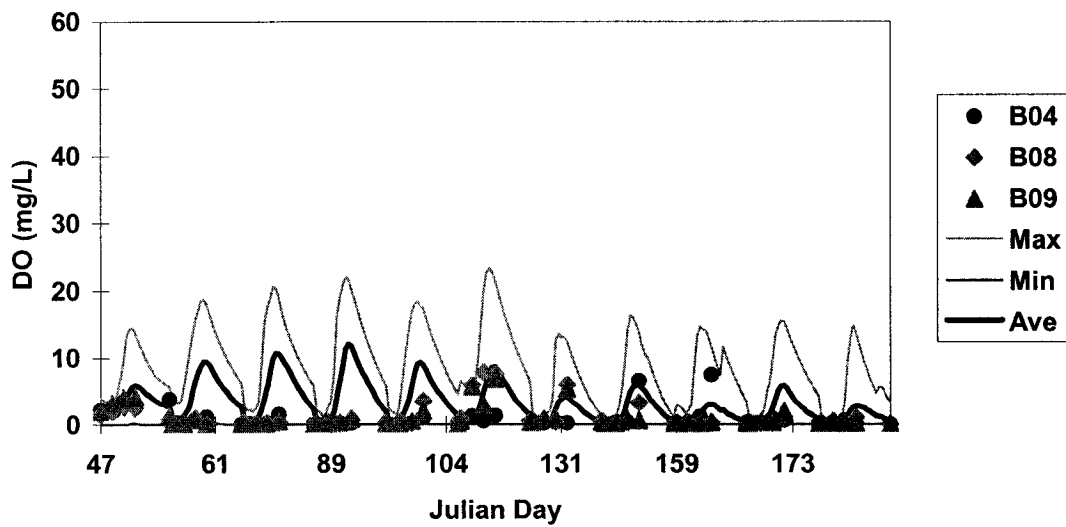


Figure 4.2.3.27. Bottom layer DO for Treatment 4 for the Honduras site

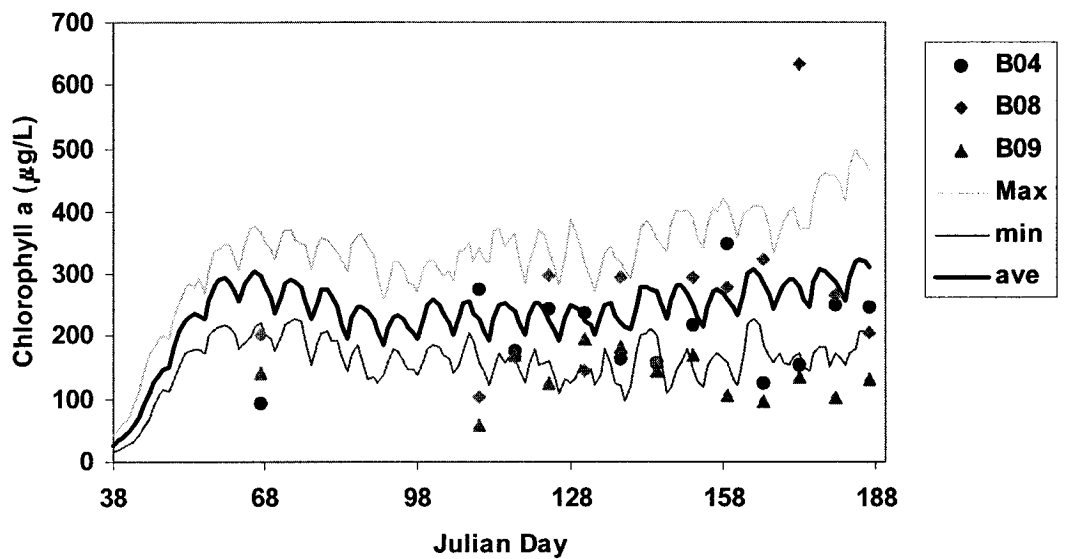


Figure 4.2.3.28. Chlorophyll a for Treatment 4 for the Honduras site

4.2.3.5. Frequency Distributions

The temperature frequency distributions at different time periods are shown in Figures 4.2.3.29 to 4.2.3.31 for the three layers. For the surface layer, the highest probability of having temperature around 25°C is at 6:00. Temperatures between 25 and 29°C occur with high probabilities at 10:00, 18:00, and 22:00. At 14:00 and 18:00, there are high probabilities corresponds to a temperatures above 33°C. Figure 4.2.3.30 shows the probabilities of temperature for the middle layer. At 6:00 and 10:00, the highest probability is to have temperature around 25°C. At 14:00 and 22:00, a temperature around 27°C has a high probability of occurring. At 18:00, the highest probability is for a temperature around 28°C. For the bottom layer, temperatures between 24 and 27°C have high probability of occurring for all times (Figure 4.2.3.31). All simulated temperatures are between 18 and 33°C for the three layers.

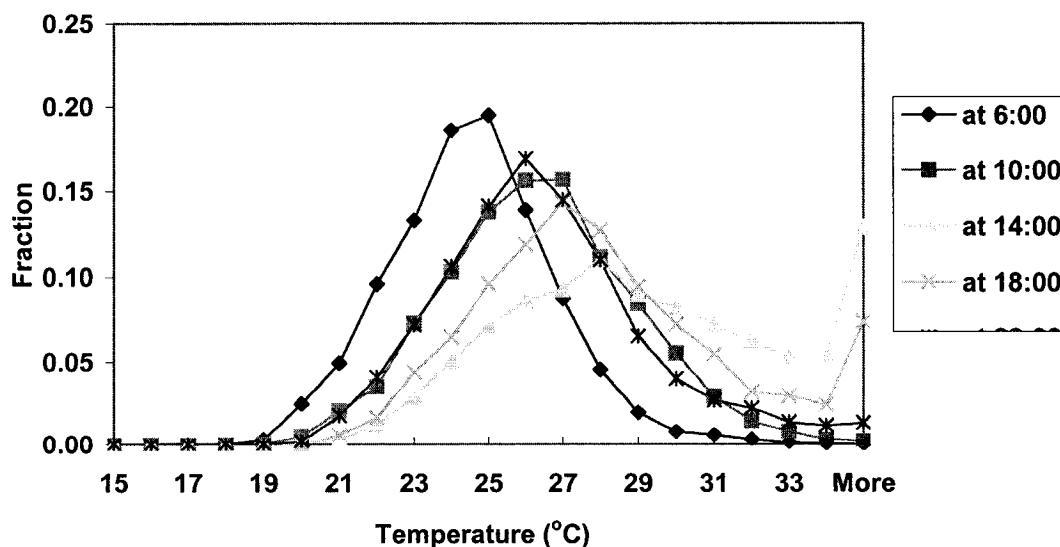


Figure 4.2.3.29. Frequency distributions for surface layer temperature (Treatment 1, Honduras site)

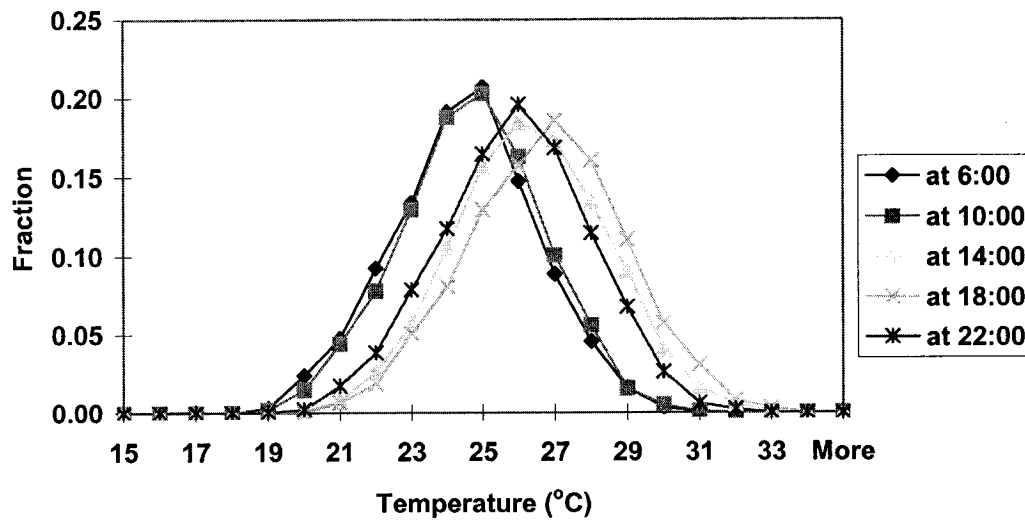


Figure 4.2.3.30. Frequency distributions for middle layer temperature (Treatment 1, Honduras site)

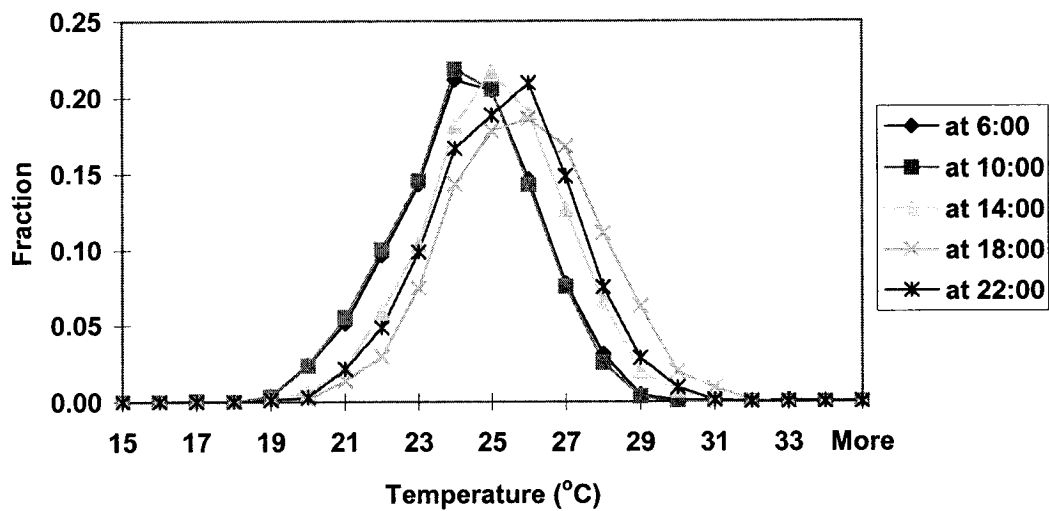


Figure 4.2.3.31. Frequency distributions for bottom layer temperature (Treatment 1, Honduras site)

Figures 4.2.3.32 to 4.2.3.34 show the probabilities of simulated DO for the three layers. DO at 0.5 mg/L has the highest probability of occurring for all three layers except during the middle of the day. At time 10:00, 14:00, and 18:00, the probability is about 0.1 for DO around 6.5 mg/L for the surface layer. The probabilities are about 0.08 and 0.05 for the middle and bottom layers when DO is around 6.5 mg/L, respectively.

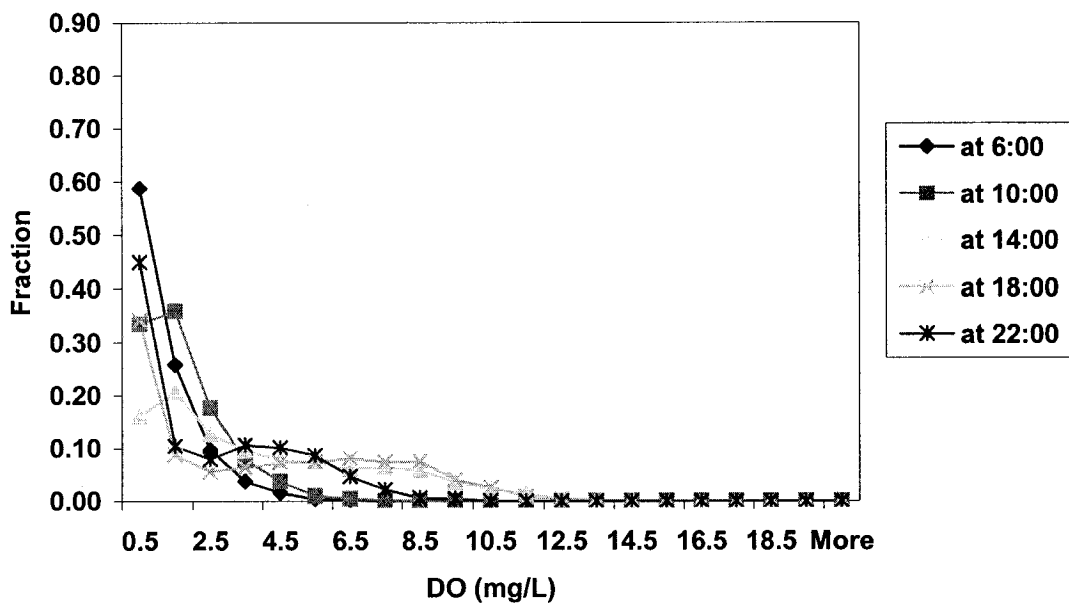


Figure 4.2.3.32. Frequency distributions for surface layer DO (Treatment 1, Honduras site)

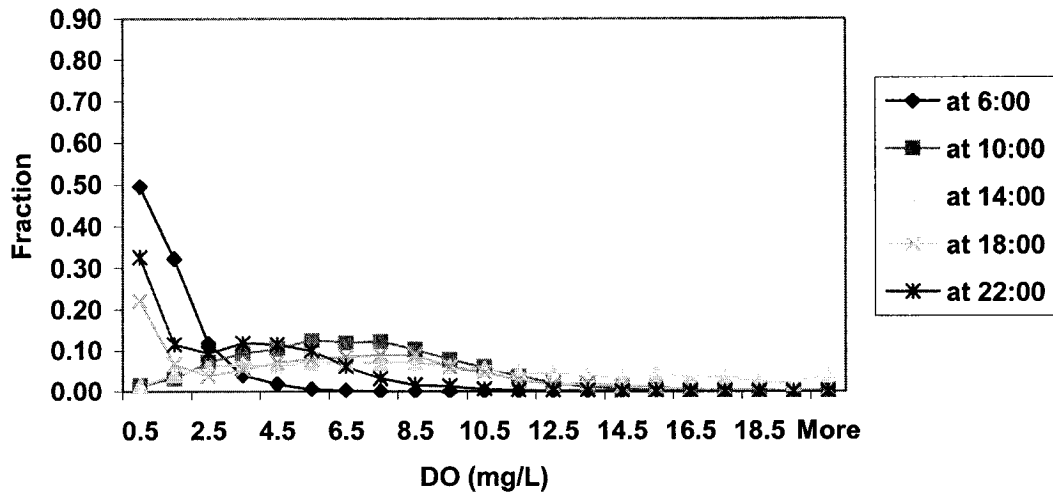


Figure 4.2.3.33. Frequency distributions for middle layer DO (Treatment 1, Honduras site)

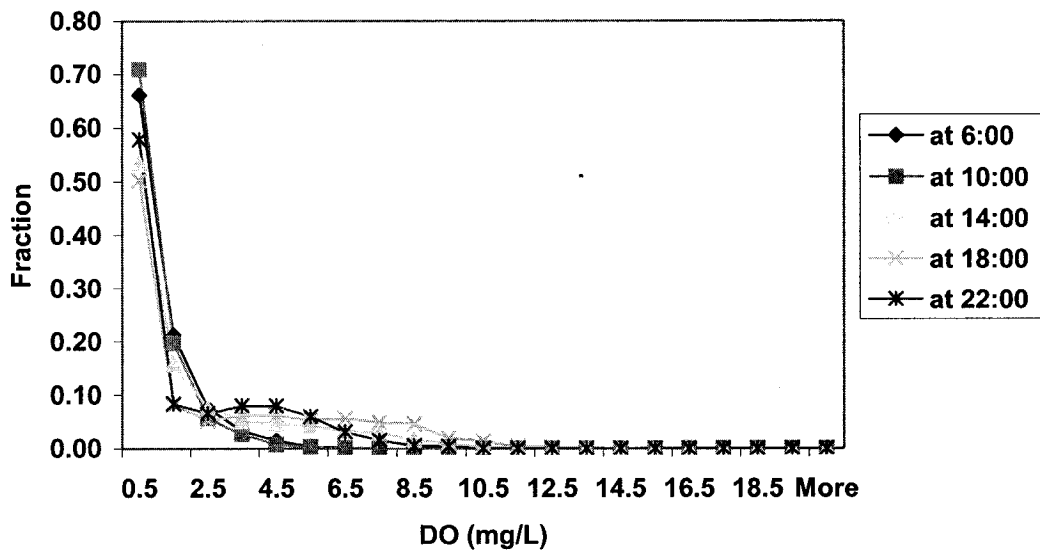


Figure 4.2.3.34. Frequency distributions for bottom layer DO (Treatment 1, Honduras site)

Data availability for the Honduras site allows the calculation of DO frequency distributions. These are shown in Figures 4.2.3.35 to 4.2.3.37. They are compared to the simulated frequency distributions. For the surface layer, the probabilities of simulated and observed DO are similar for extreme values but there are some differences for intermediate values. Figure 4.2.3.36. to 4.2.3.37 show that the simulated DO values have very similar probability distributions to those obtained from the data.

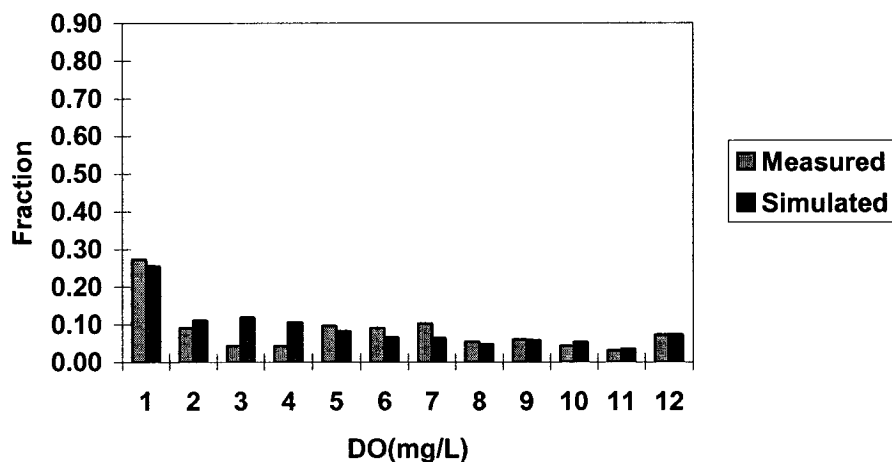


Figure 4.2.3.35. The frequency distributions of the simulated and measured surface layer DO for Treatment 1 for the Honduras site

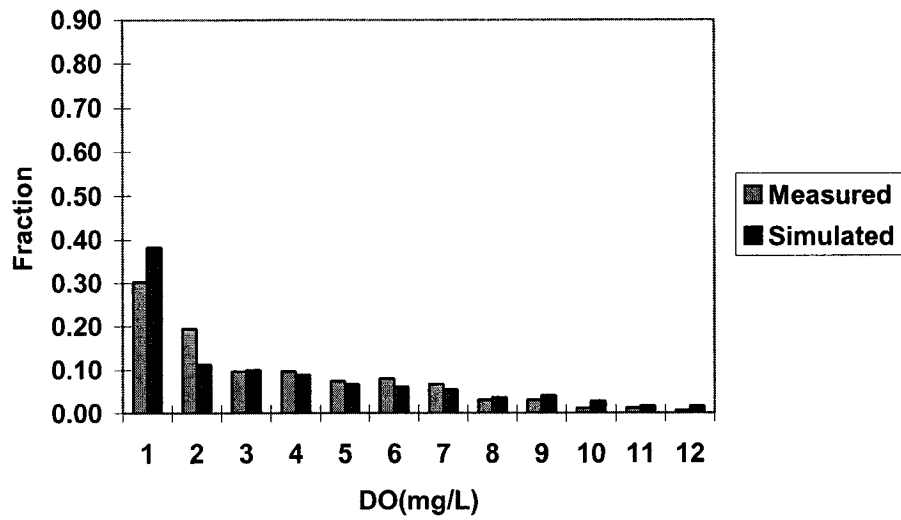


Figure 4.2.3.36. The frequency distributions of the simulated and measured middle layer DO for Treatment 1 for the Honduras site

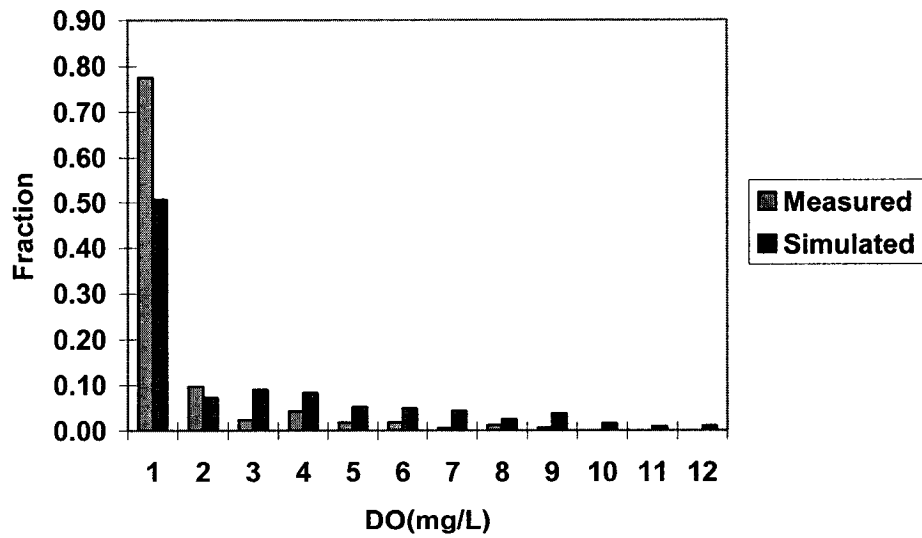


Figure 4.2.3.37. The frequency distributions of the simulated and measured bottom layer DO for Treatment 1 for the Honduras site

4.2.3.6. Long Term Simulations

The long term simulations were obtained after running the model 20 times for one growing season (3600 hours). In the previous sections, the hourly simulations are compared to the observations for specific days. In this section, the simulated water temperature and DO are presented for the entire simulation to demonstrate the influences of weather and fertilization on water temperature and DO over an entire growing season. The results present include surface, middle, and bottom layers with the maximum, minimum, and average simulations for Treatment 1.

Figures 4.2.3.38 and 4.2.3.39 show the water temperatures for the surface layer. The highest temperature was 45°C. The average water temperatures ranged from 21 to 34°C, with a mean of 26°C. Figures 4.2.3.40 and 4.2.3.41 show the simulated water temperature for the middle layer. The highest temperature is 33°C. The averages of the simulations range from 21 to 29°C with a mean of 25°C. Figure 4.2.3.42 shows the entire simulated water temperature for the bottom layer. The highest temperature is 32°C. The averages of simulations range from 21 to 27°C with a mean of 21°C. The magnitude of the fluctuations was greatest for the surface layer and smallest for the bottom layer.

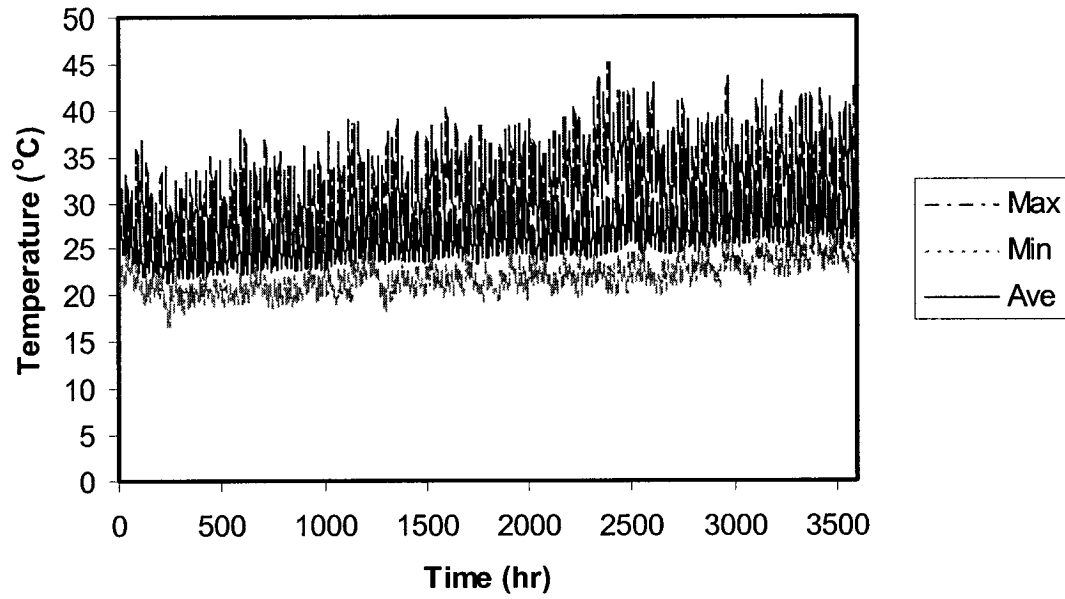


Figure 4.2.3.38. Simulated water temperatures for the surface layer (Treatment 1, Honduras)

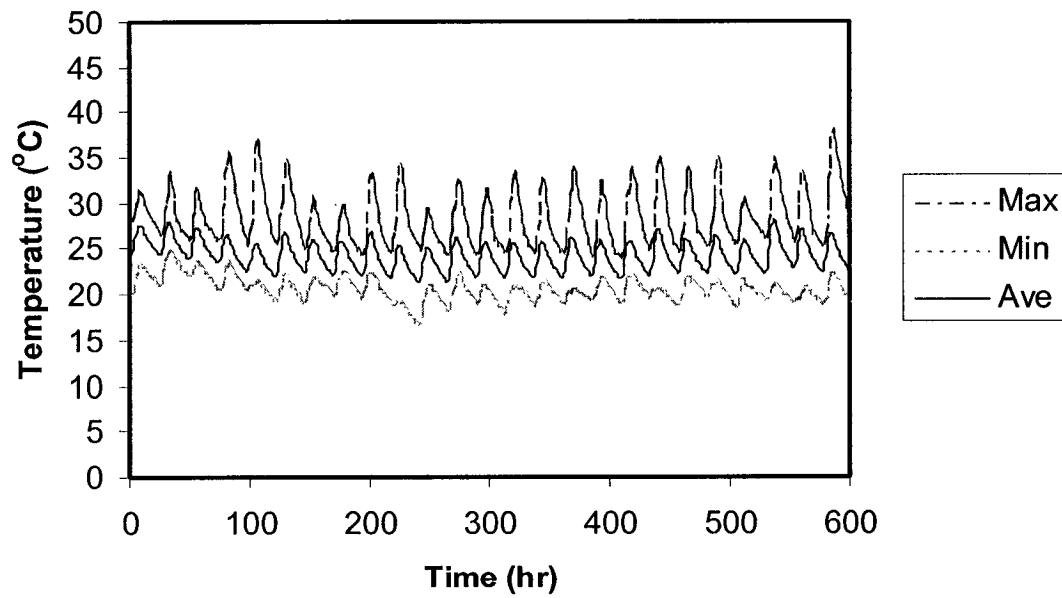


Figure 4.2.3.39. Simulated water temperatures for the surface layer for the first 600 hours (Treatment 1, Honduras)

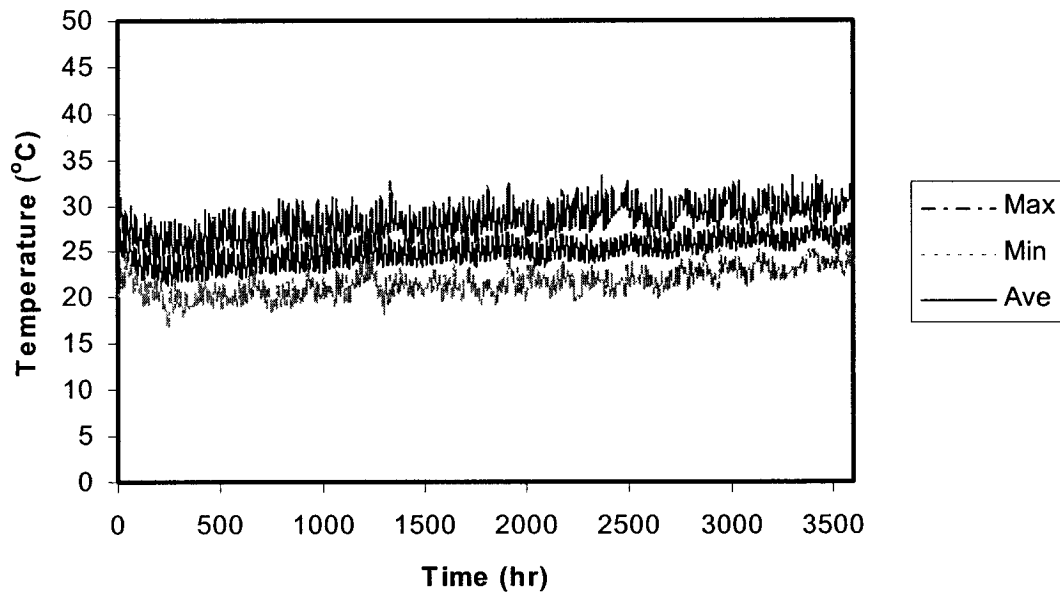


Figure 4.2.3.40. Simulated water temperatures for the middle layer (Treatment 1, Honduras)

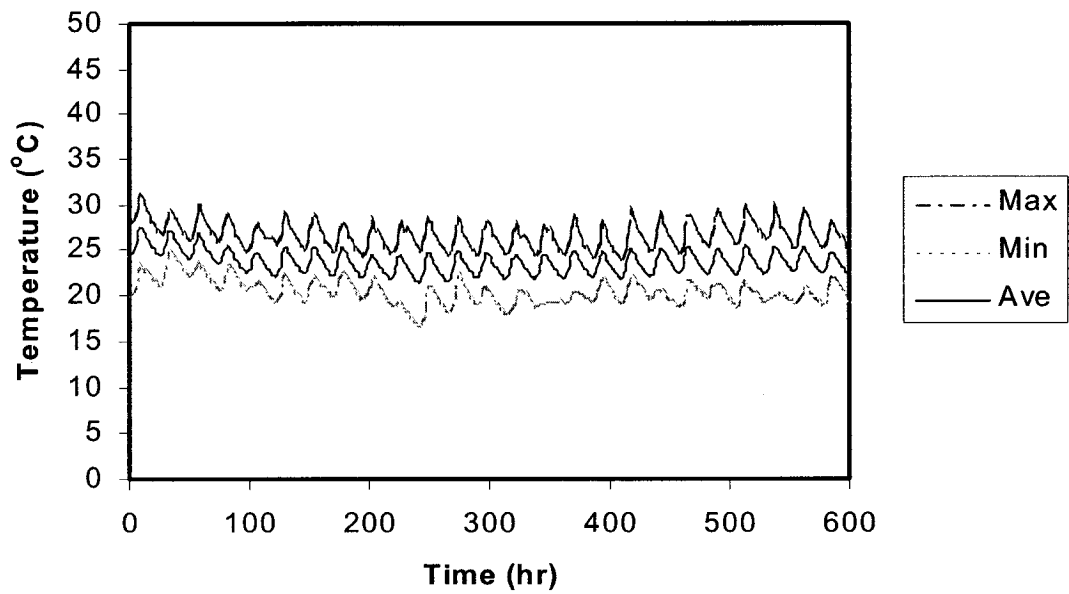


Figure 4.2.3.41. Simulated water temperatures for the middle layer for the first 600 hours (Treatment 1, Honduras)

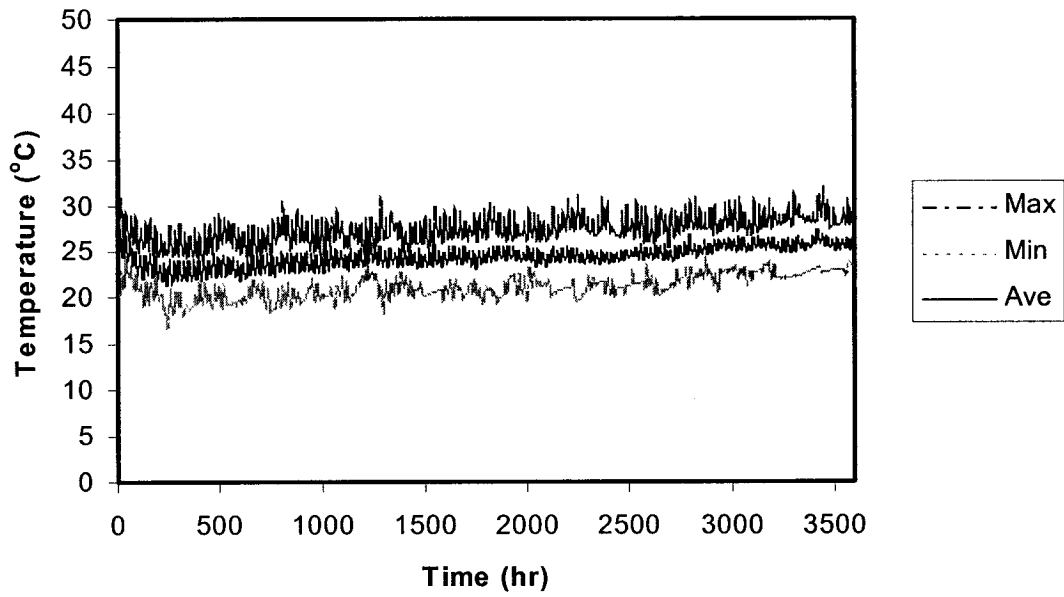


Figure 4.2.3.42. Simulated water temperatures for the bottom layer (Treatment 1, Honduras)

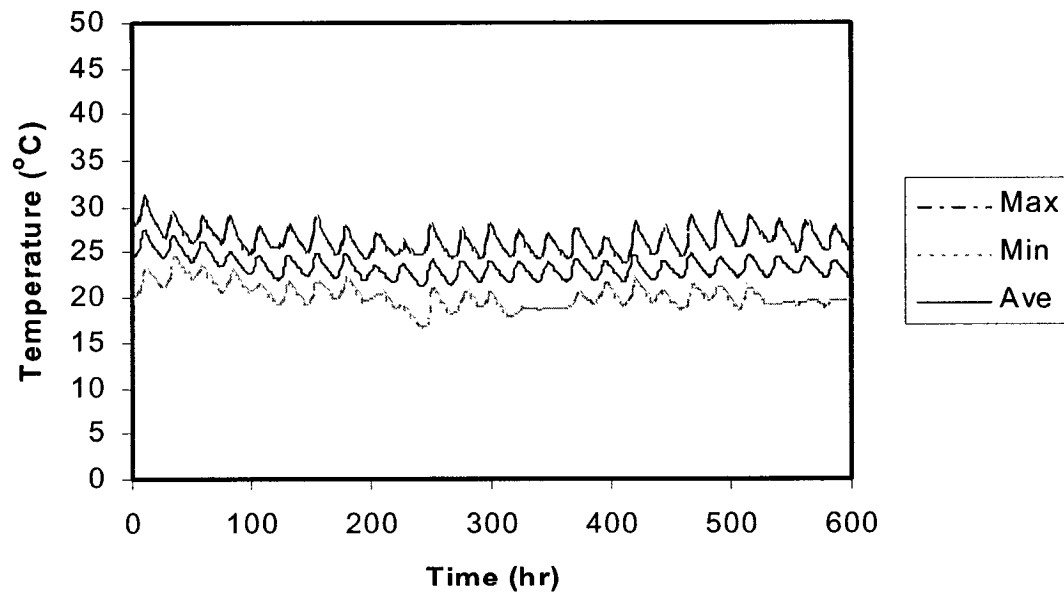


Figure 4.2.3.43. Simulated water temperatures for the bottom layer for the first 600 hours (Treatment 1, Honduras)

Figures 4.2.3.44 and 4.2.3.45 show the simulated DO for the surface layer. The highest DO is 27.36 mg/L. The average DO values are between 0.08 mg/L and 16.48 mg/L, with a mean of 4.24 mg/L. In addition to the diurnal cycle, the simulations have a noticeable fluctuation that is about seven days per cycle. The seven day cycle is due to weekly fertilizer applications. Figures 4.2.3.46 and 4.2.3.47 show the simulated DO for the middle layer. The highest DO is 15.95 mg/L, which is lower than the surface layer. The average values range from 0.02 to 8.81 mg/L, with a mean value of 2.00 mg/L. The seven day cycle is present but the ranges of the fluctuation are smaller than for the surface layer. Figures 4.2.3.48 and 4.2.3.49 show the simulated DO for the bottom layer. The range of the simulated DO is from zero to 13.56 mg/L. The averages of DO are from 0 to 7.51 mg/L, with a mean of 1.22 mg/L. Although the range of DO is much smaller than for the two upper layers, the diurnal and seven day fluctuations are still noticeable.

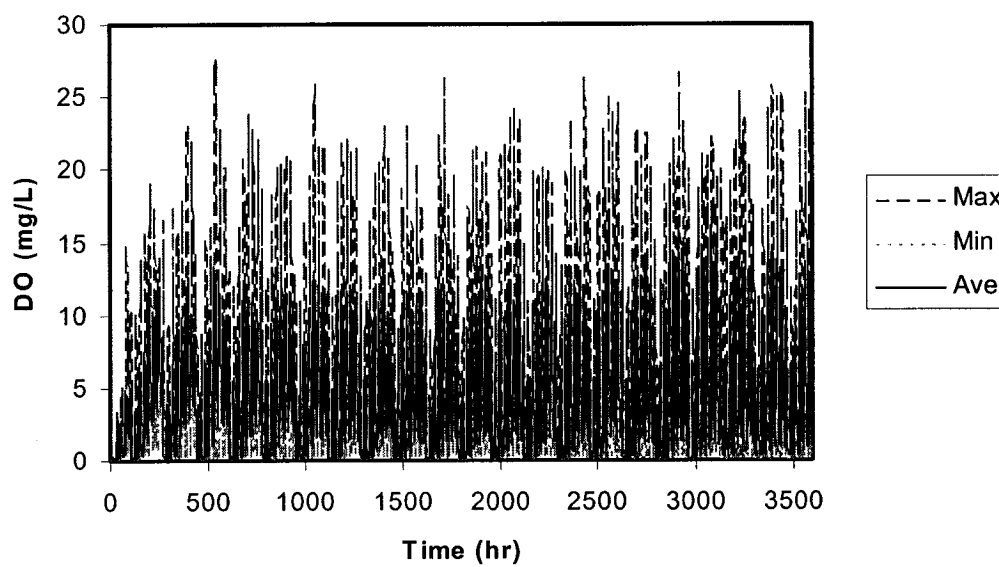


Figure 4.2.3.44. Simulated DO for the surface layer
(Treatment 1, Honduras)

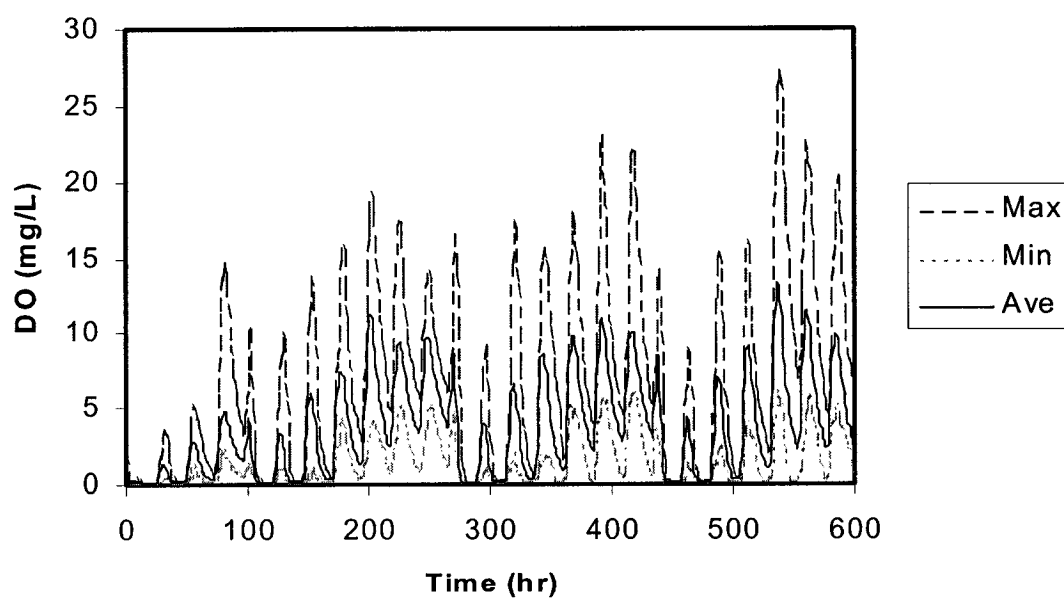


Figure 4.2.3.45. Simulated DO for the surface layer for the first 600
hours (Treatment 1, Honduras)

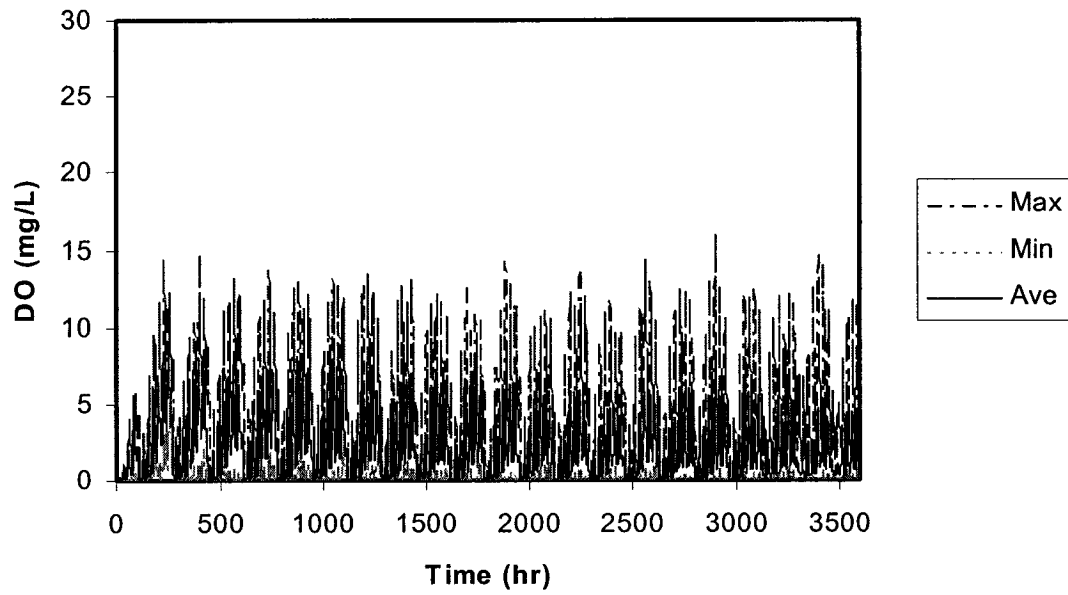


Figure 4.2.3.46. Simulated DO for the middle layer
(Treatment 1, Honduras)

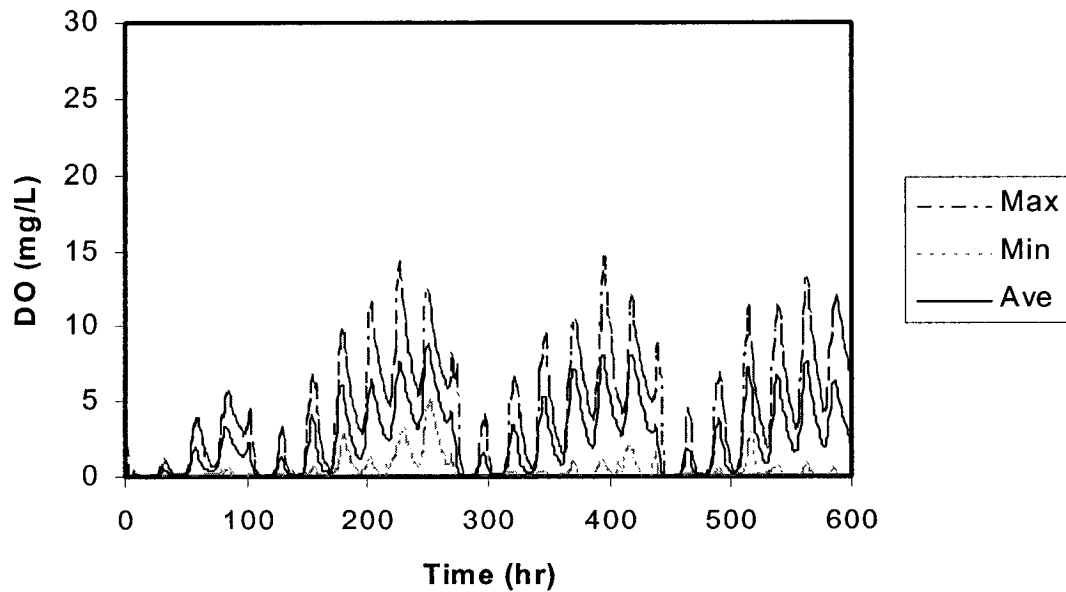


Figure 4.2.3.47. Simulated DO for the middle layer for the first 600 hours
(Treatment 1, Honduras)

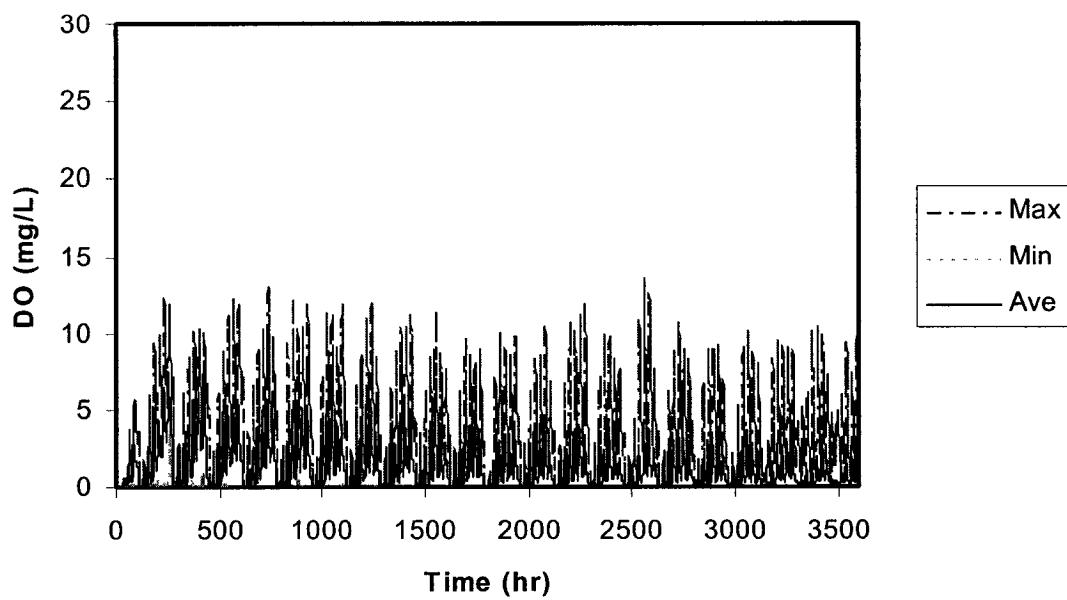


Figure 4.2.3.48. Simulated DO for the bottom layer
(Treatment 1, Honduras)

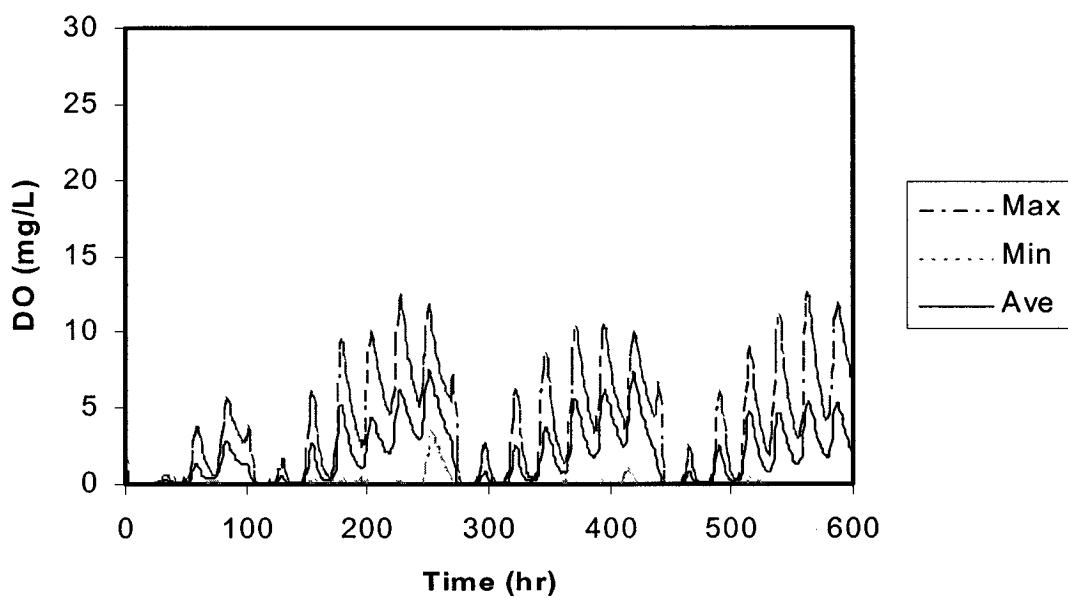


Figure 4.2.3.49. Simulated DO for the bottom layer for the first 600 hours
(Treatment 1, Honduras)

4.3. Fish Growth Simulation Results

The fish growth model was calibrated using values from the same set of data used for the water quality model calibration. The initial values for each location were the mean values obtained from all the fish ponds (Table 4-5). The calibrated parameters in the fish growth model are listed in Table 4-6. The variability of the fish masses under different treatments showed the effects of water quality and food supplies on fish growth rate. The differences between the simulated and measured fish masses at the end of the simulations were tested for significance using the Z test (Freund, 1981).

Table 4-5. Initial conditions for the fish growth model

Parameters	Thailand	Rwanda	Honduras	Description
W_f (kg)	2.6	16.0	37.0	Total fish weight
Fish _{num} (# of fish)	220	380	1012	Fish population
W (g)	11.8	42.0	36.6	Average fish weight

Table 4-6. Calibrated parameters for the fish growth model

Parameters	Thailand	Honduras	Rwanda
Average feed assimilation efficiency	0.625	0.650	0.625
Fraction of feed assimilation efficiency for feeding catabolism	0.25	0.25	0.25
Food consumption efficiency (g fish/hr)	0.03	0.03	0.03
Half-saturation factor for non-phytolankton feed uptake by fish (g/m^3)	10	60	60
Half saturation constant for Chla uptake by fish ($\mu g/L$ Chla)	30 ($W_f < 70$ g) 150 ($W_f \geq 70$ g)	60	60
Critical standing stock (kg/ha)	2000	2000	2000

4.3.1. Thailand Site

Figures 4.3.1.1 to 4.3.1.3 display the simulated and measured fish masses for Treatments 1, 2, and 3, respectively. Table 4-7 lists the means and standard deviations of simulated and observed final fish masses for the three treatments. The simulated and observed means were not significantly different for any of the three treatments ($\alpha < 0.05$).

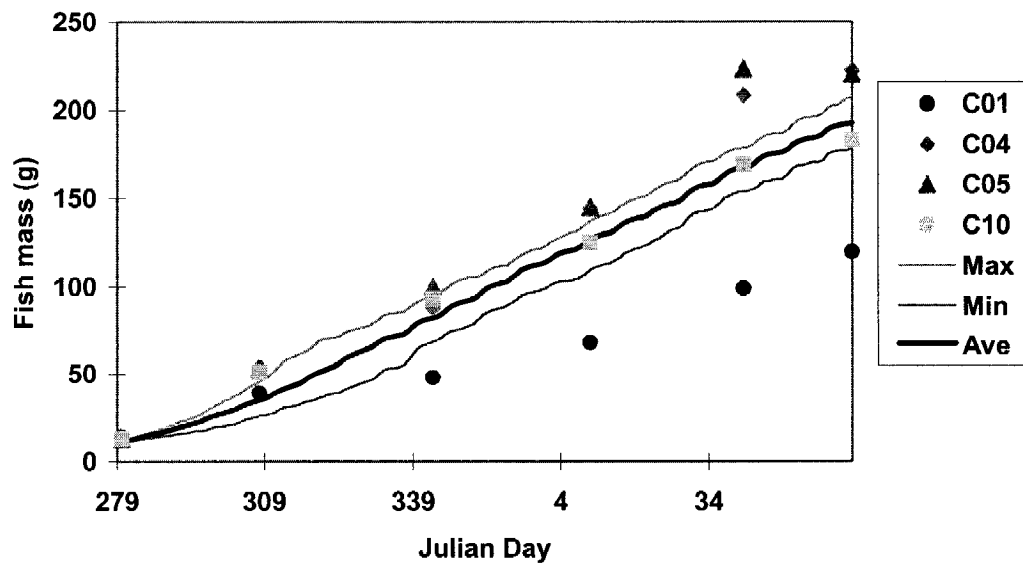


Figure 4.3.1.1. Fish masses for Treatment 1 for the Thailand site

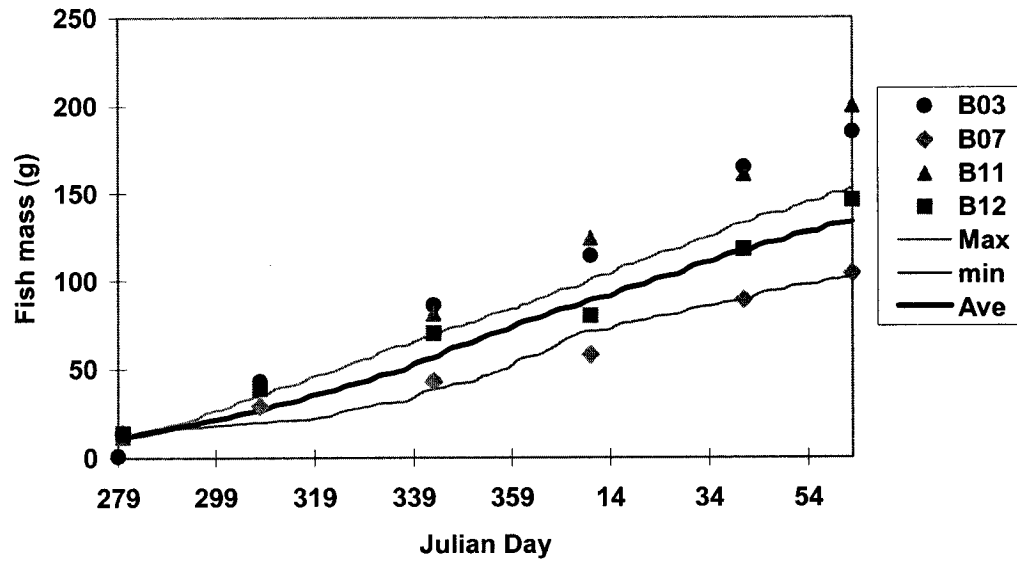


Figure 4.3.1.2. Fish masses for Treatment 2 for the Thailand site

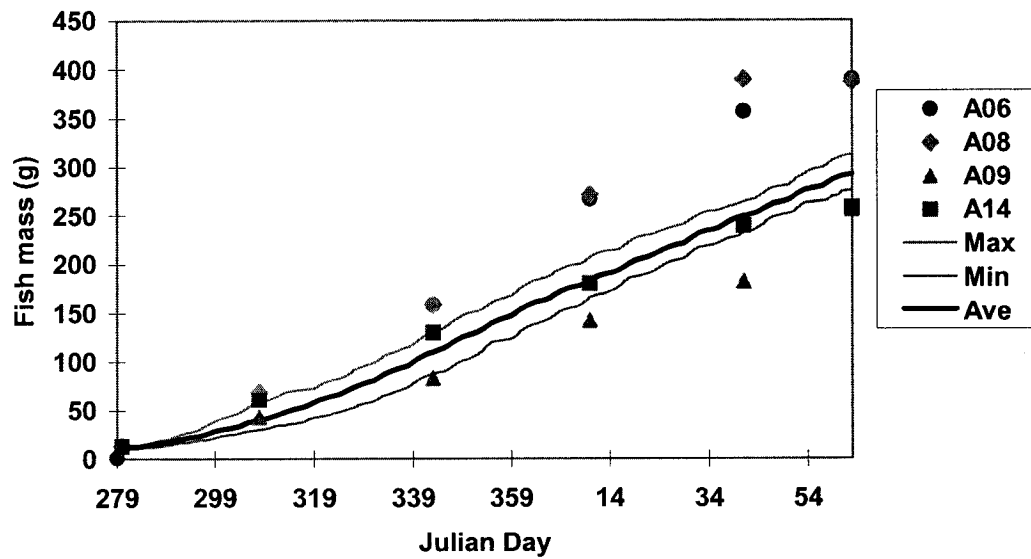


Figure 4.3.1.3. Fish masses for Treatment 3 for the Thailand site

Table 4-7. Fish mass means for different treatments (Thailand site)
(numbers in parentheses represent the standard deviations)

Treatment	Fertilizers (kg/ha/wk)	Simulated fish mass (g)	Measured fish mass (g)
Treatment 1	100 CM + 24.3 UR*	193 (± 14)	186 (± 47)
Treatment 2	44 CM + 10.8 UR	129 (± 26)	158 (± 43)
Treatment 3	200 CM + 48.6 UR	293 (± 19)	322 (± 76)

* CM is Chicken Manure, UR is Urea

4.3.2. Rwanda Site

Figures 4.3.2.1 to 4.3.2.4 show the simulated and observed fish masses for the Rwanda site. Figure 4.3.2.1 shows good agreement between the simulations and observations under Treatment 1. Simulated values were higher than observed values for Treatments 2 and 4. Table 4-8 shows the average and standard deviations of fish masses at the end of the experiments. Simulated and measured means were significantly different for Treatments 2 through 4.

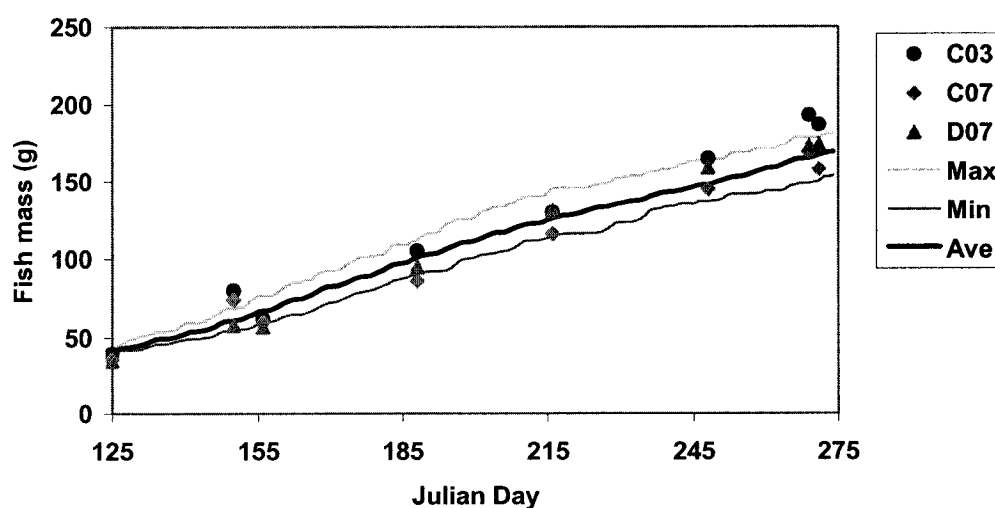


Figure 4.3.2.1. Fish masses for Treatment 1 for the Rwanda site

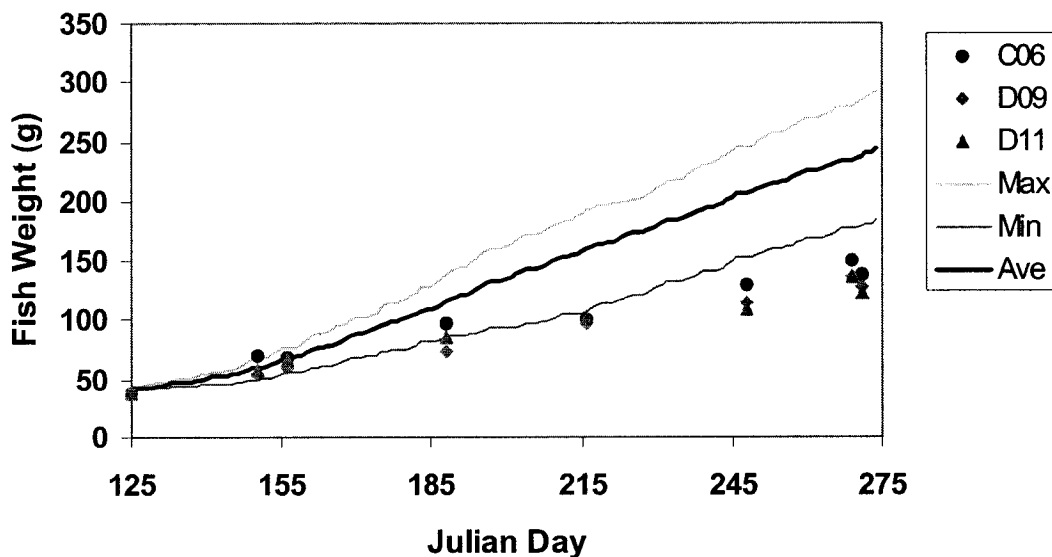


Figure 4.3.2.2. Fish masses for Treatment 2 for the Rwanda site

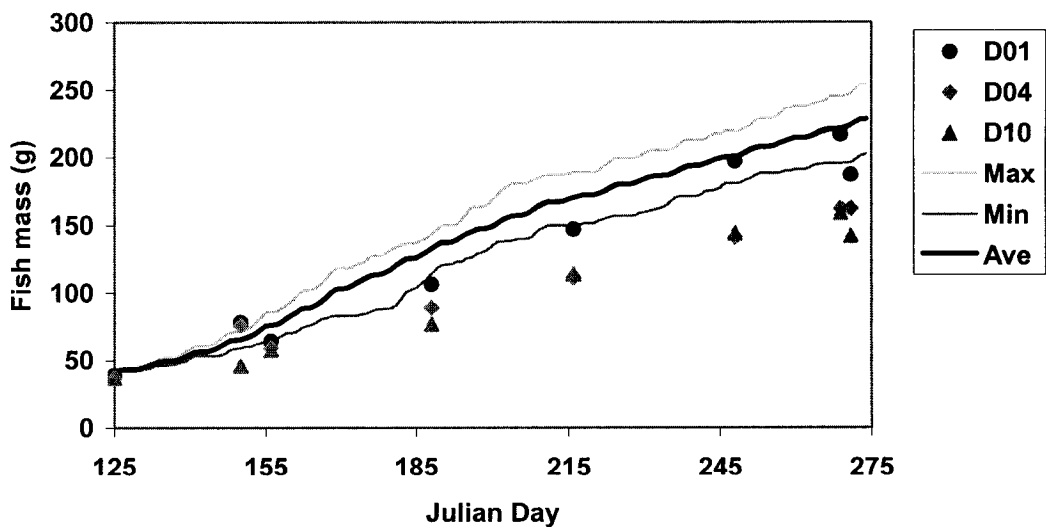


Figure 4.3.2.3. Fish masses for Treatment 3 for the Rwanda site

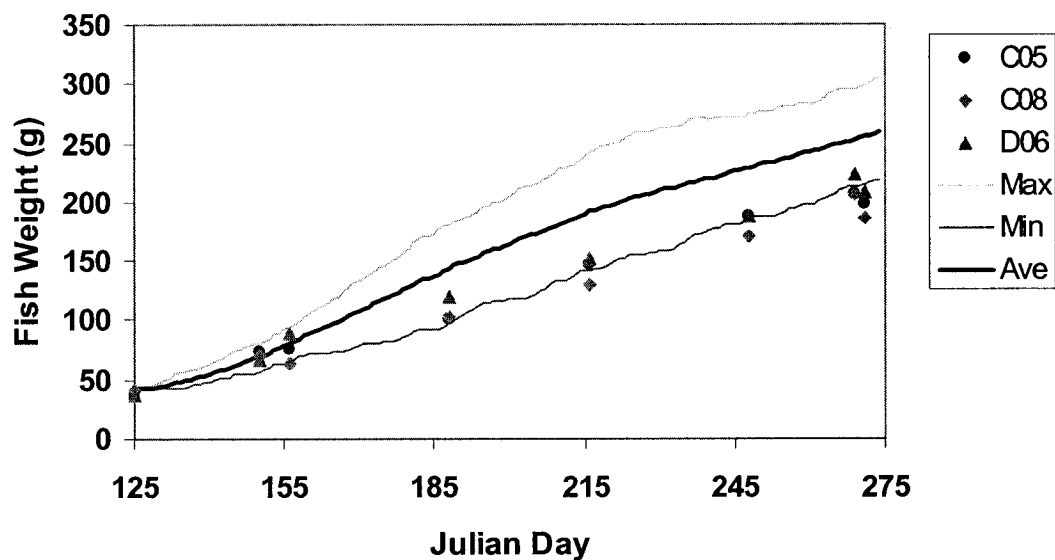


Figure 4.3.2.4. Fish masses for Treatment 4 for the Rwanda site

Table 4-8. Fish mass means for different treatments (Rwanda site)
(numbers in parentheses represent the standard deviations)

Treatment	Treatments (kg/ha/wk)	Simulated fish mass (g)	Measured fish mass (g)
Treatment 1	100 CM + 400 GR*	165 (± 14)	173 (± 15)
Treatment 2	150 CM + 600 GR	234 (± 53)	129 (± 8)**
Treatment 3	200 CM + 800 GR	222 (± 26)	164 (± 23)**
Treatment 4	100 CM + 400 GR +28.6 UR	255 (± 42)	198 (± 11)**

* CM is Chicken Manure, UR is Urea, GR is fresh cut grasses

** means are significantly different between simulated and measured fish masses at $\alpha = 0.05$ using Z test

4.3.3. Honduras Site

The comparisons of simulated and observed fish masses under Treatments 1, 2, 3, and 4 for the Honduras site are shown in Figures 4.3.3.1 to 4.3.3.4, respectively. Figure 4.3.3.1 shows that the simulated average fish masses were lower than the observations during the first three months of culture but the simulated harvested fish masses were higher than the observations. Table 4-9 lists the comparison of the simulated and observed final fish masses at the end of the culture season. There were no significant differences between the simulated and observed fish masses for any of the treatments.

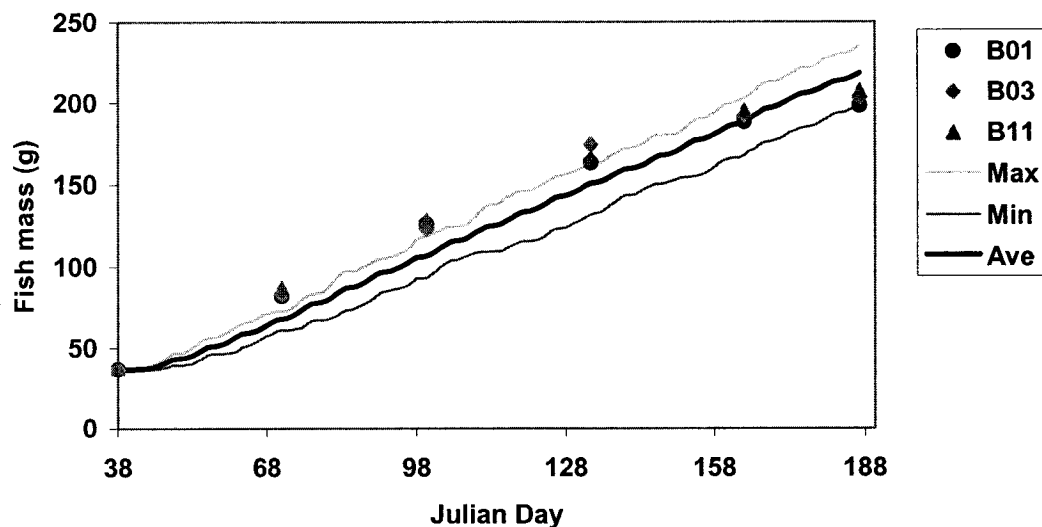


Figure 4.3.3.1. Fish masses for Treatment 1 for the Honduras site

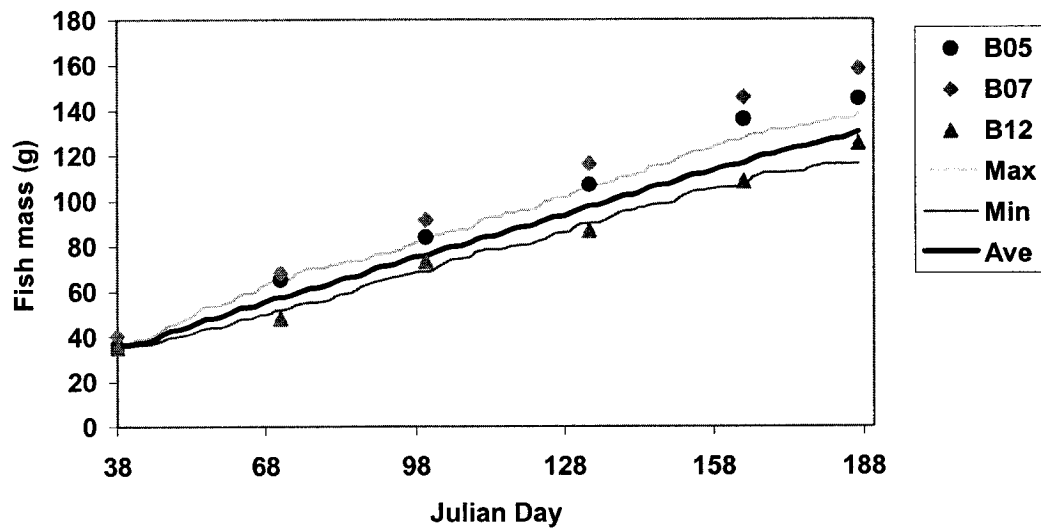


Figure 4.3.3.2. Fish masses for Treatment 2 for the Honduras site

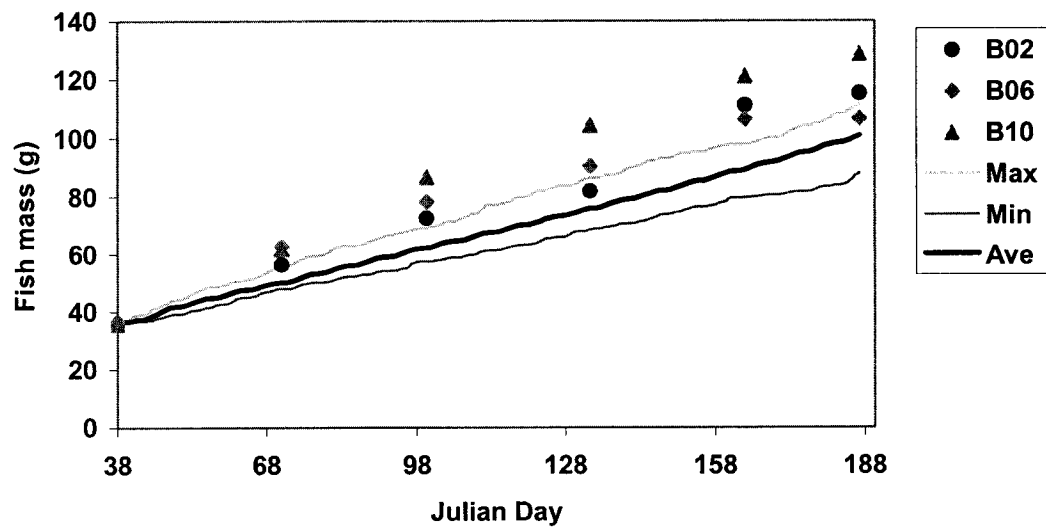


Figure 4.3.3.3. Fish masses for Treatment 3 for the Honduras site

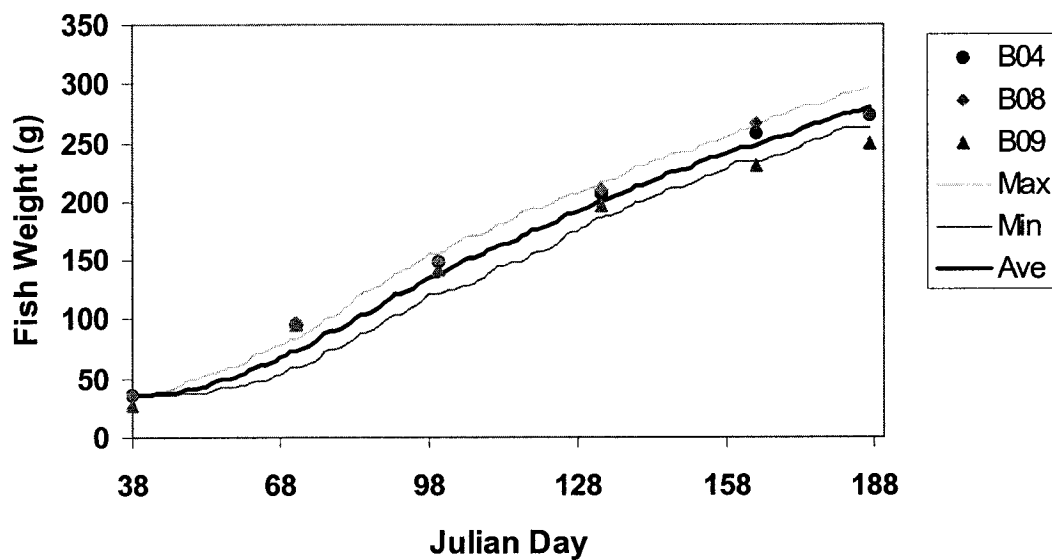


Figure 4.3.3.4. Fish masses for Treatment 4 for the Honduras site

Table 4-9. Fish mass means for different treatments (Honduras site)
(numbers in parentheses represent the standard deviations)

Treatment	Treatments (kg/ha/wk)	Simulated fish mass (g)	Measured fish mass (g)
Treatment 1	500 CM*	217 (± 18)	203 (± 5)
Treatment 2	250 CM	129 (± 11)	143 (± 17)
Treatment 3	125 CM	100 (± 12)	117 (± 11)
Treatment 4	1000 CM	280 (± 17)	266 (± 14)

* CM is Chicken manure

5. Discussion

The simulated and observed state variables are presented in Chapter 4. The differences between the simulated and observed values vary with state variables and locations.

Among the state variables, water temperature simulations are more accurate than DO and Chla. Comparing the simulation results for the three locations, the model predicts more accurately for the Honduras site than for the other two locations. Since the stochastic method is used in the model, all simulation results are presented as ranges or probability distributions. The most important objective for this model is to determine if the simulation results could be used to support decision-making. Possible reasons for the differences between the simulated and observed values are discussed in this chapter.

5.1. Solar Radiation Generation

Solar radiation is one of the major inputs for the water temperature, DO, and Chla models. The stochastic method used in the model generates daily and hourly solar radiation values that represent the local characteristics at a given site. The model was tested for three tropical sites. The generated and observed values showed good agreement for the three sites thereby indicating that the model could be used for tropical locations.

The lack of historical weather data is common for many aquaculture sites. Hence, a major objective of the solar radiation model was to devise a method to generate solar radiation values based on limited historical records. The proposed model estimates the daily solar radiation based on monthly Cumulative Frequency Distribution (CFD) from historical data. The use of monthly CFD instead of daily solar radiation values reduced

the effects of having few data on daily solar radiation. The ranges of simulated daily solar radiation cover most of the measured values for all three sites. Previous studies indicated that an average clearness index $\overline{K_t}$ and a CFD curve have a certain relationship regardless of the location (Liu and Jordan, 1963). If the relationship exists, a set of solar radiation values could be generated for a given $\overline{K_t}$ value from the corresponding CFD. The present study attempts to find whether the relationship exists among the solar radiation data from the three sites.

The three locations have different climates. Therefore, the calculated monthly average clearness indices $\overline{K_t}$ are in different ranges for the three locations (Table 4-2). The Rwanda site has the lowest range from 0.356 to 0.455, the Honduras site has the highest range from 0.514 to 0.654, and the Thailand site overlaps the other two sites with a range of 0.444 to 0.624. The ranges of $\overline{K_t}$ values and the different shapes of the CFD curves (Figures 3.2 to 3.4) indicate that there are site differences. Compared to the curves for the Thailand site, the curves for the Rwanda site tend toward low K_t values and the curves for the Honduras site tend toward high K_t values. There was no overlap of $\overline{K_t}$ for the Rwanda and Honduras sites. The higher $\overline{K_t}$ value for the Honduras site corresponds to a hot and dry climate. The low $\overline{K_t}$ value for the Rwanda site corresponds to a low temperature, medium precipitation, and high elevation climate. The climate for the Thailand site is in between that of Honduras and Rwanda. Although there were months with the same average clearness index $\overline{K_t}$ for the Thailand and Honduras sites, the CFD

curves were different for the two sites (Figure 4.1.2). There were no similar curves between locations but the curve shapes were very similar with similar \bar{K}_t values for the same location. For example, the CFD curves for May and June were almost the same and their \bar{K}_t values were very close (0.480 for May and 0.478 for June) for the Thailand site (Figure 3.1.1). It is difficult to draw a clear relationship between the curve shapes and location based on the comparisons because the calculated \bar{K}_t values may be biased due to the limited data availability. The curve shape is easily skewed if the data set is too small. For example, the January CFD curve for the Honduras site has only 35 data points (a complete data set should be 186 data points) during the six-year period, thus the curve is not as smooth as the others. The data sets were not sufficient to arrive at a general conclusion regarding the universality of \bar{K}_t and the corresponding CFD.

The daily solar radiation was generated using a first order auto-correlation equation. The current data sets have many missing values, which might cause errors in calculating the auto-correlation coefficient ρ . The calculated coefficient ρ for the three sites range from 0.29 to 0.76 which is beyond the range (0.14 to 0.70) of literature values reported by Aguiar et al. (1988). Graham and co-workers (1988) indicated that a coefficient ρ between 0.253 and 0.348 caused no significant differences in generating daily solar radiation. Although the current values are beyond the range reported, the comparison of the generated and measured CFD showed that the effects of ρ are small (Figure 4.1.6). Considering that the values of ρ calculated using the limited solar radiation data may have bias, $\rho=0.29$ was used in the model for the three sites. The comparison of generated and

simulated CFD (Figures 4.1.3a to 4.1.5b) showed small differences between any two curves.

The parameters in hourly value generation model were location independent based on previous studies for a temperate climate (Graham and Hollands, 1990; Knight, et al., 1991). The present model was examined using data from different climates. The generated hourly values covered most observed data for the Thailand and Rwanda sites (Figures 4.1.7 and 4.1.8). For the Honduras site, the generated values were lower than the observations in general (Figure 4.1.9). The major factor affecting the hourly value simulation is the daily clearness index K_t .

5.2. Water Temperature

The stratification of water temperature has been predicted well for all sites under various treatments. Table 5-1 lists the simple statistics of the averages of measured and simulated water temperatures under all treatments. The standard deviations of the simulations for the surface layer are higher than for the other two layers. The observed surface water temperature also had higher standard deviations than the other two layers for all treatments. Average water temperatures for different water layers at a given site showed slight differences. The differences between simulations and observations are higher for the Thailand site than for the other two sites. For the Thailand site, the simulations are always higher than the observations (differences are from 6 to 14%). The results show that the simulation means are significantly different from the observations for the Thailand site (Table 5-1). For the Rwanda site, the differences of the mean values

between the observations and simulations are from -8 to 5% . Statistical results show no significant differences between observation and simulation mean values for any water layer. For the Honduras site all simulations are lower than the observations (differences are from 0 to -9%). The statistical analysis results showed that the differences between the observations and simulations are significantly different only for the surface layer.

From the energy balance overestimated surface water temperatures resulted from either overestimating heat inputs or underestimating heat losses. As described above, the simulated solar radiation closely matches the data. Therefore, underestimation of heat losses appears to be the main factor accounting for the high simulated water temperature. Evaporation plays an important role in heat loss for the surface layer. The evaporation rate is an empirical function of wind speed and vapor pressure (Equation 3-2-19). Wind speed is generated using a stochastic method without calibration due to the lack of data. The vapor pressure is determined using estimated relative humidity and dew-point temperature. These parameters are not calibrated due to a lack of information.

Table 5-1 also shows that the fertilization treatments had a minor influence on the water temperature simulations. It was expected that the temperature for the bottom layer would be reduced at high fertilization rates due to increased turbidity caused by high phytoplankton concentrations. However, neither measured nor simulated temperatures showed the trends expected.

Table 5-1. Average and standard deviations of measured and simulated water temperatures for each treatment

Site	Treatment – Water layer	Measured (°C)	Simulated (°C)	Differences (%)
Thailand	Treatment1-surface	27.1 (±1.83)	30.9 (±2.27)	14%*
	Treatment2-surface	27.0(±1.78)	30.4(±2.31)	13%*
	Treatment3-surface	27.3(±1.88)	30.4(±2.02)	11%*
	Treatment1-middle	26.5(±1.50)	29.0(±1.24)	9%*
	Treatment2-middle	26.6(±1.61)	28.3(±1.52)	6%*
	Treatment3-middle	26.7(±1.57)	29.1(±1.16)	9%*
	Treatment1-bottom	26.0(± 1.40)	27.5(±1.31)	6%*
	Treatment2-bottom	26.1(±1.52)	27.1(±1.62)	4%*
	Treatment3-bottom	26.2(±1.41)	28.0(±1.17)	7%*
Rwanda	Treatment1-surface	22.8(±2.11)	23.1(±1.49)	1%
	Treatment2-surface	22.7(±2.21)	23.9(±1.34)	5%
	Treatment3-surface	22.8(±2.12)	23.0(±1.46)	1%
	Treatment4-surface	22.6(±2.17)	22.6(±1.37)	0%
	Treatment1-middle	21.9(±1.95)	21.8(±0.56)	0%
	Treatment2-middle	21.5(±3.21)	22.3(±0.24)	4%
	Treatment3-middle	21.9(±1.88)	21.6(±0.50)	-1%
	Treatment4-middle	21.5(±1.82)	19.8(±0.43)	-8%
	Treatment1-bottom	21.2(±1.77)	20.9(±0.58)	-1%
	Treatment2-bottom	20.6(±1.26)	21.3(±0.23)	3%
	Treatment3-bottom	21.1(±1.63)	20.5(±0.21)	-3%
	Treatment4-bottom	20.7(±1.67)	19.8(±0.43)	-4%
Honduras	Treatment1-surface	27.2(±2.70)	26.3(±2.34)	-3%*
	Treatment2-surface	27.4(±4.80)	26.7(±5.10)	-3%*
	Treatment3-surface	26.8(±4.60)	26.7(±4.88)	0%*
	Treatment4-surface	27.4(±4.65)	26.3(±4.89)	-4%*
	Treatment1-middle	26.6(±2.33)	25.1(±1.41)	-6%
	Treatment2-middle	25.4(±3.19)	25.2(±3.28)	-1%
	Treatment3-middle	25.3(±2.95)	25.2(±3.05)	0%
	Treatment4-middle	26.9(±2.42)	24.5(±3.07)	-9%
	Treatment1-bottom	25.8(±2.09)	24.3(±2.90)	-6%
	Treatment2-bottom	24.5(±2.83)	24.3(±2.90)	-1%
	Treatment3-bottom	24.7(±2.67)	24.6(±2.75)	0%
	Treatment4-bottom	24.5(±2.89)	24.3(±2.92)	-1%

* significantly differences between the observed and simulated mean values for each treatment and for each water layer using t-test at $\alpha=0.05$.

In general, the simulations are closer to the observations for the middle and bottom layers than the surface layer. Solar energy penetrates from the water surface into the water column affecting the heat balance. In the model the light extinction coefficient is a dynamic factor that changes with simulated Chla. The light extinction coefficient, η_{kt} is affected by turbidity caused by phytoplankton and non-phytoplankton components. Local measured Secchi disk visibility and Chla were used to estimate the relationship between light extinction coefficient and Chla. The phytoplankton light extinction coefficient is almost independent of location. The non-phytoplankton light extinction coefficient varies with location (Table 4-4). The Honduras site had the highest value and the Rwanda site had the lowest value, so the effect of Chla changes on the water temperature is much less than for the Honduras site than for Rwanda site. Compared to the DO simulation (to be discussed later), the effect of Chla on water temperature is not very strong even for the Rwanda site, where the measured Chla concentrations had high variability in replicates but the variability of the measured water temperature from those replicates was small.

5.3. Dissolved Oxygen and Phytoplankton

The simulated DO and Chla are strongly related to each other. Any failure of the Chla simulation results in errors in the DO simulation. The site specific parameters (Table 4-4) were calibrated to achieve the best overall agreement between the simulations and observations.

It was difficult to calibrate the DO model for the Thailand site. Despite the high variability of DO in pond replicates, the DO values are underestimated for most ponds

receiving Treatments 1 and 2 (Figures 4.2.1.4 to 4.2.1.6 and 4.2.1.11 to 4.2.1.13). For Treatment 3, only the surface layer DO was close to the observations and the middle and bottom layer's DO were underestimated (Figures 4.2.1.18 and 4.2.1.19). The model assumed that the Chla and nutrients are uniformly distributed and that the light extinction coefficient, η_{kt} could limit the light penetration. The light extinction coefficient was estimated using a linear regression equation with non-phytoplankton (η_{kw}), phytoplankton coefficients (η_{kc}), and the concentrations of Chla (Equation 3-2-12). Both η_{kc} and η_{kw} are considered as constants. For a heavily fertilized fish pond, light penetration could be more strongly affected by non-phytoplankton contributions than by phytoplankton. The non-phytoplankton light extinction coefficient had wide ranges among sites and between duplicates from the observed data. The applied fertilizers, the color of humic substances, and the sediment re-suspension caused by wind and fish movement could be major sources of turbidity. The high variability in η_{kw} might in part be due to the different fertilizer application and organic matter concentration (Teichert-Coddington, et al., 1990). The calculated non-phytoplankton turbidity, η_{kw} was $6.11 \pm 2.18 \text{ m}^{-1}$ with a very low correlation coefficient R^2 . Therefore, the simulated DO stratification could not be improved even with the calibration of η_{kw} . It seems inappropriate to use a constant as a non-phytoplankton light extinction coefficient for a long-term simulation.

The simulated Chla affects the light penetration and DO production. The differences of simulated and observed Chla for the Thailand site indicated that the Chla model did not predict the conditions in the ponds (Figures 4.2.1.7, 4.2.1.14, and 4.2.1.21). Jamu (1998)

suggested that the differences were partially due to zooplankton grazing. Zooplankton grazing could have a significant effect on the Chla (Reynolds, 1984).

The major Chla consumption is by fish grazing. The selective grazing behavior of tilapia could change the Chla concentration because the phytoplankton density, species, and distribution changes (Dempster et al., 1995). In the model, the half-saturation Chla uptake coefficient was calibrated (Table 4-4). For the Thailand site, the half-saturation Chla uptake rate was calibrated using two values based on fish weight: when fish weight is less than 70 g the uptake rate is 30 $\mu\text{g/L}$, otherwise, the Chla uptake is 150 $\mu\text{g/L}$ (Table 4-6). Because the initial fish weight (only 11.8 g) for the Thailand site was much smaller than for the other two sites (42.0g and 36.6 g for Rwanda and Honduras sites, respectively), the use of two values improved the Chla and fish growth simulations. For the Rwanda and Honduras sites, only one value (60 $\mu\text{g/L}$) was used for the half-saturated Chla uptake coefficient.

A critical factor for DO and Chla simulation is the ratio of carbon to Chla (CChla). CChla depends on the initial slope of the PI curve, maximum Chla growth rate, maximum light intensity (I_{max}), and temperature (Equation 3-2-49). The initial slope of the PI curve is a site-specific parameter. The calibrated value for the Thailand site is slightly higher than for the other two sites (Table 4-4). The maximum Chla growth rate is an empirical parameter that is a function of optimum temperature. The model assumed that the maximum Chla growth is independent of light intensity but is affected by the maximum light intensity. The effect of maximum light intensity was estimated by taking into

account the maximum light intensity over a running three day period. This modified I_{max} smoothed the rapid changes in maximum light intensity that could result in sudden changes in Chla growth (Reynolds, 1984). For a long-term simulation, the use of modified I_{max} is expected to be more realistic than using a constant I_{max} .

The simulated CChla varied hourly because the effect of hourly water temperature is included (Equation 3-2-50). The simulated CChla had the lowest value at 6 am and highest value at 10 am. It is difficult to explain the diurnal changes of CChla because the uncertainties in the relationship between light and carbon content (Geider et al., 1997).

The relationship between the measured DO and Chla is important in identifying potential problems in model calibration and validation. For Treatment 1 at the Thailand site, the super-saturated DO was observed at Chla below 100 $\mu\text{g/L}$ and over 600 $\mu\text{g/L}$. The difference of Chla in replicates was over 700 $\mu\text{g/L}$ (Figure 4.2.1.7). The observed Chla for Treatment 2 had a similar trend but smaller differences than for Treatment 1 (the highest difference was about 350 $\mu\text{g/L}$, Figure 4.1.14). For Treatment 3, the observed Chla was the highest because of fertilization rate. It appears that the fertilizer application affected the phytoplankton growth and consumption rates.

For the Rwanda site, the simulated Chla curves were relatively flat and covered most of the observations except for a few peak values (e.g. Figure 4.2.2.21 pond D01). The cause of the peak values is unknown and the model did not predict them accurately. For the Honduras site, the measured DO and Chla had low variability in the replicate ponds. The

simulations were very close to the observations. However, there were not many measured Chla values in the first two months of the simulation period. Therefore, it is not possible to determine whether the Chla was predicted accurately during this period.

The DO consumption terms affect the DO simulation directly. One of the main DO consumption terms is due to organic matter decomposition. The organic matter sources include applied fertilizers, dead phytoplankton, and fish feces. The decomposition rate was a constant for each organic matter source. The added fertilizers served as the nutrient supply for phytoplankton growth and the food for fish and microorganism. Fertilizer decomposition consumes oxygen and releases nitrogen that stimulates primary production, that in turn increases the oxygen supply. The ratio of oxygen consumption and organic matter decomposition was assumed to be a constant, determined in the model calibration (Table 4-4). The amount of oxygen consumed by organic matter decomposition is much less than the phytoplankton respiration. Therefore, changes in the organic matter oxidation rate do not result directly in major changes in DO.

Among the organic matter, the DO consumption due to the decomposition of dead Chla and fish feces are much smaller than that due to the decomposition of applied fertilizer. The weekly fertilizer application caused the weekly cycle of DO fluctuation (e.g. Figure 4.2.3.45). The simulated DO was reduced sharply when fertilizer was added. The fertilizer application also increased TAN concentration that stimulated the phytoplankton growth and DO concentration increased in the following days. The fluctuation suggested

that a higher frequency and lower amount of fertilizer per application would help in water quality management.

Although the fertilizer treatments are the same for replicate ponds in the current experiment, previous experiments in those ponds might have had different treatments that caused sediment differences that carry over to the new experiments (Boyd and Teichert-Coddington, 1994). This could be one of the reasons of high DO and Chla variations in the replicates.

The major advantage of the model is to predict the risks for fish losses based on the DO probability distributions. The frequency distributions change with water layers and time. The frequency distributions for DO in the upper layers were much wider than for the lower layers. For the surface layer, the frequency distributions varied with the time of day but for the bottom layer, the frequency distributions were independent of time. The low DO risks are showed well by the frequency distributions. Although the distributions vary with locations, the lowest DO (≤ 0.5 mg/L) had the highest frequency at 6:00 for all water layers. The other extreme DO value (≥ 20 mg/L) occurred at 14:00 for the Thailand site. However, the frequency distributions indicated that the frequencies were uniformly distributed from 2.5 to 10.5 mg/L (see Figures 4.2.1.25, 4.2.2.32, and 4.2.3.32).

The major difference of the model from the previous deterministic models is to predict the extreme fluctuations of water quality variables. The magnitude of the fluctuations predicted with this model is due to random weather variables. The frequency

distributions of DO at each water layer can be used to predict some of the risks associated with fish production at a given site with a given management strategy. A deterministic model can predict that low DO occurs in early morning, but the present model provides information on the probability of the low DO occurrence. The comparison of the frequency distributions of simulated and observed DO for the Honduras site showed that the model is reliable. The good simulations of Chla and DO for the Honduras site proved that the model captures the main affecting factors in the pond system. The simulated Chla and DO reflected the changes of fertilization rates.

5.4. Fish Growth

Fish growth rate is estimated based on the energy intake, losses, and transformations within a fish body. The simulated fish growth reflects the influence of weather, water quality, and fertilization treatments. The differences between the observed and simulated fish weights varied with treatments and locations. The ranges of simulated fish weights were much less than the variability of observed fish weights among replicate ponds. The causes of the high variability among the replicate ponds are not clear but the ranges of simulated fish weights are the effects of random variables. The major influences on fish growth are food supply and water quality. The associative effects on food intake, such as food competition are not included in the model. The Chla is the major food supply for fish growth in this model and the quality of Chla simulations and data availability affect the fish model directly.

For the Thailand site, the fish growth rates are similar to those observed during the first two months of culture. The Chla supply seems not to be a limiting factor on fish growth because the rapid increase of the simulated Chla concentration did not result in rapid fish growth (Figures 4.3.1.1. to 4.2.1.3). The observed fish weights had relatively small variations. However, during the last month of the fish culture trial the observed weights had high variations but not the simulated values. The differences indicate that the differences among pond replicates were not due to the uncertainty of weather variables. The average fish weights were not significantly different between the observations and simulations at harvest time for all fertilization treatments. The final average fish weights also indicate that higher fertilization rates resulted in higher fish growth rates.

The Chla appears to be a limiting factor for fish growth. For the Thailand site, the initial fish weight was much smaller than for the other two sites. Considering the larger differences between the fish weights at stocking and at harvesting, the half saturation Chla uptake coefficient used two values dependent on the fish size. It was assumed that the filter feeding ability changes as a function of fish size. A laboratory study reported that two different sizes of juvenile tilapia had different ingestion rates (Northcott, et al., 1991). For the smaller size fish (40 mm standard length, SL), the grazing rate is lower than the larger fish (85 mm SL) at the same algal concentrations. Therefore, the relationship between fish grazing rate and algal concentration was described using a logarithmic regression for smaller fish and a linear regression was used for larger fish (Northcott, et al., 1991). In the current model, the use of two half-saturated Chla uptake constants was attempted to obtain better simulation result for Chla and fish weight. In

Northcott's study, the ingestion rate was also found to increase with particle size. The high variability of Chla and fish weights in replicates might be affected partly by phytoplankton species.

For the Rwanda site as for the Thailand site, fish growth is not always proportional to the fertilizer treatment. The simulated average fish weight at the end of simulations was lower for Treatment 3 (200 kg chicken manure and 800 kg green grass per hectare per week) than for Treatment 2 (150 kg chicken manure and 600 kg green grass). Comparing the simulation fish growth curves between Treatments 2 and 3 (Figures 4 3.2.2. and 4 3.2.3), the simulated fish growth rates were slower for Treatment 3 after about three months. Chla is still a factor for fish growth, so any error in the simulated Chla could change the fish growth. However, the extremely high Chla observed in the ponds did not affect fish growth. Although the simulated fish weights were not correlated to the fertilization rate for all fertilizer treatments, the highest fertilization rate did result in the highest fish yield.

For the Honduras site, there were no significant differences between the observed and simulated average fish weights at the end of simulations (Table 4-9). However, the observed fish weight curves showed slow increases in the last month of fish culture (Figures 4 3.3.1 to 4.3.3.4). Fish growth rate is described using a power form. It was expected to have the fish growth slow at certain time because of physiological and environmental influences. The flatter curve of observed fish weights indicated a slowing of fish growth but the simulated curves showed a different trend, especially for Treatment

1 (Figure 4. 3.3.1). Pond carrying capacity is used to describe the limitation of fish growth under certain conditions (Nath, 1996). In the fish model, a relative feeding level λ_f represents the effects of pond carrying capacity (Equation 3-3-2). If the standing crops of fish exceed the critical standing crop the natural food availability declines and the relative feed level is reduced. The critical standing stock varies with pond management. For a fertilized pond without artificial food, the amount of natural food can be increased up to a certain maximum level, and increasing the pond carrying capacity (Cuenco et al., 1985c). In the model, the slow growth rates for the high fertilize ponds were limited by TAN not by food supply.

The simulated fish weights showed the effects of water quality and food supply. The present model includes the effects of water quality, food supply, fish size, and stocking density but does not consider the effects of food competition, appetite, digestion, and disease. The variations of simulated fish weight are due to the effects of stochastically generated weather variables only.

6. Conclusions

The model development was focused on the construction of the solar radiation model, the effects on the stratification of water temperature and DO as well as on the fish growth rate. The major contribution of the model is to illustrate the impacts of weather on water quality and subsequently on fish growth over both short and long terms in a fishpond. In general, the probability distributions of water temperature and DO under the influence of weather variables, especially solar radiation can be predicted for a stratified fishpond. To examine the capability of the model, the model simulation results were carried out for 36 ponds at 11 fertilization treatments for three different locations. The model can be used to predict the effects of fertilization practices on water quality and fish growth and to assess the risk that water quality will degrade affecting fish growth and survival.

6.1. Model Approach and Performance

All weather variables including solar radiation, air temperature, wind direction and speed are generated using stochastic methods. Randomly generated weather variables are the inputs for deterministic water quality models. The deterministic models simulate water temperature, DO, Chla, and TAN.

A major difficulty in developing a solar radiation model is to obtain the local climate characteristics from the limited data available for aquaculture sites. Fortunately, the monthly cumulative frequency distribution (CFD) curves can be obtained from limited historical weather data and daily solar radiation values can be generated from site specific CFD. For the three locations, the monthly average clearness index values (\bar{K}_t) were

different, most likely representing climate characteristics. The three sites have different average air temperature and annual precipitation. The calculated \bar{K}_t values can be divided into three ranges corresponding to weather differences. The Rwanda site weather is cool and humid, the calculated \bar{K}_t values are in the lowest range. The Thailand site is warm and humid, the \bar{K}_t values are in the middle range. The Honduras site is cool and dry and the \bar{K}_t values are in the highest range. Although there is some overlap in \bar{K}_t values between locations, CFD differ for different locations even with the same \bar{K}_t value.

The development of the solar radiation model is crucial for the water quality model because the randomly generated hourly solar radiation affects the water quality simulation. The comparison of the observations and simulations showed that the solar radiation models performed satisfactorily for all three locations. The hourly model can be used for any locations because the fixed parameters are independent of the locations. However, the hourly values are dependent on the daily clearness index \bar{K}_t .

The water temperature model is built on well-established concepts, so the simulated water temperatures are close to the observations for most ponds. The hourly solar radiation plays a major role in the water temperature simulation. Although other weather variables, such as air temperature, wind speed, and wind direction are important factors for the water temperature simulation, their effects were not evaluated. The effect of

fertilization treatment on water temperature appears minor based on the simulations at various treatments.

The DO model predicted well for the Honduras and Rwanda sites but not for the Thailand site. The probability distributions indicated the possible risks for extremely high and low DO during certain time periods. The DO model also predicted the DO changes under different fertilization treatments. The DO model is constructed for both short and long-term simulation. The long-term simulations revealed the effects of fertilizer application. The simulation results suggested that changes of fertilizer application rate and frequency could reduce the low DO occurrences.

The Chla model is a key component of the DO model. The Chla were predicted well for the Honduras site but not for the Thailand site. The observations for the Thailand site had high variability among pond replicates. The exact reasons for the high variability in the replicated ponds could not be identified. It is common for ecological system to have high variability in replicates because of the uncertainty of ecological system. The deterministic model cannot describe the uncertainty of the pond system. However, the Chla model may be improved if the model includes zooplankton and the species of phytoplankton. At the current stage, the model could not include these two factors because no data were available to support model calibration and validation.

The Fish growth model predicted well for most fishponds. The variability of simulated fish due to weather variables is much smaller than that of any water quality variables.

Higher fertilization resulted in higher fish growth rate for the Thailand and Honduras sites but the higher fertilization resulted in lower fish growth for some ponds for the Rwanda site. This is probably due to high TAN concentrations under high fertilization rates. Fish death due to low DO is not simulated in the present model.

Based on the simulation results, the study reached its objectives. The advantages of the model:

- (1) The model can predict both long- and short-term water temperature as well as DO for a stratified fish pond.
- (2) The randomness and uncertainty of weather variables are taken into account in the water quality model.
- (3) The outputs provide the probability distributions of water quality and fish growth under certain site characteristics.
- (4) The model application is simple and requires a few input variables.
- (5) The model is easy to update and refine as additional information available.

6.2. The CRSP Database

The CRSP database provides detailed information about the weather and water quality in several countries. The database contains different treatments at different locations for similar fish species. Without these data, the model could not be developed. Since the experiment design was not prepared for this specific study, the weather data are not ideal for the model development. The weather data were recorded only during experiment periods but the model requires continues data. The wind speed and direction are random variables that can significantly affect stratification and water quality distribution, while

the local measured data will help to improve the accuracy of simulations. Inclusions of relative humidity and precipitation will be useful in future model modifications. More detailed information about zooplankton and species of phytoplankton may help to construct a random term in phytoplankton model and in fish growth model.

6.3. Future Work

The present model is used to predict water quality and fish growth under randomly generated weather variables. Based on the results of the study, the following are recommended for future research:

- Weather variables: the current model includes air temperature, wind speed and direction models. These models use a simple structure and most of the parameters were adapted from the literature. The models were not validated due to lack of data. It is necessary to validate these models when additional data become available.
- Account for precipitation: the current model does not include precipitation. Rainfall could impact the stratification of water temperature and DO directly, and impact the other water quality parameters indirectly. It is particularly important for the sites that have high precipitation rates.
- Phytoplankton: the dynamic behavior of phytoplankton needs to be explored further. The phytoplankton distribution in the water column in terms of size, species, and Chla concentrations should be considered. Filter feeding fish grazing rate depends on the fish species and size. A detailed model for fish grazing may help in the Chla simulation if the phytoplankton size and species are known.

- Zooplankton: a model for zooplankton should be developed. Zooplankton could affect the phytoplankton and DO mass balances significantly.
- Light extinction coefficient: the light extinction coefficient estimation needs to be modified for a long-term simulation. A stochastic model may be suitable to estimate the light extinction coefficient based on the concentration of Chla and inorganic matter.
- Nitrogen model: a detailed nitrogen distribution model for fish pond has been developed by Jamu (1998). The model includes a nitrogen cycle in the water column and sediment. It is possible to combine the present model with Jamu's model. The information may be more useful for pond management. The combined model could improve the prediction of the impact of fertilization.
- Sediment model: a detailed model to describe organic matter decomposition in the sediments is necessary. It may improve the DO simulation for the bottom water layer.
- Fish mortality: death rate is estimated from the data using a constant in the model. The mortality rate due to DO deficiency may need to be included if the model is used for different fish species. TAN caused mortality needs to be considered in the model after a detailed TAN model is included.

REFERENCES

- Almazan, G. and C. E. Body. 1978. Evaluation of secchi disk visibility for estimating plankton density in fishponds. *Hydrobiologia*, 61:205-208.
- Aguiar, R. J., M. Collares-Pereira, and J. P. Conde. 1988. Simple procedure for generating sequences of daily radiation values using a library of Markov transition matrices. *Solar Energy*, 40(3): 269-279.
- Amato, U., A. Andretta, B. Bartoli, B. Coluzzi, and V. Cuomo. 1986. Markov processes and Fourier analysis as a tool to describe and simulate daily solar irradiance. *Solar Energy* 37(3): 179-194.
- Balarin, J. D. and R. D. Haller. 1982. The intensive culture of tilapias in tanks, raceways and cages. In J.F. Muir and R.J. Roberts (editors). *Recent Advances in Aquaculture*. Croom Helm Ltd., London. 265-356.
- Balousktsis, A., D. Tsanakas, and G. Vachtsevanos. 1986. Stochastic simulation of hourly and daily average wind speed sequences. *Wind Engineering* Vol. 10, No. 1: 1-11.
- Banks, R. B. and F. F. Herrera. 1977. Effect of wind and rain on surface reaeration. *Jour. of Envir. Engineering Division*. ASCE, 103(EE3):489-504.
- Bendt, P. M., M. Collares-Pereira, and A. Rabl. 1981. The frequency distribution of daily insolation values. *Solar Energy* 27: 1-5.
- Box, G. E. P. and G. M. Jenkins. 1976. *Time series analysis forecasting and control*. Holden-Day, San Francisco, 575 pp.
- Bolte, J. P., R. O. Smitherman, and D. T. Hill. 1986. Applications of mathematical modeling to pond aquaculture: a state of the art review. Presented at the 1986 Summer Meeting Am. Soc. Ag. Engr., San Luis Obispo, California, June 29-July 2, 1986. ASAE Paper No. 86-5049.
- Bolte, J. P., S. S. Nath, and D. E. Ernst. 1994. Pond: A decision support system for pond aquaculture. In: H. Egna, J. Bowman, B. Goetze, and N. Weidner (Editors) *Twelfth Annual Technical Report. Pond Dynamics/Aquaculture CRSP, Office of International Research and Development, Oregon State University, Corvallis, Oregon*, pp 48-67.
- Boyd, C. E., R. P. Romaine, and E. Johnson. 1978. Predicting early morning dissolved oxygen concentrations in channel catfish ponds. *Transactions of the American Fisheries Society*, 107(3):484-492.

- Boyd, C. E. 1979. Water quality in warmwater fish ponds. Auburn University Agricultural experiment station, Auburn, Alabama, 359 pp.
- Boyd, C. E. and D. Teichert-Coddington, 1994. Pond bottom soil respiration during fallow and culture periods in heavily-fertilized tropical fish ponds. *Jour. of the world aquaculture societ.* 25:417-423.
- Brett, J. R., J. E. Shelbourn, and C. T. Shoop 1969. Growth rate and body composition of fingerling sockeye salmon, *Onchorhynchus nerka*, in relation to temperature and body size. *J. Fish. Res. Board Can.*, 26:2363-2394.
- Caulton, M. S. 1978. The effect of temperature and mass on routine metabolism in *Sarotherodon (Tilapia) mossambicus* (Peters). *J. Fish. Biol.*, 13:195:201.
- Card, W. H. E. E. Drucker, M. Ucar, and J. E. LaGraff. 1976. Generalized weather functions for computer analysis of solar-assisted HVAC systems. Presented at the winter 1976 meeting of the American Society of Mechanical Engineers.
- Cathcart, T. P. and F. W. Wheaton. 1987. Modeling temperature distribution in freshwater ponds. *Aquacultural Engineering*, 6(1987):237-257.
- Chapra, S. C. and K. H. Reckhow. 1983. Engineering approaches for lake management, volume 2:mechanistic modeling. Butterworth Publishers, Boston. 492 pp.
- Cosper, E. 1982. Influence of light intensity on diel variations in rates of growth, respiration and organic release of marine diatom: comparison of diurnally constant and fluctuating light. *J. Plankton Res.* 4:705-724.
- Cuenco, M. L., R. R. Stickney, and W. E. Grant. 1985a. Fish bioenergetics and growth in aquaculture ponds: I. Individual fish model development. *Ecol. Modelling*, 27:169-190.
- Cuenco, M. L., R. R. Stickney, and W. E. Grant. 1985b. Fish bioenergetics and growth in aquaculture ponds: II. Effects of interactions among size, temperature, dissolved oxygen, un-ionized ammonia and food on growth of individual fish. *Ecol. Modelling*, 27: 191-206.
- Cuenco, M. L., R. R. Stickney, and W. E. Grant. 1985c. Fish bioenergetics and growth in aquaculture ponds: III. Effects of intraspecific competition, stocking rate, stocking size and feeding rate on fish productivity. *Ecol. Modelling*, 28: 73-95.
- Culberson, S. D. 1993. Simplified model for prediction of temperature and dissolved oxygen in aquaculture ponds: using reduced data inputs. M.S. Thesis. University of California, Davis. 212 pp

- Dempster, P., D. J. Baird, and M. C. M. Beveridge. 1995. Can fish survive by filter-feeding on microparticles? Energy balance in tilapia grazing on algal suspensions. *Jour. of Fish Biology* 47:7-17.
- dos Santos Neto, C. P., and R. H. Piedrahita. 1994. Stochastic modeling of temperature in stratified aquaculture ponds. Twelfth Annual Administrative Report -Pond Dynamics/Aquaculture, Collaborative Research Support Program 1994. Corvallis, Oregon. PD/A CRSP Management Office. pp 169-178.
- Duffie, J. A., and W. A. Beckman. 1991. Solar engineering of thermal processes. John Wiley & Sons, Inc. New York. 919 pp.
- Emerson, K., R. C. Russo, R. Lund, and R. V. Thurston. 1975. Aqueous ammonia equilibrium calculations: effects of pH and temperature. *J. Fish Res. Board Can.*, 32:2379-2388.
- Ephrath, J. E., J. Goudriaan, and A. Marani. 1996. Modelling diurnal patterns of air temperature, radiation, wind speed and relative humidity by equations from daily characteristics. *Agricultural Systems* 0308-521x. 377-393.
- Ernst, D. H. 2000. AquaFarm: simulation and decision-support software for aquaculture facility design and management planning. Ph.D. dissertation. Oregon State University. 383 pp.
- Freund, J. E. 1981. Statistics: a first course. Prentice-Hall, Inc. Englewood Cliffs, New Jersey 07632. 466 pp.
- Geider R. J., M. L. MacIntyre, and T. M. Kana. 1997. Dynamic model of phytoplankton growth and acclimation: responses of the balanced growth rate and the chlorophyll a:carbon ratio to light, nutrient-limitation and temperature. *Marine ecology progress series* Vol 148:187-200.
- Giovannini, P. 1994. Water quality dynamics in aquaculture ponds: an investigation of photosynthetic production and efficiency variations. Ph.D. dissertation. University of California, Davis. 219 pp.
- Goldman, C. R. and A. J. Horne. 1983. Limnology. McGraw-Hill Publishing Company, New York. 464 pp.
- Gordon, J. M. and T. A. Reddy. 1988a. Time series analysis of daily horizontal solar radiation. *Solar Energy* 40(3): 215-226.

- Gordon, J. M. and T. A. Reddy. 1988b. Time series analysis of hourly global horizontal solar radiation. *Solar Energy* 40(5): 423-429.
- Graham, V. A., K. G. T. Hollands, and T.E. Unny. 1988. A time series model for K_t with application to global synthetic weather generation. *Solar Energy* 40(2): 83-92.
- Graham, V. A. and K. G. T. Hollands. 1990. A method to generate synthetic hourly solar radiation globally. *Solar Energy* 44(6): 333-341.
- Hsieh, J. S. 1986. *Solar energy engineering*. Prentice-Hall Inc. NJ. 533 pp.
- Huang, Z. and Z. S. Chalabi. 1995. Use of time-series analysis to model and forecast wind speed. *Jour. of Wind Engineering and Industrial Aerodynamics* 56:311-322.
- Jamu, D. M., 1998. Modeling organic matter and nitrogen dynamics in integrated aquaculture/agriculture systems: effects of cycling pathways on nitrogen retention and system productivity. Ph.D. Dissertation. 297 pp.
- Jamu, D. M. and R. H. Piedrahita, 1996. Aquaculture pond modeling for the analysis of integrated aquaculture/agriculture systems. In H. Egna, B. Goetze, M. McNamara, and D. Clair (Editors) Thirteenth Annual Technical Report. Pond Dynamics/Aquaculture CRSP, Office of International Research and Development, Oregon State University, Corvallis, Oregon, pp 172-177.
- Jamu, D. M., Z. Lu, and R. H. Piedrahita, 1999. Relationship between secchi disk visibility and chlorophyll a in aquaculture ponds. *Aquaculture* 170(1999):205-214.
- Jørgensen, S. E. and M. J. Gromiec. 1989. *Mathematical submodels in water quality systems*. New York, NY, USA Elsevier Science Pub. 409 pp.
- Jobling, M. 1994. *Fish Bioenergetics*. The Norwegian College of Fishery Science University of Tromso, Norway. Chapman&Hall. London. 309 pp.
- Knight, K. M., S. A. Klein and J. A. Duffie. 1991. A methodology for the synthesis of hourly weather data. *Solar Energy* 46(2): 109-120.
- Lee, J. H. W., R. S. S. Wu, Y. K. Cheung, and P. P. S. Wong, 1991a. Dissolved oxygen variations in marine fish culture zone. *Jour. of Environmental Engineering*. Vol. 117, No. 6:799-815.
- Lee, J. H. W., R. S. S. Wu and Y. K. Cheung, 1991b. Forecasting of dissolved oxygen in marine fish culture zone. *Jour. of Environmental Engineering*. Vol. 117, No. 6:816-833.

- Leohle, C. 1997. A hypothesis testing framework for evaluating ecosystem model performance. *Ecological Modelling* 97: 153-165.
- Liu, B. Y. H. and R. C. Jordan. 1960. The interrelationship and characteristic distributions of direct, diffusion, and total solar radiation. *Solar Energy* 4: 1-19.
- Liu, K. M. and W. Y. B. Chang. 1992. Bioenergetic modelling of effects of fertilization, stocking density, and spawning on growth of Nile tilapia, *Oreochromis niloticus*. *Aquaculture and Fisheries management* 23: 291-301.
- Losordo, T. M. 1988. The characterization and modeling of thermal and oxygen stratification in aquaculture ponds. Ph.D. dissertation. University of California, Davis. 416 pp.
- Meyer, D. I. 1980. Modeling diel oxygen flux in a simulated catfish pond. Master thesis. University of California, Davis, California, 123 pp.
- Meyer, D. I. and D. E. Brune. 1982. Computer simulation of the diurnal oxygen levels in a stillwater aquaculture pond. *Aquacultural Engineering*, 1(1982):245-261.
- Nath, S. 1996. Development of a decision support system for pond aquaculture. Ph.D. Dissertation, Oregon State University, Corvallis. 273 pp.
- Northcott, M. E., M. C. M. Beveridge, and G. R. Lindsay. 1991. A laboratory investigation of the filtration and ingestion rates of the tilapia, *Oreochromis niloticus*, feeding on two species of blue-green algae. *Environ. Biology of Fishes* 31:75-85.
- PD/A CRSP 1987. Pond Dynamics/Aquaculture Collaborative Research Data Reports. PD/A CRSP program Management Office. Oregon State University, Corvallis, Oregon 97331.
- PD/A CRSP 1988. Pond Dynamics/Aquaculture Collaborative Research Data Reports. PD/A CRSP program Management Office. Oregon State University, Corvallis, Oregon 97331.
- PD/A CRSP 1989. Pond Dynamics/Aquaculture Collaborative Research Data Reports. PD/A CRSP program Management Office. Oregon State University, Corvallis, Oregon 97331.
- PD/A CRSP. 2003. PD/A CRSP Database. <http://www.aqua-information.ait.ac.th/crspdb>

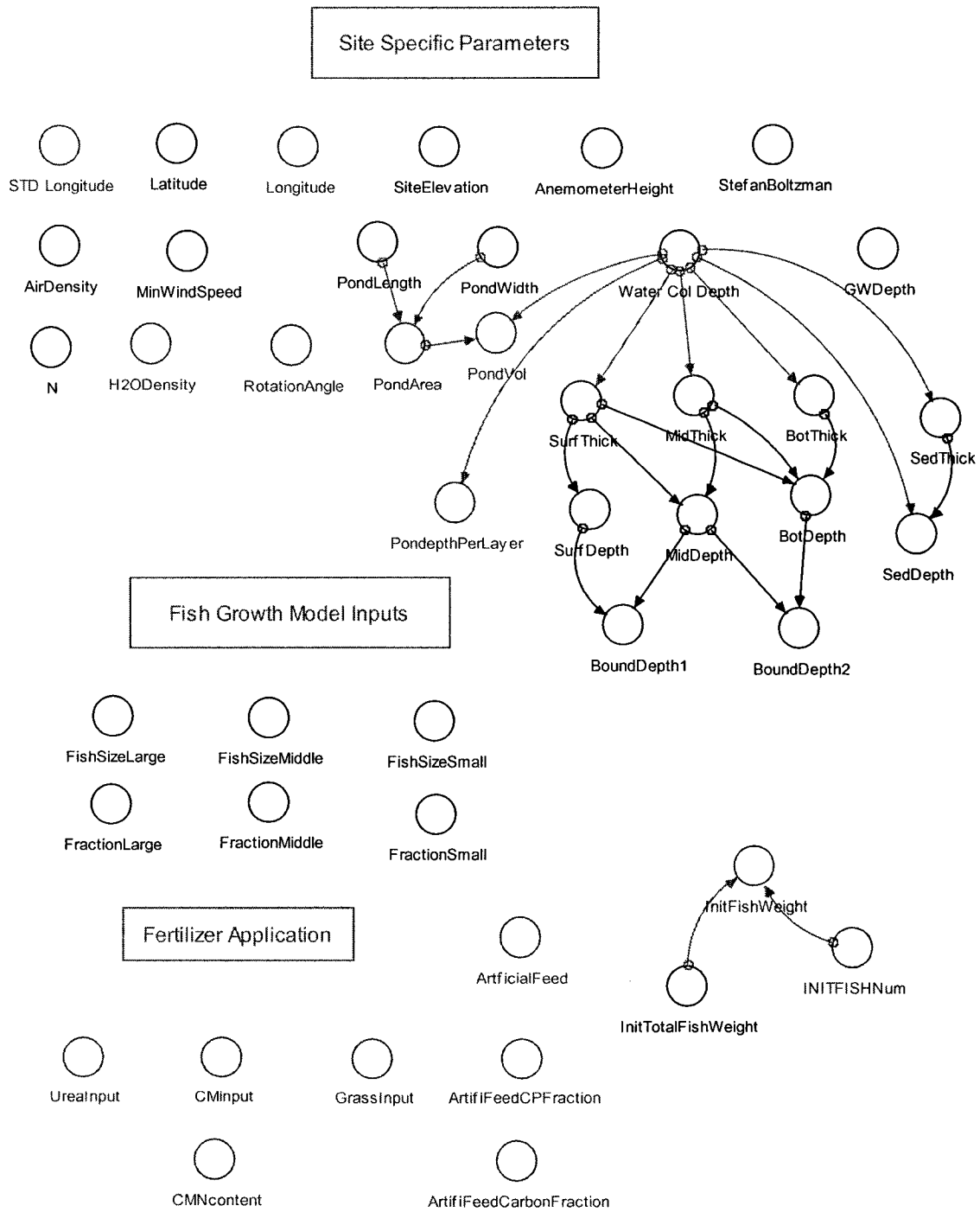
- Pearl, R. and L. J. Reed. 1920. On the rate of growth of the population of the United States since 1790 and its mathematical representation. *Proc. Natl. Acad. Sci.* 6:275-288.
- Piedrahita, R. H. 1984. Development of a computer model of the aquaculture pond ecosystem. Ph.D. dissertation. University of California, Davis, California, 162 pp.
- Piedrahita, R. H. 1990. Calibration and validation of TAP, an aquaculture pond water quality model. *Aquaculture Eng.* 9:75-96.
- Reynolds, C. S. 1984. The ecology of freshwater phytoplankton. University of Cambridge Press, Cambridge, England. 384 pp.
- Romaire, R. P. and C. E. Boyd. 1979. Effects of solar radiation on the dynamics of dissolved oxygen in channel catfish ponds. *Transactions of the American Fisheries Society*, 108(1979):472-478.
- Saunier, G. Y., T. A. Reddy and S. K. Kumar. 1987. A monthly probability distribution function of daily global irradiation values appropriate for both tropical and temperate locations. *Solar Energy* 38(3): 169-177.
- Schroeder, G. L. 1987. Carbon and nitrogen budgets in manured fish ponds on Israel's coastal plain. *Aquaculture*, 62:259-279.
- Steele, J. H. 1962. Environmental control of photosynthesis in the sea. *Limnol. Oceanogr.*, 7:137-150.
- Straskraba, M. and A. H. Gnauck, 1985. Freshwater ecosystems: Modelling and simulation. *Developments in environmental modelling* 8, Elsevier, Amsterdam. 309 pp.
- Svirezhev, Y. M., V. P. Krysanova, and A. A. Voinov. 1984. Mathematical modelling of a fish pond ecosystem. *Ecological Modelling*, 21:315-337.
- Szumiec, M. A. 1990. Stochastic model of carp fingerling growth. *Aquaculture*, 91: 87-99. Elsevier Science Publishers B.V. Amsterdam.
- Tanji, K. 1981. Modeling Wastewater Renovation Land Treatment. Edited by Iskandar, John Wiley & Sons, pp 21-41.
- Teichert-Coddington, D., B. Green, C. E. Boyd, and M. I. Rodriguez. 1990. Supplemental nitrogen fertilization of organically fertilized ponds. In H. Egna, J.

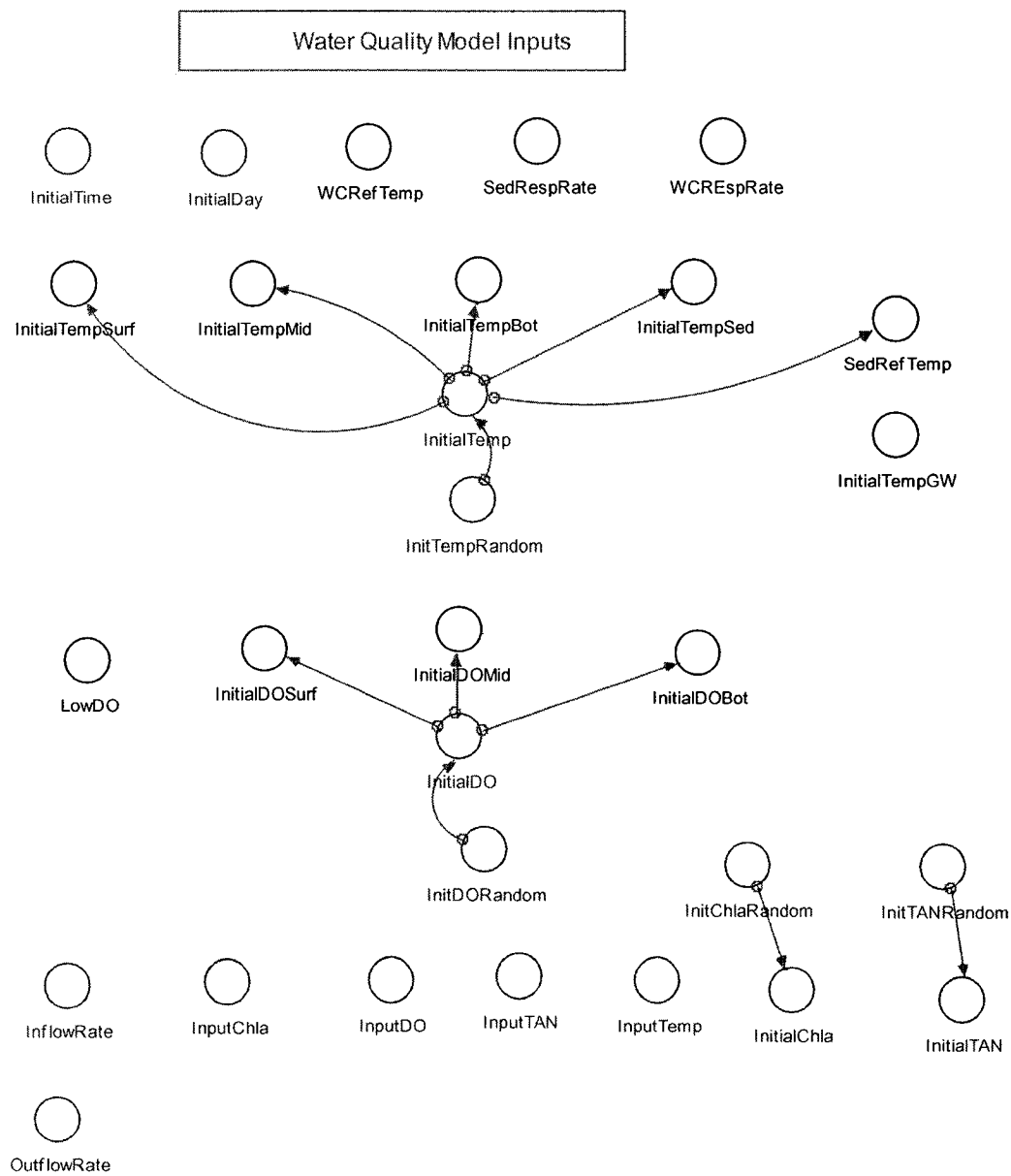
Bowman and M. McNamara (Editors). Eighth Annual Administrative Report, PD/A CRSP, Corvallis, Oregon, pp18-21.

Thomann, R. V. and J. A. Mueller, 1987. Principles of surface water quality modeling and control. Harper and Row. New York 644 pp.

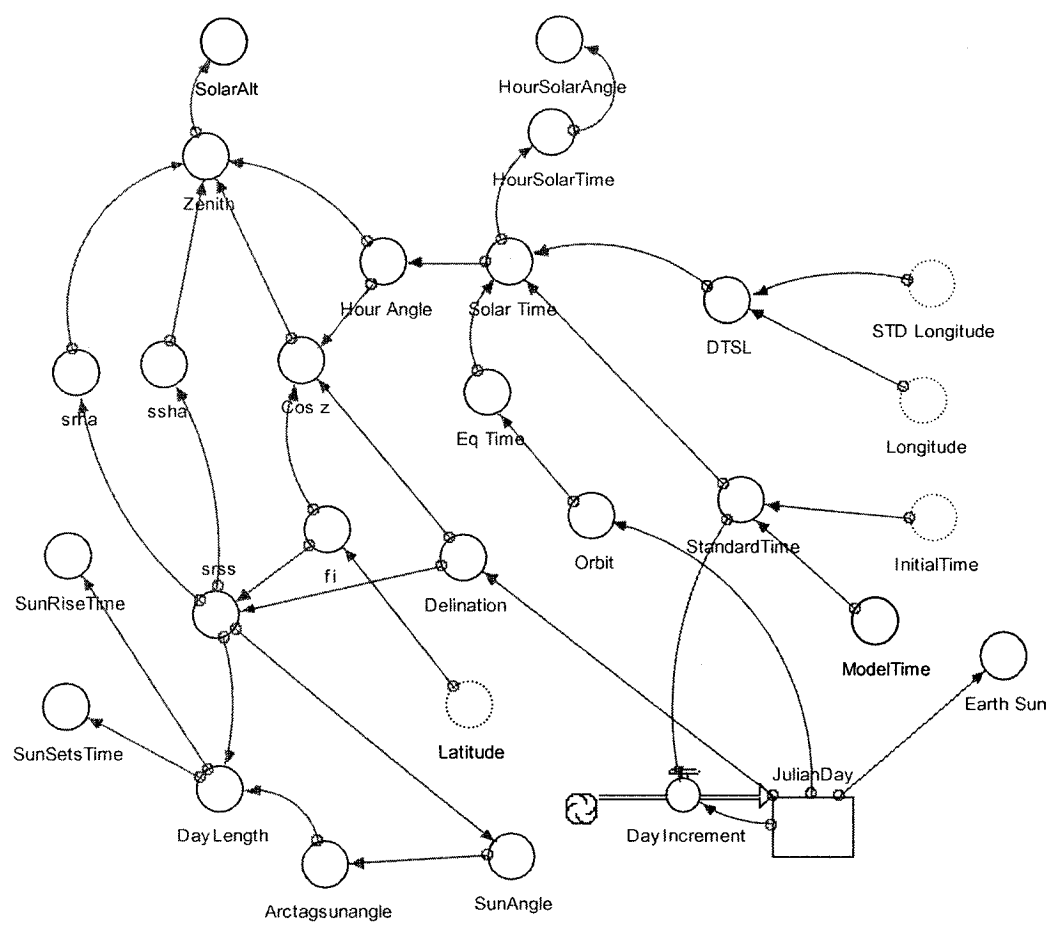
APPENDICES

A. Stella Icon Diagram

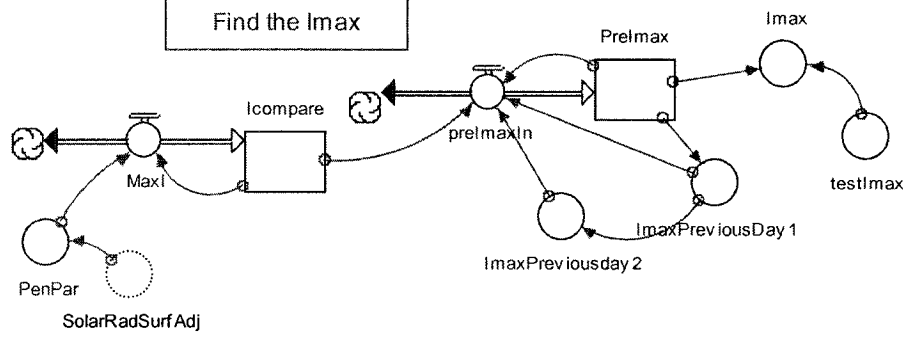




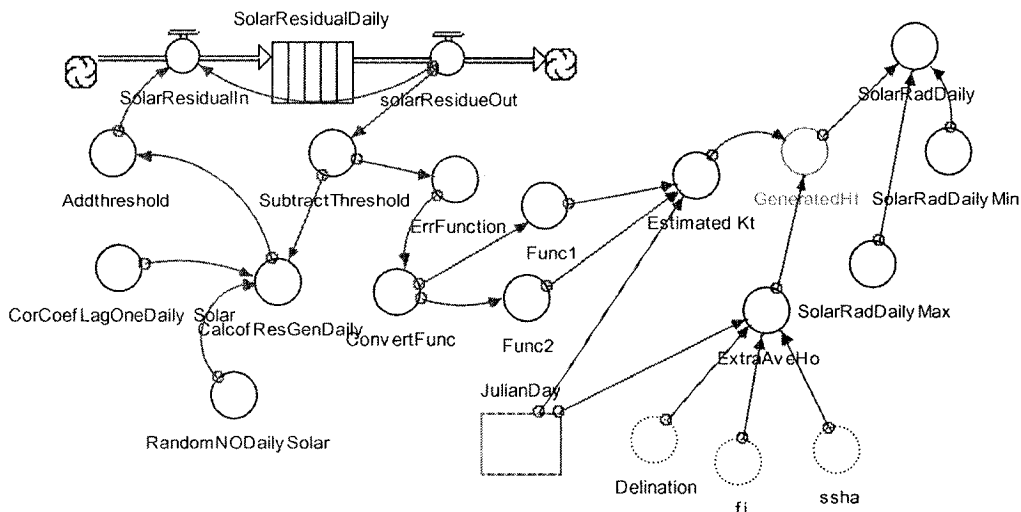
Solar Angle



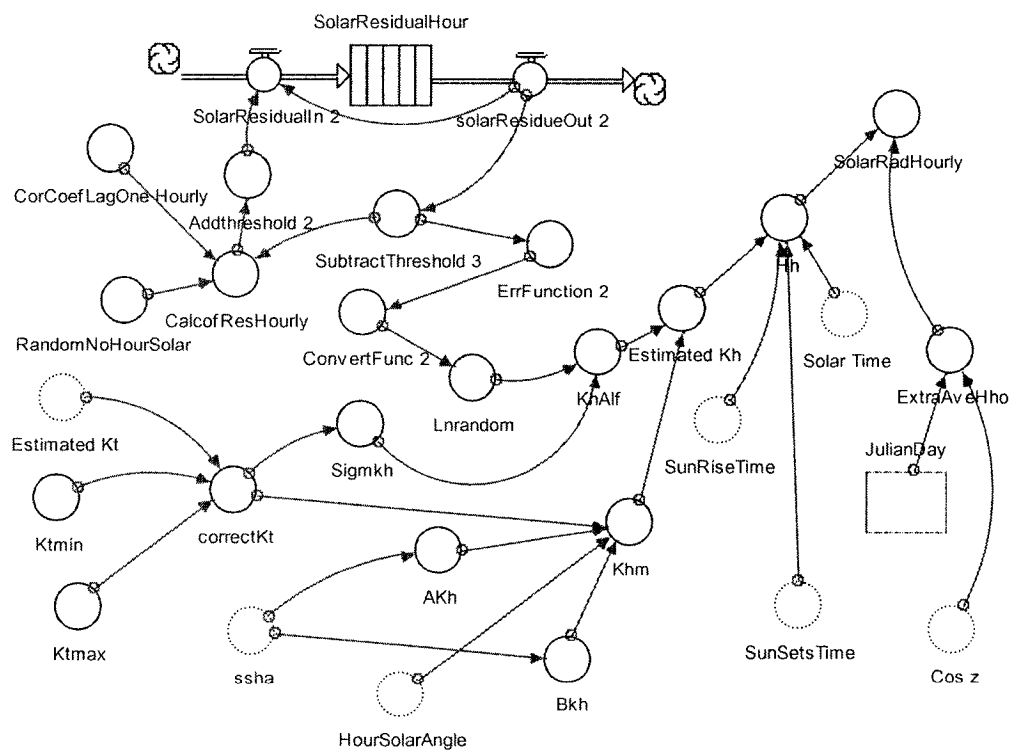
Find the I_{max}

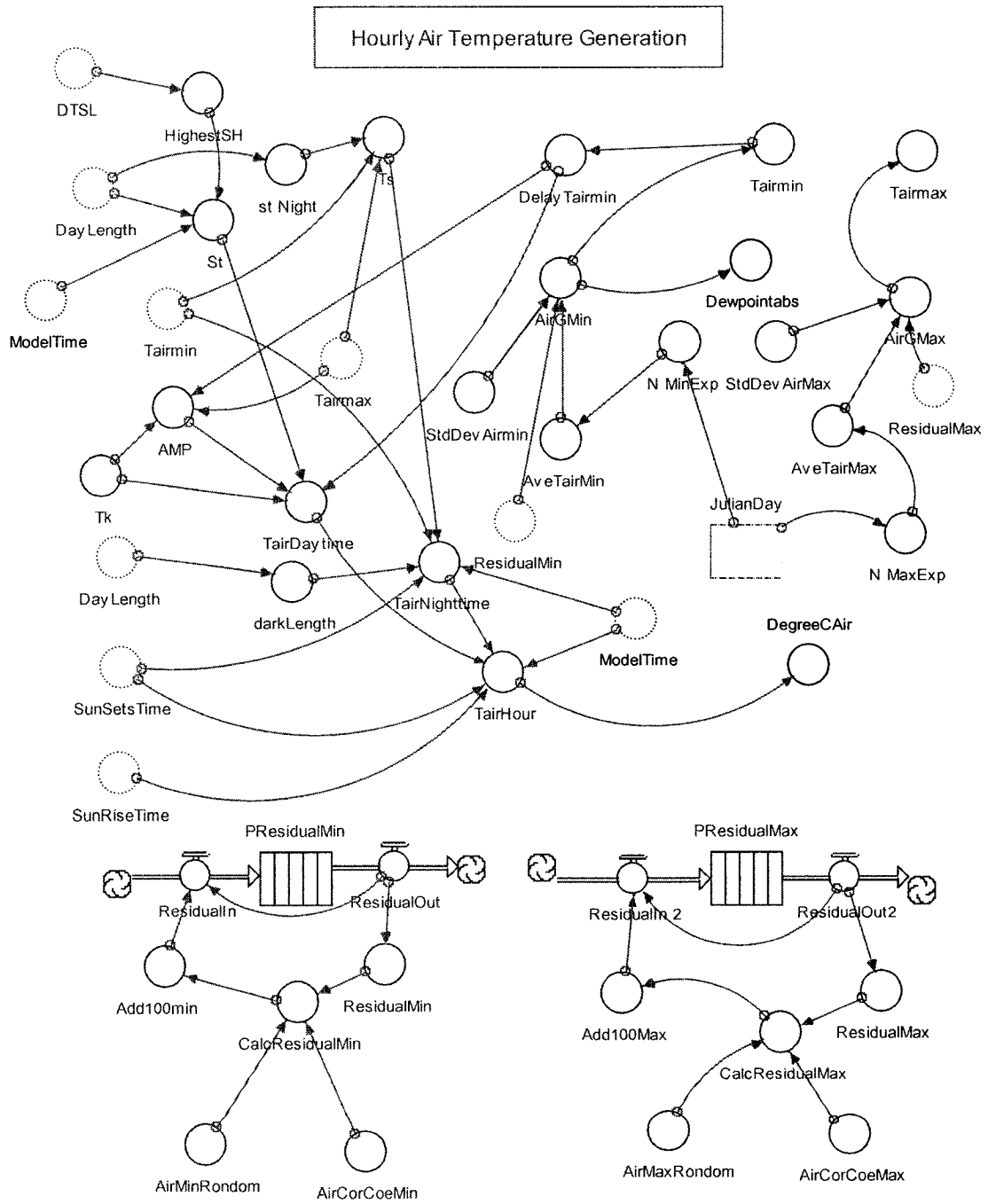


Daily Solar Radiation Generation

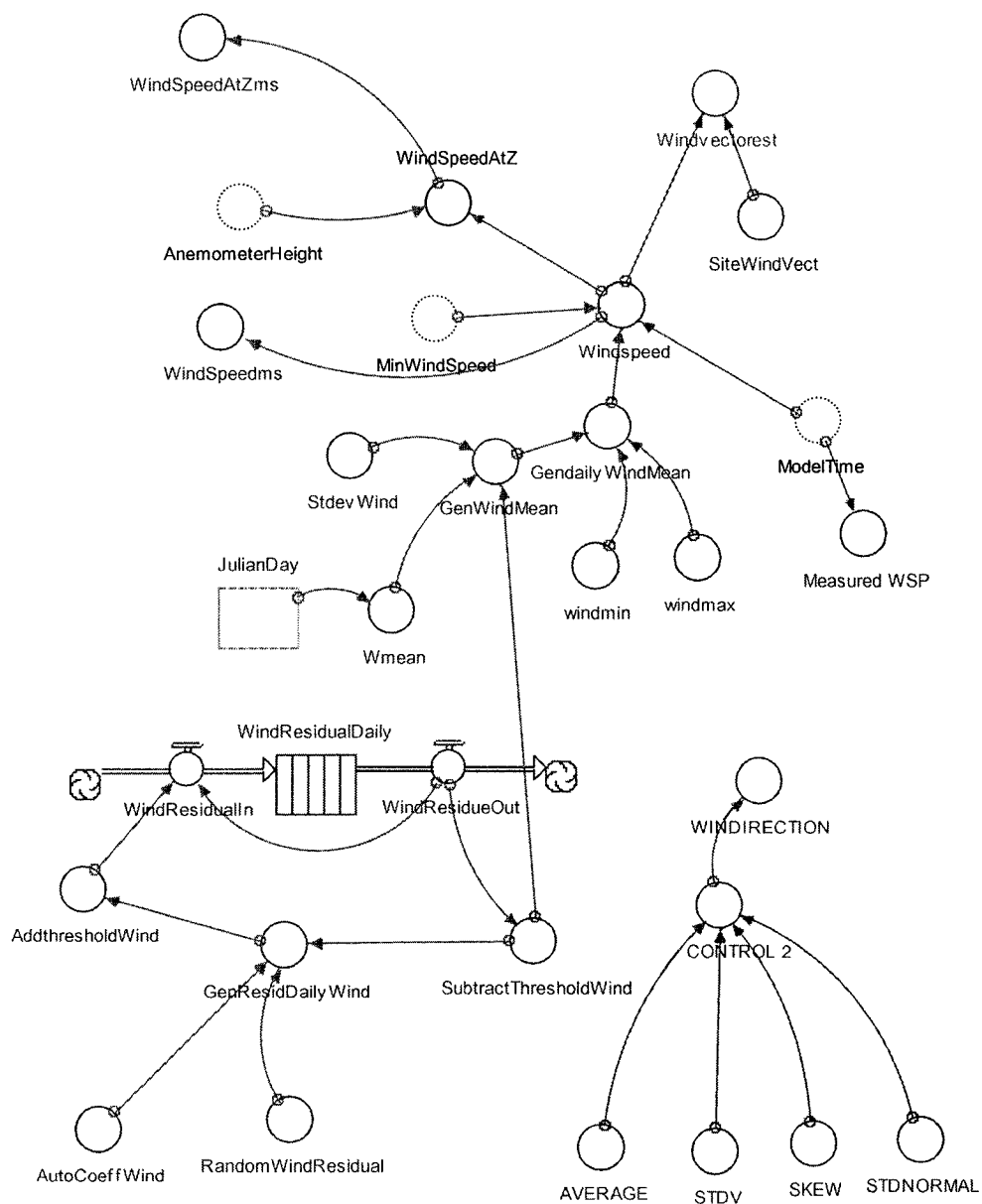


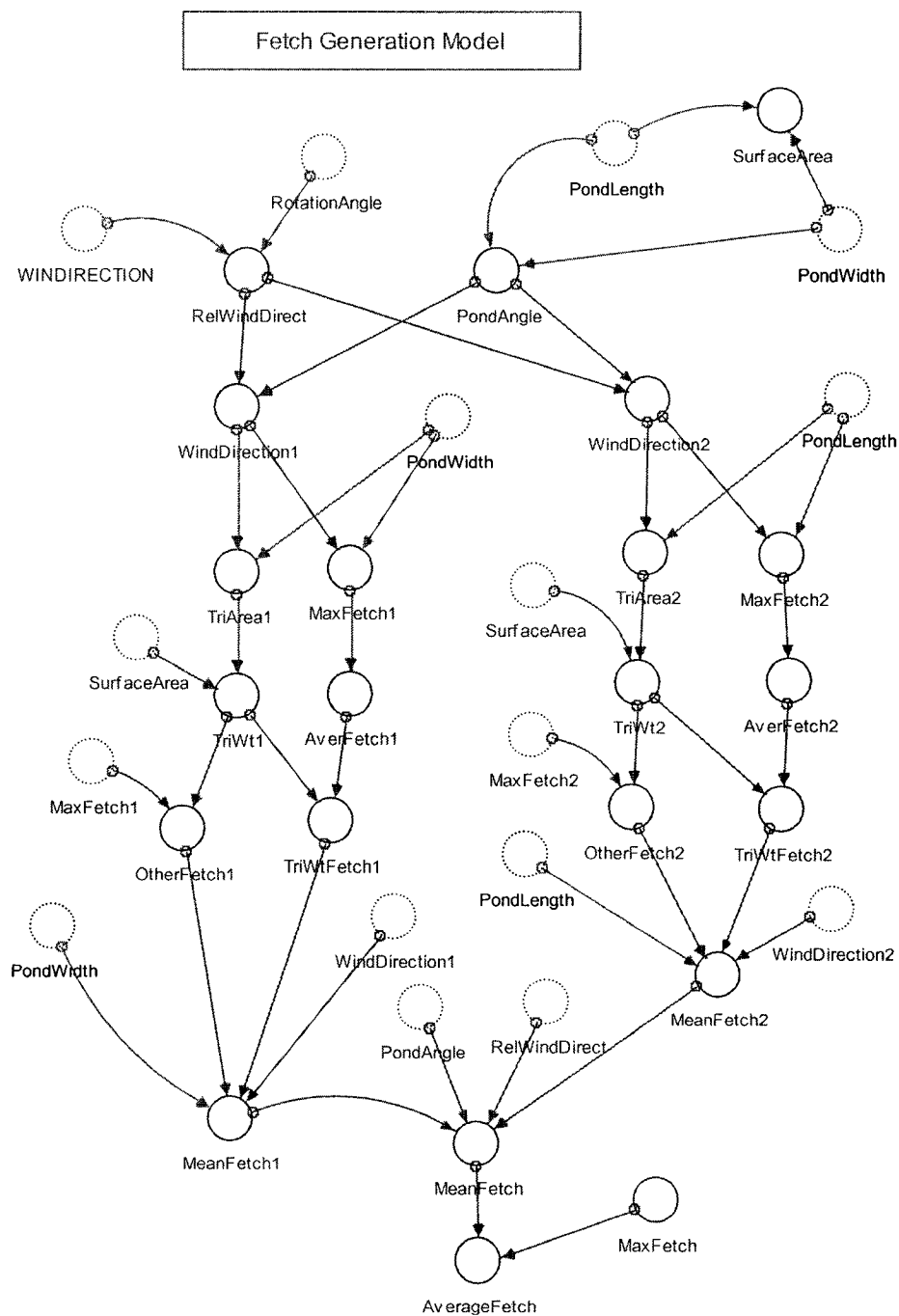
Hourly Solar Radiation Generation

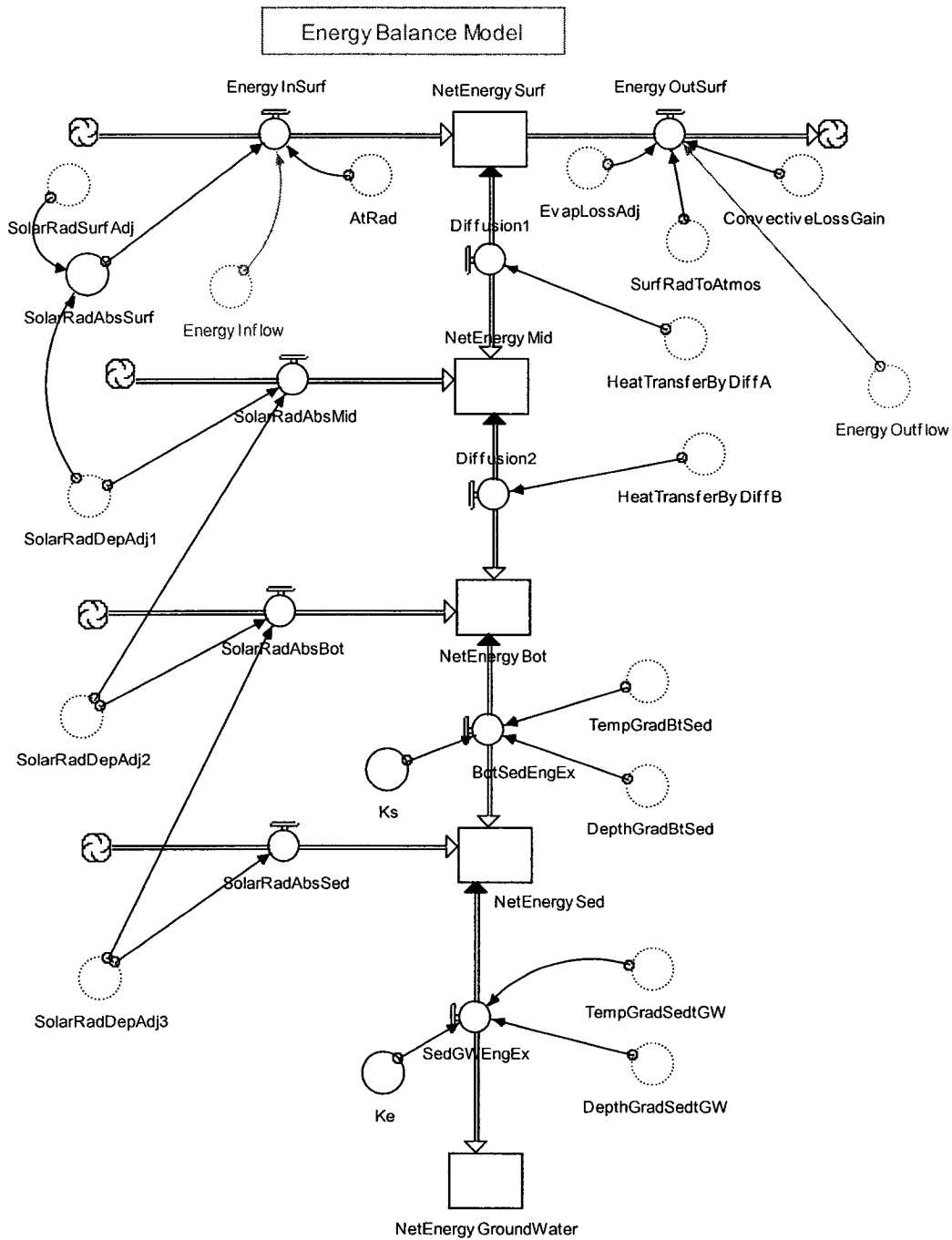




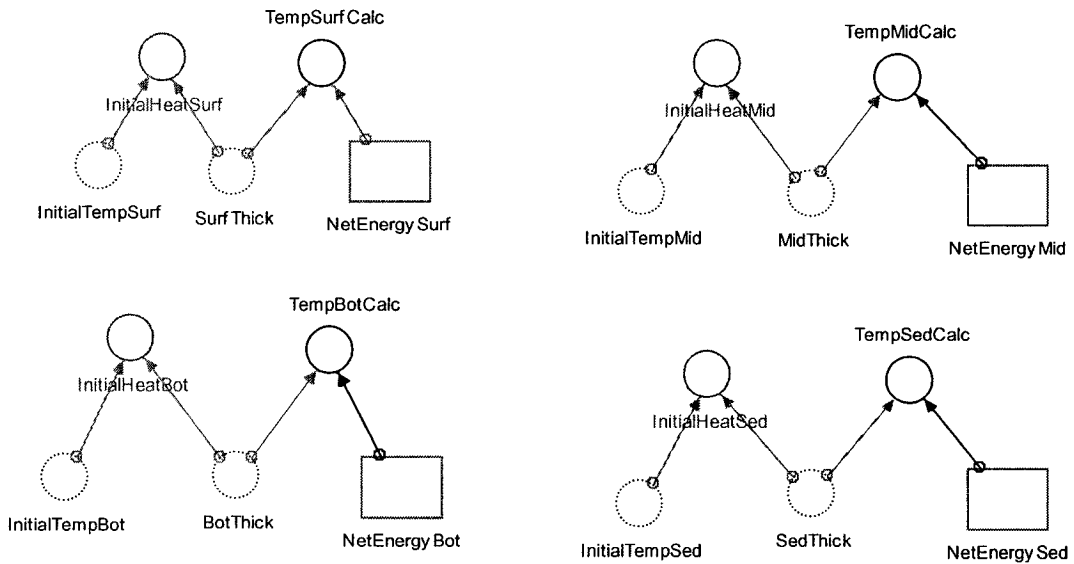
Wind Speed and Wind Direction Generation Models



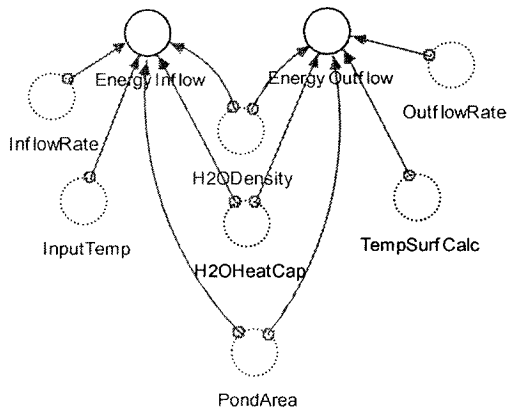




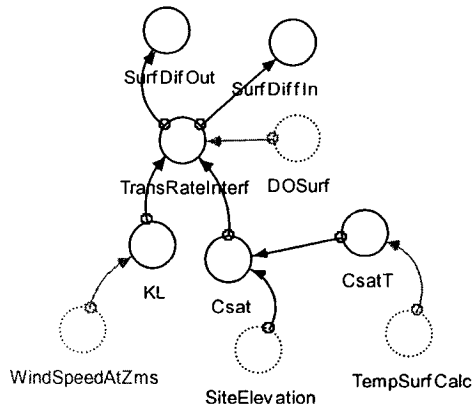
Calculation of Water Temperature



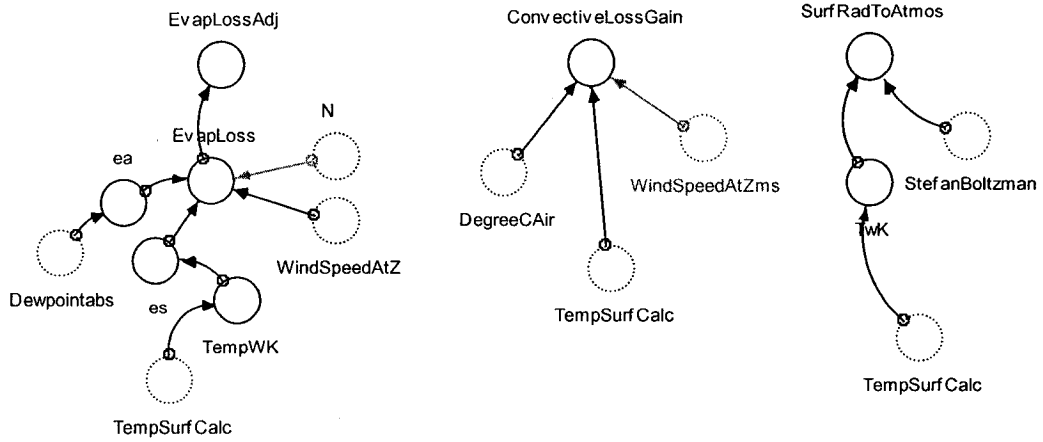
Energy Input and Output in Water Influent and Effluent



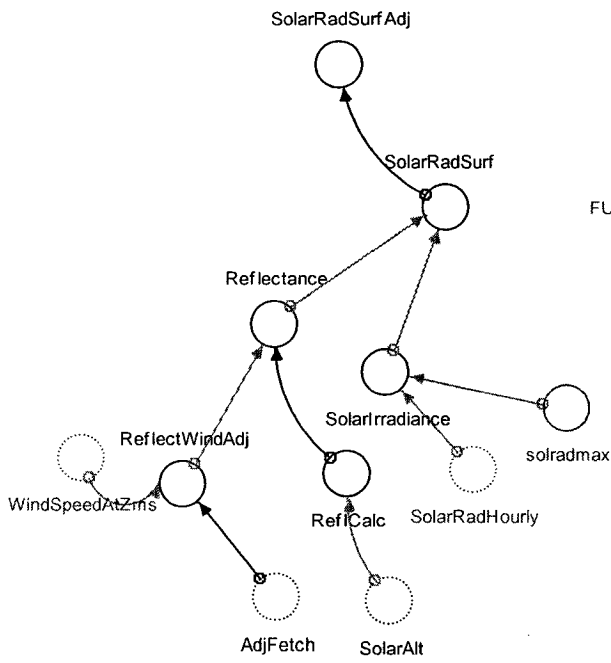
Surface Diffusion



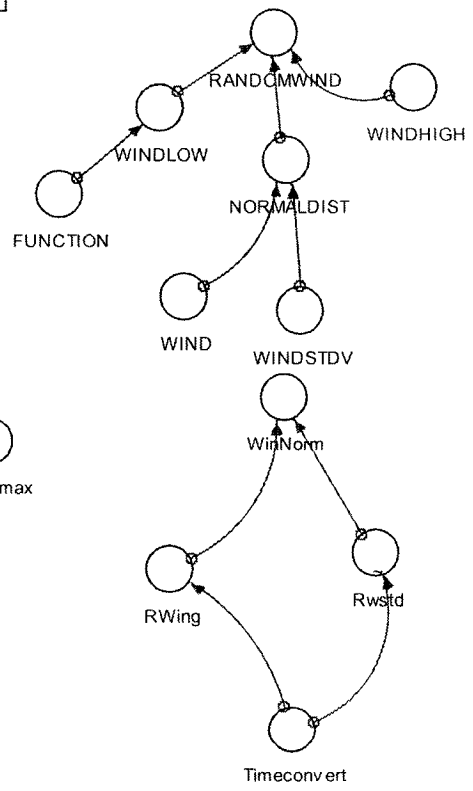
Heat losses at the Surface



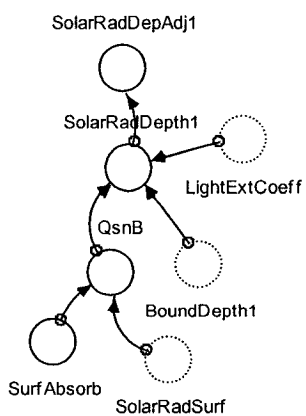
Solar radiation surface adjustment



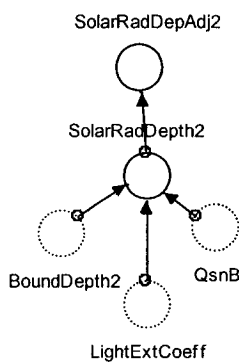
Wind Speed Generation



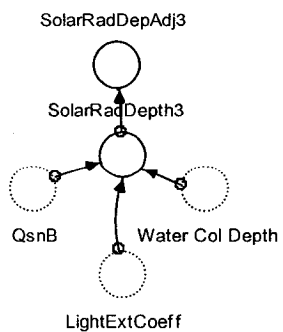
Middle Layer Adjustment



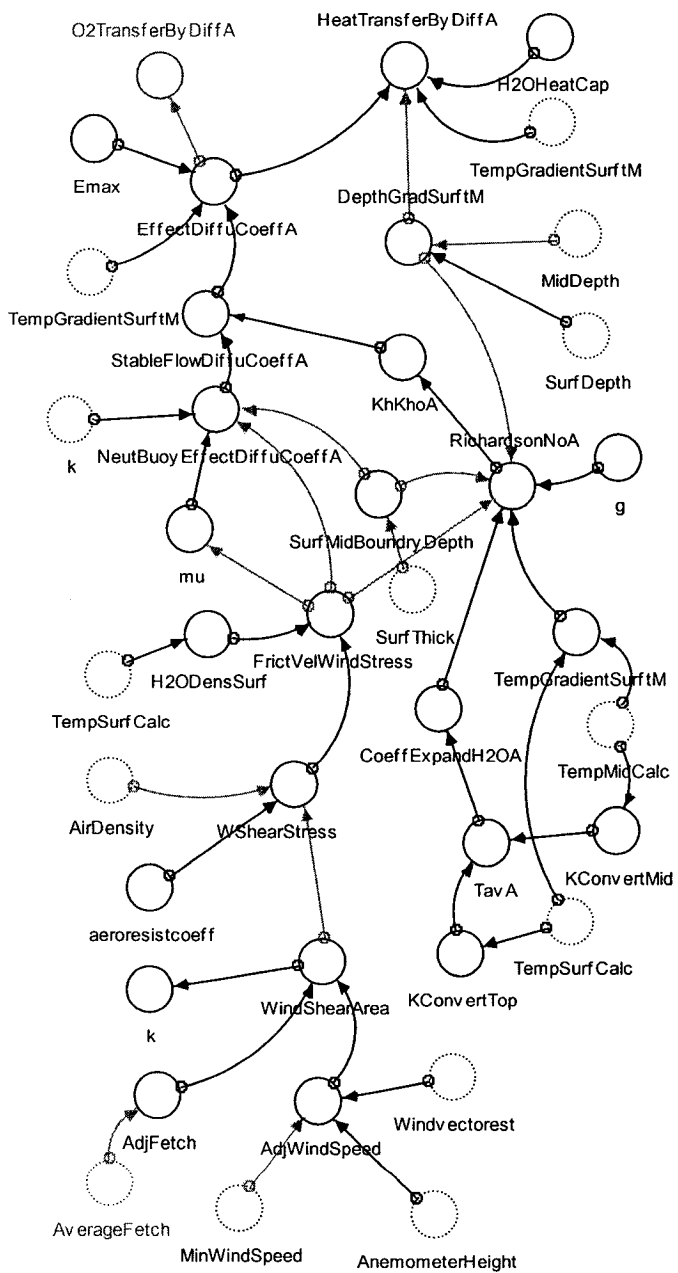
BOTTOM LAYER



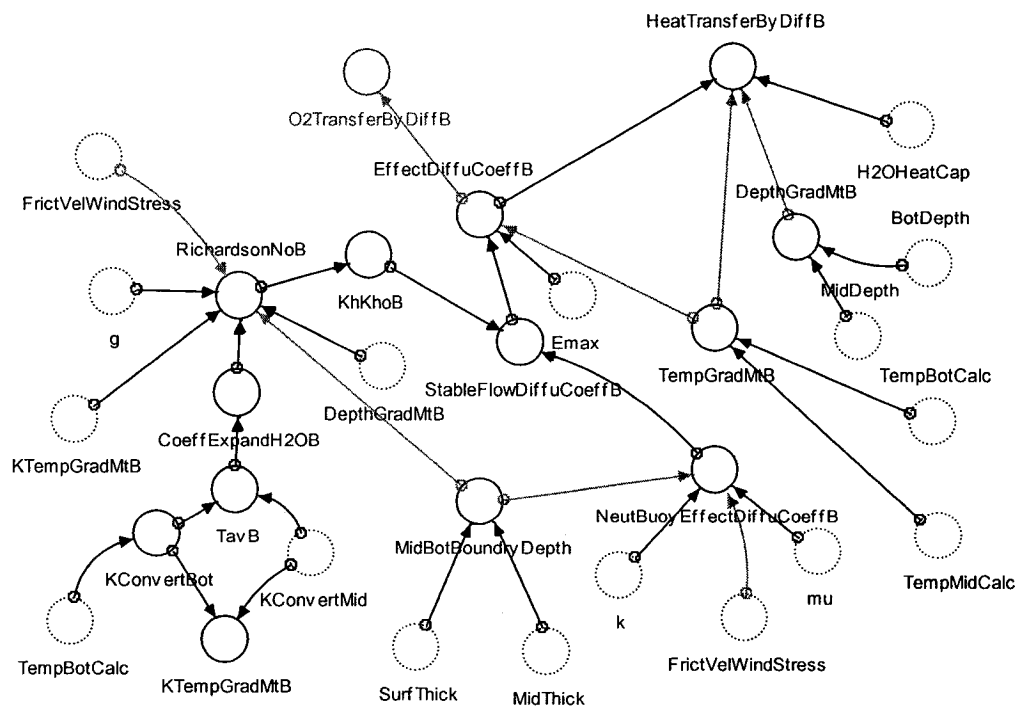
SEDIMENT LAYER



TRANSFER FROM SURFACE TO MIDDLE LAYER

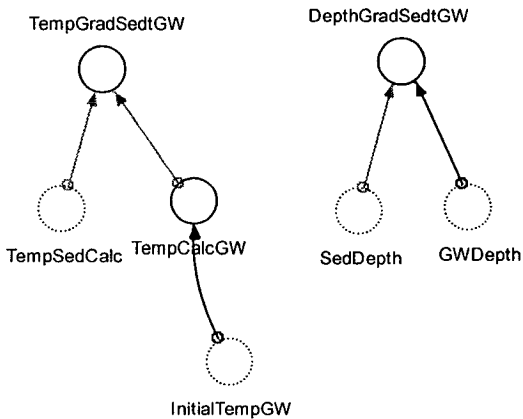
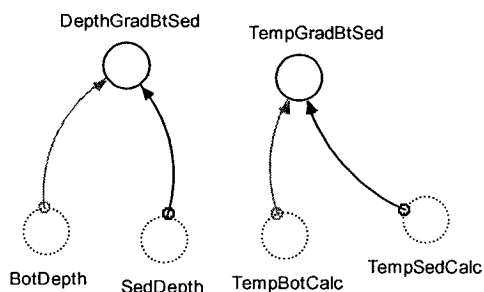


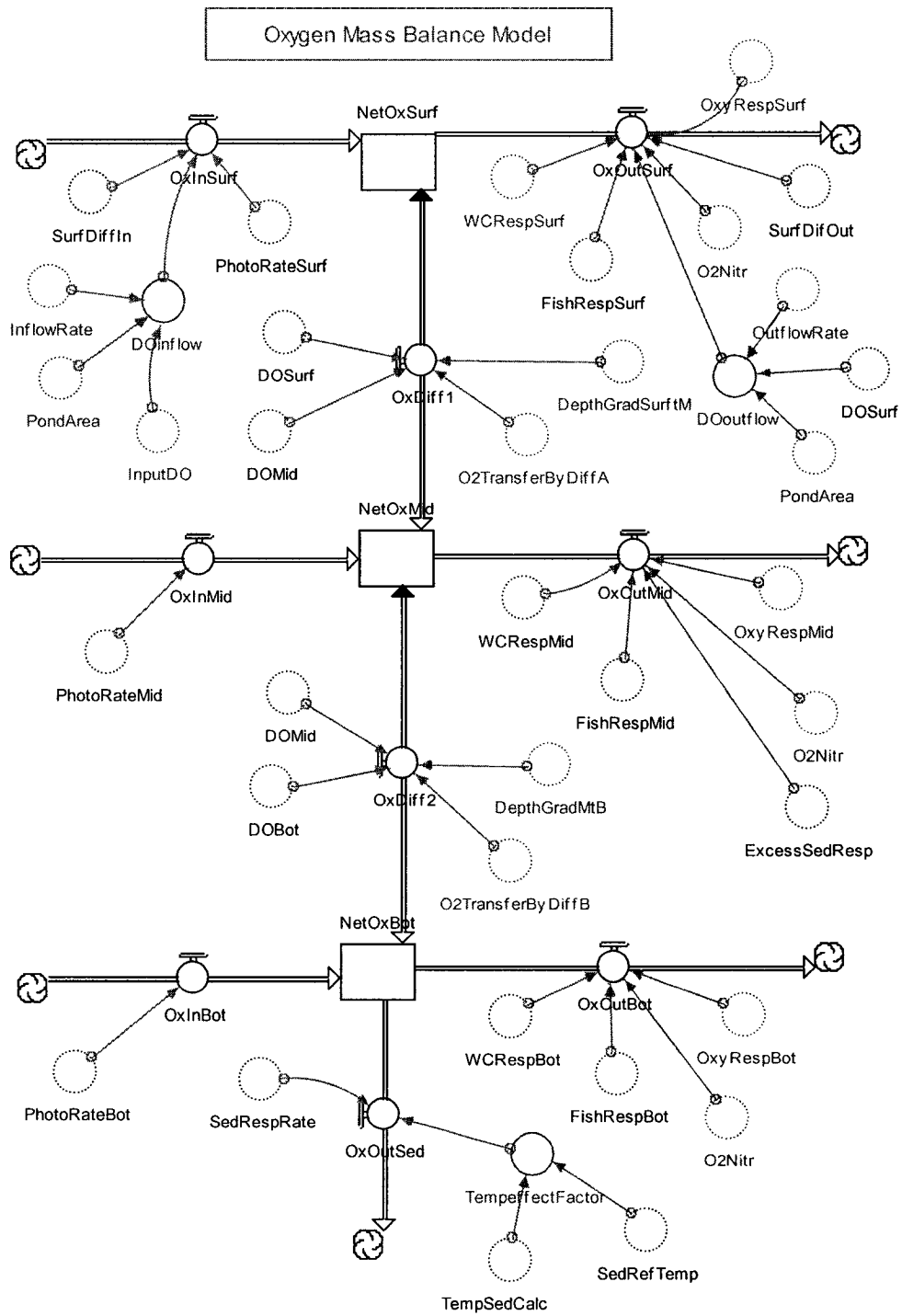
Transfer From Middle to Bottom Layer



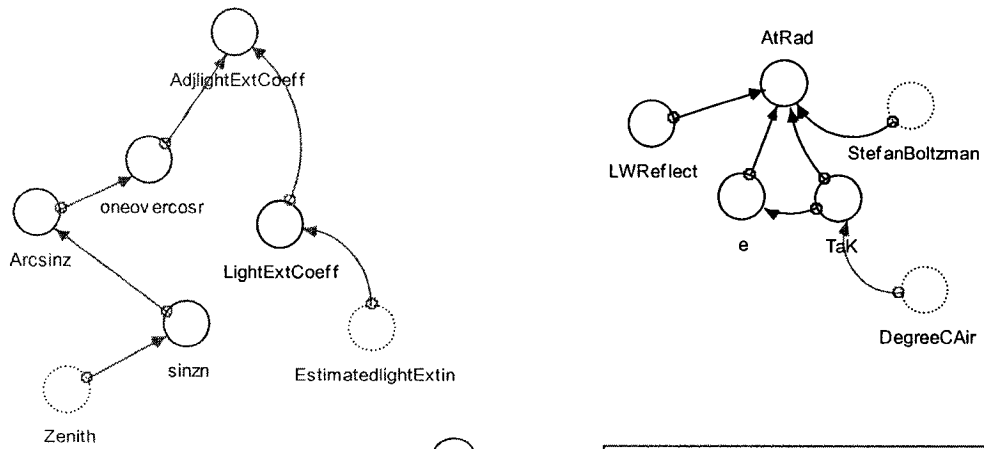
Transfer From Sediment To Ground Water

Transfer From Bottom To Sediment

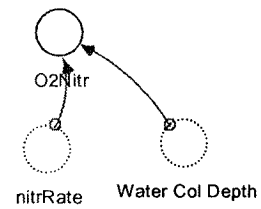




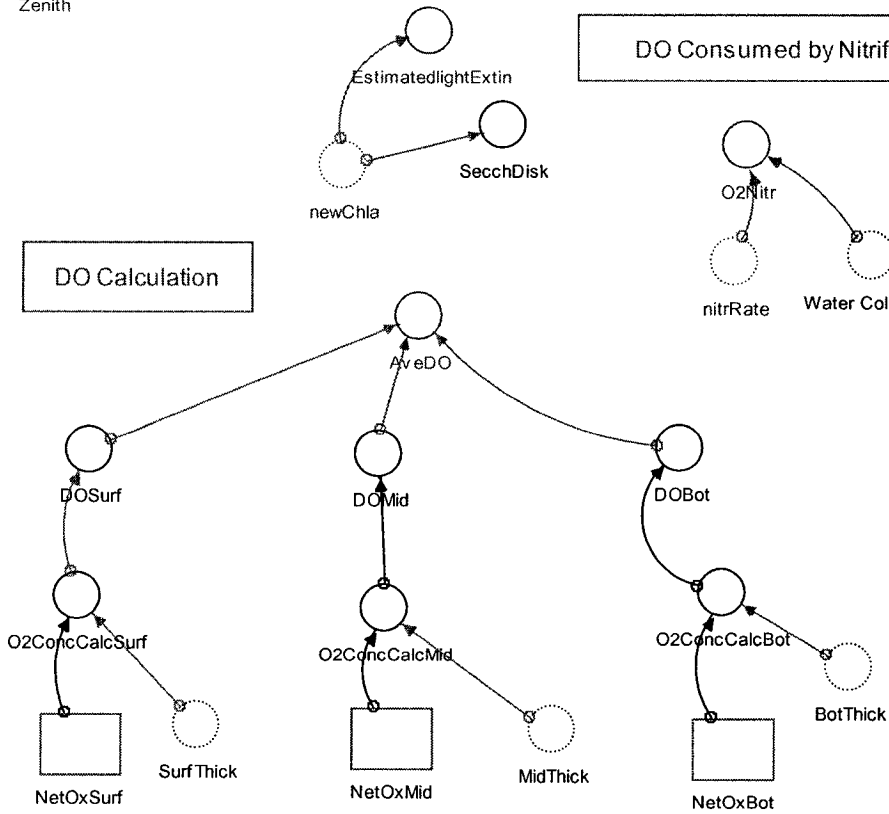
Adjusted Light Extension Coefficient



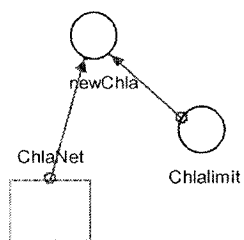
DO Consumed by Nitrification



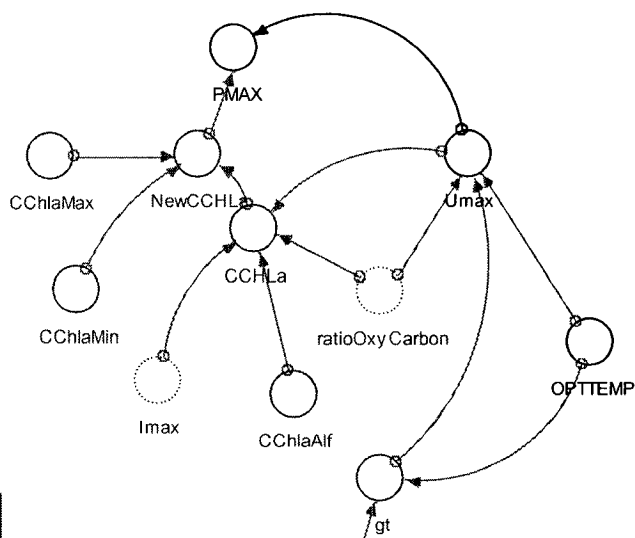
DO Calculation



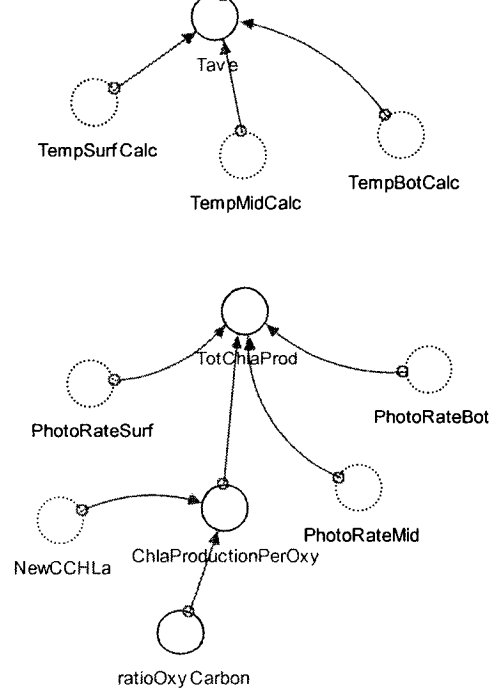
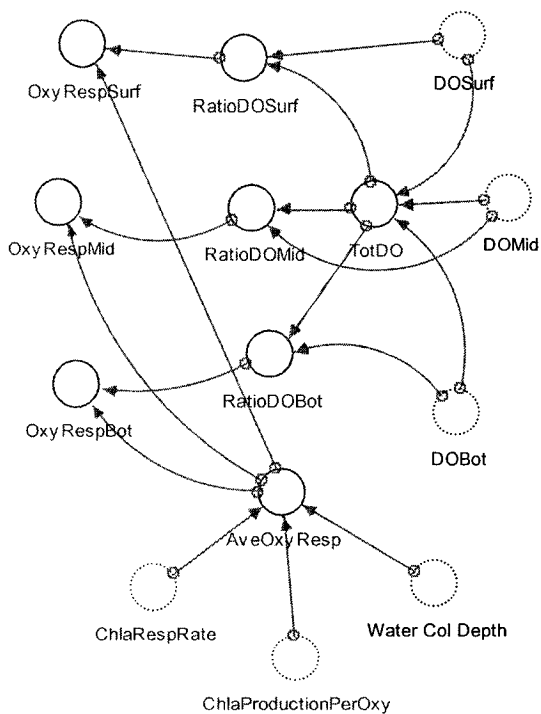
The dynamic Chlorophyll-a Conc.

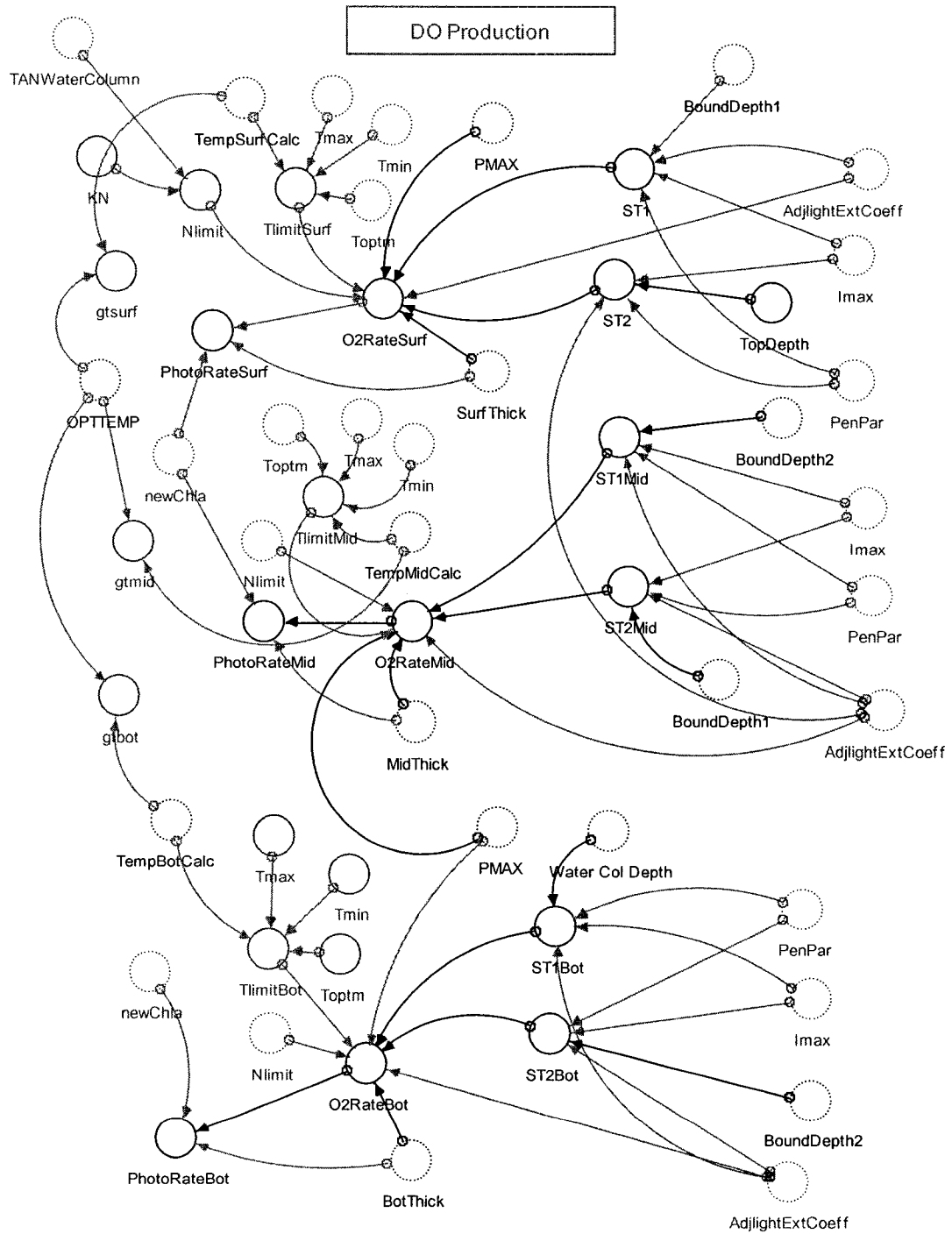


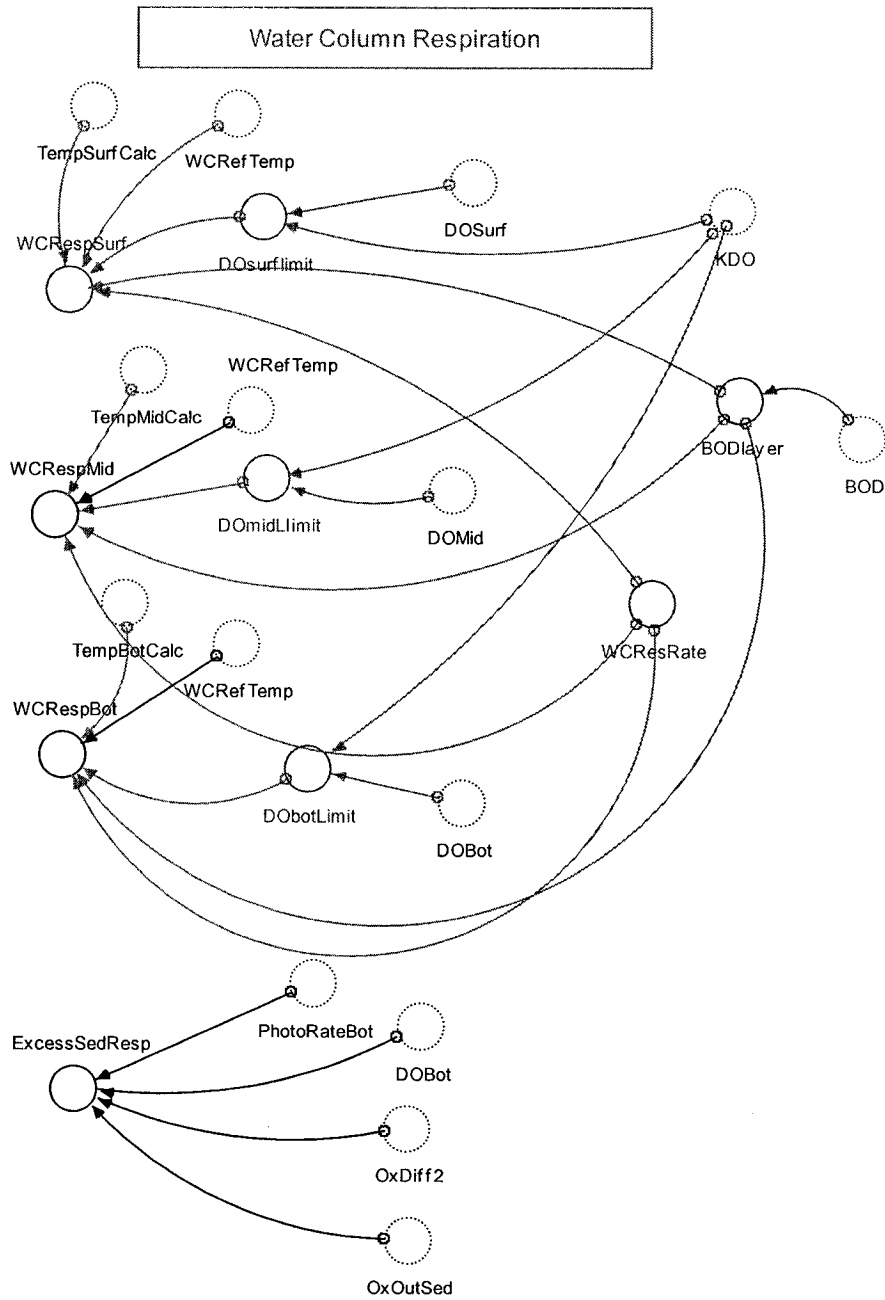
Ratio of Carbon to Chlorophyll a



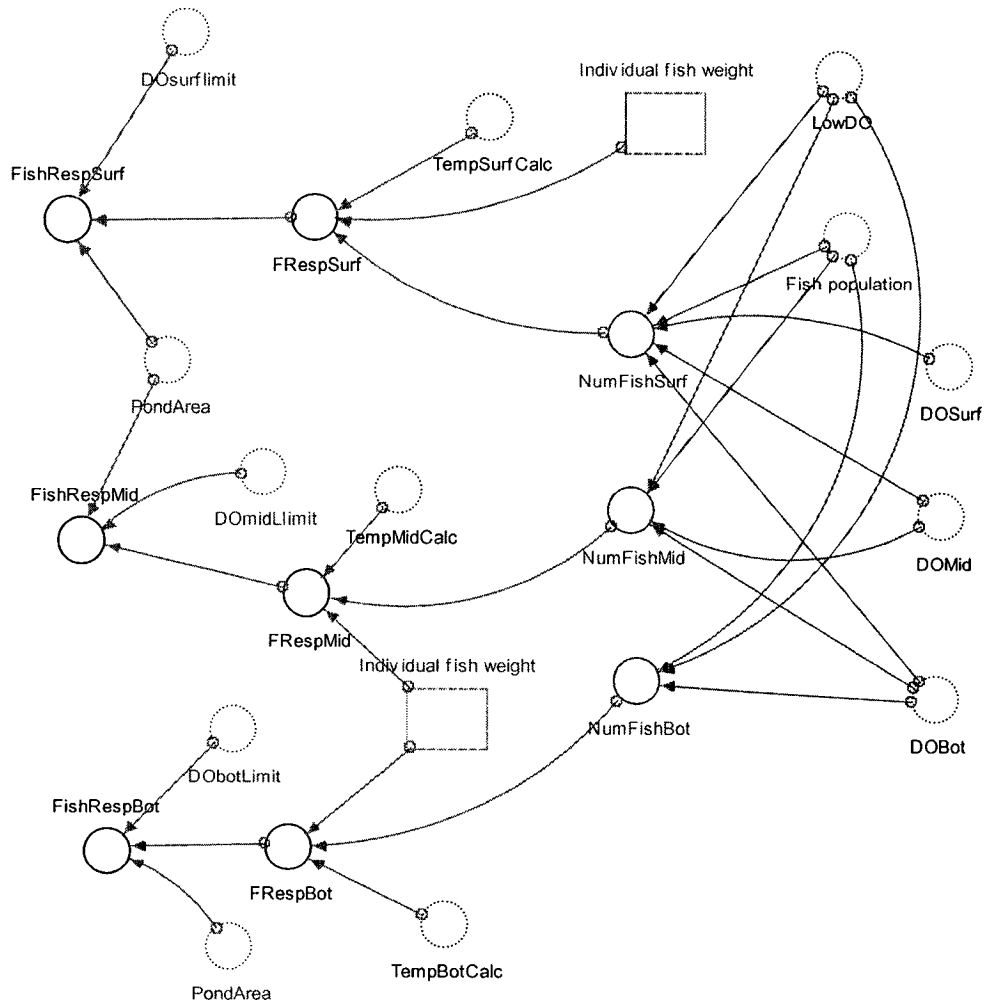
Phytoplankton Respiration

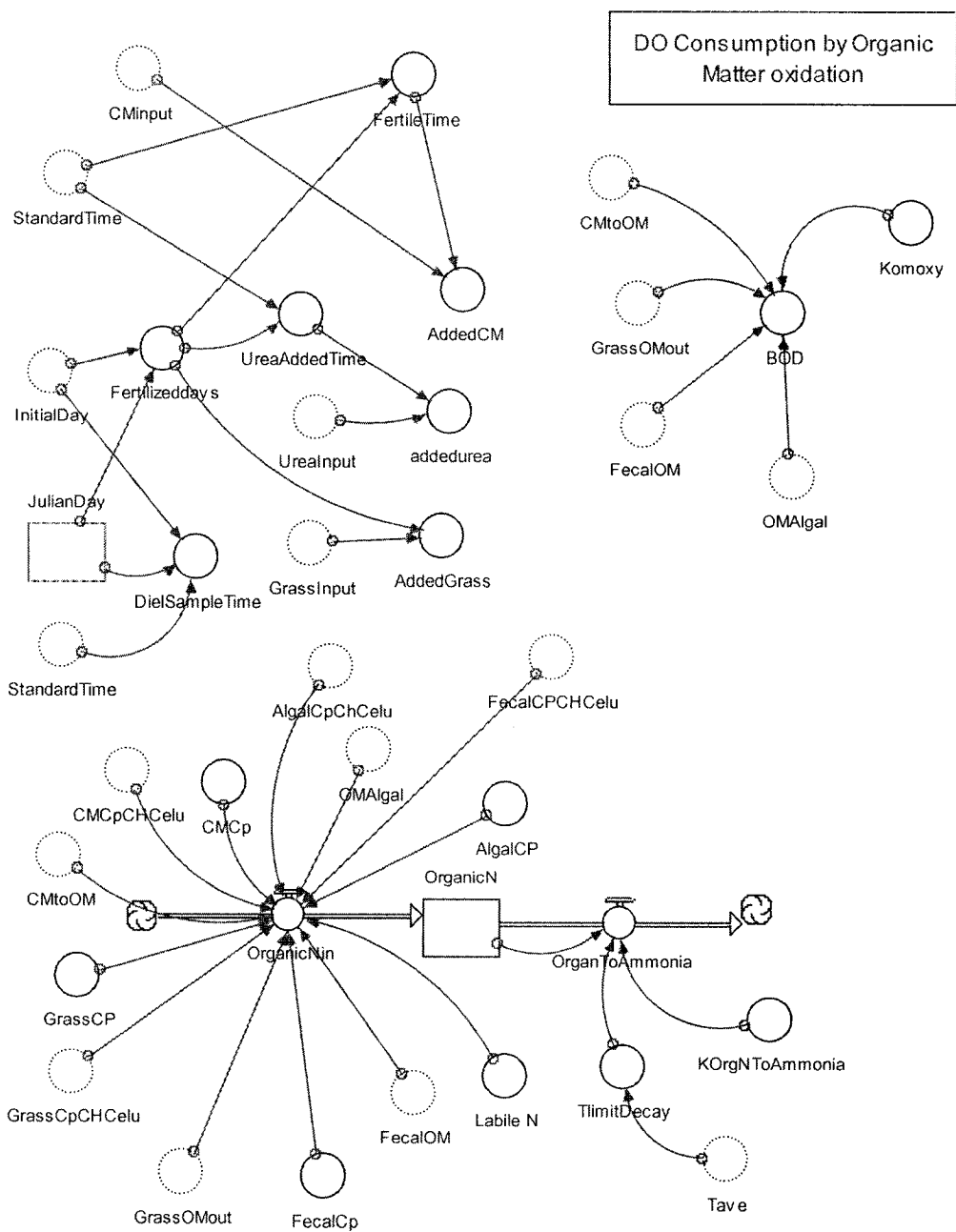


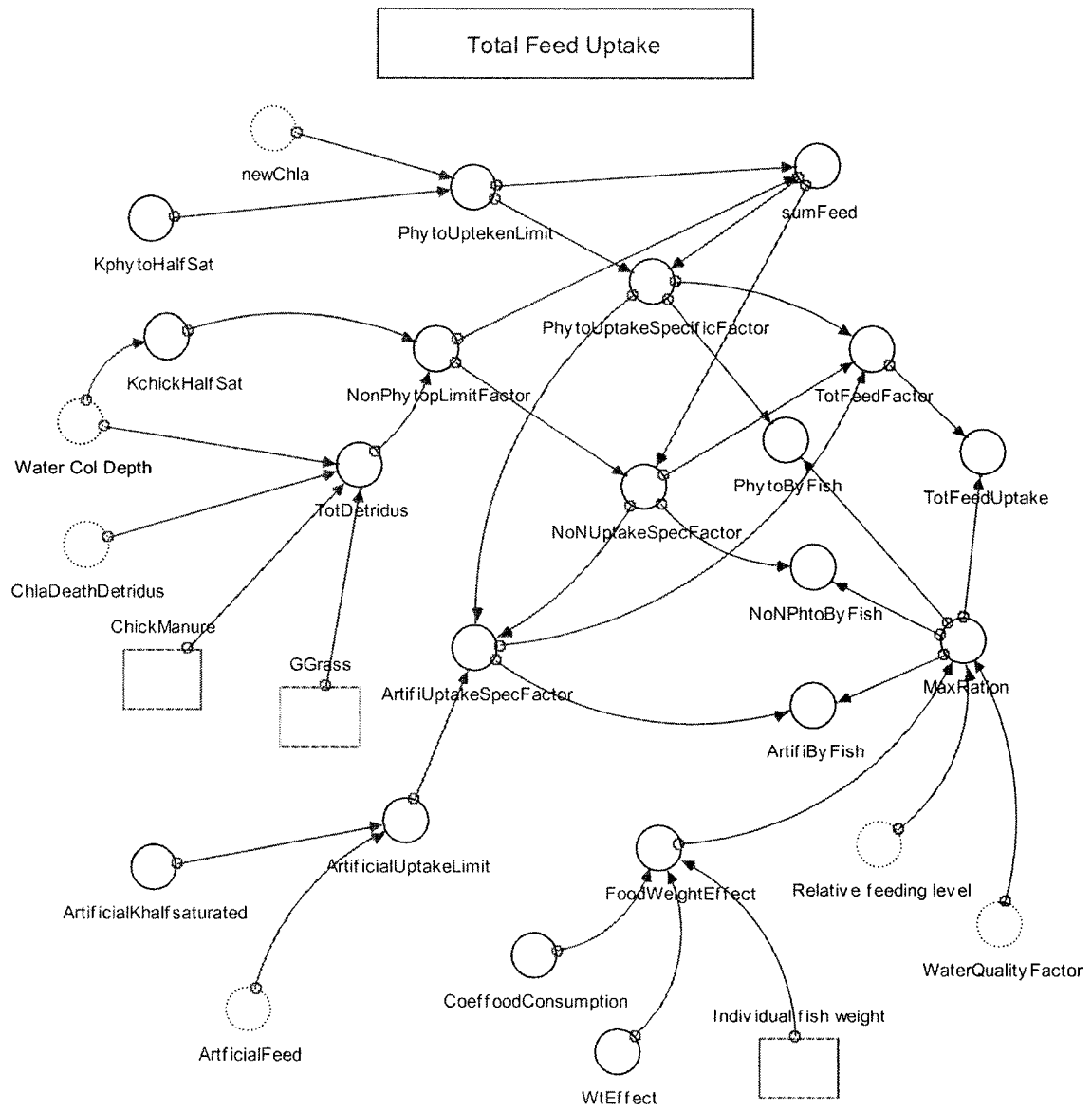


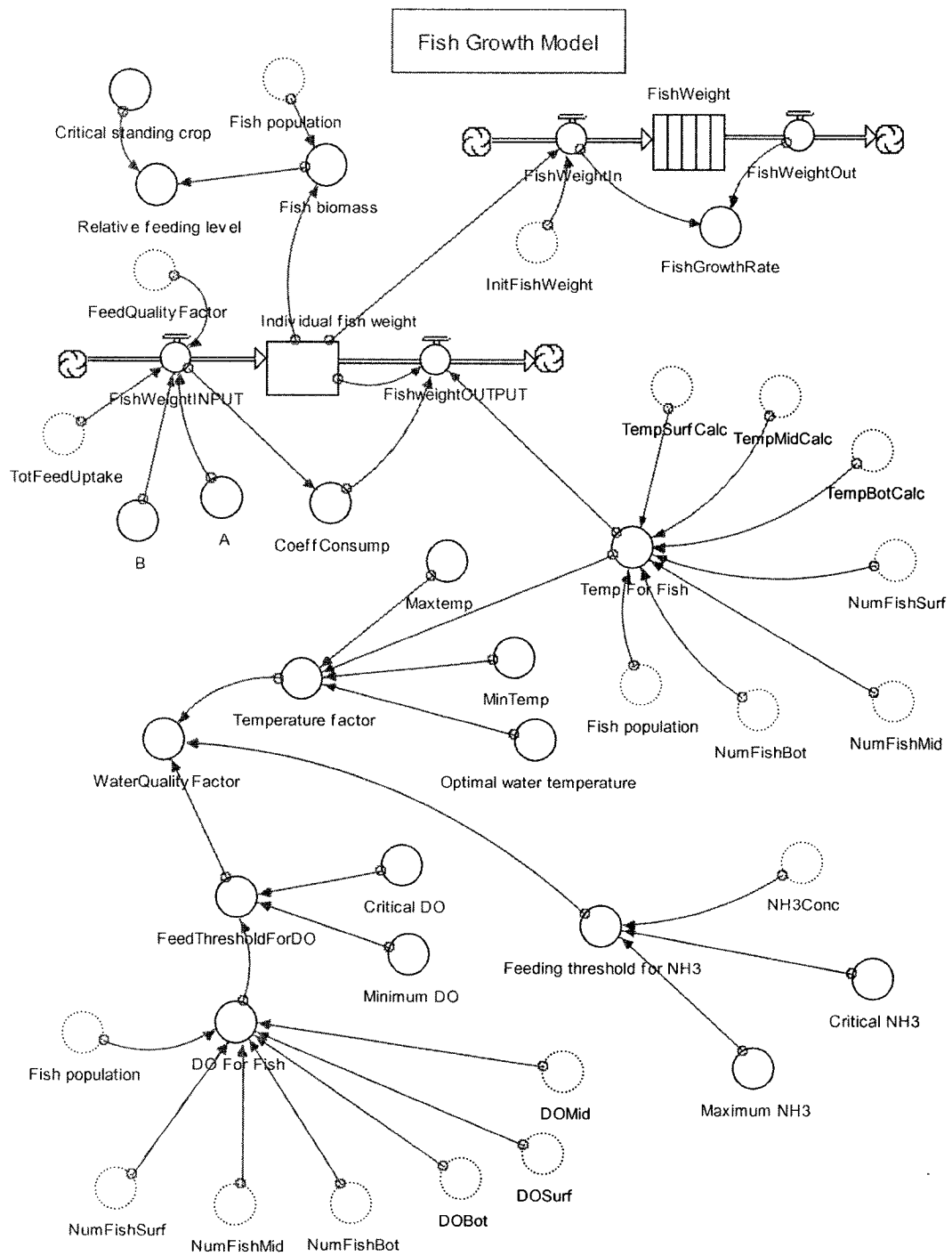


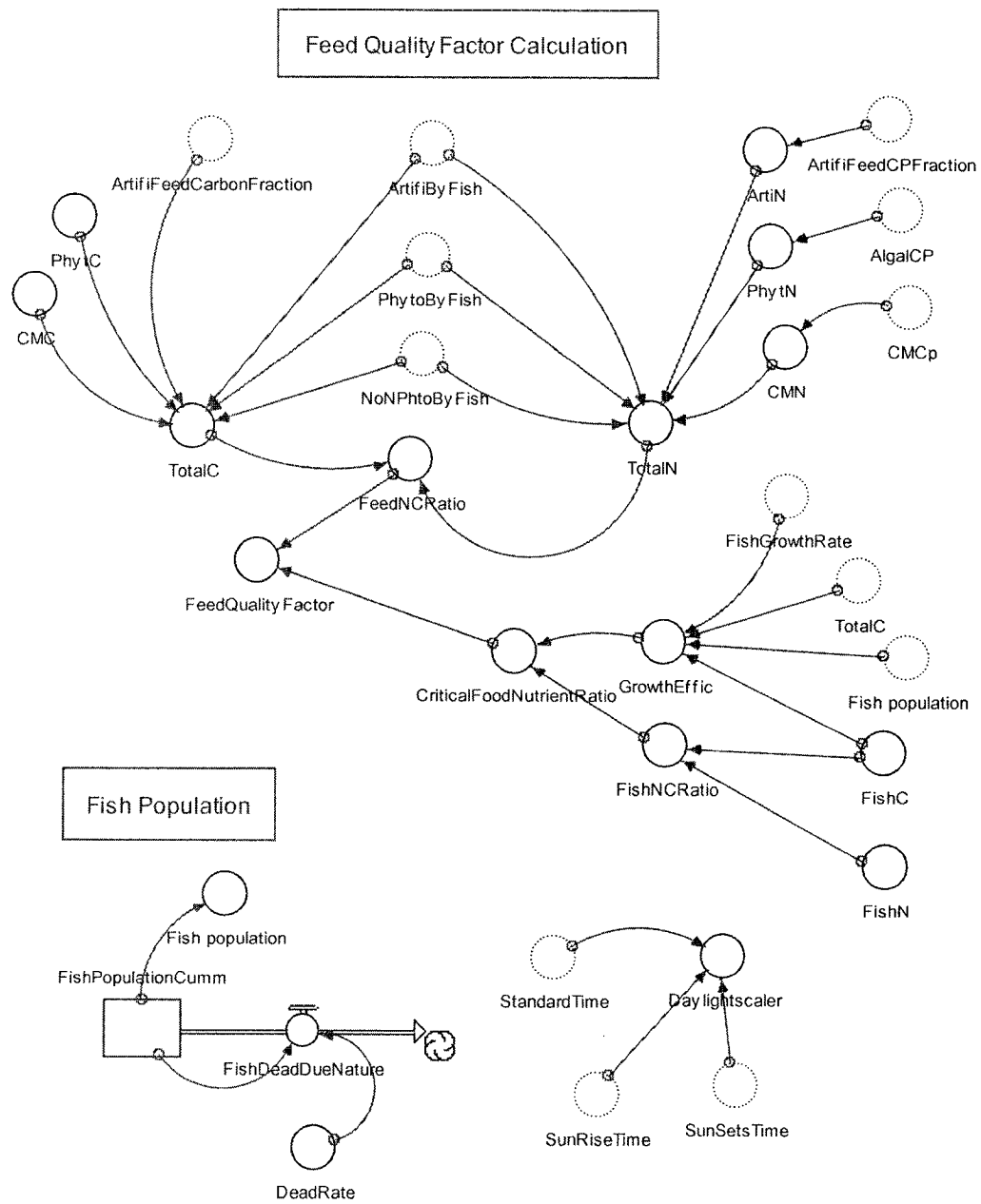
Fish Repiration

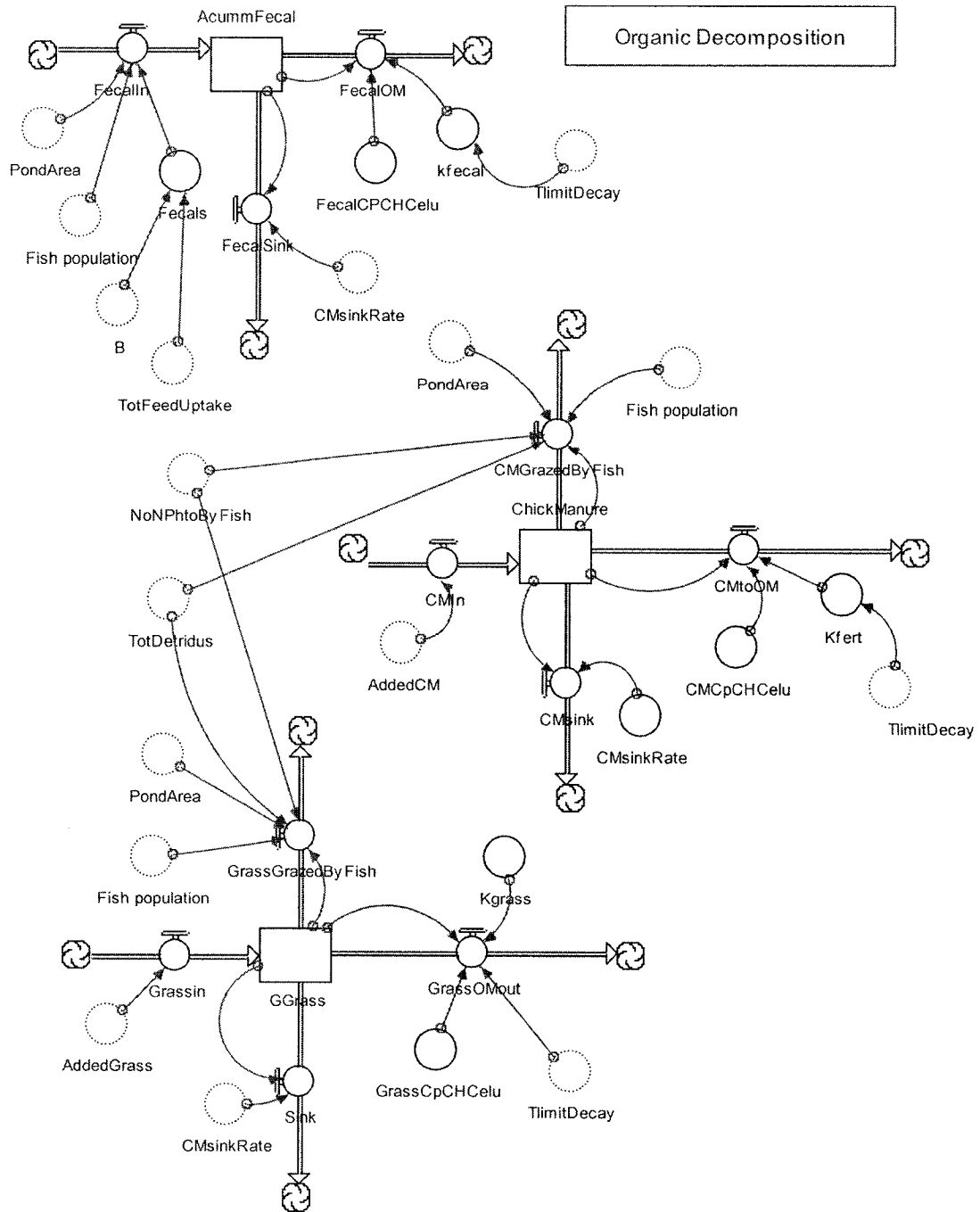


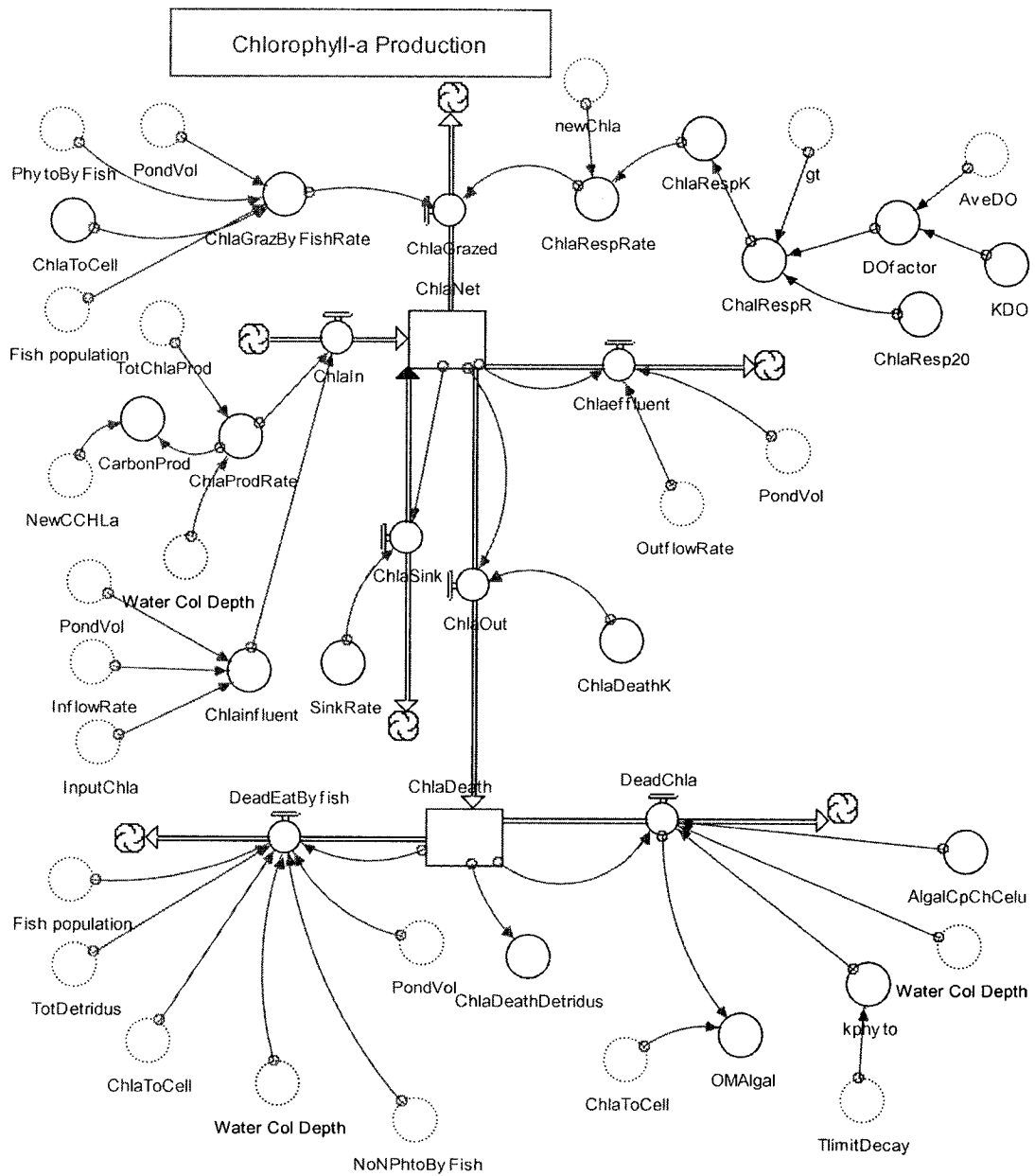




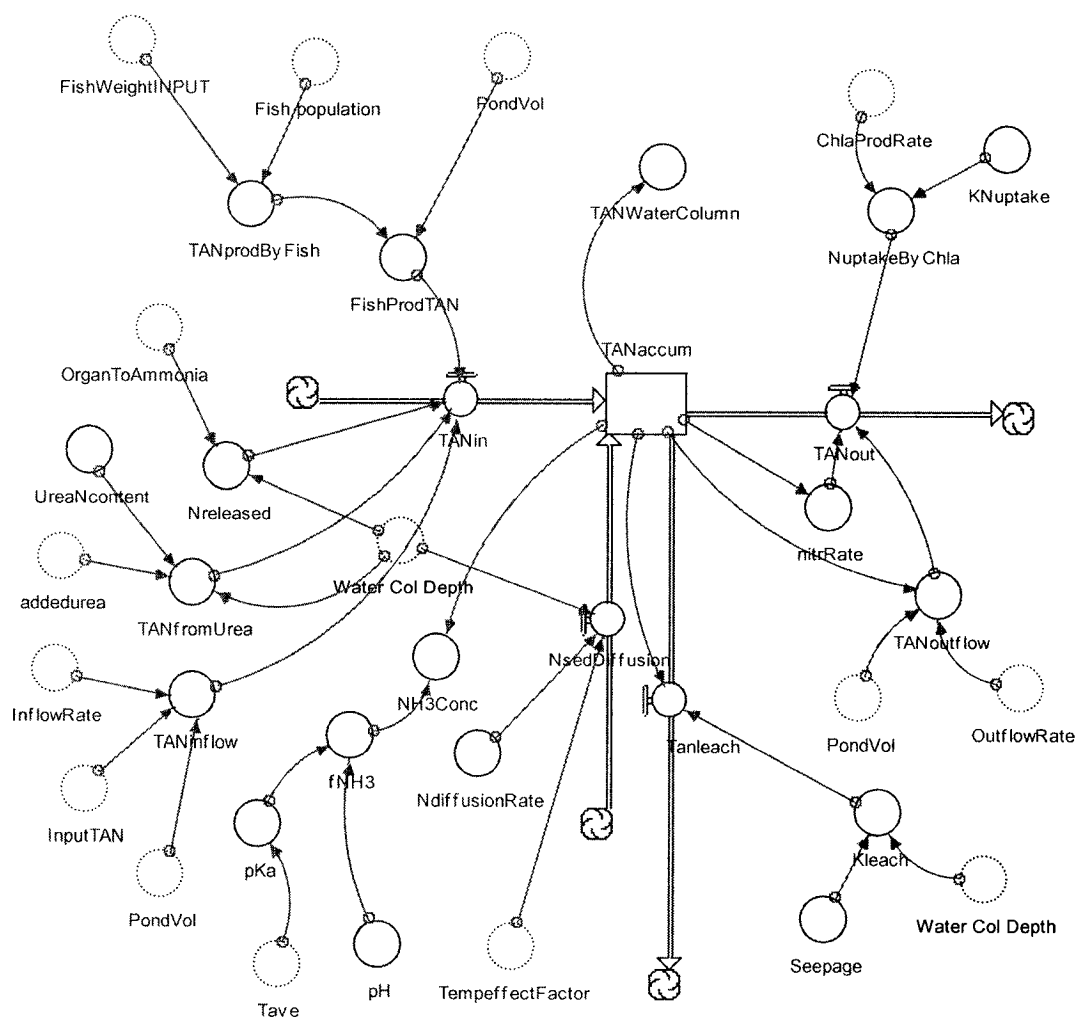








Total Ammonia Nitrogen Balance



B. Stella Equations

AcummFecal(t) = AcummFecal(t - dt) + (FecalIn - FecalOM - FecalSink) * dt
 INIT AcummFecal = 0.0 {g/m2}

INFLOWS:

FecalIn = Fecals*Fish_population/PondArea {g /m2/hr}

OUTFLOWS:

FecalOM = kfecal*AcummFecal*FecalCPCHCelu {g/m2/hr}

FecalSink = CMSinkRate*AcummFecal

ChickManure(t) = ChickManure(t - dt) + (CMIn - CMtoOM - CMSink - CMGrazedByFish) * dt

INIT ChickManure = CMinput*0.1 { 23.4 g/m2}

INFLOWS:

CMIn = AddedCM {g/m2/hr}

OUTFLOWS:

CMtoOM = ChickManure*Kfert*CMCpCHCelu {g OM/hr/m2}

CMSink = ChickManure*CMSinkRate

CMGrazedByFish = NoNPhtoByFish*(ChickManure/TotDetritus)*Fish_population/PondArea {g CM/m2}

ChlaDeath(t) = ChlaDeath(t - dt) + (ChlaOut - DeadChla - DeadEatByfish) * dt

INIT ChlaDeath = 0.5 {mg Chla /m3}

INFLOWS:

ChlaOut = ChlaDeathK*ChlaNet {mg Chla /m3/hr}

OUTFLOWS:

DeadChla = if ChlaDeath>0 then ChlaDeath*AlgalCpChCelu*kphyto*Water_Col_Depth else 0
 {mg/hr/m2 chla}

DeadEatByfish =

NoNPhtoByFish*(ChlaDeath/(TotDetritus*1000/Water_Col_Depth))*ChlaToCell*Fish_population/Pond
 Vol*1000 {mg chla/m3/hr}

ChlaNet(t) = ChlaNet(t - dt) + (ChlaIn - ChlaOut - ChlaSink - ChlaGrazed - Chlaeffluent) * dt

INIT ChlaNet = InitialChla {mg Chla /m3}

INFLOWS:

ChlaIn = ChlaProdRate+Chlainfluent {mgchla/m3/hr}

OUTFLOWS:

ChlaOut = ChlaDeathK*ChlaNet {mg Chla /m3/hr}

ChlaSink = SinkRate*ChlaNet {mgchla/m3/hr}

ChlaGrazed = ChlaGrazByFishRate+ChlaRespRate {mg/m3/hr}

Chlaeffluent = OutflowRate*ChlaNet/PondVol {mg/m3/hr, chla in the effluent}

FishPopulationCumm(t) = FishPopulationCumm(t - dt) + (- FishDeadDueNature) * dt

INIT FishPopulationCumm = INITFISHNum

OUTFLOWS:

FishDeadDueNature = DeadRate*FishPopulationCumm

FishWeight(t) = FishWeight(t - dt) + (FishWeightIn - FishWeightOut) * dt

INIT FishWeight = 39.8 {g fish}

TRANSIT TIME = 1

INFLOW LIMIT = INF

CAPACITY = INF

INFLOWS:

FishWeightIn = if time<=1 then InitFishWeight else Individual_fish_weight {g fish/fish}

OUTFLOWS:

FishWeightOut = CONVEYOR OUTFLOW

GGrass(t) = GGrass(t - dt) + (Grassin - GrassOMout - Sink - GrassGrazedByFish) * dt

INIT GGrass = 0.0 {g/m²}

INFLOWS:

Grassin = AddedGrass

OUTFLOWS:

GrassOMout = GGrass*K_{grass}*GrassCpCHCelu*TlimitDecay {g OM/hr/m²}

Sink = GGrass*CMsinkRate

GrassGrazedByFish = NoNPhtoByFish*(GGrass/TotDetridus)*Fish_population/PondArea {g/m²/hr}

Icompare(t) = Icompare(t - dt) + (MaxI) * dt

INIT Icompare = 0

INFLOWS:

MaxI = if mod(time,24)>=24-dt then (PenPar-Icompare)*1/dt else (max(PenPar, Icompare)-Icompare)*1/dt
{find the maximum value of Solarrad }

Individual_fish_weight(t) = Individual_fish_weight(t - dt) + (FishWeightINPUT - FishweightOUTPUT) * dt

INIT Individual_fish_weight = InitFishWeight {g/fish }

INFLOWS:

FishWeightINPUT = B*(1-A)*FeedQualityFactor*TotFeedUptake { g fish /fish/hr}

OUTFLOWS:

FishweightOUTPUT = (CoeffConsump*EXP(0.015*(Temp_For_Fish-15))*Individual_fish_weight^{0.81})
{0.81; g/hr}

JulianDay(t) = JulianDay(t - dt) + (DayIncrement) * dt

INIT JulianDay = InitialDay

INFLOWS:

DayIncrement = if JulianDay>=365 and StandardTime=23+(1-dt) then (-1*364/dt) else IF
(StandardTime>23+(1-DT)) THEN (1/DT) ELSE 0

NetEnergyBot(t) = NetEnergyBot(t - dt) + (Diffusion2 + SolarRadAbsBot - BotSedEngEx) * dt

INIT NetEnergyBot = InitialHeatBot {KJ/m²/hr}

INFLOWS:

Diffusion2 = HeatTransferByDiffB {transfer from middle to bottom layer; KJ/m²/hr}

SolarRadAbsBot = SolarRadDepAdj2 - SolarRadDepAdj3 {KJ/m²/hr}

OUTFLOWS:

BotSedEngEx = K_s * (TempGradBtSed/DepthGradBtSed) * 3.6 {KJ/m²/hr}

NetEnergyGroundWater(t) = NetEnergyGroundWater(t - dt) + (SedGWEngEx) * dt

INIT NetEnergyGroundWater = InitialHeatSed {KJ/m²/hr}

INFLOWS:

SedGWEngEx = K_e * (TempGradSedtGW/DepthGradSedtGW) * 3.6 {KJ/m²/hr}

NetEnergyMid(t) = NetEnergyMid(t - dt) + (SolarRadAbsMid + Diffusion1 - Diffusion2) * dt

INIT NetEnergyMid = InitialHeatMid {KJ/m²}

INFLOWS:

SolarRadAbsMid = SolarRadDepAdj1 - SolarRadDepAdj2 {KJ/m²/hr}

Diffusion1 = HeatTransferByDiffA {transfer from surface to middle layer; KJ/m²/hr}

OUTFLOWS:

Diffusion2 = HeatTransferByDiffB {transfer from middle to bottom layer; KJ/m²/hr}

NetEnergySed(t) = NetEnergySed(t - dt) + (SolarRadAbsSed + BotSedEngEx - SedGWEngEx) * dt

INIT NetEnergySed = InitialHeatSed {KJ/m²/hr}

INFLOWS:

SolarRadAbsSed = SolarRadDepAdj3 {KJ/m2/hr}
 BotSedEngEx = Ks * (TempGradBtSed/DepthGradBtSed) * 3.6 {KJ/m2/hr}
 OUTFLOWS:
 SedGWEngEx = Ke * (TempGradSedtGW/DepthGradSedtGW) * 3.6 {KJ/m2/hr}
 NetEnergySurf(t) = NetEnergySurf(t - dt) + (EnergyInSurf - EnergyOutSurf - Diffusion1) * dt
 INIT NetEnergySurf = InitialHeatSurf {KJ/m2}

INFLOWS:

EnergyInSurf = AtRad + SolarRadAbsSurf+EnergyInflow {KJ/m2/hr}

OUTFLOWS:

EnergyOutSurf = SurfRadToAtmos + EvapLossAdj + ConvectiveLossGain+EnergyOutflow {KJ/m2/hr}

Diffusion1 = HeatTransferByDiffA {transfer from surface to middle layer; KJ/m2/hr}

NetOxBot(t) = NetOxBot(t - dt) + (OxDiff2 + OxInBot - OxOutSed - OxOutBot) * dt

INIT NetOxBot = InitialDOBot*1000*BotThick {mgO2/m2}

INFLOWS:

OxDiff2 = (O2TransferByDiffB) * ((DOMid - DOBot)/DepthGradMtB) * 1000 {l/m3; yields mgO2/hr/m2}

OxInBot = PhotoRateBot {mgO2/hr/m2}

OUTFLOWS:

OxOutSed = SedRespRate * TempeffectFactor {mgO2/hr}

OxOutBot = OxyRespBot + WCRespBot + FishRespBot + O2Nitr {mgO2/hr/m2}

NetOxMid(t) = NetOxMid(t - dt) + (OxDiff1 + OxInMid - OxDiff2 - OxOutMid) * dt

INIT NetOxMid = InitialDOMid*1000*MidThick {mgO2/m2}

INFLOWS:

OxDiff1 = (O2TransferByDiffA) * ((DOSurf - DOMid)/DepthGradSurfM) * 1000 {l/m3; yields mgO2/m2/hr}

OxInMid = PhotoRateMid {mgO2/m2/hr}

OUTFLOWS:

OxDiff2 = (O2TransferByDiffB) * ((DOMid - DOBot)/DepthGradMtB) * 1000 {l/m3; yields mgO2/hr/m2}

OxOutMid = OxyRespMid + WCRespMid + FishRespMid + O2Nitr+ExcessSedResp {mgO2/hr/m2}

NetOxSurf(t) = NetOxSurf(t - dt) + (OxInSurf - OxDiff1 - OxOutSurf) * dt

INIT NetOxSurf = InitialDOSurf*1000*SurfThick {mg/m2}

INFLOWS:

OxInSurf = (SurfDiffIn + PhotoRateSurf + DOinflow) {mgO2/hr/m2}

OUTFLOWS:

OxDiff1 = (O2TransferByDiffA) * ((DOSurf - DOMid)/DepthGradSurfM) * 1000 {l/m3; yields mgO2/m2/hr}

OxOutSurf = (SurfDifOut + FishRespSurf + OxyRespSurf + WCRespSurf + O2Nitr + DOoutflow) {mg/hr/m2}

OrganicN(t) = OrganicN(t - dt) + (OrganicNin - OrganToAmmonia) * dt

INIT OrganicN = 0.7 {0.74 g/m2}

INFLOWS:

OrganicNin =

Labile_N*((GrassOMout*GrassCP/GrassCpCHCelu+CMtoOM*CMCp/CMCpCHCelu+FecalOM*FecalCp/FecalCpCHCelu+AlgalCP*OMAlgal/AlgalCpChCelu))/6.25 {g/m2/hr available organic nitrogen}

OUTFLOWS:

OrganToAmmonia = KOrgNToAmmonia*OrganicN*TlimitDecay {g/m2/hr}

PreImax(t) = PreImax(t - dt) + (preImaxIn) * dt

INIT PreImax = 857 {1144 for Honduras; 857 for Rwanda; 1543 for Thailand; umol/m2/s}

INFLOWS:

$preI_{maxIn} = \text{if } \text{mod}(\text{time}, 24) \geq 24 - dt \text{ and } \text{time}/24 > 2 \text{ then}$
 $((0.1 * I_{maxPreviousDay2} + 0.2 * I_{maxPreviousDay1} + 0.7 * I_{compare}) - preI_{max}) * (1/dt)$ else if $\text{mod}(\text{time}, 24) \geq 24 - dt \text{ and } \text{time}/24 \leq 2$ then $(I_{compare} - preI_{max}) * 1/dt$ else 0
 $PR_{residualMax}(t) = PR_{residualMax}(t - dt) + (ResidualIn_2 - ResidualOut2) * dt$
 $INIT PR_{residualMax} = 0$

TRANSIT TIME = varies

INFLOW LIMIT = INF

CAPACITY = INF

INFLOWS:

$ResidualIn_2 = \text{if } \text{mod}(\text{time}, 24) \geq 24 - dt \text{ then Add100Max}$ else $ResidualOut2$ { delay 24 hours }

OUTFLOWS:

$ResidualOut2 = \text{CONVEYOR OUTFLOW}$

TRANSIT TIME = dt

$PR_{residualMin}(t) = PR_{residualMin}(t - dt) + (ResidualIn - ResidualOut) * dt$

$INIT PR_{residualMin} = 0$

TRANSIT TIME = varies

INFLOW LIMIT = INF

CAPACITY = INF

INFLOWS:

$ResidualIn = \text{if } \text{mod}(\text{time}, 24) \geq 24 - dt \text{ then Add100min}$ else $ResidualOut$ { delay 24 hours }

OUTFLOWS:

$ResidualOut = \text{CONVEYOR OUTFLOW}$

TRANSIT TIME = dt

$SolarResidualDaily(t) = SolarResidualDaily(t - dt) + (SolarResidualIn - solarResidueOut) * dt$

$INIT SolarResidualDaily = 0$

TRANSIT TIME = varies

INFLOW LIMIT = INF

CAPACITY = INF

INFLOWS:

$SolarResidualIn = \text{if } \text{mod}(\text{time}, 24) \geq 24 - dt \text{ then Addthreshold}$ else $solarResidueOut$ { delay 24 hours }

OUTFLOWS:

$solarResidueOut = \text{CONVEYOR OUTFLOW}$

TRANSIT TIME = dt

$SolarResidualHour(t) = SolarResidualHour(t - dt) + (SolarResidualIn_2 - solarResidueOut_2) * dt$

$INIT SolarResidualHour = 0$

TRANSIT TIME = varies

INFLOW LIMIT = INF

CAPACITY = INF

INFLOWS:

SolarResidualIn_2 = if mod(time, 24) >= 24-dt then 100 else if mod(time, 1) >= 1-dt then Addthreshold_2
 else solarResidueOut_2 { delay one hour }

OUTFLOWS:

solarResidueOut_2 = CONVEYOR OUTFLOW

TRANSIT TIME = dt

TANaccum(t) = TANaccum(t - dt) + (TANin + NsedDiffusion - TANout - Tanleach) * dt
 INIT TANaccum = InitialTAN {ug/L}

INFLOWS:

TANin = Nreleased + FishProdTAN + TANfromUrea + TANinflow {ugN/L/hr}

NsedDiffusion = NdiffusionRate/Water_Col_Depth*TempeffectFactor/24*1000 {ug/L/hr}

OUTFLOWS:

TANout = nitrRate + NuptakeByChla + TANoutflow {ug/L/hr, nitrogen consum by nitrification and
 chlorophyll}

Tanleach = Kleach*TANaccum {ug/L/hr}

WindResidualDaily(t) = WindResidualDaily(t - dt) + (WindResidualIn - WindResidueOut) * dt

INIT WindResidualDaily = 0

TRANSIT TIME = varies

INFLOW LIMIT = INF

CAPACITY = INF

INFLOWS:

WindResidualIn = if mod(time, 24) >= 24-dt then AddthresholdWind else WindResidueOut { delay 24 hours
 }

OUTFLOWS:

WindResidueOut = CONVEYOR OUTFLOW

TRANSIT TIME = dt

A = 0.25 { 0.25; DIMENSIONLESS; FRACTION OF FOOD ASSIMILATED BUT USED FOR
 CATABOLISM (DIMENSIONLESS)}

Add100Max = CalcResidualMax + 100

Add100min = CalcResidualMin + 100

AddedCM = if FertileTime = 1 then CMinut * 0.1/4 else 0 {g dry chicken manure matter/m² }

AddedGrass = if Fertilizeddays = 1 then GrassInput * 0.1/4 else 0 {g/m²}

addedurea = if UreaAddedTime = 1 then (UreaInput * 0.1)/4/2 else 0 {g/m²}

Addthreshold = CalcofResGenDaily + 100 {rise the threshold}

AddthresholdWind = GenResidDailyWind + 100 {rise the threshold}

Addthreshold_2 = CalcofResHourly + 100 {rise the threshold}

AdjFetch = IF AverageFetch > 1 THEN 1 ELSE IF AverageFetch < 0.5 THEN 0.5 ELSE AverageFetch
 {adjustment to fetch calculations, see Losordo pg.167}

AdjLightExtCoeff = LightExtCoeff * oneovercosr {1/m }

AdjWindSpeed = if Windvectorest * 1000/3600 * (10/AnemometerHeight)^(1/7) < MinWindSpeed then
 MinWindSpeed else Windvectorest * 1000/3600 * (10/AnemometerHeight)^(1/7) {wind speed, adjusted for
 windspeed less than MINIMUMWINDSPEED and anemometer height}

aeroresistcoeff = 0.0013 {approximation for all wind speeds, see Losordo pg.160}

AirCorCoeMax = 0.431 {Correlation Coefficient of Lag One.}

AirCorCoeMin = 0.694 {Correlation Coefficient of Lag One.}

AirDensity = 1.0375 {1.1988 at sea level; 1.0375 is at 1700m; dry air density kg/m³}

AirGMax = ResidualMax * StdDevAirMax + AveTairMax {estimated solar radiation total for the day}

AirGMin = ResidualMin * StdDevAirmin + AveTairMin {estimated solar radiation total for the day}

AirMaxRondom = NORMAL(0,1) {Random number from a normal distribution with mean 0 and standard deviation 1}
 AirMinRondom = NORMAL(0,1) {Random number from a normal distribution with mean 0 and standard deviation 1}
 AKh = 0.409+0.5016*sin((ssha-1.047))
 AlgalCP = 0.45 {crude protein content}
 AlgalCpChCelu = 0.86 {decomposable, CP, CH, and Cellulose}
 AMP = (Tairmax-DelayTairmin)*(1+(Tairmax-DelayTairmin)/Tk)
 AnemometerHeight = 2.0 {m}
 Arcsinz = if sinzn>=1 then pi/2 else if sinzn<=-1 then -pi/2 else arctan(sinzn/(1-sinzn^2)^0.5) { use arctan() to calculate arcsin(zenith) }
 Arctagsunangle = arctan(SunAngle/(1-SunAngle^2)^0.5)
 ArtificialFeed = 0*12.5 {g/m2/hr, Cassava}
 ArtifiByFish = ArtifiUptakeSpecFactor*MaxRation
 ArtificialKhalfsaturated = 1 {g/m3}
 ArtificialUptakeLimit = ArtificialFeed/(ArtificialKhalfsaturated+ArtificialFeed)
 ArtifiFeedCarbonFraction = 0.5 {g C/g feed dry matter}
 ArtifiFeedCPFraction = 0.08 {g CP/g feed}
 ArtifiUptakeSpecFactor = if 1-(NoNUptakeSpecFactor+PhytoUptakeSpecificFactor)<=0 then 0 else (1-(NoNUptakeSpecFactor+PhytoUptakeSpecificFactor))*ArtificialUptakeLimit

 ArtiN = ArtifiFeedCPFraction/6.25
 AtRad = (1-LWReflect) * e * StefanBoltzman * ((TaK)^4)
 {net atmospheric radiation into pond; kJ/m2/hr}
 AutoCoeffWind = 0.65 {Correlation Coefficient of Lag One. Obtained from miniTAB using the measured data from Rwanda}
 AveDO = (DOBot+DOMid+DOSurf)/3 {average DO, mg/L }
 AveOxyResp = ChlaRespRate/ChlaProductionPerOxy*(Water_Col_Depth) {mgO2/m2/hr}
 AVERAGE = 191.1628 { }
 AverageFetch = MeanFetch/MaxFetch }
 AverFetch1 = 0.5*MaxFetch1
 AverFetch2 = 0.5*MaxFetch2
 AveTairMax = 26.63+(7.16*4*N_MaxExp/(1+N_MaxExp)^2)
 AveTairMin = 15.42+(5.84*4*N_MinExp/(1+N_MinExp)^2)
 B = 0.65 {unitless; EFFICIENCY OF FOOD ASSIMILATION; 0.5 average values for phytoplankton not artificial food }
 Bkh = 0.6609-0.4767*sin((ssha-1.047))
 BOD = Komoxy*(CMtoOM+GrassOMout+FecalOM+OMAlgal) {gO2/hr/m2}
 BODlayer = BOD/3*1000 {mg/m2/hr}
 BotDepth = SurfThick + MidThick + (BotThick/2) {meters, measurement depth}
 BotThick = Water_Col_Depth/3 {meters thick}
 BoundDepth1 = (SurfDepth + MidDepth)/2 {depth at boundry between surface and middle layers; m}
 BoundDepth2 = (MidDepth + BotDepth)/2 {depth at boundry between middle depth and bottom depth; m}
 CalcOfResGenDaily = (CorCoeffLagOneDaily_Solar*SubtractThreshold) +sqrt(1-(CorCoeffLagOneDaily_Solar)^2)*RandomNODailySolar {Generated Residual }
 CalcOfResHourly = (CorCoeffLagOne_Hourly*SubtractThreshold_3) +sqrt(1-(CorCoeffLagOne_Hourly)^2)*RandomNoHourSolar {Generated Residual }
 CalcResidualMax = (AirCorCoeMax)*ResidualMax+sqrt(1-(AirCorCoeMax)^2)*AirMaxRondom {Generated Residual }
 CalcResidualMin = (AirCorCoeMin)*ResidualMin+sqrt(1-(AirCorCoeMin)^2)*AirMinRondom {Generated Residual }
 CarbonProd = ChlaProdRate*NewCCHLa {mgC/hr/m3}
 CCHLa = (CChlaAlf*Imax)/(Umax/ratioOxyCarbon*2.718) {mg c/ mg chla, predicted ratio of carbon to chlorophyll a. }
 CChlaAlf = 1./24 {0.45 (Rwanda); 1.4 (thailand); 1.85 ; mgC/mg chla*umol/m2.s; 35 mg c/(mg chla *(umol/m2)), slope of PI curve}

```

CChlaMax = 600 { maximum CChla, mgC/mg Chla }
CChlaMin = 10 { minimum CChla, mg C/mg Chla }
ChalRespR = ChlaResp20*gt*DOfactor {1/hr}

ChlaDeathDetritus = if ChlaDeath>0 then ChlaDeath else 0
ChlaDeathK = 0.01/24 {0.02/24, 1/hr; death rate}
ChlaGrazByFishRate = ((PhytoByFish*Fish_population*ChlaToCell/PondVol)*1000) {mg chla/m3/hr}
Chlainfluent = InflowRate*InputChla/PondVol {mg/m3 chla in the influent}
Chlalimit = 1500 {800, mg chla/m3, the maximum chla in the pond}
ChlaProdRate = TotChlaProd/Water_Col_Depth {mgChla/hr/m3}
ChlaProductionPerOxy = (1/(ratioOxyCarbon*NewCCHLa)) { mgchla/mg O2, the amount of chla
produced}
ChlaResp20 = 0.002{0.008; 0.002 1/hr; from Zhu, S}
ChlaRespK = ChalRespR { 0.05/24; 1/hr; phytoplankton respiration rate}
ChlaRespRate = ChlaRespK*newChla {mg chla/hr/m3}
ChlaToCell = 0.01 { 0.014; range is from 0.005 to 0.02 mg Chla/ mg Cell dry weight }
CMC = 0.278 {assumed carbon}
CMCp = 0.14 { Fraction of Chicken manure is Crude protein; Msiska, 1981}
CMCpCHCelu = 0.69 {g/g ChickManure; 0.12 celloclose and 0.43 CarbonHydrate; 0.283 crude Protein}
CMinput = 500 {kg/ha/wk dry matter, then maximum is 1000}
CMN = CMCp/6.25
CMNcontent = 0.022 {g N/g dry chicken manure}
CMsinkRate = 0.05/24 {1/hr}
CoeffConsump = if FishWeightINPUT>=0.03 then 0.025/24 else 0
CoeffExpandH2OA = (0.000015 * (TavA - 277)) - (0.0000002 * ((TavA - 277)^2)) {coefficient for
expansion of water}
CoeffExpandH2OB = (0.000015 * (TavB - 277)) - (0.0000002 * ((TavB - 277)^2)) {coefficient for
expansion of water}
CoeffoodConsumption = 0.8/24 {0.55/24; g fish^(1-m)/g fish/hr, COEFF OF Food consumption =h IN
BEI 0.8 from calibration using CRSP data}
CONTROL_2 = (PI/180)*(STDV*(2/SKEW)*((1+(SKEW/6)*(STDNORMAL-(SKEW/6)))^3 -1)
+AVERAGE) { radians }
ConvectiveLossGain = 1.5701 * WindSpeedAtZms * (TempSurfCalc - DegreeCAir) {Sensible/convective
loss of heat; KJ/m2/hr}
ConvertFunc = if ErrFunction>=0.99 then 0.5+0.5*0.98 else if ErrFunction <=(-0.96) then 0.5+0.5*(-0.96)
else 0.5+0.5*ErrFunction
ConvertFunc_2 = if ErrFunction_2>0.98 then 0.5+0.5*0.98 else if ErrFunction_2<=(-0.96) then 0.5+0.5*(-
0.96) else 0.5+0.5*ErrFunction_2
CorCoefLagOneDaily_Solar = 0.29 {Correlation Coefficient of Lag One. Obtained from literature,
Graham, 1988}
CorCoefLagOne_Hourly = 0.54 {Correlation Coefficient of Lag One. Obtained from literature, Graham,
1988}
correctKt = if Estimated_Kt>=Ktmin and Estimated_Kt<= Ktmax then Estimated_Kt else if
Estimated_Kt>Ktmax then Ktmax else Ktmin {limit the value of Kt in a reseable range}
Cos_z = SIN(fi)*SIN(Delination)+COS(fi)*COS(Delination)*COS(Hour_Angle)
CriticalFoodNutrientRatio = FishNCRatio*GrowthEffic
Critical_DO = 6.2 {6.2 mg oxygen/liter. Critical DO level above which food intake is not affected (Balarin
and Haller 1979) }
Critical_NH3 = 0.06 {mg/L, Critical NH3 level above which food intake is affected. Chervinski (1982) }
Critical_standing_crop = 100 {kg fish biomass; maximum biomass in the specific fish pond, based on the
measured data. kg Fish biomass above which fish will be fed limited}
Csat = CsatT * (1 - (0.0001 * SiteElevation)) {saturation concentration value for oxygen in water, corrected
for elevation; mg/l}
CsatT = 14.625 - (0.41022 *TempSurfCalc) + (0.007991 * (TempSurfCalc)^(2)) - (0.0000778 *
(TempSurfCalc)^(3)) {saturation concentration of oxygen in water of temperature given; mg/l}
darkLength = 24-DayLength {dark time}

```

```

DayLength = if srss<=0 then (2/15)*(180-Arctagsunangle*180/pi) else (2/15)*(Arctagsunangle*180/pi)
Daylightscaler = if StandardTime>=(SunRiseTime+2) and StandardTime<=(SunSetsTime-2) then 1 else 0
{day light scaler, because only day time feeding}
DeadRate = 4e-5 {1/hr, death rate}
DegreeCAir = TairHour {air temperature model from Ephrath et al, 1996}
DelayTairmin = delay(Tairmin,24)
Delination = (23.45*SIN(360/365*(284+JulianDay)*pi/180))*pi/180 { delination in radians}
DepthGradBtSed = SedDepth - BotDepth {m}
DepthGradMtB = BotDepth - MidDepth {m}
DepthGradSedtGW = GWDepth - SedDepth {m}
DepthGradSurfM = MidDepth - SurfDepth {m}
Dewpointabs = (AirGMin - 2.0) + (273.15) {°K; from Koon et. al. -- dry-bulb temp at 600 a.m. minus 2°C}
DielSampleTime = if (mod((JulianDay-(InitialDay+9)), 14) =0 and StandardTime>=6) or
(mod((JulianDay-(InitialDay+9)), 14) =1 and StandardTime<=6) then 1 else 0
DOBot = IF O2ConcCalcBot < 0 THEN 0 ELSE O2ConcCalcBot {eliminates negative values}
DObotLimit = DOBot/(KDO+DOBot)
DOfactor = AveDO/(AveDO+KDO) {unitless}
DOinflow = (InputDO*1000)*InflowRate/PondArea {mg/m2/hr}
DOMid = IF O2ConcCalcMid < 0 THEN 0 ELSE O2ConcCalcMid {eliminates negative values}
DOmidLimit = DOMid/(KDO+DOMid)
DOoutflow = (DOSurf*1000)*OutflowRate/PondArea {mg/m2/hr}
DOSurf = IF O2ConcCalcSurf < 0 THEN 0 ELSE O2ConcCalcSurf {mg/L; eliminates negative values}
DOSurflimit = DOSurf/(KDO+DOSurf)
DO_For_Fish = if (DOSurf*NumFishSurf+DOMid*NumFishMid+DOBot*NumFishBot)/Fish_population
<=0 then DOSurf else
(DOSurf*NumFishSurf+DOMid*NumFishMid+DOBot*NumFishBot)/Fish_population
DTSL = 4*(STD_Longitude - Longitude)/60 {Solar time difference between Standard Longitude, and Site
Longitude, hr}
e = 0.398 * (10^(-5)) * ((TaK)^2.148)
{average emittance of the atmosphere; dimensionless}
ea = (610.78 * EXP(17.2649 * (Dewpointabs - 273.15)/(Dewpointabs - 35.86))) * 0.001 * 7.5006 {water
vapor pressure above pond surface; mm Hg}
Earth_Sun = 1 + 0.017 * COS(0.0172 * (186 - JulianDay))
EffectDiffuCoeffA = IF TempGradientSurfM <= 0 THEN Emax ELSE IF StableFlowDiffuCoeffA < 0
THEN 0.0054 ELSE IF StableFlowDiffuCoeffA > Emax THEN Emax ELSE StableFlowDiffuCoeffA
{m2/hr}
EffectDiffuCoeffB = IF TempGradMtB <= 0 THEN Emax ELSE IF StableFlowDiffuCoeffB < 0 THEN
0.054 ELSE IF StableFlowDiffuCoeffB > Emax THEN Emax ELSE StableFlowDiffuCoeffB {m2/hr}
Emax = 0.4 {0.4 ;m2/hr}
EnergyInflow = InputTemp*InflowRate*H2OHeatCap*H2ODensity/PondArea {kJ/m2/hr}
EnergyOutflow = TempSurfCalc*OutflowRate*H2ODensity*H2OHeatCap/PondArea {kJ/m2/hr, effluent
energy, energy loss is due to water effluent}
Eq_Time = (9.87*sin(2*Orbit)-7.53*cos(Orbit)-1.5*sin(Orbit))/60 {equation time, hr}
ErrFunction = if SubtractThreshold>=0 then 0.016040162+1.4902455*SubtractThreshold+(-
0.66947908)*SubtractThreshold^2+0.13026229*SubtractThreshold^3+(-
0.048797198)*exp(SubtractThreshold) else (-1)*(0.016040162+(-1.4902455)*(SubtractThreshold)+(-
0.66947908)*SubtractThreshold^2+(-0.13026229)*SubtractThreshold^3+(-0.048797198)*exp(-
SubtractThreshold))
ErrFunction_2 = if SubtractThreshold_3>=0 then 0.016040162+1.4902455*SubtractThreshold_3+(-
0.66947908)*SubtractThreshold_3^2+0.13026229*SubtractThreshold_3^3+(-
0.048797198)*exp(SubtractThreshold_3) else (-1)*(0.016040162+(-1.4902455)*(SubtractThreshold_3)+(-
0.66947908)*SubtractThreshold_3^2+(-0.13026229)*SubtractThreshold_3^3+(-0.048797198)*exp(-
SubtractThreshold_3))
es = 25.374 * EXP(17.62 - (5271/TempWK)) {saturated vapor pressure at WaterTemp; mm Hg}
EstimatedlightExtin = 7.67+0.013*newChla {estimated light extinction coefficient}
Estimated_Kh = if (Khm+KhAlf)>1.0 then 1.0 else if (Khm+KhAlf)<0 then 0 else (Khm+KhAlf)

```

```

Estimated_Kt = if (JulianDay>=1 and JulianDay<91) then func1 else Func2
EvapLoss = (N * WindSpeedAtZ * (es - ea)) {KJ/m2/hr}
EvapLossAdj = EvapLoss {KJ/m2/hr}
ExcessSedResp = IF DOBot <= 0 THEN -(PhotoRateBot + OxDiff2 - OxDiffSed) ELSE 0
ExtraAveHho = 4.921*(1+0.033*cos(360/365*JulianDay*pi/180))*Cos_z {extraterrestrial daily solar
radiation, MJ/m2}
ExtraAveHo =
24/Pi*4.921*(1+0.033*cos(360/365*JulianDay*pi/180))*(ssha*sin(fi)*sin(Delination)+cos(fi)*cos(Delinat
ion)*sin(ssha)) {extraterrestrial solar radiation, MJ/m2}
FecalCp = 0.03 {Nitrogen content, 0.02 to 0.046 cp for marine fish}
FecalCPCHCelu = 0.94 { content of CP, CH, & cellulose in fish fecal}
Fecals = TotFeedUptake*B {g /hr, total produced fecals}
Feeding_threshold_for_NH3 = IF NH3Conc<Critical_NH3 then 1 ELSE if NH3Conc>Maximum_NH3
then 0 else (Maximum_NH3-NH3Conc)/(Maximum_NH3-Critical_NH3) {Dimensionless. captures the
effect of high unionized levels of ammonia that result in feeding cessation}

FeedNCRatio = if TotalC>0 then TotalN/TotalC else 0 {g N/g C uptake by fish}
FeedQualityFactor = (if FeedNCRatio<=0 then 0 else if FeedNCRatio<CriticalFoodNutrientRatio then
FeedNCRatio/CriticalFoodNutrientRatio else 1) {effect of feed on fish growth}
FeedThresholdForDO = If DO_For_Fish>Critical_DO then 1 else if DO_For_Fish >= Minimum_DO and
DO_For_Fish <=Critical_DO then (DO_For_Fish-Minimum_DO)/(Critical_DO-Minimum_DO) else 0
{Dimensionless function describing the effect of high DO levels on feeding cessation by fish}
FertileTime = if Fertilizeddays=1 and (StandardTime>10 and StandardTime<=14) then 1 else 0 { assumed
at 10:00 am to add fertilizer}
Fertilizeddays = if mod((JulianDay-(InitialDay+4)), 7) =0 and JulianDay<188 then 1 else 0 { Hoduras,
from Data F301, fertilization was stoped three weeks before end of season}
fi = Latitude * PI / 180 {Latitude in radians}
FishC = 0.33 {g C/g fish; fish carbon}
FishGrowthRate = FishWeightIn-FishWeightOut {g fish/fish/hr}
FishN = 0.7/6.25 {0.7 is crude protein, g CP/g fish}
FishNCRatio = FishN/FishC
FishProdTAN = (TANprodByFish/PondVol)*1000 {ug N/L/hr}
FishRespBot = DObotLimit*FRespBot/PondArea {mgO2/hr/m2}
FishRespMid = DOfmidLimit*FRespMid/PondArea {mgO2/m2/hr}
FishRespSurf = DOSurfLimit*FRespSurf/PondArea {mgO2/m2/hr}
FishSizeLarge = 0 {average size large fish; g}
FishSizeMiddle = 0 {average size of medium fish; g}
FishSizeSmall = 34.0 {average weight of small fish; g}
Fish_biomass = Fish_population*Individual_fish_weight/1000 { kg, total biomass}
Fish_population = int(FishPopulationCumm) {number of fish}

fNH3 = 1/(10^(pKa-pH)+1) {NH3 fraction, Boyd, 1990}
FoodWeightEffect = (Individual_fish_weight^WtEffect )*CoeffoodConsumption{g fish/fish/hr}
FractionLarge = 0.0 {% of population}
FractionMiddle = 0.0 {% of population}
FractionSmall = 1.0 {% of population, as fraction}
FRespBot = (10^(-0.999 - 0.000957 * Individual_fish_weight + 0.0000006 * Individual_fish_weight^2 +
0.0327 * TempBotCalc - 0.0000087 * TempBotCalc^2 + 0.0000003 * Individual_fish_weight *
TempBotCalc)) * (Individual_fish_weight*NumFishBot) {mgO2/hr}
FRespMid = (10^(-0.999 - 0.000957 * Individual_fish_weight + 0.0000006 * Individual_fish_weight^2 +
0.0327 * TempMidCalc - 0.0000087 * TempMidCalc^2 + 0.0000003 * Individual_fish_weight *
TempMidCalc)) * Individual_fish_weight*NumFishMid {mgO2/hr}
FRespSurf = (10^(-0.999 - 0.000957 * Individual_fish_weight + 0.0000006 * Individual_fish_weight^2 +
0.0327 * TempSurfCalc - 0.0000087 * TempSurfCalc^2 + 0.0000003 * Individual_fish_weight *
TempSurfCalc)) * (Individual_fish_weight*NumFishSurf) {mgO2/hr}
FrictVelWindStress = ((WShearStress/(H2ODensSurf * 1000))^(0.5)) {m/s; shown as Ws* in Losordo}

```

```

Func1 = 0.62601177-0.088785601*(LOGN(1.05574/(ConvertFunc+0.01)-1)) {accumulate frequency
distribution function for month Jan, Feb, and March}
Func2 = 0.53013909-0.072482258*(logn(1.0177006/(ConvertFunc+0.01)-1)) {this function is for months
April to Dec, Honduras}
FUNCTION = (10/36)*(-0.045094133+3.9603766*EXP(-0.5*(((5+COUNTER(6,30))-
14.428748)/2.8386295)^2)) { m/sec. }
g = 9.81 {m/s/s}
GendailyWindMean = if GenWindMean<windmin then windmin else if GenWindMean>windmax then
windmax else GenWindMean
GeneratedHt = Estimated_Kt*ExtraAveHo {calculated solar radiation values, mJ/m2}
GenResidDailyWind = (AutoCoeffWind*SubtractThresholdWind) +sqrt(1-
(AutoCoeffWind)^2)*RandomWindResidual {Generated Residual }
GenWindMean = SubtractThresholdWind*StdevWind+Wmean {km/hr}
GrassCP = 0.13 { organic nitrogen content from CP}
GrassCpCHCelu = 0.85 {kg decomped matter/kg grass}
GrassInput = 0 {kg/ha/wk grass in dry matter}
GrowthEffic = if (TotalC/Fish_population) <=0 or FishGrowthRate<=0 then 0 else if
(FishGrowthRate*FishC/(TotalC/Fish_population)) >1 then 0 else
FishGrowthRate*FishC/(TotalC/Fish_population) {unitless, growth efficiency}
gt = 1.066^(Tave-OPTTEMP) {1.066 temperature correction, 1/hr from Lee, 1991}
gtbot = 1.049^(TempBotCalc-OPTTEMP) { temperature correction, 1/hr from Lee, 1991}
gtmid = 1.049^(TempMidCalc-OPTTEMP) { temperature correction, 1/hr from Lee, 1991}
gtsurf = 1.066^(TempSurfCalc-OPTTEMP)
GWDepth = 6.0 {meters, measurement depth; "earth"}
H2ODensity = 1000 {kg/m3, water density}
H2ODensSurf = 0.99987 + ((0.0000069) * (TempSurfCalc)) - ((0.00000889) * ((TempSurfCalc)^2)) +
((0.00000074) * ((TempSurfCalc)^3)) {kg/l}
H2OHeatCap = 4.1819 {KJ/°K/kg at 20C; 4.1718 at 30 C}
HeatTransferByDiffA = (H2OHeatCap * EffectDiffuCoeffA *1000 {kg/m3} *
((TempGradientSurftM)/(DepthGradSurftM))) {KJ/m2/hr}
HeatTransferByDiffB = H2OHeatCap * EffectDiffuCoeffB * 1000 {kg/m3} *
(TempGradMtB/(DepthGradMtB)) {KJ/m2/hr}
Hh = if Solar_Time<SunRiseTime or Solar_Time>SunSetsTime then 0 else Estimated_Kh
HighestSH = 12-DTSL -1.5/60 {the time of heighest position of the sun which is at the decline angle 23.5}
HourSolarAngle = ( HourSolarTime-12 ) * 15 * PI/180 {radians}
HourSolarTime = int(Solar_Time)
Hour_Angle = ( Solar_Time-12 ) * 15 * PI/180 {radians}
Imax = testImax*PreImax { max solarRad, umole/m2/s }
ImaxPreviousDay1 = delay(PreImax,24)
ImaxPreviousday2 = delay(ImaxPreviousDay1,24)
InflowRate = 0./24 {inflow rate, m3/hr}
InitChlaRandom = Normal(19.5, 13.3) {ug/L, initial chla}
InitDORandom = normal(0.8, 1.1) {mg/L, initial DO at 6:00 middle layer}
INITFISHNum = 1012 {Initial number of fish }
InitFishWeight = InitTotalFishWeight/INITFISHNum*1000 {g, initial fish weight}
InitialChla = if InitChlaRandom<15 then 15 else InitChlaRandom {477, mg chla /m3, Inital chla
canc.3/11/91 }
InitialDay = 38
InitialDO = if InitDORandom<0 then 0 else InitDORandom {7.9, initial DO for all layers; average on
5/26/89 ponds CO5, DO6, DO8}
InitialDOBot = InitialDO {mg/l; input value on day 40}
InitialDOMid = InitialDO {mg/l; input value}
InitialDOSurf = InitialDO {mg/l; input value}
InitialHeatBot = InitialTempBot * 1000 * 4.1816*BotThick {Kj/m2; 1000 is the density; 4.1816 is specific
heat at 20°C}

```

InitialHeatMid = InitialTempMid * 1000 * 4.1816*MidThick {Kj/m2; 1000 is the density; 4.1816 is specific heat at 20°C}
 InitialHeatSed = InitialTempSed * 1000 * 4.1816*SedThick {Kj/m2; 1000 is the density; 4.1816 is specific heat at 20°C}
 InitialHeatSurf = InitialTempSurf * 1000 * 4.1816*SurfThick {Kj/m2; 1000 is the density; 4.1816 is the specific heat at 20°C}
 InitialTAN = if InitTANRandom<50 then 50 else InitTANRandom {100, mg/M3, initial TAN}
 InitialTemp = if InitTempRandom <15 then 15 else InitTempRandom {21, C; initial temperature for all three layers on 5/26/89 average from ponds b01, b05, and b11}
 InitialTempBot = InitialTemp
 InitialTempGW = 20 {°C}
 InitialTempMid = InitialTemp
 InitialTempSed = InitialTemp
 InitialTempSurf = InitialTemp
 InitialTime = 6.00 { Initial time, hr }
 InitTANRandom = Normal(150, 120) {ug/L, TAN, initial TAN}
 InitTempRandom = Normal(25.4, 2.01) {C, inintial temperature, from Honduras site F03D-E file}
 InitTotalFishWeight = 37 {kg}
 InputChla = 0 {mg/m3, chla in the influent}
 InputDO = 7 {mg/L, DO in the influent water}
 InputTAN = 10 {ug/L TAN, TAN in inflow}
 InputTemp = 20 {C, the inflow water temperature }
 k = (6 * (WindShearArea)^(-1.84)) {empirical drift coefficient; m/s}
 KchickHalfSat = 60*Water_Col_Depth {g/m2, 60 g/m3 }
 KConvertBot = TempBotCalc + 273.15 {conversion to Kelvin degrees}
 KConvertMid = TempMidCalc + 273.15 {°C to °K}
 KConvertTop = TempSurfCalc + 273.15 {°C to °K}
 KDO = 1 {half satuation DO constand, mg O2/L}
 Ke = 0.667 {watts/m°C}
 kfecal = TlimitDecay*0.24/24 {1/hr, fecal decomposition rate}
 Kfert = TlimitDecay*0.7/24 {1/hr; 0.7/24 from ref. average decomposition rate}
 Kgrass = 0.53/24 {1/h, decomposition rate}
 KhAlf = (-1)*(Sigmkh/1.58)*Lnrandom {calculate random component, Knight, 1991}
 KhKhoA = IF RichardsonNoA < 0 THEN 1 ELSE (1 + (0.05 * RichardsonNoA))^(-1) {dimensionless ratio; Losordo pg. 32, 161}
 KhKhoB = IF RichardsonNoB < 0 THEN 1 ELSE (1+ (0.05 * RichardsonNoB))^(-1) {dimensionless ratio; Losordo pg. 32, 161}
 Khm = correctKt*(AKh+Bkh*cos(HourSolarAngle)) {empirical equation, Hsieh, 1986. p58}
 KL = (0.0036 * (8.43 * (WindSpeedAtZms)^(0.5) - 3.67 * (WindSpeedAtZms) + (0.43 * (WindSpeedAtZms)^(2)))) {oxygen transfer coefficient; m/hr}
 Kleach = Seepage/Water_Col_Depth {1/hr; sink rate }
 KN = 30 { 15 ug/L, half saturation constant for N, 10-20 ug/L, frm Lee, 1991a }
 KNuptake = 5 {nutrient uptake rate, ug N/ug chla 10 is from Lee; the value is 4.6 from calculation based on Thailand }
 Komoxy = 3 {1.08; 3.0 g O2 removed/ g Organic matter}
 KOrgNToAmmonia = 0.05/24 {1/hr, range is 0.05 to 0.1 (1/day)}
 kphyto = TlimitDecay*0.72/24 { 1/hr, phytoplankton decomposition rate}
 KphytoHalfSat = 30 { mg/m3; 80 }
 Ks = 0.667 {W/m/°C}
 KTempGradMtB = KConvertMid - KConvertBot
 Ktmax = 0.8 {0.8; the maximum Kt value, from CRSP}
 Ktmin = 0.1 {the minimum value of Kt}
 Labile_N = 1 {Labile N fraction;0.45}
 Latitude = 14.43 {degrees south}
 LightExtCoeff = EstimatedlightExtin { 1.7/SECCHIDISK ,m-1}
 Lnrandom = logn(1/ConvertFunc_2-1)

Longitude = 87.68 {degrees west}
 LowDO = 2.0 {mg/l; limit before fish move to higher DO}
 LWReflect = 0.05 {0.03 reflectance of water surface to Lw radiaton, as decimal}
 MaxFetch = 65 { m, measured from pond }
 MaxFetch1 = IF WindDirection1>0 THEN PondWidth/COS(WindDirection1) ELSE 0
 MaxFetch2 = IF WindDirection2>0 THEN PondLength/COS(WindDirection2) ELSE 0
 Maximum_NH3 = 0.14 {Maximum NH3 level above which tilapia will not feed (Hassan, 1989)}
 MaxRation = FoodWeightEffect*WaterQualityFactor*Relative_feeding_level {g fish/fish/hr; Rmax}
 Maxtemp = 41 {41, maximum temperature}
 MeanFetch = IF RelWindDirect >= PondAngle THEN MeanFetch2 ELSE MeanFetch1 }
 MeanFetch1 = IF WindDirection1=0 THEN PondWidth ELSE TriWtFetch1+OtherFetch1 { }
 MeanFetch2 = IF (WindDirection2 = 0) THEN PondLength ELSE (OtherFetch2+TriWtFetch2) { }
 Measured_WSP = if ModelTime>=0 and ModelTime<4 then 1.53 else if ModelTime>=4 and
 ModelTime<10 then 2.47 else if ModelTime>=10 and ModelTime<18 then 2.72 else 0.86 {m/s measured
 from Thailand}
 MidBotBoundryDepth = SurfThick + MidThick {m; midlayer/bottom layer boundry depth}
 MidDepth = SurfThick + (MidThick/2) {meters, measurement depth}
 MidThick = Water_Col_Depth/3 {meters thick}
 Minimum_DO = 2.5 { 2.5 mg/l. Minimum DO below which fish will not feed. Mabaye (1971) 2.5 ; 0.5}
 MinTemp = 15 {minimum temperature}
 MinWindSpeed = 0.1*3.6 {km/hr; used in calculating evaporation, shear, etc...}
 ModelTime = MOD(time,24)
 mu = FrictVelWindStress * 30 {drift velocity; m/s}
 N = 5.0593 {empirical "Lake Hefner" coefficient; kJ/m2/km/mmHg}
 NdiffusionRate = 0.075 {g TAN/m2/d}
 NeutBuoyEffectDiffuCoeffA = (((FrictVelWindStress^(2))/(mu * k)) * EXP(-k *
 SurfMidBoundryDepth)) {m2/sec; neutrally buoyant diffusion coefficient at surf/middepth boundry Kho in
 Losordo, but adjusted for depth}
 NeutBuoyEffectDiffuCoeffB = (((FrictVelWindStress^(2))/(mu * k)) * EXP(-k * MidBotBoundryDepth))
 {m2/sec; neutrally buoyant diffusion coefficient at middepth/bottomdepth boundry}
 NewCCHLa = if CCHLa>CCHLaMax then CCHLaMax else if CCHLa<CCHLaMin then CCHLaMin else
 CCHLa {mg C/mg chla}
 newChla = if ChlaNet>Chlalimit then Chlalimit else if ChlaNet<0 then 0 else ChlaNet {mg/m3, net chla}
 NH3Conc = TANaccum*fNH3/1000 {mg/L, estimated NH3 conc.}
 nitrRate = (0.01)*TANaccum {ug/L/hr; nitrification rate, Lee 1991a}
 Nlimit = (TANWaterColumn/(KN+TANWaterColumn)) {unitless, nitrogen limitation, from Lee 1991a}
 NonPhytoByFish = MaxRation*NonUptakeSpecFactor
 NonPhytopLimitFactor = TotDetritus/KchickHalfSat {unitless, the factor limits the nonphytoplankton
 food uptake}
 NonUptakeSpecFactor = NonPhytopLimitFactor/(1+sumFeed)
 NORMALDIST = NORMAL((10/36)*WIND, (10/36)*WINDSTDV){ m/sec }
 Nreleased = (OrganToAmmonia)/Water_Col_Depth*1000 {ug N/L/hr}
 NumFishBot = if DOBot>=LowDO then Fish_population/3 else 0 {number of fish}
 NumFishMid = if DOMid<LowDO then 0 else if dobot<LowDO and DOMid>=LowDO then
 Fish_population/2 else Fish_population/3 {number of fish}
 NumFishSurf = if DObot<LowDO and DOMid>=LowDO then Fish_population/2 else if
 DOSurf>=LowDO and DOMid>=LowDO and DOBot>=LowDO then Fish_population/3 else if
 DOSurf<LowDO then 0 else Fish_population {number of fish }
 NuptakeByChla = ChlaProdRate*KNuptake
 N_MaxExp = exp(-(JulianDay-183.83)/78.07)
 N_MinExp = exp(-(JulianDay-194.57)/83.52)
 O2ConcCalcBot = if NetOxBot<0 then 0 else NetOxBot/BotThick/1000 {mg/l}
 O2ConcCalcMid = if NetOxMid<0 then 0 else NetOxMid/MidThick/1000 {mg/l}
 O2ConcCalcSurf = if NetOxSurf<0 then 0 else NetOxSurf/SurfThick/1000 {mg/l; initial plus net change
 (mg/m3) divided by liters in a m2 element of given thickness}
 O2Nitr = 4.57*nitrRate*Water_Col_Depth/3 {mg O2/hr/m2, oxy consumed by Nitrification in the segment}

$O2RateBot = (P_{MAX} * (ST1_{Bot} - ST2_{Bot}) * EXP(1)) / (AdjLightExtCoeff * (BotThick)) * Nlimit * Tlimit_{Bot}$
 $O2RateMid = (P_{MAX} * (ST1_{Mid} - ST2_{Mid}) * EXP(1)) / (AdjLightExtCoeff * MidThick) * Nlimit * Tlimit_{Mid}$
 $O2RateSurf = (P_{MAX} * (ST1 - ST2) * EXP(1)) / (AdjLightExtCoeff * (SurfThick)) * Nlimit * Tlimit_{Surf}$ {mgO2/mgChla/hr}
 $O2TransferByDiffA = EffectDiffuCoeffA$ {m2/hr. }
 $O2TransferByDiffB = EffectDiffuCoeffB$ {m2/hr}
 $OMA_{Algal} = DeadChla / ChlaToCell / 1000$ {g/m2/hr OM from algal cell}
 $oneovercosr = 1 / \cos(Arcsinz / 1.33)$
 $Optimal_water_temperature = 30$ {optimal temperature for fish growth}
 $OPTTEMP = 25.5$ {25.5 degrees C; optimum phytoplankton temp. in "middle to upper range of pond water temperatures" in Giovannini, part 1 in press 1992}
 $Orbit = (360 / 364 * (JulianDay - 81)) * \pi / 180$ {Angular position of earth in orbit around sun - Radians}
 $OtherFetch1 = MaxFetch1 * (1 - TriWt1)$
 $OtherFetch2 = MaxFetch2 * (1 - TriWt2)$
 $OutflowRate = 0. / 24$ { outflow rate}
 $OxyRespBot = AveOxyResp * RatioDO_{Bot}$ {mgO2/m2/hr}
 $OxyRespMid = AveOxyResp * RatioDO_{Mid}$ {mgO2/m2/hr}
 $OxyRespSurf = AveOxyResp * RatioDO_{Surf}$ {mgO2/m2/hr}
 $PenPar = \text{if } SolarRadSurfAdj \leq 0 \text{ then } 0 \text{ else } (5.5958 + 1.8228 * (SolarRadSurfAdj * 1000 / 3600))$ {umol/m2/s, is converted from Kj/m2/hr, penetrating photosynthetically active radiation }
 $pH = 8.5$
 $PhotoRateBot = O2RateBot * newChla * BotThick$ {mgO2/m2/hr}
 $PhotoRateMid = O2RateMid * newChla * MidThick$ {mgO2/m2/hr}
 $PhotoRateSurf = O2RateSurf * newChla * SurfThick$ {mgO2/m2/hr; gross growth}
 $PhytC = 0.4$ {g carbon/g phytoplankton}
 $PhytN = AlgalCP / 6.25$
 $PhytoByFish = MaxRation * PhytoUptakeSpecificFactor$
 $PhytoUptakeSpecificFactor = PhytoUptekenLimit / (1 + sumFeed)$
 $PhytoUptekenLimit = newChla / KphytoHalfSat$ {unitless, the factor for limiting the grazing by fish due to conc. of chla}
 $pKa = 0.09018 + 2729.92 / (Tave + 273)$ {estimated pKa, Emerson et al., 1975}
 $P_{MAX} = NewCCHLa * Umax$ {mgO2/mgChla/h; see Giovannini, part 1, in press 1992}
 $PondAngle = ARCTAN(PondLength / PondWidth)$ { }
 $PondArea = PondLength * PondWidth$ {m2 }
 $PondepthPerLayer = Water_Col_Depth / 3$ {m, water depth per layer}
 $PondLength = 50$ {m, need to check! }
 $PondVol = Water_Col_Depth * PondArea$ {m3 }
 $PondWidth = 20$ {m}
 $QsnB = (1 - SurfAbsorb) * SolarRadSurf$ {KJ/m2/hr}
 $RandomNODailySolar = NORMAL(0,1)$ {Random number from a normal distribution with mean 0 and standard deviation 1}
 $RandomNoHourSolar = NORMAL(0,1)$ {Random number from a normal distribution with mean 0 and standard deviation 1}
 $RANDOMWIND = \text{IF } (NORMALDIST < WINDHIGH) \text{ AND } (NORMALDIST > WINDLOW) \text{ THEN } NORMALDIST \text{ ELSE } 0$ { m/sec }
 $RandomWindResidual = NORMAL(0,1)$ {Random number from a normal distribution with mean 0 and standard deviation 1}
 $RatioDO_{Bot} = \text{if } TotDO > 1.0 \text{ then } DO_{Bot} / TotDO \text{ else } 1/3$
 $RatioDO_{Mid} = \text{if } TotDO > 1.0 \text{ then } DO_{Mid} / TotDO \text{ else } 1/3$
 $RatioDO_{Surf} = \text{if } TotDO > 1.0 \text{ then } DO_{Surf} / TotDO \text{ else } 1/3$
 $ratioOxyCarbon = 2.67$ {oxygen / carbon; 36/12=2.67; 2.3}
 $ReflCalc = \text{IF } SolarAlt > 0.017453 \text{ THEN } 2.2 * EXP(-0.97 * LOGN(SolarAlt * 180 / PI)) \text{ ELSE } 0$ {reflectivity of a smooth water surface under scattered clouds; as a fraction of incoming radiaton}
 $Reflectance = \text{IF } ReflCalc > 1 \text{ THEN } 1 \text{ ELSE } ReflCalc * ReflectWindAdj$


```

ReflectWindAdj = (1 - (0.04 * (WindSpeedAtZms * AdjFetch))) { adjustment of reflectivity of water
surface for WINDSPEED}
Relative_feeding_level = IF Fish_biomass <= Critical_standing_crop THEN 1 ELSE
Critical_standing_crop / (Fish_biomass) {RELATIVE FEEDING LEVEL = ACTUAL FOOD
INTAKE / MAXIMUM POSSIBLE INTAKE; DIMENSIONLESS}
RelWindDirect = ARCTAN(ABS(SIN(WINDIRECTION - RotationAngle) / COS(WINDIRECTION -
RotationAngle))) { }
ResidualMax = if time <= 24 - dt then (ResidualOut2) else (ResidualOut2 - 100) {subtract the threshld}
ResidualMin = if time <= 24 - dt then (ResidualOut) else (ResidualOut - 100) {subtract the threshld}
RichardsonNoA = ((CoeffExpandH2OA * g * (SurfMidBoundaryDepth)^2) / FrictVelWindStress^(2)) *
(TempGradientSurfM / DepthGradSurfM) {Richardson number for diffusion at surf/mid boundary}
RichardsonNoB = ((CoeffExpandH2OB * g * (MidBotBoundaryDepth)^2) / FrictVelWindStress^(2)) *
(KTempGradMtB / DepthGradMtB) {Richardson number for diffusion at mid/bot boundary}
RotationAngle = 0.0 * PI / 180 { }
RWind = 0.49607887 + 1.8431325 * exp(-0.5 * ((Timeconvert - 785.11185) / 163.10768)^2) {generated the
wind speed in m/s}
SecchDisk = 124.739 / (newChla + 3.00)^0.306 / 100 { m, Honduras data from Shree}
SedDepth = Water_Col_Depth + (SedThick / 2) {meters, measurement depth}
SedRefTemp = InitialTemp { °C}
SedRespRate = 0.16 / 24 {0.015, 0.5 mgO2/m2/hr}
SedThick = Water_Col_Depth / 3 {m}
Seepage = 3 / 1000 / 24 {3 / 1000 / 24 ; m/hr, infiltration rate}
Sigmkh = 0.1557 * sin(PI * correctKt / 0.933)
SinkRate = 0.05 / 24 {0.05 / 24 m/hr; algal sink rate, 1 to 1.3m/d; ref. Lee, 1991b}
sinzn = sin(Zenith) / 1.33
SiteElevation = 583 {meters above sea level}
SiteWindVect = 1.5 {site specific parameter, unitless}
SKEW = -1.08868 { }
SolarAlt = 1.570796 - Zenith {solar altitude angle; radians}
SolarIrradiance = if SolarRadHourly > solradmax then solradmax * 1000 else SolarRadHourly * 1000 {
Mj/m2/hr}
SolarRadAbsSurf = SolarRadSurfAdj - SolarRadDepAdj1
SolarRadDaily = if GeneratedHt >= SolarRadDailyMin and GeneratedHt <= SolarRadDailyMax then
GeneratedHt else if GeneratedHt > SolarRadDailyMax then SolarRadDailyMax else SolarRadDailyMin {
average daily solar radiation values, mj/m2}
SolarRadDailyMax = 31.14 {MJ/m2, the maximum value is measured from the Honduras site in 1991}
SolarRadDailyMin = 3.17 {MJ/m2, the minimum value from CRSP data Honduras site in 1991}
SolarRadDepAdj1 = IF SolarRadDepth1 > 0 THEN SolarRadDepth1 ELSE 0 {KJ/m2/hr; eliminates
negative values}
SolarRadDepAdj2 = IF SolarRadDepth2 > 0 THEN SolarRadDepth2 ELSE 0 {KJ/m2/hr; eliminates
negative values}
SolarRadDepAdj3 = IF SolarRadDepth3 > 0 THEN SolarRadDepth3 ELSE 0 {KJ/m2/hr; eliminates
negative values}
SolarRadDepth1 = QsnB * (EXP(-LightExtCoeff * (BoundDepth1))) {adjustment for middepth}
SolarRadDepth2 = QsnB * EXP(-LightExtCoeff * (BoundDepth2)) {KJ/m2/hr; adjusted for middle/bottom
depth}
SolarRadDepth3 = QsnB * EXP(-LightExtCoeff * (Water_Col_Depth)) {KJ/m2/hr}
SolarRadHourly = Hh * ExtraAveHho {average hourly solar radiation value, MJ/m2/hr}
SolarRadSurf = SolarIrradiance * (1 - Reflectance) { Mj/m2/hr, light intensity at the surface of the pond,
adjusted for roughness of water surface}
SolarRadSurfAdj = IF SolarRadSurf > 0 THEN SolarRadSurf ELSE 0 {KJ/m2/hr}
Solar_Time = StandardTime + Eq_Time + DTSL
solradmax = 4.500 {4.5; Mj/m2/hr}
srha = - (PI / 2 - ARCTAN( srss / SQRT(1 - srss^2) )) {Sun Rise Hour Angle}
srss = -TAN(fi) * TAN(Delination) {Sunrise & Sunset huor, same as cos HA}
ssha = ( PI / 2 - ARCTAN( srss / SQRT(1 - srss^2) )) {Sun Set Hour Angle}

```

```

St = sin((pi*(ModelTime+6+dt-HighestSH+DayLength/2)/(DayLength+2)))
ST1 = EXP((-PenPar/Imax) * EXP(-AdjLightExtCoeff * (BoundDepth1)))
ST1Bot = EXP((-PenPar/Imax) * EXP(-AdjLightExtCoeff * Water_Col_Depth))
ST1Mid = EXP((-PenPar/Imax) * EXP(-AdjLightExtCoeff * (BoundDepth2)))
ST2 = EXP((-PenPar/Imax) * EXP(-AdjLightExtCoeff * (TopDepth)))
ST2Bot = EXP((-PenPar/Imax) * EXP(-AdjLightExtCoeff * BoundDepth2))
ST2Mid = EXP((-PenPar/Imax) * EXP(-AdjLightExtCoeff * (BoundDepth1)))
StableFlowDiffuCoeffA = NeutBuoyEffectDiffuCoeffA * 3600 * KhKhoA {m2/hr}
StableFlowDiffuCoeffB = NeutBuoyEffectDiffuCoeffB * 3600 * KhKhoB {m2/hr}
StandardTime = if (InitialTime+ModelTime) > 24 then ModelTime-InitialTime-12 else
(InitialTime+ModelTime) {assumed standard equals model time, hr}
StdDevAirMax = 3.20 {standard deviation, air temperature}
StdDevAirmin = 2.02 { standard deviation of minimim air temperature, C}
StdevWind = 4.43 {km/hr}
STDNORMAL = NORMAL(0,1) { }
STDV = 74.41835 { }
STD_Longitude = 90
StefanBoltzman = 2.042 * 10(-7) {kJ/m2/hr/°K4}
st_Night = sin(pi*(DayLength/(DayLength+2)))

SubtractThreshold = if time<=24-dt then (solarResidueOut) else (solarResidueOut-100) {subtract the
threshld}
SubtractThresholdWind = if time<=24-dt then (WindResidueOut)/(20.5) else (WindResidueOut-
100)/(20.5) {subtract the threshld}
SubtractThreshold_3 = if time<=1-dt then (solarResidueOut_2) else (solarResidueOut_2-100) {subtract
the threshld}
sumFeed = NonPhytopLimitFactor+PhytoUptekenLimit
SunAngle = (1-srss2)0.5 {arcsin(x)}
SunRiseTime = 12-DayLength/2 {sunrise time}
SunSetsTime = 12+DayLength/2 {Sunset time}
SurfAbsorb = 0.045 {0.05; decimal %; SW radiation absorbed at water surface}
SurfaceArea = PondLength*PondWidth { }
SurfDepth = SurfThick/2 {meters, measurement depth}
SurfDiffIn = IF TransRateInterf > 0 THEN TransRateInterf ELSE 0
SurfDifOut = IF TransRateInterf < 0 THEN -TransRateInterf ELSE 0
SurfMidBoundryDepth = SurfThick {m; boundry layer depth}
SurfRadToAtmos = 0.97 * StefanBoltzman * ((TwK)4) {kJ/m2/hr; loss of energy from water body due to
Lw radiation}
SurfThick = Water_Col_Depth/3 {meters thick}
TairDaytime = if (Tk2+4*AMP*Tk*St)<=0 then DelayTairmin-Tk/2 else DelayTairmin-
Tk/2+0.5*(Tk2+4*AMP*Tk*St)0.5
TairHour = if ModelTime+6>=SunRiseTime-1 and ModelTime+6 <=SunSetsTime then TairDaytime else
TairNighttime
Tairmax = if AirGMax>37 then 37 else AirGMax
Tairmin = if AirGMin<13 then 13 else if AirGMin>25 then 25 else AirGMin
TairNighttime = (Tairmin-Ts*exp(-darkLength/4)+(Ts-Tairmin)*exp(-(ModelTime+6-
SunSetsTime)/4))/(1-exp(-darkLength/4)) {Air temperature at night }
TaK = 273.15 + DegreeCAir {conversion to degrees K}
TANfromUrea = ((UreaNcontent*addedurea)/(Water_Col_Depth))*1000 {ug ammonia/L/hr}
TANinflow = InputTAN*InflowRate/PondVol {ug/L/hr TAN}
TANoutflow = OutflowRate*TANaccum/PondVol {ug/L hr}
TANprodByFish = 0.03*FishWeightINPUT*Fish_population {g/hr; total TAN production which is based
on the feed intake}
TANWaterColumn = if TANaccum<0 then 0 else TANaccum
TavA = (KConvertTop + KConvertMid)/2
TavB = (KConvertBot + KConvertMid)/2

```

```

Tave = (TempBotCalc+TempMidCalc+TempSurfCalc)/3 {average water temperature }
TempBotCalc = NetEnergyBot/(1000 * 4.1816*BotThick) {°C}
TempCalcGW = InitialTempGW {°C}
TempeffectFactor = 1.049^(TempSedCalc - SedRefTemp)
Temperature_factor = IF Temp_For_Fish<Optimal_water_temperature THEN EXP(-
4.6*((Optimal_water_temperature-Temp_For_Fish)/
(Optimal_water_temperature-MinTemp))^4) ELSE EXP(-4.6*((Temp_For_Fish-
Optimal_water_temperature)
/(Maxtemp-Optimal_water_temperature))^4) {Describes effects of temp on food intake =TAU IN BEI;
dimensionless}
TempGradBtSed = TempBotCalc - TempSedCalc {°C}
TempGradientSurfM = TempSurfCalc - TempMidCalc
TempGradMtB = TempMidCalc - TempBotCalc
TempGradSedtGW = TempSedCalc - TempCalcGW {°C}
TempMidCalc = NetEnergyMid/(1000 * 4.1816*MidThick) {°C}
TempSedCalc = NetEnergySed/(1760*SedThick) {KJ/m3/°C}
TempSurfCalc = NetEnergySurf/(1000 * 4.1816*SurfThick) {°C; energy/mass * specific heat; 4.1816 is
specific heat at 20°C}
TempWK = TempSurfCalc + 273.15
Temp_For_Fish = if
(TempSurfCalc*NumFishSurf+TempMidCalc*NumFishMid+TempBotCalc*NumFishBot)/Fish_populatio
n<=TempBotCalc then TempSurfCalc else
(TempSurfCalc*NumFishSurf+TempMidCalc*NumFishMid+TempBotCalc*NumFishBot)/Fish_populatio
n
testlmax = 0.7
Timeconvert = mod(time,24)*100
Tk = 15 {C, parameter for the sensible heat}
TlimitBot = IF TempBotCalc<Toptm THEN EXP(-4.6*((Toptm-TempBotCalc)/(Toptm-Tmin))^4) ELSE
EXP(-4.6*((TempBotCalc-Toptm)/(Tmax-Toptm))^4)
TlimitDecay = 1.08^(Tave-20)
TlimitMid = IF TempMidCalc<Toptm THEN EXP(-4.6*((Toptm-TempMidCalc)/(Toptm-Tmin))^4)
ELSE EXP(-4.6*((TempMidCalc-Toptm)/(Tmax-Toptm))^4)
TlimitSurf = IF TempSurfCalc<Toptm THEN EXP(-4.6*((Toptm-TempSurfCalc)/(Toptm-Tmin))^4)
ELSE EXP(-4.6*((TempSurfCalc-Toptm)/(Tmax-Toptm))^4)
Tmax = 41 {41 assumed value}
Tmin = 10 {10 assumed value}
TopDepth = 0.0 {m}
Toptm = 25
TotalC = ArtifiFeedCarbonFraction*ArtifiByFish+CMC*NoNPhtoByFish+PhytC*PhytoByFish {g C/hr,
total uptake Carbon}
TotalN = ArtifiByFish*ArtiN+CMN*NoNPhtoByFish+PhytN*PhytoByFish {g N/hr; total uptake
Nitrogen}
TotChlaProd = (PhotoRateBot+PhotoRateMid+PhotoRateSurf)*ChlaProductionPerOxy {mg chla/m2/hr}
TotDetridus = ChickManure+GGrass+ChlaDeathDetridus*Water_Col_Depth/1000 {g/m2}
TotDO = DOBot+DOMid+DOSurf
TotFeedFactor = PhytoUptakeSpecificFactor+NoNUptakeSpecFactor+ArtifiUptakeSpecFactor {unitless;
total feed uptake specific factor}
TotFeedUptake = MaxRation*TotFeedFactor {g fish/fish/hr}
TransRateInterf = (KL * (Csat - DOSurf)) * 1000 { area of interface; yields rate of oxygen transfer across
interface per unit area; mg/hr/m2}
TriArea1 = IF WindDirection1<>-1 THEN (PondWidth^2)*TAN(WindDirection1)/2 ELSE 0 { }
TriArea2 = IF WindDirection2<>-2 THEN 0.5*(PondLength^2)*TAN(WindDirection2) ELSE 0 { }
TriWt1 = 2*TriArea1/SurfaceArea { }
TriWt2 = 2*TriArea2/SurfaceArea
TriWtFetch1 = AverFetch1*TriWt1
TriWtFetch2 = AverFetch2*TriWt2 { }

```

```

Ts = Tairmin+(Tairmax-Tairmin)*st_Night {the temperature connects the day time and night time curve}
TwK = 273 + TempSurfCalc {conversion to degrees K}
Umax = (((10^(0.0275 * OPTTEMP - 0.23))/12))^ratioOxyCarbon*gt {0.83; mgO2/mgC/hr; from
Giovannini, in press 1992; part 1}
UreaAddedTime = if (Fertilizeddays=1 or Fertilizeddays=4) and (StandardTime>10 and
StandardTime<=14) then 1 else 0 { assumed at 10:00 am to add fertilizer}
UreaInput = 0 {77.04 ; kg urea/ha/wk}
UreaNcontent = 0.38 {38 % of urea is Ammonia from Honduras data}
WaterQualityFactor = Feeding_threshold_for_NH3*FeedThresholdForDO*Temperature_factor { unitless,
water quality factor}
Water_Col_Depth = 0.9 {m, sediment depth}
WRefTemp = 27 {°C; 28.8 temperature at which water column respiration rate was measured}
WRespBot = (1.049^(TempBotCalc - WRefTemp)) *( BODlayer+WResRate)*DObotLimit
{mgO2/hr/m3}
WRespMid = (1.049^(TempMidCalc - WRefTemp)) *(BODlayer+WResRate)*
DOMidLlimit{mgO2/hr/m2}
WCREspRate = 0*50 {200; (DOfactor*0.5+0.2)*0.23*1000 ; 0.4 mg/m2/hr}
WRespSurf = (1.049^(TempSurfCalc-WRefTemp))*(BODlayer+WResRate)*DOSurflimit {
mgO2/hr/m2}
WResRate = 50 {mg O2/m2/hr}
WIND = 5.5655218+2.44074073*SIN((2*PI*(5+TIME)/19.555564)+2.633405) { }
WindDirection1 = IF RelWindDirect<PondAngle THEN RelWindDirect ELSE -1 { }
WindDirection2 = IF (RelWindDirect >= PondAngle) THEN (IF (1.570796 - RelWindDirect) <= 0.001
THEN 0 ELSE (1.50796-RelWindDirect)) ELSE -2 { DIFERENCA NO VALOR DE DT PODE PEDIR
MUDANCA NO 0.001 }
WINDHIGH = (10/36)*(11.366296+7.4485281*EXP(-0.5*(((5+COUNTER(6,30))-
16.091399)/1.4503812)^2)) { m/sec }
WINDIRECTION = IF CONTROL_2<0 THEN ABS(CONTROL_2) ELSE CONTROL_2 {radian }
WINDLOW = IF COUNTER(6,30)<18 THEN FUNCTION ELSE 0 { m/sec. }
windmax = 37 {km/hr}
windmin = 2.5 {km/hr}
WindShearArea = AdjWindSpeed * AdjFetch
Windspeed = if GendailyWindMean*(0.575+0.899*exp(-0.5*((ModelTime-9.928)/3.687)^2))
<MinWindSpeed then MinWindSpeed else GendailyWindMean*(0.575+0.899*exp(-0.5*((ModelTime-
9.928)/3.687)^2))
WindSpeedAtZ = (Windspeed) * (10/AnemometerHeight)^(1/7) {Wind speed at 2m above pond,
converted to Km/hr}
WindSpeedAtZms = WindSpeedAtZ/3.6 {m/s}
WindSpeedms = (Windspeed*1000/3600) {m/s}
WINDSTDV = 3.193815+0.294170*SIN( (2*PI*(5+TIME)/25.007263)+1.8247152) { }
Windvectorest = SiteWindVect*Windspeed {needs to be determined through initialization; relates wind
speed to wind vector estimation}
WinNorm = normal(RWing,Rwstd)
Wmean = 7.55+1.458*sin(2*pi*JulianDay/313.605+0.5517) {km/hr}
WShearStress = IF WindShearArea > 0 THEN AirDensity * aeroresistcoeff * (WindShearArea)^2 ELSE 0
{N/m2; see Losordo pg.387}
WtEffect = 0.67 { 0.67, unitless, exponent of anabolism, body weight effect to feeding}
Zenith = IF (Hour_Angle > ssha ) OR (Hour_Angle < srha ) THEN 1.5707963 ELSE PI/2 - ARCTAN(
Cos_z / ( SQRT ( 1 - (Cos_z)^2 ) ) ) {radians}
Rwstd = GRAPH(Timeconvert {0.50874873+0.43*exp(-0.5*((Timeconvert/100-9.5760451)/-
1.366834)^2)})
(0.00, 9.80), (250, 0.9), (500, 0.8), (750, 0.8), (1000, 1.00), (1250, 0.9), (1500, 0.8), (1750, 0.8), (2000,
0.8), (2250, 0.7), (2500, 0.7)

```